Distribution Agreement

In presenting this thesis or dissertation as a partial fulfillment of the requirements for an advanced degree from Emory University, I hereby grant to Emory University and its agents the non-exclusive license to archive, make accessible, and display my thesis or dissertation in whole or in part in all forms of media, now or hereafter known, including display on the world wide web. I understand that I may select some access restrictions as part of the online submission of this thesis or dissertation. I retain all ownership rights to the copyright of the thesis or dissertation. I also retain the right to use in future works (such as articles or books) all or part of this thesis or dissertation.

Signature:

_____ _____

Stephanie Jones Date

The Polyadenosine RNA Binding Protein ZC3H14 is Required in Mice for Proper Working Memory, Synaptosomal Composition, and Dendritic Spine Density and Morphology

By

Stephanie Jones
Doctor of Philosophy

Graduate Division of Biological and Biomedical Science
Genetics and Molecular Biology

_____
Anita H. Corbett, Ph.D.
Advisor

_____
Tamara Caspary, Ph.D.
Committee Member

_____
Andrew Escayg, Ph.D.
Committee Member

_____
Paul S. Garcia, MD., Ph.D.
Committee Member

_____
Kenneth H. Moberg, Ph.D.
Committee Member

Accepted:

_____
Lisa A. Tedesco, Ph.D.
Dean of the James T. Laney School of Graduate Studies

_____
Date

The Polyadenosine RNA Binding Protein ZC3H14 is Required in Mice for Proper Working Memory, Synaptosomal Composition, and Dendritic Spine Density and Morphology

By

Stephanie Jones

B.S., Pacific Lutheran University, 2012

Advisor: Anita H. Corbett, Ph.D.

An abstract of

A dissertation submitted to the Faculty of the

James T. Laney School of Graduate Studies of Emory University

in partial fulfillment of the requirements for the degree of

Doctor of Philosophy

in Genetics and Molecular Biology

2020

Abstract

The Polyadenosine RNA Binding Protein ZC3H14 is Required in Mice for Proper Working Memory, Synaptosomal Composition, and Dendritic Spine Density and Morphology

By Stephanie Jones

ZC3H14 (Zinc finger CysCysCysHis domain-containing protein 14), an evolutionarily conserved polyadenosine (poly(A)) RNA binding protein, is lost in a form of heritable, nonsyndromic autosomal recessive intellectual disability. This observation shows that ZC3H14 is essential for proper brain function. To investigate the role of ZC3H14 in the mammalian brain, we have generated a novel *Zc3h14*$^{\Delta ex13/\Delta ex13}$ mutant mouse model. Utilizing these mice, we provide the first *in vivo* functional characterization of ZC3H14. The *Zc3h14*$^{\Delta ex13/\Delta ex13}$ mice show defects in working memory, suggesting that loss of ZC3H14 may affect brain regions associated with memory, such as the hippocampus. Analysis of *Zc3h14*$^{+/+}$ and *Zc3h14*$^{\Delta ex13/\Delta ex13}$ hippocampi show loss of ZC3H14 results in elongated bulk RNA poly(A) tails, decreased dendritic spine density both *in situ* and *in vitro*, and altered steady-state proteins to include postsynaptic proteins such as CaMKIIα. CaMKIIα is critical in synaptic plasticity, which is a process highly implicated to underlie learning and memory. Loss of ZC3H14 results in increased levels of CaMKIIα in synaptosomes, as well as reduction of *in vitro* mushroom spine density, which is rescued upon exogenous ZC3H14 expression. In addition, ZC3H14 associates with *CaMKIIα* mRNA and is detected in synaptosomes, suggesting *CaMKIIα* may be a ZC3H14 RNA target. Together, the results generated from this novel mouse model suggest that ZC3H14 is required in higher order brain function by regulating targets critical to proper neuronal function.

The Polyadenosine RNA Binding Protein ZC3H14 is Required in Mice for Proper Working Memory, Synaptosomal Composition, and Dendritic Spine Density and Morphology

By

Stephanie Jones

B.S., Pacific Lutheran University, 2012

Advisor: Anita H. Corbett, Ph.D.

A dissertation submitted to the Faculty of the

James T. Laney School of Graduate Studies of Emory University

in partial fulfillment of the requirements for the degree of

Doctor of Philosophy

in Genetics and Molecular Biology

2020

Table of Contents

List of Figures

Chapter 1:

Chapter 2:

Chapter 3:

Chapter 4:

Chapter 1

General Introduction

1.1 RNA Binding Proteins Confer Fundamental Cellular Functions and Their Dysregulation Can Result in Major Tissue-Specific Disorders

Life as we know it would not exist without RNA. The RNA world hypothesis suggests that before the earliest form of "life" even took shape RNA was present in primordial conditions and capable of functioning both as genetic material and as a biochemical catalyst, otherwise known as ribozymes. While the hypothesis is incomplete [1], it is well supported [2-6] and provides a model where RNA can serve as the template for the earliest instances for stable and self-reproducible biological systems to occur. Over the course of billions of years of evolution, RNA has remained a vital component of all living life; acting as the essential bridge between genetic integrity and protein synthesis.

There is a wide diversity of different RNA classifications, including but not limited to messenger (mRNA), transfer (tRNA), ribosomal (rRNA), long noncoding (lncRNA), microRNA, small nuclear (snRNA), circular (circRNA), small interfering (siRNA), and many more, each of which confers a specific cellular function. In order to perform their functions, RNAs first go through a series of post-transcriptional processing and regulatory events to achieve their proper functional sequences/forms. Precise control over this complex RNA processing is paramount, especially in higher-order organisms in which the differentiation of distinct tissues and the ability to maintain tissue-specific functionality is thoroughly dependent not only on how specific RNAs are differentially expressed and processed, but also how fully mature RNAs are regulated, maintained, and eventually destroyed [7-11].

To exert precise control over RNA processing, a large class of RNA binding proteins interacts (directly or indirectly) with RNA. Of the ~20,000 annotated protein-coding genes in the human genome, at least 7% are RNA binding proteins [12], indicating the functional importance

of direct RNA regulation by this class of proteins. The role of specific RNA binding proteins varies widely and depends on which step(s) in RNA processing/maintenance they are involved in. RNA binding proteins can interact with RNAs at specific or numerous steps of RNA processing, including addition of a 5' methyl cap [13], RNA splicing [14], 3' end cleavage that occurs co-transcriptionally or post-transcriptionally and the addition of a 3' polyadenosine (poly(A)) tail [15], export of quality-checked mature RNA from the nucleus to the cytoplasm [16], RNA stabilization [17], transport/subcellular localization [18], translation [19], and/or RNA turnover/decay [20]. Many RNA binding proteins have been identified to cause Mendelian disease upon mutation [21], and **Figure 1-1** highlights how impairment of RNA-binding proteins at any one of the RNA processing steps has the potential to cause detrimental cellular and/or organismal phenotypes. This further emphasizes the necessity for proper and finely tuned control at each level of RNA processing as well as the advantage of involving numerous RNA processing proteins at each step.

The genetic, molecular, and functional roles of specific RNA binding proteins is an active area of investigation. Due to the fundamental requirement for cells to maintain proper control of RNA, RNA binding proteins are predominantly expressed ubiquitously, with only 2-6% of RNA binding proteins exhibiting tissue-specific expression in humans [12, 22]. However, of 1502 examined RNA binding proteins, at least 157 (~10%) have thus far been linked to over 200 tissue-specific Mendelian diseases upon mutation, to include neuropathies, muscular atrophies, sensorial disorders, cancer, anemias, cardiovascular, and hepatic disorders [21, 23-30]. This number may increase as additional proteins have been implicated to have RNA-binding potential [31] and as more uncharacterized RNA binding proteins are investigated. **Figure 1-1** illustrates examples of tissue-specific diseases can result from mutated RNA binding proteins, despite their

ubiquitous expression. The following few examples represent how various RNA binding proteins involved in regulating different stages of RNA processing generate a diverse range of tissue-specific diseases upon mutation.

One of the best characterized examples of an RNA binding protein linked to disease is Fragile X syndrome (FXS), the most common inherited form of intellectual disability [32] with prevalence in the general population estimated at ~1:5000 in males and ~1:8000 in females [33]. This disorder most often manifests due to a 200+ repeat CGG trinucleotide expansion in the 5' UTR region of the *FMR1* gene, resulting in epigenetic silencing due to hypermethylation of the allele [34], and subsequent silencing of *FMR1* expression [35]. *FMR1* encodes the Fragile X Mental Retardation Protein (FMRP), an RNA binding protein that normally represses protein translation [36, 37]. Evidence indicates that FMRP may play a role in translation at both the initiation [38, 39] and elongation [40, 41] stages, but the exact mechanism remains under active investigation [42]. As a result, steady-state levels of several proteins critical to neuronal and synaptic function are significantly altered in models of FXS [43-45], leading to neuronal dysfunction. Despite the normally ubiquitous expression of FMRP, its loss in FXS causes adverse phenotypes principally in neuronal tissue [46] although functional impairment has also been observed in connective tissue [47] and the testes [48]. Therefore, FXS serves as a classic example of how loss of a ubiquitous RNA binding protein results in tissue-specific impairment.

Another example of a tissue-specific disorder arising from impairment of a ubiquitously expressed RNA binding protein is Oculopharyngeal Muscular Dystrophy (OPMD), a rare (~1:100,000) [49] adult-onset disorder that severely weakens skeletal muscles. OPMD specifically weakens a subset of skeletal muscle—those of the eyelids, pharynx, and potentially the proximal limbs [50]. OPMD arises due to a CGC trinucleotide expansion in the first exon of

the Polyadenylate-Binding Protein Nuclear 1 (*PABPN1*) gene [26]. This expansion expands the normal ten alanine tract in the PAPBN1 N-terminal to 13-18 alanines [51] with a potential correlation between expansion size and disease severity/progression [52]. The PABPN1 protein is a polyadenosine RNA binding protein that promotes 3' polyadenylation of RNAs [53] through recruitment of poly(A) polymerase [54, 55]. Proper regulation of poly(A) tail length is critical for mRNA stability, and can influence later steps of RNA regulation such as nuclear export and translation. Beyond this primary role, PABPN1 also serves additional RNA regulatory roles, including splicing [56] and RNA turnover [57].

One final example is Spinal Muscular Atrophy (SMA), a progressive neuromuscular disorder characterized by loss of motor neurons in the anterior horn of the spinal cord and muscle weakening, which affects ~1:10,000 births [58]. Survival of Motor Neuron (SMN) protein is encoded by both the *SMN1* and *SMN2* genes in humans [59], which provide ~90% and ~10% SMN function, respectively. SMA arises due to loss of SMN protein [28] from loss of function mutations in *SMN1*, with disease severity often corresponding to the degree of SMN deficiency which can be dictated by *SMN2* copy number [60]. SMN is an RNA binding protein [61] whose best characterized function is promoting the assembly of small nuclear ribonucleoproteins (snRNPs) [62, 63], an integral component of the spliceosome machinery [64]. Loss of SMN leads to reduced capacity for snRNP assembly [65, 66], and in a related role is potentially associated with RNA splicing defects [67-70]. SMN has also been implicated in additional regulatory roles, including RNA localization and local translation [71-73]. Showcasing just these few examples indicates a wider precedent where mutation/loss of ubiquitously expressed RNA binding proteins has the capacity to result in tissue-specific disorders, despite often playing fundamental roles that are required in all cell types.

This small handful of examples illustrates the wide range in which loss of a ubiquitously expressed RNA-binding protein can dysregulate RNA processing at different specific stages, as well as result in unique tissue-specific disorders. The reason as to why tissue-specific disorders arise from loss of such RNA-binding proteins with fundamental roles in regulating RNA remains a major area of investigation. Therefore, investigating tissue-specific regulatory features is essential when trying to identify the underlying mechanism(s) of differential tissue impairment upon loss of individual RNA binding proteins.

1.2 Neurons Rely on Complex Regulation of RNA: Long-Distance mRNP Transport/Localization and Local Translation

Proper RNA control is essential in all cell types, but neurons possess distinctive features that make these cells particularly sensitive to dysregulation of RNA binding proteins. Many of these key distinctions stem from the unique morphological traits of neurons in comparison to other cells types. Neurons possess dendrites and axons (collectively called neurites), which are processes that extend outward from the soma and are accessed via active transport along microtubules [74] together with a low level of cellular diffusion. The length of individual dendrites and axons is highly dependent on a number of internal, external, developmental and spatiotemporal variables [75], but in humans dendrites have been found to extend out as far as 1000 μm from the soma (principal cell of globus pallidus) [76], and axons as far as over one meter (sciatic nerve). As neurites extend further from the soma, the more critical and challenging it is to have an efficient method of reliably providing cellular components. This is largely achieved through two neuron-centric processes: long-distance mRNP transport and local translation of mRNA, both of which rely on a suite of RNA binding proteins.

While in the soma, mRNAs are packaged with additional components including RNA binding proteins, microRNAs, and translational machinery, which collectively form messenger ribonucleoprotein (mRNP) complexes. mRNPs associate with molecular motors/adaptors as RNA granules to facilitate transport along cytoskeletal microtubules. Quantification of mRNA within RNA granules has shown that several different mRNAs can coexist within the same RNA granule [77], while other granules can contain a low number or even possibly only a single mRNA [78, 79]. The role of this distinction in mRNA cargo has yet to be confirmed, but it is hypothesized that transporting multiple mRNAs together could aid in coordinating the regulation of similar RNAs [77], as well as being more energy efficient by transporting fewer RNA granules. In contrast, transport of single mRNAs would confer the advantage of individualized RNA regulation.

Packaging and transport of RNAs within RNA granules to their target sites is dependent upon the interaction between *cis*-acting RNA elements and *trans*-acting factors that recognize/interact with specific mRNA sequences. The presence/absence of various types of common sequence motifs is not unique to neurons, however, studies have shown that critical neuronal mRNAs including *CaMKIIα*, *MAP2*, *ARC*, and *BDNF* contain *cis*-acting dendritic targeting elements (DTEs), affirming that *cis*-acting elements contribute to providing neuron-specific localization [80-83]. In addition, the brain exhibits a very high degree of alternative splicing in comparison to other tissues [84, 85] as well as different coding exons [86]. Increased alternative splicing events produce greater regulatory potential through new combinations of included/excluded *cis*-acting regulatory elements, which can create neuron-specific mRNA localization patterns [87, 88]**.** These enhanced features could contribute at least partially to a model for prompting neuron-specific RNA dysregulation as well as neuron-specific disorders.

In tandem with *cis*-acting elements, *trans*-acting components of mRNPs, particularly RNA binding proteins, contribute to determining how and where RNAs will be transported /localized, which in turn affects mRNA translation [89-91]. Consistent with this, loss of RNA binding proteins implicated in RNA transport/localization is linked to mislocalized RNA and, commonly, neurological impairment [92, 93], including FMRP [94], SMN [95], Pum2 [96, 97], CPEB [98], TLS/FUS [99], Sam68 [100], and RNG105/caprin1 [101]. While RNAs can be localized within the cytoplasm of neuronal compartments, such as soma, dendrites, and axons, RNAs can also be localized to sub-compartments within these structures as well. For example, one factor that can contribute to dendrite-specific patterns of RNA localization is distance from the soma (proximal dendrites vs proximal and distal dendrites), which occurs in the transcriptome localization profile of hippocampal synaptic neuropil [102]. RNA localization can also be specific to dendritic spines, with certain RNAs enriched or nearly exclusively localized to spines [103, 104]. Specificity in RNA localization is hypothesized to be attributed at least in part to mRNPs and RNA granules that have distinct associated RNA binding proteins. For example, although the RNA binding proteins Staufen1 (Stau1) and Staufen2 (Stau2) are paralogues and confer dendritic localization, they do not colocalize and Stau2 is more readily detected in distal dendrites than Stau1 [105]. In cultured hippocampal neurons Stau1-positive RNA granules are more likely to be localized to the dendritic shaft, whereas Puralpha-positive RNA granules are localized to both the dendritic shaft and spines [106]. ZBP1 is required for persistence of β-actin mRNA localization to stimulated dendritic spines [107]. Overall, *cis*-acting RNA sequences and *trans*-acting RNA binding proteins cooperate to facilitate neuron-specific localization of RNAs, which is essential for ensuring proper spatiotemporal production of proteins required for neuronal function.

In addition to RNA transport, proper neuronal function is dependent upon effective spatiotemporal regulation of protein translation. While most of the proteins required in the neurites are synthesized in the soma and actively transported along microtubules to their required site [91], a number of proteins are instead synthesized at distal sites as a mechanism to readily respond to local needs and adjust the local proteome accordingly [108, 109]. As illustrated in **Figure 1-2**, local translation is particularly concentrated at sites of synaptic activity. Local translation contributes to modulating the makeup, number, and/or distribution of important neuronal proteins, including those critical to synaptic function [110-114]. This method of on-site regulated protein synthesis allows for synapses to quickly and appropriately adapt their local proteomes in response to changes in frequency of synaptic signaling. As such, a wide range of neurological disorders are associated with dysregulation of RNA binding proteins implicated in local translation, including Fragile X syndrome, autism spectrum disorders, epilepsy, and neurodegenerative diseases [73, 115, 116].

Regulation of translation by RNA binding proteins can occur at one or multiple steps of translation, including initiation, elongation, and termination. Due to the long distances which mRNAs must be transported before local translation occurs, preventing premature initiation of translation is of particular importance and could be considered a rate-limiting step in protein synthesis. Within the family of eukaryotic initiation factors (eIFs), a subset are RNA binding proteins that interact with the 5’ mRNA cap and initiate translation by recruiting translational machinery to the start site [117]. Additional RNA binding proteins such as HuD [118], PABP [119], and PAIP1 [120] promote translation through direct interactions with eIFs. RNA binding proteins that have been implicated in repressing translation initiation often interact or compete with eukaryotic initiation factors. Such proteins include FMRP [39], Gemin5 [121], and Msi1

[122]. Once translation is initiated, specific RNA binding proteins regulate translation elongation either positively such as HuR [123], which is also suggested to promote translation initiation, or negatively (FMRP [124], UPF1 [125]). Repression of elongation in these examples is often associated with polyribosome stalling. In fact, an alternative model to transporting translation-uninitiated mRNAs has been proposed where mRNAs are instead transported in a translationally paused conformation with incomplete proteins, to later reinitiate and complete protein synthesis [126]. This could support a model where RNA binding proteins contribute to priming paused mRNAs/polyribosomes to provide more immediate production of required proteins in neuronal compartments, including synapses. Finally, several RNA binding proteins are associated with promoting (PABP [127]) or inhibiting (PAIP1 [128], PAIP2 [128], UPF1 [129]) translation termination, especially through interactions with the poly(A) tail and/or eukaryotic release factors (eRFs). Much more needs to be uncovered regarding the effect of specific RNA binding proteins on translation, particularly local translation in neurons, but these questions are challenging to address due to experimental limitations on inhibiting local translation for an extended period of time *in vivo*. However, neuronal function depends on precise temporal and spatial translational control in comparison to other tissue types, particularly due to local translation. This could potentially provide an explanation as to why neurons are more susceptible to tissue-specific disorders that result from mutations in genes encoding ubiquitous RNA binding proteins, as numerous RNA binding proteins have roles that directly or indirectly impact translation.

1.3 Dendritic Spines are a Spatiotemporally Dynamic Morphological Feature of Neurons

Local translation in neurons takes place in various compartments within the neurites, but is particularly associated functionally with structures produced along dendrites known as dendritic spines [108]. Dendritic spines constitute the postsynaptic component of excitatory synapses, partnered with presynaptic axon terminals. Dendritic spines are generated once developed neurons begin initiating interneuronal contact to establish synapses during a process called synaptogenesis [130]. Postsynaptic neurons project long finger-like extensions known as filopodia from the base of the dendritic shaft in search of a presynaptic contact. If contact is established, the filopodia retracts back towards the dendritic shaft while maintaining its presynaptic contact and has the potential to mature into a full dendritic spine, depending on synaptic input. If there is sufficient stimulation, a dendritic spine is produced and can act as the postsynaptic site of interneuronal signaling. The spine then relays excitatory signaling for the postsynaptic neuron to integrate amongst a collection of additional excitatory and inhibitory signals.

Although dendritic spines are the potential final product produced from immature filopodia, generation of dendritic spines does not produce morphologically static structures. Remaining structurally plastic is critical for dendritic spines to efficiently adapt to ever-changing synaptic activity. Individual spines continue to remodel their cytoskeleton in response to synaptic input, by growing or shrinking in a manner that allows them to respond to an increase or reduction in synaptic stimulation [131-133]. As shown in **Figure 1-3**, morphologically the classic example of a dendritic spine consists of a distinct “head” atop a thin neck that forms the base and connects to the dendritic shaft. The dynamic cytoskeleton allows for a wider range in morphology though, and can present as the classical structure described above, as well as

potentially lacking a distinct head or a noticeable neck [134]. In terms of individual dendritic spines, “stubby”, “thin”, and “mushroom” shaped dendritic spines are used as general morphological classifications within the research field, even though the physical parameters are not fully standardized [135-137]. While not standardized, individual spines can be classified as stubby, thin, or mushroom-shaped based off of two criteria: the length of the spine and the ratio between the width of the head and the neck [138]. It is also very important to note that these categories are assigned as single snapshots of individual dendritic spines. The inherently plastic morphology of dendritic spines allows single spines to switch between morphological categories. The development of live imaging techniques has allowed for more in-depth studies of these morphological dynamics [139], which has been essential in understanding pathways integral to dendritic spine function such as spine formation, maturation, stability, and elimination, as well as distinguishing differential impairment of these processes in different models of neuronal impairment.

These qualitative morphological categories can be used as a basic visual indicator of spine maturity/synaptic strength. In addition, dendritic spines play a key role in learning/memory in the brain [140-143], with different spine types potentially playing distinct roles in learning/memory [144]. Stubby spines are generally quite short and lack a clear distinctive head and neck. Of the three morphology types stubby spines are thought of as the most immature. This degree of morphological immaturity could be interpreted as the stubby spine being captured while receiving a low level of synaptic input or as the result of a loss of stimulation. Thin spines are characterized as being long enough to possess a discernable neck but do not exhibit a clear distinction between the spine head and neck. Thin spines are considered highly plastic in their morphology and possess the highest potential for synaptic strengthening or weakening as their

structure acts as a sort of “midpoint”. This heightened capacity for synaptic responsiveness has led thin type spines to be termed colloquially as “learning” spines [144]. Mushroom spines are similar to thin spines in average spine length, but are instead defined by a clear distinction between the head and neck. The size of the spine head is generally correlated with the strength of the synapse, with larger mushroom spines approaching a potential upper limit on additional synapse size/strength. Due to their structural stability and synaptic strength, mushroom spines are known colloquially as “memory” spines [144]. However, while major advances in characterizing the role of dendritic spines and their components in both learning/memory and higher order brain function have been made in recent years [145-147], the exact way in which dendritic spines facilitate these processes as well as the underlying biochemical mechanisms remain a major area of investigation.

The dynamic nature of dendritic spines is even more evident when considering brain-wide phases of spine regulation that occur over the course of developmental and life stages. In addition to the dynamics of individual dendritic spines, **Figure 1-4** shows the three overarching phases of spine regulation: spinogenesis, spine pruning, and spine maintenance [148]. These three phases are characterized by the respective balance between spine formation and elimination. The spinogenesis phase generates a net abundance of dendritic spines, starting *in utero* and continuing until adolescence [149, 150]. At adolescence, the brain enters the spine pruning phase, in which an increase in spine elimination creates a net reduction in spine density that lasts until adulthood [151, 152]. After the spine pruning phase, the brain enters the spine maintenance phase in which an equilibrium is reached between spine formation and elimination, maintaining the overall spine density [152]. Outside of these programmed phases of spine formation/elimination, normal aging may also affect spine density and morphology [153].

Importantly, individual dendritic spines are continuously undergoing the morphological fluctuations described earlier throughout spinogenesis, spine pruning, and spine maintenance. These brain-wide phases are an additional level of spine regulation that affect overall spine density as well as the distribution and proportion of specific types of spines throughout brain development [140, 148, 154]. Overall, accounting for both the dynamics of individual spines and spatiotemporal characteristics generates a gigantic range of unique dendritic spine landscapes. These considerations are essential when characterizing the role of dendritic spines in enabling proper neuronal function and defining the underlying molecular mechanisms.

1.4 Dendritic Spine Function and Structure is Dependent on Components of the Post-Synaptic Density

To better understand the importance of dendritic spines in regulating neuronal function, it is essential to not only investigate their morphological characteristics, but also the inner molecular and proteomic composition that underlie such morphological restructuring. The cytoskeleton of filopodia and dendritic spines is enriched for F-actin, the polymerized filamentous form of actin [155]. F-actin provides the cytoskeletal scaffolding within filopodia and spines and serves as the base from which all morphological changes in these dendritic protrusions originate. Depending upon positive or negative changes in synaptic input, F-actin destabilizes and allows for restructuring of the cytoskeleton to either grow or shrink, especially in spine heads [147]. In addition to stabilizing the cytoskeleton, F-actin also stabilizes the composition of the postsynaptic density (PSD), which is an extensive structured proteomic matrix located along the synaptic contact zone within the spine head. The PSD organizes the arrangement and density of components necessary for synaptic function and plasticity, including

receptors, channels, structural proteins, and signaling molecules [156]. Therefore, the ability to effectively modulate the size and composition of the PSD in response to synaptic activity is essential for dendritic spines to accurately receive, integrate, and relay synaptic input. F-actin associates with components of the PSD [157, 158], which allows the PSD to restructure components while F-actin is destabilized. This association between the PSD and F-actin contributes to the general maturity of a dendritic spine and can be loosely implied from spine morphology, with spine size generally correlated with the size of the PSD and increased synaptic strength [159]. However, it is important to stress that this inference is not consistent amongst all dendritic spines [160], so conclusions on the actual maturity of a dendritic spine as well as its molecular composition, internal biochemical activity, or degree of synaptic activity cannot be drawn based on this type of qualitative inference alone.

There are numerous proteins critical to ensure the proper function of dendritic spines and the PSD, but for the purposes of this thesis significant focus will be placed on Calcium(Ca^{2+})/calmodulin(CaM)-dependent protein kinase II (CaMKII). While the CaMKII protein is detected in a wide range of tissues, *CaMKII* mRNA contains a 30nt DTE sequence in the 3'UTR, emphasizing the importance of its presence in neuronal dendrites [80, 161]. CaMKII is an evolutionarily conserved serine/threonine-specific phosphokinase within the CaM-kinase family that affects both dendritic spine morphology and function. CaMKII is a large holoenzyme consisting of 12 subunits, arranged into two layered rings of six [162]. Each monomer possesses an N-terminal catalytic domain, a C-terminal association domain, and a regulatory domain which controls monomer activation status through either binding of Ca^{2+}/CaM to its binding site, or autophosphorylation [163]. Binding of Ca^{2+}/CaM results in a conformational change to that subunit that exposes the catalytic domain. The conformational change subsequently exposes the

regulatory domains of the neighboring subunits, allowing for additional subunit Ca^{2+}/CaM binding and/or autophosphorylation [164]. In addition, while not required for CaMKII activity, autophosphorylation of Thr286/287 produces a 1000-fold increase in affinity for Ca^{2+}/CaM, thus allowing CaMKII activity even when [Ca^{2+}] is low [165]. Coupled with this trait, CaMKII also detects changes in the frequency of fluctuating [Ca^{2+}] [166]. Even after dissociation of Ca^{2+}/CaM, phosphorylated CaMKII can still have kinase activity as Thr286/287 phosphorylation inhibits returning to the closed, inactive conformation. CaMKII activity is inhibited when dephosphorylated by a phosphatase [167], or if Thr305/306 becomes autophosphorylated [168]. Therefore, CaMKII is dependent upon binding Ca^{2+}/CaM to initiate activation, but also possesses phosphorylation-based autoregulatory measures that contribute to modulating its activity independent of Ca^{2+} activity.

CaMKII is associated with synaptic plasticity in neurons, particularly long-term potentiation (LTP) induction in which a long-lasting increase in strength of a single synapse, which can last up to over a month [169], is generated from a brief period of synaptic activity. LTP induction creates an influx of Ca^{2+}, thereby activating CaMKII within seconds following synaptic stimulation. CaMKII activation is compartmentalized to just the stimulated spine and does not extend to additional spines or the dendritic shaft [170]. CaMKII subsequently promotes potentiation through binding and phosphorylating NMDA- and AMPA-type glutamate receptors and subunits [162, 171]. In addition to modulating the strength of existing synapses, CaMKII is also implicated in promoting filopodia growth and spine formation in rat hippocampal slices [172]. While enzymatic activation within dendritic spines may take place over a short period of time, the effects can be long-lasting due to the autoregulation of CaMKII. The possibility to sustain CaMKII activity through autophosphorylation even after synaptic activity concludes has

been proposed to be a mode of "molecular memory" within dendritic spines [171, 173]. Consistent with this idea, CaMKII is also strongly associated with learning/memory, which is affected when LTP is impaired. Numerous CaMKII mutant models have been generated that exhibit impaired LTP and/or learning and memory [174-178]. Consistent with this critical role in LTP, dysregulation of CaMKII is associated with a number of neurological disorders, including mouse models of Fragile X syndrome [179], Angelman syndrome [180], Alzheimer's disease [181], schizophrenia [182], epilepsy [183], and Down syndrome [184].

Mammalian CaMKII protein is expressed as four isoforms (α, β, γ, δ), each encoded by a separate gene [185]. All four protein isoforms have the same overall structure, with only minor differences [186]. However, each isoform displays different properties with respect to subcellular localization, Ca^{2+}/CaM kinetics, rate of autophosphorylation, and protein binding [186, 187]. While CaMKII holoenzymes can be composed of homomeric subunits, an even wider range of variability is introduced with heteromeric CaMKII holoenzymes [188]. This heterogeneity introduces a level of complexity that is largely undefined with regard to the range of potential structural conformations and functions of CaMKII. Therefore, most research devoted to CaMKII function in different cells/tissues has been directed towards either the total holoenzyme population, or the role of specific isoforms. Steady-state mRNA and protein levels of these CaMKII isoforms vary between tissues, but CaMKIIα and CaMKIIβ are almost exclusively expressed in neuronal tissue, making up ~1% of total brain protein and up to 2% of total hippocampal protein [189]. CaMKIIγ and CaMKIIδ are less prevalent in neuronal tissue, but display an overall more ubiquitous pattern across tissues [185, 190]. Importantly, deletion of CaMKIIα and CaMKIIβ together causes lethality in mice, both as a germline deletion and as an induced deletion in adults [191]. This suggests the combined expression and activity of

CaMKIIα and CaMKIIβ is essential to neuronal function, both during and after brain development. Furthermore, these findings demonstrate that while CaMKIIα and CaMKIIβ have a high degree of homology to other CaMKII isoforms, they have non-redundant roles in neurons.

While studies are ongoing, CaMKIIα is the most characterized isoform in relation to learning and memory. Experimental findings describing how CaMKIIα impacts LTP, learning, and memory are variable, largely depending on the exact way CaMKIIα expression was manipulated as well the brain region and point in development investigated [175-178, 192, 193]. Among these findings, loss of CaMKIIα significantly impairs working memory [194]. In addition, CaMKIIα is implicated in modulating dendritic spine volume, where loss of CaMKIIα activity is associated with impairing dendritic spine enlargement [193] and accumulation of postsynaptic CaMKIIα is associated with an increase in spine volume [195, 196]. Although CaMKIIβ is less characterized, there is also an association between CaMKIIβ and LTP, learning, and memory [197, 198]. Unlike CaMKIIα, CaMKIIβ contains an F-actin binding domain and is thus proposed to play a structural role in regulating dendritic spine morphology [157]. As shown in **Figure 1-5**, inactive CaMKIIβ binds and stabilizes F-actin [199]. Influx of Ca^{2+} into the spine via synaptic stimulation activates CaMKII, thereby triggering dissociation from F-actin. While unbound, F-actin can restructure and allow for morphological change. The cytoskeleton restabilizes once F-actin is rebound by inactive CaMKIIβ. The association between CaMKIIβ and F-actin also allows CaMKIIα to be localized to the cytoskeleton and PSD components via CaMKII heteromeric holoenzymes [200]. In summary, the current model suggests that CaMKIIα and CaMKIIβ serve distinct functions within dendritic spines, but they are also able to influence the function of one another and ultimately act cooperatively to achieve proper control of LTP,

learning, and memory through the activation of dendritic spine proteins and contributing to the modulation of spine morphology.

1.5 Spine Dynamics in Neuronal Disorders

The hippocampus is canonically known as the central hub for learning and memory consolidation in the brain [201-203]. In animals with lower cognition, the hippocampus serves a critical role for survival by converting short-term memory into long-term memory to access information critical to assess the safety/danger of an event or situation. In humans, hippocampal damage can impair working, short-term, and long-term memory [204-208] as well as learning [208-210]. Furthermore, numerous neurological disorders are associated with hippocampal abnormalities/impairment in patients and/or mouse models, including Fragile X syndrome [211, 212], Alzheimer's disease [213, 214], autism spectrum disorder [215, 216], epilepsy [217, 218], schizophrenia [219, 220], and Down syndrome [221, 222].

The hippocampus is composed of distinct subregions, including the dentate gyrus (DG) and the cornu ammonis (CA) subfields (CA1, CA2, CA3, and CA4). Of the various hippocampal subregions, the DG, CA3, and CA1 are the regions primarily studied in learning/memory, as well as hippocampal synaptic plasticity [223-226]. A tremendous degree of signaling interconnectivity exists between these subregions, but a highly simplistic model would be as follows: DG granule cells receive incoming signals from the entorhinal cortex (EC) (an adjacent structure to the hippocampus), the DG stimulates CA3 neurons, CA3 stimulates CA1, and CA1 completes the circuit through stimulation of the EC again [226]. Due to the high level of interconnectivity, it is inaccurate to definitively assign a specific type of learning/memory to a single hippocampal subregion, but studies have provided general associations between specific

subregions and learning/memory characteristics. Various hypotheses have been proposed regarding the contribution of different subregions to learning/memory, but suggested roles describe the DG as a preprocessor and enforcer of signaling relayed to CA3 [224], the CA3 region as the core of rapid memory/association storage, and the CA1 region detects mismatching signals in the input and output between the hippocampus and EC [227]. In addition, neurological disorders that affect the hippocampus commonly display heterogeneous phenotypes in specific subregions rather than evenly throughout the whole hippocampus [228-234]. Thus, investigations into the potential role of the hippocampus in neurological disorders should take into consideration the possible heterogeneous contributions of different hippocampal subregions.

A common neuronal abnormality that occurs in a wide range of neurological disorders is aberrant dendritic spine morphology. As depicted in **Figure 1-6**, defects including altered spine density, length, head size, and head-to-neck ratio are independent parameters that may or may not change, depending on the neurological disorder [235]. For example, spine density is characteristically decreased in both Angelman syndrome [236] and Down syndrome [237], but head size is significantly increased in hippocampal spines examined in a mouse model of Down syndrome [238]. In contrast, there is high variability in hippocampal spine length and head size in a mouse model of Angelman syndrome [239]. Consequently, differences in spine morphology and density can disrupt the typical ratio between filopodia, stubby-, thin-, and mushroom-type spines. Importantly, such changes in dendritic spine morphology and density are not necessarily detected ubiquitously throughout the brain. For example, spine density in Fragile X mice is rather irregular with respect to brain region, with various regions displaying an increase, decrease, or no change in density [240]. However, the hallmark morphological phenotype in Fragile X neurons is the presence of consistently longer and thinner dendritic spines [241], which

has been largely characterized in regions of the forebrain [240], including the DG [242] and CA1 [243] regions of the hippocampus in mouse models. These spines more closely resemble filopodia and thus have been described as more immature. These observations support a model where FMRP may be required for proper spine maturation [212]. Surprisingly, this hallmark morphology is not observed in the CA3 region of the hippocampus [244], suggesting that FMRP may play a region-specific role within the hippocampus. The explanation for this distinction remains unclear, though this finding is of particular significance as this provides an example of how loss of a critical ubiquitous RNA-binding protein may selectively alter neuron-specific features.

In addition to spatial considerations, temporal regulation is another parameter to account for when investigating dendritic spine dysregulation in neurological disorders. The presence of specific dendritic spine abnormalities can depend on the stage of brain development [235]. Studies of spine morphology, but particularly spine density, over the course of brain development are often compared across spinogenesis, spine pruning, and spine maintenance phases of spine regulation. For example, studies measuring spine density in Fragile X mice (Layer 5 pyramidal neurons in the primary somatosensory cortex) have suggested that spine density is elevated at postnatal day 7 (P7), with no change detected at P14 or P28, then elevated density again at 7 weeks old [240, 245, 246]. In contrast, dendritic spine density in the hippocampal DG of Fragile X mice was found to increase with age between P14-60 without evidence of a defined spine pruning phase [242]. Altered spine density specifically in the spinogenesis, pruning, or maintenance phase(s) may indicate specific impairment in either spine formation or turnover, since each phase is distinguished by distinct ratios of spine formation/elimination. This topic is still being investigated, particularly as more studies of

dendritic spine dynamics are conducted with *in vivo* live-cell imaging. Overall, characterizing what specific alterations occur to dendritic spine morphology/density, the affected regions of the brain, and when they occur together further our comprehension as to how an individual cellular component implicated in neurological disorder results in dysregulated neuronal function. These studies and finding also contribute to further understanding how underlying neuronal-specific biological processes manifest phenotypically as distinct types of neuronal dysfunction.

1.6 ZC3H14 Function in Neurons

Human ZC3H14 (Zinc finger CysCysCysHis domain-containing protein 14) is a member of an evolutionarily conserved polyadenosine (poly(A)) RNA binding protein [247, 248]. Despite ubiquitous expression [249], mutations in *ZC3H14* are associated with a form of nonsyndromic autosomal recessive intellectual disability in humans [250]. This adds ZC3H14 to a growing list of RNA-binding proteins that are altered in tissue-specific disorders. The primary characterized ZC3H14 orthologue at the time of this association was nuclear polyadenylated RNA-binding 2 (Nab2) in *S. cerevisiae* [251], with very little known about the function of ZC3H14 and orthologues in multicellular model systems, let alone the role of ZC3H14 in mammals. The following section describes the research that has characterized orthologues of ZC3H14, leading up to the start of this thesis in characterizing ZC3H14 in mice and its role in neurons to specifically maintain higher order brain function.

ZC3H14 as well as its orthologues in *S. cerevisiae* (nuclear polyadenylated RNA-binding 2, Nab2) [251], *D. melanogaster* (Nab2) [247], and *C. elegans* (suppressor of tau-2, SUT-2) directly bind poly(A) tracts of RNA through a functionally conserved C-terminal tandem CysCysCysHis (CCCH) Zinc Finger (ZnF) domain [252]. This tandem ZnF domain is essential

and sufficient for poly(A) RNA binding [248, 253]. As shown in **Figure 1-7**, the RNA-binding domain of ZC3H14 is composed of repeating CCCH ZnFs. While highly conserved, some ZC3H14 orthologues have varying numbers of repeats or difference in spacing between repeats [253, 254]. For example, *D. melanogaster* Nab2, SUT-2, and ZC3H14 each contain five CCCH repeats, while *S. cerevisiae* Nab2 consists of seven. In budding yeast, binding of poly(A) RNA by Nab2 is mediated primarily through ZnF 5-7, as deletion of these three zinc fingers reduces the interaction between Nab2 and poly(A) RNA by 90% [253]. Nab2 ZnF 5-7 are structurally homologous to ZnF 1-3 in ZC3H14, which may suggest the vast majority of ZC3H14-poly(A) RNA interactions occur through the first three zinc fingers. ZC3H14 and the ZC3H14 orthologues also possess an N-terminal Proline-Tryptophan-Isoleucine (PWI)-like domain, which is necessary for efficient poly(A) RNA export from the nucleus in budding yeast [255]. This PWI-like domain is implicated in protein-protein interactions, particularly in mediating interactions with the nuclear pore [256]. There is also a predicted nuclear targeting signal, which is an arginine-glycine-glycine (RGG) motif in budding yeast, and a classical nuclear localization signal (cNLS) in flies, worms, mice, and humans.

As ZC3H14 has affinity for polyadenosine RNA [248, 252], models suggest ZC3H14 and RNA interactions may be mediated though the 3’ poly(A) tail added to mRNA. Poly(A) RNA binding proteins impact RNA regulation at various stages of RNA processing, including transcript polyadenylation [53, 257], translation [119, 258], splicing [56], stability [259, 260], and nuclear export [261, 262]. ZC3H14 has a conserved role in regulating poly(A) tail length, with loss resulting in longer bulk poly(A) tails [247, 263, 264]. There are currently two main non-mutually exclusive mechanisms proposed for how ZC3H14 may naturally restrict poly(A) tail length: a polyadenylation limiting model postulates that ZC3H14 restricts activity of poly(A)

polymerase, while a poly(A) trimming model suggests ZC3H14 promotes ribonuclease activity to trim poly(A) tails back to an appropriate length [265]. Polyadenylation is a required step for mRNA nuclear export, therefore dysregulation in poly(A) tail length could impact nuclear export [266]. Altered poly(A) tail length is also associated with defects in translation [267-269] and altered RNA stability [270, 271]. In fact, extension of poly(A) tail length is induced in a subpopulation of *CaMKIIα* mRNA present in rat visual cortices following visual experience, which is accompanied by an increase in CaMKIIα protein in synaptosomes [272].

The binding affinity for poly(A) tracts implies ZC3H14 could interact with virtually all polyadenylated RNAs. However, there is growing evidence to suggest that ZC3H14 may regulate target RNAs. Analysis of the co-crystal structure of three ZnFs of *C. thermophilum* Nab2 bound to an A8 chain of RNA revealed an adenosine binding pattern of AAXAAXXA or AAXAXXAA, which allows flexibility in direct RNA sequence beyond a simple tract of As [273]. A separate study using a genome-wide RNA-IP in budding yeast shows Nab2 binds to RNAs with a consensus A-rich 12nt sequence ($A_{11}G$) [274]. Identifying transcriptome-wide targets of Nab2-containing mRNPs revealed enrichment for mRNAs that encode translational proteins [275]. Identifying whether there are specific RNA targets of mammalian ZC3H14, especially transcripts unique to brain tissue, may provide additional rationale as to how ZC3H14 loss results specifically in higher order brain dysfunction.

The majority of previous studies have focused on analysis of Nab2 using *S. cerevisiae* and *D. melanogaster* model systems. While appropriate to use less complex systems to investigate foundational cellular roles of an evolutionarily conserved protein, it is essential to account for potential differences in gene expression when investigating potential conserved or unique functions of ZC3H14 in more complex organisms such as mammals. As depicted in

Figure 1-7, Nab2 and SUT-2 are expressed as a single isoform. ZC3H14 in mice and humans is expressed from a single gene as at least four distinct isoforms generated by alternative splicing [249], shown in **Figure 1-8**. Isoforms 1, 2, and 3 contain all three domains mentioned above, with isoform 1 encoding the full-length 17 exon transcript, while isoform 2 skips exons 11-12 and isoform 3 skips exons 10-12. Isoform 4 contains the RNA-binding domain, yet is distinguished by lack of the N-terminal PWI-like domain and cNLS, instead encoding an alternative first exon spliced to exon 10, and skipping exons 11-12. The presence of multiple protein isoforms may confer redundancy, or possibly isoform-specific functionality, which could contribute to the heightened degree of precise/complex RNA regulation required in higher-order systems.

The initial studies linking the ZC3H14 gene to intellectual disability was through classical genetic studies. A large-scale homozygosity mapping study was performed in 2011 with a cohort of >200 consanguineous Iranian families to identify autosomal recessive mutations associated with intellectual disability [250]. Intellectual disability was assessed through administration of an IQ test in which a score <70 indicated moderate and <50 severe intellectual disability. Two independent families were identified that showed nonsyndromic autosomal recessive intellectual disability associated with homozygous inheritance of mutations in the *ZC3H14* gene. One family has three affected males with IQ ~50 linked to inheritance of a *ZC3H14* homozygous nonsense mutation (R154X) located in exon 6, as shown in **Figure 1-9**. This mutation introduces a premature stop codon and thus eliminates expression of isoforms 1, 2, and 3, with isoform 4 intact [247]. The second family has three affected males with IQ ~35 linked to an inherited *ZC3H14* homozygous 25bp deletion, located in the intronic sequence between exons 16-17. This mutation affects all four isoforms and disrupts expression of the last

amino acid [247]. While the functional effect of this deletion has not been characterized as extensively as the nonsense mutation, intronic mutations may interfere with proper ZC3H14 protein expression through disrupted RNA splicing such as exon skipping or intron retention. It is extremely difficult to determine from just two affected families, but one hypothesis that may address an observed difference in intellectual disability severity between these two families could potentially be related to the contrast in number of ZC3H14 isoforms affected/left intact by each mutation. Unfortunately, experiments have not been performed to distinguish whether there are unique cellular and functional consequences of these different mutations. Even without fully defining the functional differences between the mutations present in these two families, this association study presents two major implications regarding ZC3H14. First, while Nab2 is essential for viability in yeast [251] and flies [264], ZC3H14 is not essential for viability in humans. Second, the association of *ZC3H14* mutations with nonsyndromic intellectual disability adds ZC3H14 to the growing list of ubiquitous RNA-binding proteins associated with tissue-specific disorders in humans. Therefore, it is critical to investigate the function of ZC3H14 in the brain.

As ZC3H14 is a ubiquitously expressed protein [249], it is important to examine its expression in the brain. The *ZC3H14* transcript is expressed in both adult and fetal tissue [247], suggesting ZC3H14 may play a role during and after human early brain development. Furthermore, immunohistochemical staining of post-mortem Alzheimer's disease patients shows a decrease in overall ZC3H14 (termed MSUT2 in this study) in the hippocampus [276]. Immunofluorescent staining of ZC3H14 protein in the brain, specifically in adult mouse hippocampus indicates that ZC3H14 is enriched in hippocampal neurons, including the DG, CA1, and CA3 regions, as compared to glia [247]. This indicates ZC3H14 likely could play a

role in neurons. Investigations in *C. elegans* also suggest neuron-specific function, where loss of SUT-2 function suppresses neurodegenerative changes in a tauopathy model [254] and SUT-2 overexpression enhances tau-induced neuronal dysfunction [276]. To further emphasize the importance in neurons, Nab2 in flies is essential for viability [264], and neuron-specific expression of Nab2 in null flies is sufficient to rescue viability to 93% [264]. Additionally, neuron-specific expression of human ZC3H14 isoform 1 in Nab2-null flies also rescues viability [264], implying a high degree of functional conservation between Nab2 and ZC3H14 isoform 1.

Within the 3% Nab2-null surviving adult flies, which are hypothesized to escape death via maternally-deposited Nab2 in the oocyte, the brain demonstrates severe highly penetrant morphological defects, most notably in the morphology of the mushroom bodies [277]. The mushroom bodies are functionally analogous to the hippocampus and are required for learning/memory in the fly brain [278]. Together with this finding, a behavioral assay showed Nab2-null flies have intact learning but are impaired in short-term memory [277]. Overall, the role of ZC3H14 should be investigated throughout the brain, but the data compiled from immunofluorescence, brain morphology, behavioral impairment, and link to intellectual disability suggests ZC3H14 has a key role in specific regions of the brain, especially the hippocampus.

1.7 Summary and Prevailing Questions

ZC3H14 is a ubiquitous polyadenosine RNA binding protein that is lost in an autosomal recessive form of nonsyndromic intellectual disability. Prior to the work reported here, no studies of ZC3H14 had been performed in any vertebrate model. In this thesis, I describe the first vertebrate loss of function model of ZC3H14, which was developed to investigate the role of

ZC3H14 in higher order brain function. This novel *Zc3h14*$^{\Delta ex13/\Delta ex13}$ mouse model is used in Chapter 2 to assess functional and molecular consequences that occur with zygotic loss of ZC3H14, which models the case in patients. This characterization includes investigations of the viability of *Zc3h14*$^{\Delta ex13/\Delta ex13}$ mice, as well as gross brain size and morphology, learning/memory behavior, bulk poly(A) tail length, and an analysis of the hippocampal proteome. Chapter 3 exploits the *Zc3h14*$^{\Delta ex13/\Delta ex13}$ moue model to assess how loss of ZC3H14 impacts hippocampal neurons, both *in situ* and *in vitro*. Furthermore, I analyze the morphological and proteomic consequences that loss of ZC3H14 has for hippocampal dendritic spines, which are essential postsynaptic sites required for proper neuronal function and are commonly dysregulated in neurological disorders. Together, the results of this thesis suggest that ZC3H14 is necessary for higher order brain function due to a role in regulating critical RNA targets that maintain proper neuronal function. These findings suggest a working model for how loss of ZC3H14, a ubiquitous RNA-binding protein, may result in brain dysfunction. Finally, Chapter 4 discusses these findings as well as the implications of my work and future open areas of investigation.

Figures:

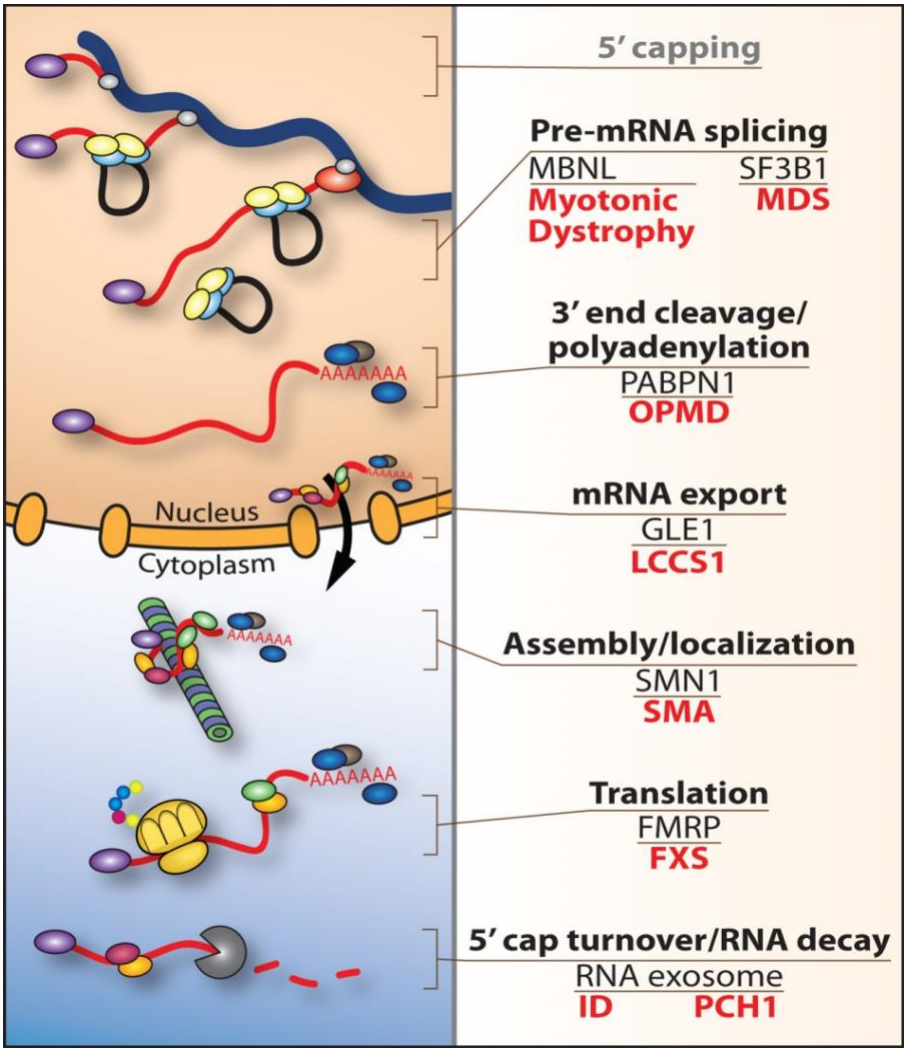

Figure 1-1: Steps of post-transcriptional RNA processing, with examples of dysregulated RNA binding proteins resulting in tissue specific disorders. A schematic (*left*) illustrating steps in post-transcriptional regulation of gene expression (*right*) is shown highlighting representative RNA binding proteins that are altered in disease. Processing of the mRNA (red) begins co-transcriptionally with the addition of an mRNA cap (5' capping), splicing to remove introns (Pre-mRNA splicing), and 3' end cleavage/polyadenylation. Specific RNA binding proteins associate with the mRNA to form an export-competent mRNA ribonucleoprotein (mRNP) complex that is exported through the nuclear pore to the cytoplasm (mRNA export). In

the cytoplasm, the mRNP can undergo remodeling but the RNA binding proteins assembled into the mRNA within the nucleus can also dictate the cytoplasmic fate of mRNA. The mRNA can undergo specific localization (Assembly/localization), can be translated (Translation), or can undergo regulated decay (5’ cap turnover/RNA decay). Here, a small subset of diseases that result from altered function of post-transcriptional regulators of gene expression is illustrated (*right*): Muscleblind (MBNL) is one alternative splicing factor sequestered in Myotonic Dystrophy type 1; SF3B1 is one of several splicing factors that is mutated in myelodysplastic syndrome (MDS), a cancer syndrome of the blood; the nuclear poly(A) RNA binding protein PABPN1 is altered in oculopharyngeal muscular dystrophy (OPMD); the mRNA export factor, GLE1 is altered in lethal congenital contracture syndrome 1 (LCCS1) causing loss of motor neurons; the mRNA chaperone protein SMN1 is lost in spinal muscular atrophy (SMA); a key regulator of translation, the fragile X mental retardation protein (FMRP) is lost in fragile X syndrome (FXS); and components of mRNA decay and processing including: the DCPS protein, which mediates turnover of the 5’ cap linked to an inherited form of intellectual disability (ID); and the RNA exosome, which mediates both RNA decay and precise RNA processing, has been linked to multiple diseases including pontocerebellar hypoplasia (PCH).

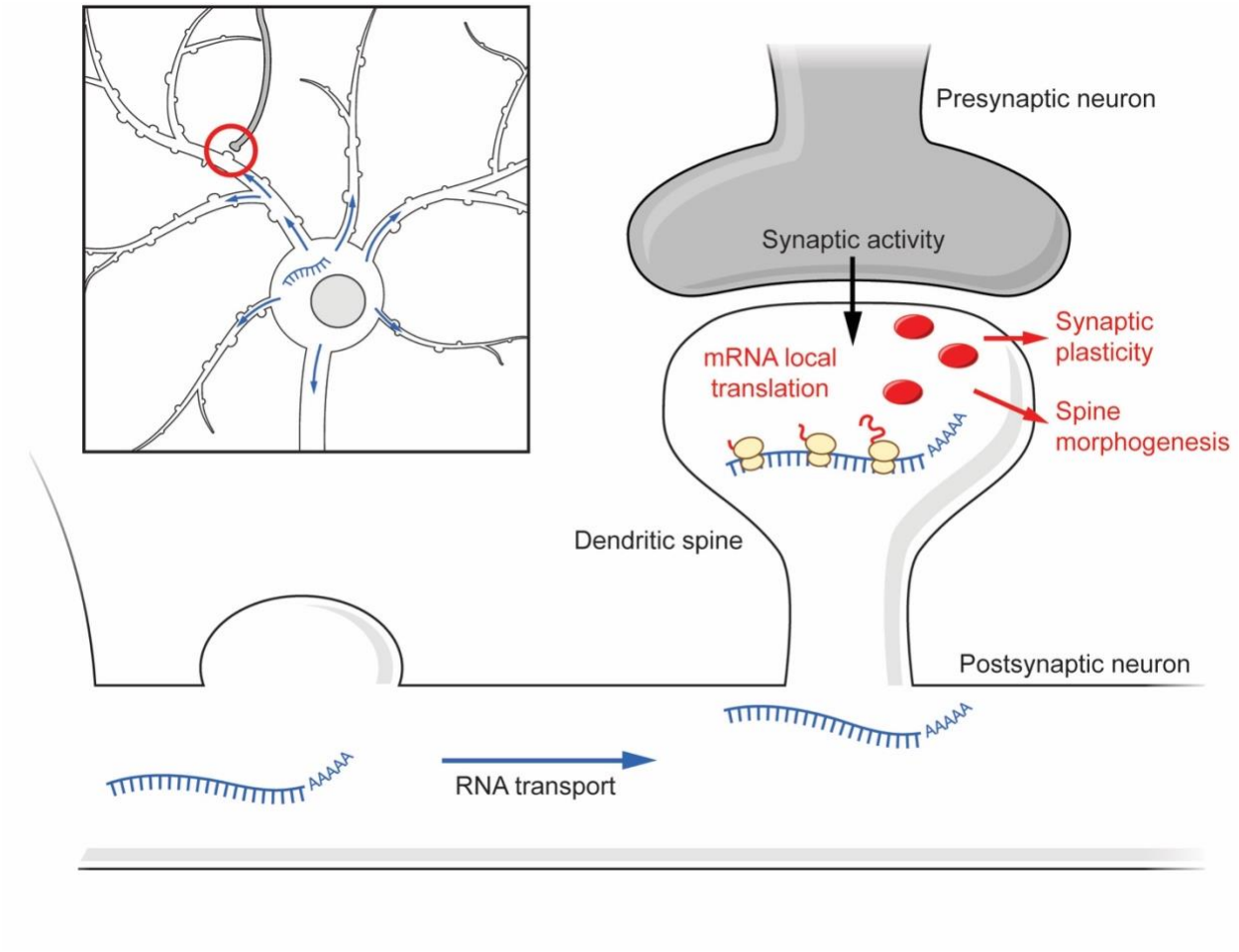

Figure 1-2: Dendritic spines serve as major postsynaptic sites of local translation. A representative neuron (*top left*) is shown covered with dendritic spines. After mRNA (blue) is exported into the cytoplasm, active mRNA transport (blue arrows) moves the transcript away from the soma along a neurite. The transported mRNA may localize to a dendritic spine; postsynaptic sites that arise from the dendritic shaft and respond to excitatory synaptic activity from a paired axon terminal. Synaptic activity may activate local translation of mRNA, and produce proteins (red) that can locally contribute to synaptic plasticity and spine morphogenesis. This figure is adapted from Medioni *et al.* (2012) [279].

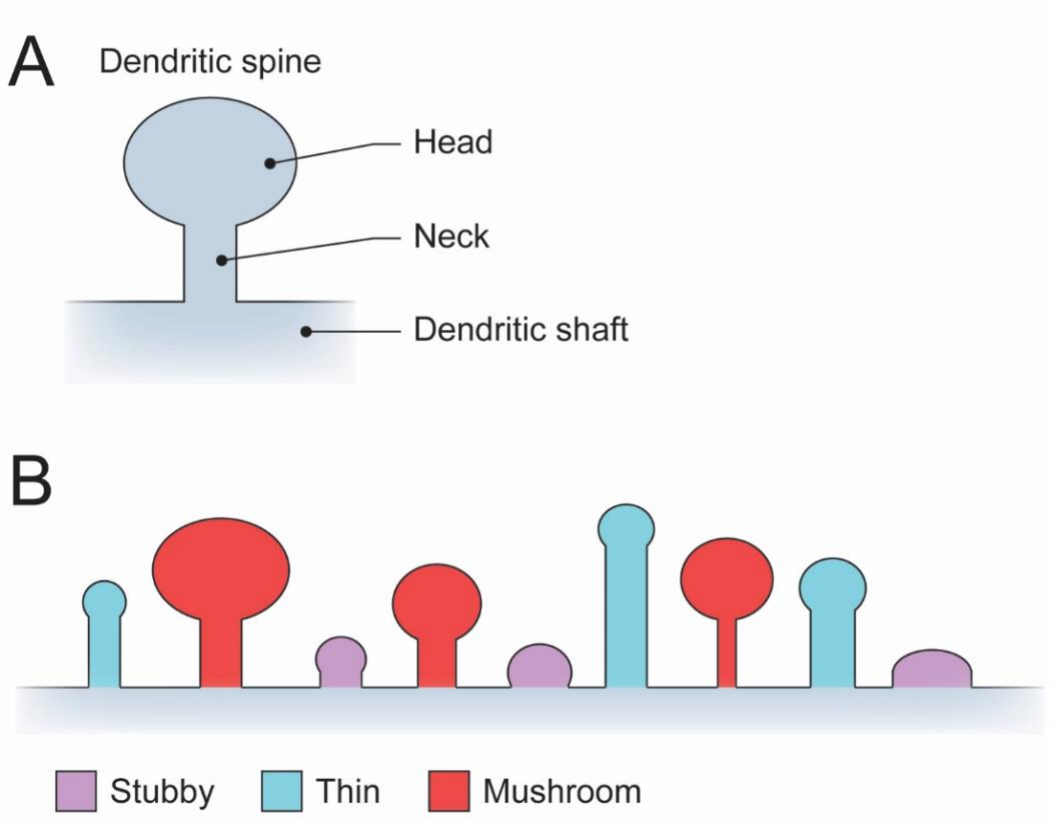

Figure 1-3: General schematic of different dendritic spine morphology classifications. A. A classic example of dendritic spine morphology, consisting of a distinct "head" atop a thin neck that connects to the dendritic shaft. B. A schematic of the range of morphologies available for dendritic spines due to structural plasticity. Single spines are morphologically categorized as stubby (purple), thin (blue), or mushroom (red) spines, typically based off of the length of the spine and the ratio between the width of the head and neck. This schematic does not represent real-life distribution of dendritic spine types, ratios, and differences in morphology occurring along a dendrite.

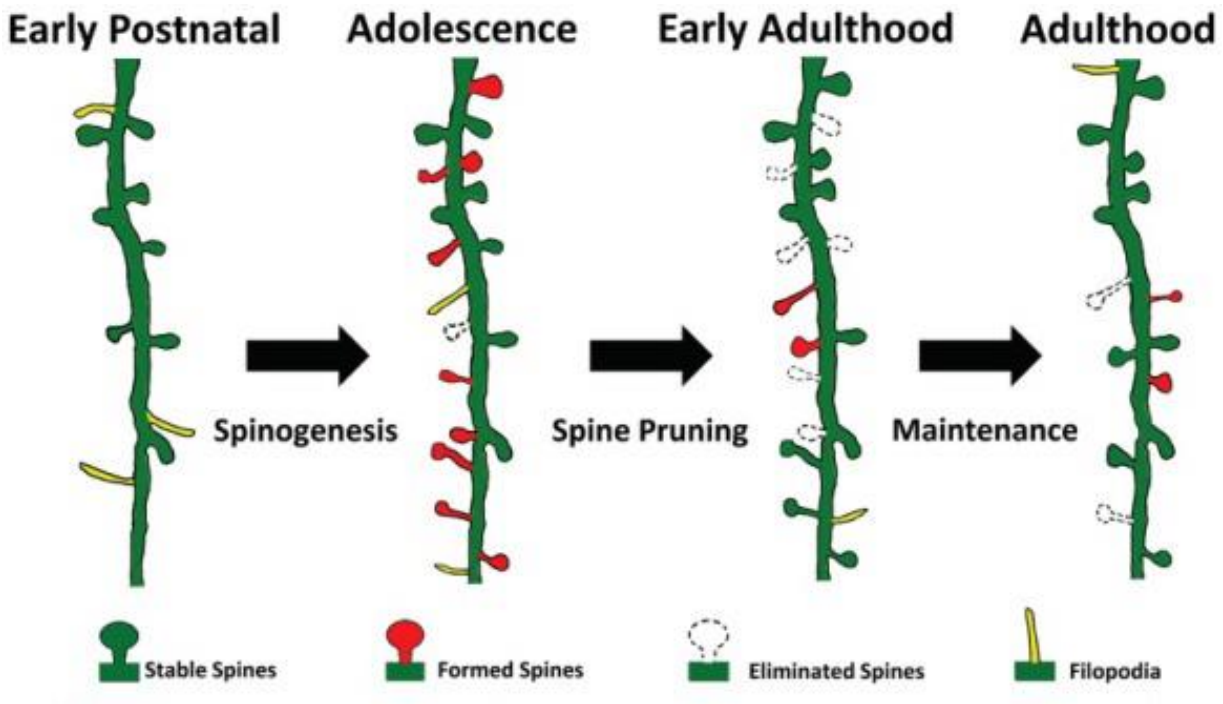

Figure 1-4: Schematic of the brain-wide phases that regulate dendritic spine density over the course of life in mammals. Distinct phases of spine density are characterized by the relative rate between spine formation/elimination. Spinogenesis starts in early postnatal development as a period of dendritic spine overproduction, creating a net abundance of dendritic spines that lasts until adolescence. Spine pruning increases spine elimination at adolescence into early adulthood, which results in an overall reduction in spine density. Spine maintenance reaches equilibrium between spine formation and elimination, thereby maintaining spine density throughout adulthood. This figure is adapted from Chen *et al.* (2014) [148].

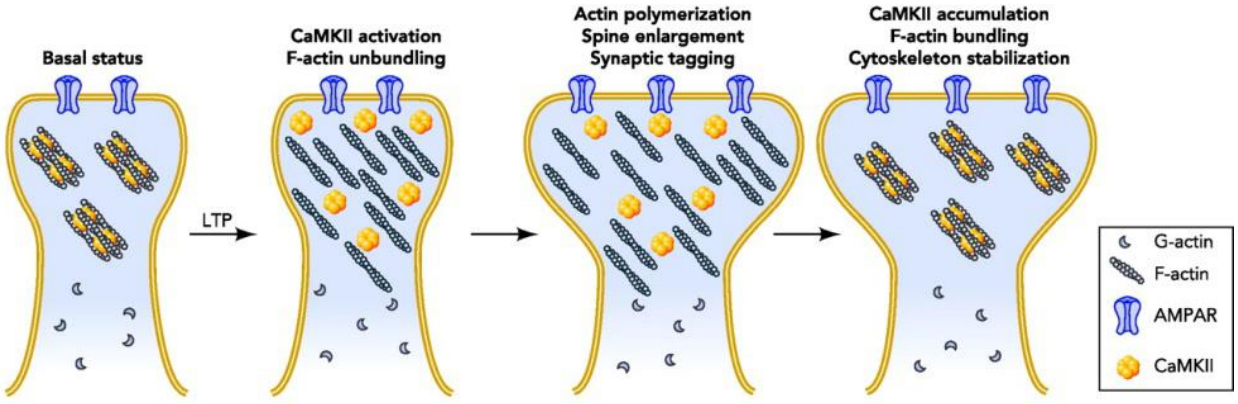

Figure 1-5: The role of CaMKII in cytoskeletal stabilization within dendritic spines. The cytoskeletal structure of dendritic spines is enriched for filamentous actin (F-actin). CaMKII is bound to bundled F-actin in the dendritic spine's basal state. Upon induction of long-term potentiation (LTP), CaMKII is activated and unbinds F-actin, allowing for unbundling and polymerization of globular actin (G-actin) to produce addition F-actin. During this period, the dendritic spine can expand and incorporate proteins into the postsynaptic membrane, such as the AMPA receptor (AMPAR), strengthening the synapse. The structural and proteomic changes in the dendritic spine are stabilized once inactive CaMKII binds/bundles F-actin again. This figure is adapted from Okamoto *et al*. (2009) [157].

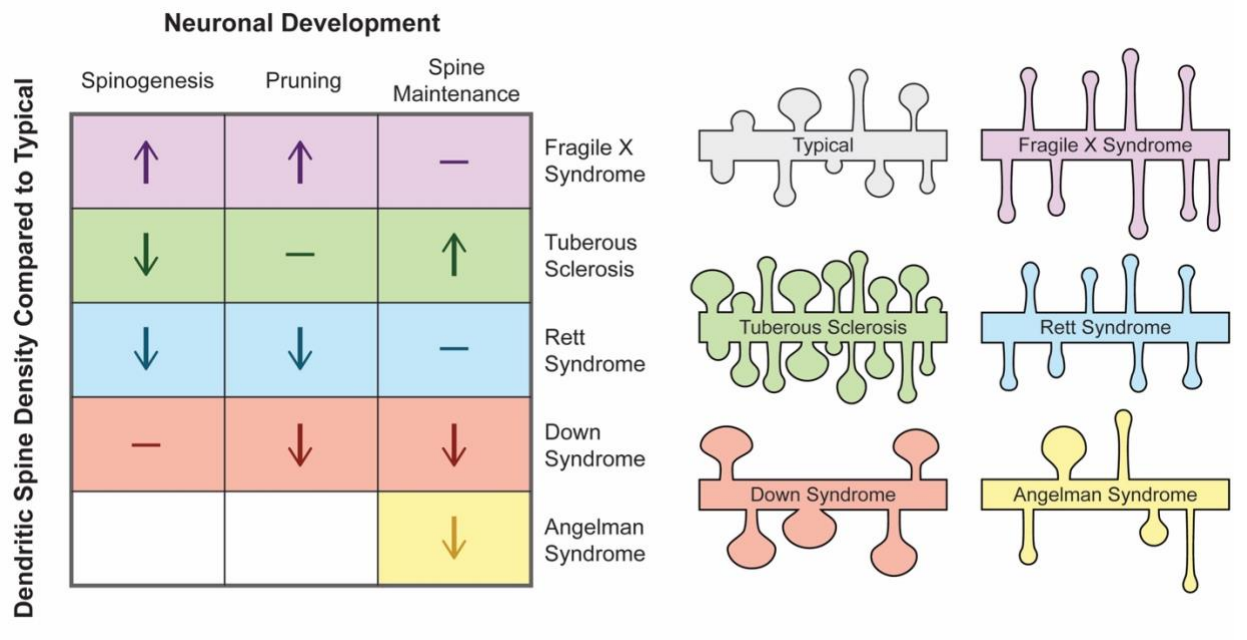

Figure 1-6: Changes in dendritic spine density, morphology, and proportion of spine types associated with various neurological disorders over the course of neuronal development. Dendritic spine density naturally changes over the course of spinogenesis, pruning, and spine maintenance phases of neuronal development. Dendritic spine density exhibited by various neurological disorders (Fragile X Syndrome (purple), Tuberous Sclerosis (green), Rett Syndrome (blue), Down Syndrome (red), and Angelman Syndrome (yellow)) can differ from typical (grey) spine density (arrows) or exhibit similar spine density during specific neuronal development phases (horizontal line) (*left*). White boxes indicate lack of data for a disorder during a specific phase of neuronal development. Changes in spine morphology, such as spine length, head size, and prevalence of spine type, are also unique to specific neurological disorders (*right*). This figure is adapted from Phillips & Pozzo-Miller (2015) [235].

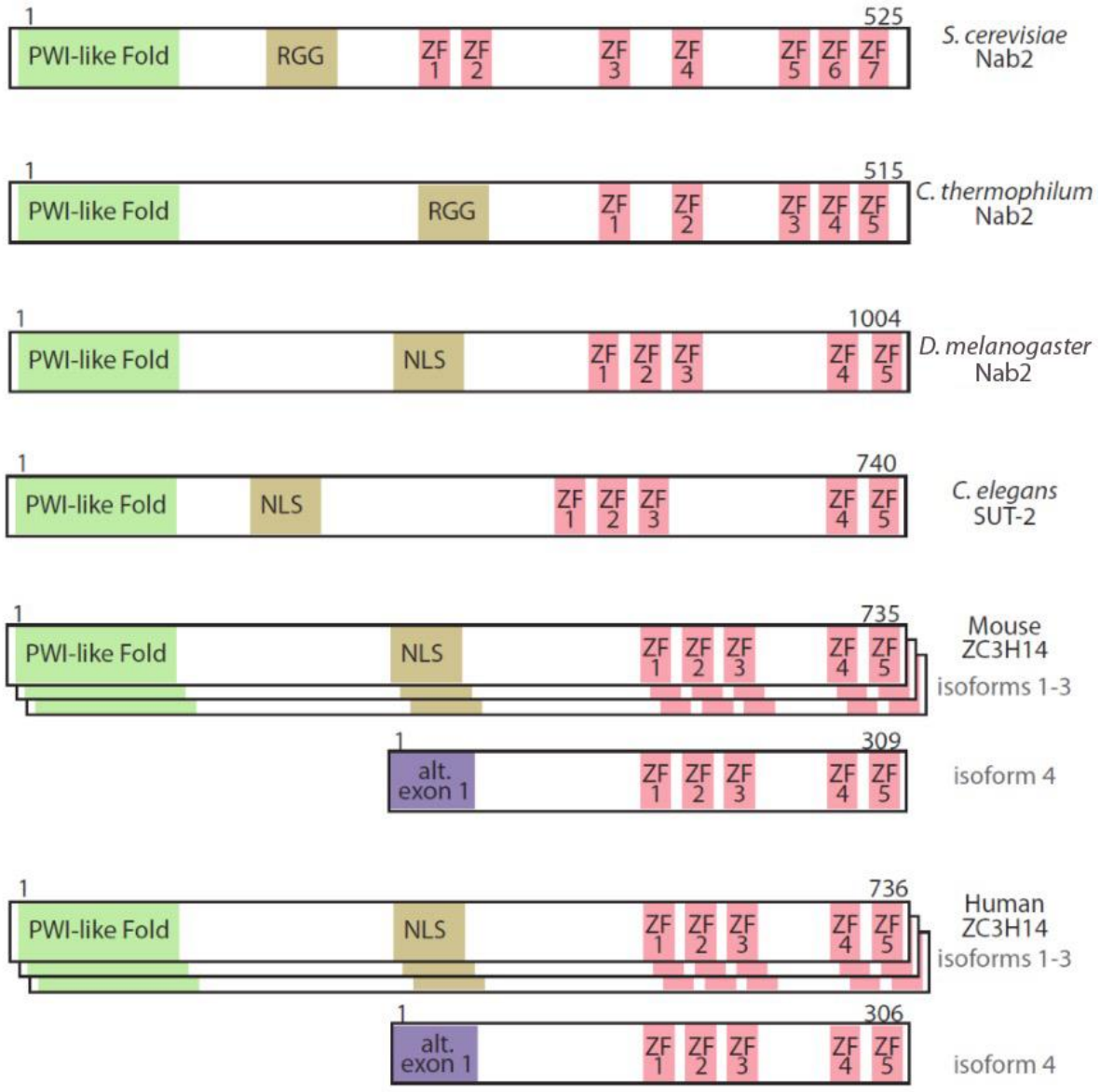

Figure 1-7: Evolutionarily conserved domain structure of ZC3H14 protein and its orthologues. Comparisons of evolutionarily conserved ZC3H14 orthologues, which contain an N-terminal Proline-Tryptophan-Isoleucine (PWI)-like domain (green), nuclear targeting signal (an arginine-glycine-glycine (RGG) motif or a classical nuclear localization signal (cNLS)) (brown), and the RNA binding domain composed of five to seven zinc fingers (ZF, pink). Mammalian ZC3H14 orthologues result from alternative splicing that produces at least four protein isoforms, with an alternative exon 1 (purple) in isoform 4 likely generated through an

alternative transcriptional stat site. Numbers above each protein indicate amino acid number. The spacing between domains is not drawn to scale. The clustered spacing of ZFs within the RNA binding domain reflects the actual spacing.

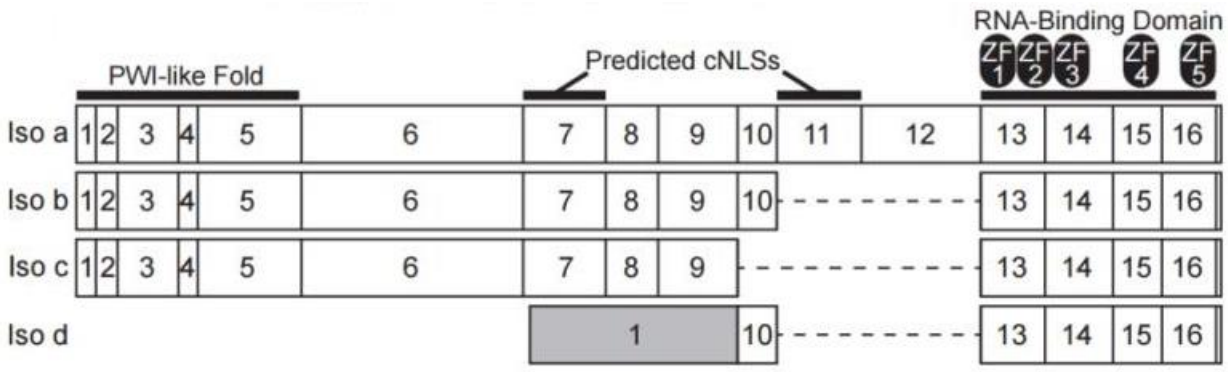

Figure 1-8: ZC3H14 domain structure and isoform alternative splicing. ZC3H14 in mice and humans is expressed from a single gene as at least four distinct isoforms generated by alternative splicing. All isoforms contain the C-terminal RNA binding domain, encoded by exons 13-16. Isoforms 1 (a), 2 (b), and 3 (c) contain the N-terminal PWI-like domain encoded by exons 1-5 and the cNLS predicted to be encoded in exon 7 or 11, with alternative splicing occurring between exons 10-12. Isoform 4 (d) lacks the PWI-like domain and cNLS and encodes an alternative first exon.

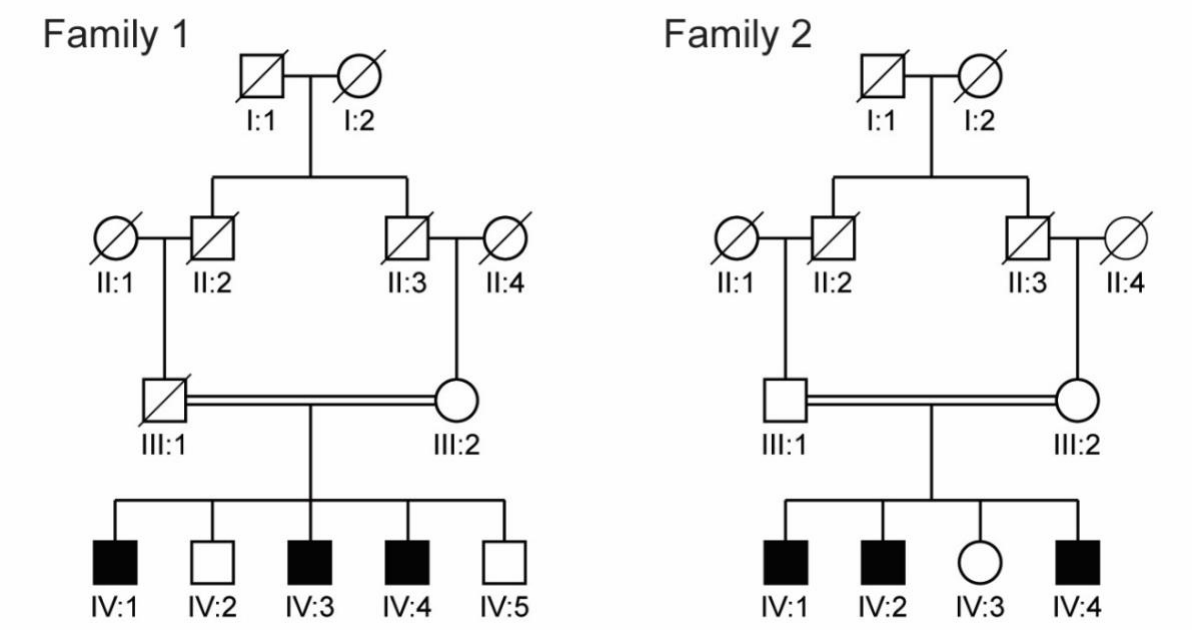

Figure 1-9: Pedigree of Family-1 and Family-2 of independent ZC3H14 mutation inheritance. Family pedigrees of Family 1 (*left*) carrying a ZC3H14 nonsense mutation (R156X) in exon 6, and Family 2 (*right*) carrying a 25nt deletion in ZC3H14 exon 17. ZC3H14 homozygous recessive affected individuals are shown in black. This figure is adapted from Pak *et al.* (2013) [247].

Chapter 2

The RNA-binding protein, ZC3H14, is required for proper polyadenylation, expression of synaptic proteins, and brain function in mice

This Chapter was published as:

J. Rha, S.K. Jones, J. Fidler, A. Banerjee, S.W. Leung, K.J. Morris, J.C. Wong, G.AS. Inglis, L. Shapiro, Q. Deng, A.A. Cutler, A.M. Hanif, M.T. Pardue, A. Schaffer, N.T. Seyfried, K.H. Moberg, G.J. Bassell, A. Escayg, P.S. Garcia, and A.H. Corbett (2017) *Human Molecular Genetics* **20**, 1372-138. "The RNA-binding Protein, ZC3H14, is Required for Proper Poly(A) Tail Length Control, Expression of Synaptic Proteins, and Brain Function in Mice."

I was second author on the published paper, but I made substantial contributions to the work including addressing revisions after the first author graduated. I was integral to the husbandry, genotyping, tissue collection, and experimental selection/gathering of the *Zc3h14*$^{+/+}$, *Zc3h14*$^{F/F}$, and *Zc3h14*$^{\Delta ex13/\Delta ex13}$ mouse lines, which was required for all of the data collected and thus figures presented in this chapter. I contributed directly to the execution and/or generation of all data presented in Figures 2, 7, and S2. I contributed directly to the execution and/or generation of data that composed parts of Figures 3 (hippocampus imaging), Table S1 (open field and novel cage behavioral assays), and S3 (wire-hang and rotarod assays).

2.1 Introduction

Post-transcriptional processing of mRNA, which is critical to ensure proper gene expression, is mediated by numerous RNA-binding proteins that associate with RNA from the start of transcription in the nucleus to degradation in the cytoplasm [280, 281]. There are a growing number of examples where mutations in genes that encode ubiquitously expressed RNA-binding proteins required for post-transcriptional processing cause tissue-specific human disease [282]. Many of these mutations cause diseases of the nervous system such as fragile X syndrome [283] and spinal muscular atrophy [284]. Understanding the functions of these RNA-binding proteins within the nervous system is an important step towards defining the molecular mechanism underlying these tissue-specific diseases.

Fine-tuning of the size and number of synaptic connections in the brain is critical for cognition and underlies fundamental processes such as learning and memory [285]. One key mechanism by which neurons finely tune synapses is through spatio-temporal regulation of gene expression at the site of the synapse [286, 287]. Much of this regulation is mediated by RNA-binding proteins that modulate steps in post-transcriptional processing of mRNAs to achieve local protein synthesis in neurites [286]. A number of mRNA binding proteins, such as Fragile X Mental Retardation Protein (FMRP) and Zipcode Binding Protein 1 (ZBP1), regulate local protein synthesis [287] in neurons. FMRP binds to target mRNAs and represses their local translation, allowing for finely-tuned expression of key synaptic plasticity proteins [29]. ZBP1 guides target mRNAs to the growth cone and synchronizes their translation in response to external stimuli [287]. Such specific functions that may be most essential in neurons could explain why mutations in genes encoding ubiquitously expressed RNA-binding proteins commonly cause neurological defects.

Recently, mutations in the gene encoding the evolutionarily conserved polyadenosine RNA-binding protein, ZC3H14 (Zinc finger CysCysCysHis protein 14), were identified as the cause of a form of nonsyndromic, autosomal recessive intellectual disability [247]. ZC3H14 is evolutionarily-conserved [247-249, 264, 277], and orthologues are essential in budding yeast [251] and flies [247]. The critical functionally conserved domains present in ZC3H14 (Fig. 1A) include an N-terminal Proline-Tryptophan-Isoleucine (PWI)-like domain that mediates interactions with the nuclear pore [256], predicted nuclear targeting signals, and a C-terminal tandem CysCysCysHis (CCCH) Zinc Finger (ZF) domain that mediates high affinity binding to polyadenosine RNA [252]. As shown in Figure 1A, alternative splicing in mammals generates several isoforms of ZC3H14 (isoforms a-d in mice) including one, isoform d, that lacks the exons that encode the N-terminal PWI domain and nuclear targeting signals.

Patients that suffer from intellectual disability caused by mutation of *ZC3H14* are homozygous for a *ZC3H14* allele with a premature stop codon in exon 6 (R154X) that eliminates expression of the protein isoforms that most resemble the essential orthologues found in yeast [251] and flies [247]. Isoform d of ZC3H14, which lacks exon 6, is unaffected by the mutation [249]. Although this form of the protein and is localized to the cytoplasm and appears to be expressed primarily in testes [249], possibly this short ZC3H14 isoform could fulfill an essential function in these patients [288]. While there could be a functional orthologue of ZC3H14 that does not share extensive amino acid similarity in key domains, the human genome does not encode any other CCCH zinc finger proteins that contain a PWI-like domain or key conserved residues within the zinc finger domain that are critical for RNA binding in ZC3H14 orthologues [273] raising the possibility that ZC3H14 function may not be essential in mammals. Prior to the current study there was no way to assess the requirement for mammalian ZC3H14.

ZC3H14 binds with high-affinity binding to polyadenosine RNA [247, 248]. Studies in cultured human cell lines show that ZC3H14 is localized primarily to nuclear speckles [249, 276] suggesting functions within the nucleus. In fact, characterization of ZC3H14 orthologues in model organisms reveals a number of nuclear functions for this zinc finger polyadenosine RNA-binding protein including reported roles in transcription [289], control of poly(A) tail length [263, 264], splicing [290] and RNA export from the nucleus [253]. These functions are consistent with the steady-state localization of the protein to the nucleus and the confirmed nucleocytoplasmic shuttling of the *S. cerevisiae* orthologue [255, 291, 292]. However, such functions alone cannot readily explain why loss of ZC3H14 in patients leads to brain-specific deficits. The specific cellular requirement for ZC3H14 has been addressed by studies exploiting loss-of-function models of the *Drosophila* orthologue, dNab2. Flies lacking both zygotic and maternally-deposited dNab2 are not viable [247] while zygotic mutants show reduced viability as well as defects in brain morphology [277]. Neuron-specific knockdown of dNab2 impairs short-term memory as determined in a courtship conditioning assay [277]. Furthermore, neuron-specific re-expression of dNab2 or expression of human ZC3H14 is sufficient to rescue behavioral defects in *dNab2* zygotic mutant flies [247, 264]. These studies establish a critical, functionally conserved requirement for *Drosophila* ZC3H14 (dNab2) in neurons.

To examine the function of ZC3H14 in a mammalian brain and provide insight into why a loss-of-function mutation in *ZC3H14* causes brain-specific defects in humans, we generated mice that lack *Zc3h14* exon 13, an exon common to all *Zc3h14* splice variants (denoted as $Zc3h14^{\Delta ex13/\Delta ex13}$). Here, we report an evolutionarily conserved function of ZC3H14 in poly(A) tail length control in the mammalian brain. Furthermore, $Zc3h14^{\Delta ex13/\Delta ex13}$mice show morphological changes in ventricles with the brain as well as a deficit in working memory.

Quantitative label-free proteomic analysis reveals key pathways with roles in synaptic function affected upon the loss of ZC3H14. The *Zc3h14*$^{\Delta ex13/\Delta ex13}$ mouse and these findings reveal the importance of ZC3H14 within the mammalian brain and provide an important tool to further define the role of ZC3H14 in the brain.

2.2 Results

2.2.1 Generation and confirmation of *Zc3h14*$^{\Delta ex13/\Delta ex13}$ mice

As with humans [249], mice express multiple splice variants of the *Zc3h14* gene, which encode four protein isoforms termed ZC3H14 isoforms a-d (Fig. 1A). These isoforms share 90% amino acid sequence identity with the human ZC3H14 isoforms. Exon 13 is the first common exon among the *Zc3h14* splice variants. This exon encodes the start of the zinc finger domain that mediates binding to RNA [247-249, 252, 273, 293] and is essential for the function of the budding yeast ZC3H14 orthologue, Nab2 [253]. As described in Materials and Methods, we obtained embryonic stem cells in which *Zc3h14* exon 13 is flanked by *loxP* sites from the Knockout Mouse Project (Fig. 1B). These cells were utilized to generate a conditional knockout mouse line expressing a floxed allele for *Zc3h14* which was induced to create an out-of-frame deletion of *Zc3h14* exon 13 (Δex13) upon Cre-mediated recombination.

To examine the function of ZC3H14, we inactivated *Zc3h14* by mating homozygous floxed *Zc3h14*$^{F/F}$ mice to *EIIa-Cre* transgenic mice, which express Cre-recombinase under the control of a strong adenovirus EIIa promoter in a wide range of tissues in the mouse embryo including germ cells [294, 295]. *EIIa-Cre* transgenic mice are commonly used to generate germ-line deletion of *loxP*-flanked genes [296-302]. Following several generations of breeding as described in Materials and Methods, the floxed *Zc3h14* conditional allele was efficiently

recombined to yield *EIIa-Zc3h14*$^{\Delta ex13/\Delta ex13}$ mice as determined by genomic PCR analysis (primers indicated in Fig. 1B) to detect the control, floxed, and recombined alleles. The recombination event was confirmed by the appearance of a lower molecular weight band at the predicted size (230 bp) upon Cre-mediated deletion of exon 13 (Fig. 1C, *top* panel). Additional PCR analyses confirmed the loss of exon 13 in the recombined mice (Fig. 1C, *bottom* panel). Mice with confirmed recombination were mated to wildtype mice to breed out the *EIIa-Cre* allele. *EIIa-Cre*-negative, *Zc3h14*$^{\Delta ex13/+}$ mice were mated to generate *Zc3h14*$^{\Delta ex13/\Delta ex13}$ homozygous mice for a minimum of four generations for subsequent analyses.

To validate the loss of ZC3H14 protein in these mice, we immunoblotted tissue isolated from the hippocampus, cerebral cortex, cerebellum, and spinal cord, using an antibody that detects the N-terminal PWI-like domain of ZC3H14 [249]. As shown in Figure 1D, the *Zc3h14*$^{\Delta ex13/\Delta ex13}$ mice show no detectable expression of ZC3H14 isoforms a-c, which are readily detectable in the *Zc3h14*$^{+/+}$ control mice. Note that in the *Zc3h14*$^{\Delta ex13/\Delta ex13}$ homozygous mice, we did observe a small amount of a lower molecular weight band (asterisk in Figure 1D) that is specifically detected by the N-terminal ZC3H14 antibody. Using mass spectrometry, we determined that this lower molecular weight band corresponds to a truncated form of ZC3H14. Peptides of ZC3H14 from the *Zc3h14*$^{\Delta ex13/\Delta ex13}$ mouse map only to the N-terminal region of the ZC3H14 protein within exons 5 and 6 (Supplementary Material, Fig. S1), suggesting low-level expression of a truncated protein that lacks the essential RNA-binding domain [253]. In contrast, peptides from the control mouse map to both the N- and C-terminal regions of the ZC3H14 protein (Supplementary Material, Fig. S1). Furthermore, the amount of ZC3H14 immunoprecipitated from *Zc3h14*$^{+/+}$ mice is at least ten-fold more than the amount of truncated protein immunoprecipitated from *Zc3h14*$^{\Delta ex13/\Delta ex13}$ mice showing that the level of this truncated

protein is very low. Thus, *Zc3h14*$^{\Delta ex13/\Delta ex13}$ mice do express a small amount of truncated ZC3H14, which is devoid of the functionally essential RNA-binding zinc finger domain [248, 253]. As no antibody is available to detect ZC3H14 isoform d by immunoblotting, we performed real-time PCR analysis of mouse brain to confirm that this variant was also absent from the *Zc3h14*$^{\Delta ex13/\Delta ex13}$ mice. The *Zc3h14 isoform d* transcript was not detectable above background in *Zc3h14*$^{\Delta ex13/\Delta ex13}$ mice, but was readily detected in *Zc3h14*$^{+/+}$ mice (Fig. 1E). Taken together, these analyses confirm that we have generated mice lacking any full-length ZC3H14 isoform.

2.2.2 ZC3H14 is not essential but is required for normal litter and testis size

To assess the requirement for ZC3H14 in mice, we bred heterozygous *Zc3h14*$^{\Delta ex13/+}$ mice to one another, calculated ratios of the genotypes produced, and compared them to expected Mendelian ratios. While *Zc3h14*$^{\Delta ex13/\Delta ex13}$ mice are viable, there was a statistically significant difference between the expected (1:2:1) and observed (1.0:1.8:0.6, $p<0.0205$) ratios of the genotypes produced (Fig. 2A). To assess differences in litter size, we bred homozygous *Zc3h14*$^{\Delta ex13/\Delta ex13}$ mice to one another. We detected a modest but statistically significant decrease in average litter size (4.14 pups/litter) generated from these *Zc3h14*$^{\Delta ex13/\Delta ex13}$ pairings when compared with *Zc3h14*$^{+/+}$ pairings (6.10 pups/litter) (Fig. 2B). This decrease in litter size may at least partially be due to a trend toward a decrease in the number of male *Zc3h14*$^{\Delta ex13/\Delta ex13}$ births as shown in Fig. 2C. Together, these data indicate that although *Zc3h14* is not essential for viability, but loss of ZC3H14 may impair survival *in utero*.

As a general indication of overall health and development, we systematically measured the body weight of the mice starting at 3 weeks after birth and continuing until they were 5 months old (Supplementary Material, Fig. S2A). Analysis of mean values for body weight of

male and female *Zc3h14*$^{+/+}$ and *Zc3h14*$^{\Delta ex13/\Delta ex13}$ mice showed no statistically significant difference between the two genotypes. The sample size, standard error of the means (SEMs), and *p* values are reported in Supplementary Material, Fig. S2B-D. We also observed no statistically significant difference between the mean values for whole brain weight (Fig. 2D) or hippocampal weight (Fig. 2E) when we compared male *Zc3h14*$^{+/+}$ and *Zc3h14*$^{\Delta ex13/\Delta ex13}$ adult mice.

As the testes express high levels of ZC3H14 [249], we compared testis weight in *Zc3h14*$^{+/+}$ versus *Zc3h14*$^{\Delta ex13/\Delta ex13}$ mice. Although no gross differences in body weight or brain weight were detected, *Zc3h14*$^{\Delta ex13/\Delta ex13}$ mice had testes that were half the size of *Zc3h14*$^{+/+}$ testes (Fig. 2F). ZC3H14 is thus required for normal litter size and is important for normal testis size.

2.2.3 *Zc3h14*$^{\Delta ex13/\Delta ex13}$ mice show altered ventricles in the brain

Although the brain and hippocampi of *Zc3h14*$^{\Delta ex13/\Delta ex13}$ mice showed no detectable change in weight as compared to *Zc3h14*$^{+/+}$ mice (Fig 2D,E), we examined overall brain morphology by histology. We analyzed coronal histological sections (as diagrammed in Fig. 3A) comparing *Zc3h14*$^{+/+}$ and *Zc3h14*$^{\Delta ex13/\Delta ex13}$ mouse brains. Haematoxylin and eosin (H&E) staining revealed that the anterior portion of the lateral ventricles is enlarged in *Zc3h14*$^{\Delta ex13/\Delta ex13}$ mice as compared to *Zc3h14*$^{+/+}$ mice (Fig. 3B and 3C). In contrast, there was no detectable effect on the size of the lateral ventricles at a more caudal level at the hippocampus proper (Fig. 3D). To examine hippocampal morphology, we stained matched sections from *Zc3h14*$^{+/+}$ and *Zc3h14*$^{\Delta ex13/\Delta ex13}$ mice with cresyl violet (Fig. 3E). At this level of analysis, no gross morphological differences were detected between the *Zc3h14*$^{+/+}$ and *Zc3h14*$^{\Delta ex13/\Delta ex13}$ hippocampi when sections from five independent mice were examined.

2.2.4 *Zc3h14*$^{\Delta ex13/\Delta ex13}$ mice have impaired working memory but intact learning

Loss of the ZC3H14 orthologue in *Drosophila* causes defects in short-term memory while learning remains intact [277]. To assess the consequences of loss of ZC3H14 in mice, we performed a variety of behavioral assays including spontaneous alternation Y-maze, open field test, light-dark box, fear conditioning, novel cage activity, and water radial arm maze (Fig. 4 and Supplemental Material, Table S1). For all studies, we employed adult mice between 3 and 4 months of age. Cohorts of mice were carefully age and gender matched for all assays. In several of the assays including the novel cage, light-dark box, and fear conditioning, we did not detect statistically significant differences in the behaviors we examined when comparing the *Zc3h14*$^{+/+}$ and *Zc3h14*$^{\Delta ex13/\Delta ex13}$ mice (Table S1). A Y-maze paradigm was employed as an initial approach to assess working memory [303]. We did not detect a statistically significant difference in the percentage of correct alternation in arm entries when we compared *Zc3h14*$^{+/+}$ and *Zc3h14*$^{\Delta ex13/\Delta ex13}$ mice (Fig. 4A); however, there was a trend toward a deficit in the sequence of arm entries for *Zc3h14*$^{\Delta ex13/\Delta ex13}$ mice. As shown in Figure 4B, we did detect a statistically significant difference ($p=0.004$) in the number of arm entries between the two groups The *Zc3h14*$^{\Delta ex13/\Delta ex13}$ mice had 40% more arm entries than the *Zc3h14*$^{+/+}$ mice (Fig. 4B). These data suggest there are some differences in the behavior of *Zc3h14*$^{\Delta ex13/\Delta ex13}$ mice compared to control *Zc3h14*$^{+/+}$ mice.

Based on the results obtained in the Y-maze, we employed a more sensitive assay to further explore aspects of learning and memory, the water radial arm maze (WRAM) [304-307]. As illustrated in Figure 4C, the WRAM is an eight-arm arena in which mice are evaluated on their ability to *learn* the location of submerged platforms in order to escape from having to swim, and *remember* the location of the hidden platforms. Learning is indicated, across nine days of

testing, by a decrease in the amount of time required to find all four platforms and a decrease in the number of errors made. Errors include mistakes in which a mouse enters an arm that: (a) does not contain a platform, (b) contains a platform but the mouse does not locate it, (c) contained a platform on a previous trial on the same day, or (d) has already been entered previously during the trial (i.e. deficit in working memory). Both *Zc3h14*$^{+/+}$ and *Zc3h14*$^{\Delta ex13/\Delta ex13}$ adult mice were able to learn the locations of the hidden platforms, as evidenced by a decrease in the time required to locate the platforms (Fig. 4D, $p<0.0001$), a decrease in the number of overall total errors (Fig. 5E, $p<0.0001$), and a decrease in the number of working memory errors (Fig. 4F, $p<0.0001$), across the course of the nine-day testing period.

Though both *Zc3h14*$^{+/+}$ and *Zc3h14*$^{\Delta ex13/\Delta ex13}$ mice show the ability to *learn* as assessed in the WRAM (Fig. 4D-F), data uniformly indicate a trend toward an impairment in efficient learning by the *Zc3h14*$^{\Delta ex13/\Delta ex13}$ mice, which require one to three additional days to perform at a similar level to *Zc3h14*$^{+/+}$ mice. Furthermore, analyzing the WRAM data to assess *working memory* function, *Zc3h14*$^{\Delta ex13/\Delta ex13}$ mice showed a statistically significant deficit in working memory when compared with *Zc3h14*$^{+/+}$ mice (Fig. 4F). Specifically, working memory errors are repeated entries into any arm on a given trial, indicating the subject's inability to remember which arm was explored within the previous two minutes (the length of a single trial). As illustrated in Fig. 4F, *Zc3h14*$^{\Delta ex13/\Delta ex13}$ mice exhibited a statistically significant ($p=0.035$) persistence in the number of working memory errors that is not exhibited by control mice. *Zc3h14*$^{\Delta ex13/\Delta ex13}$ mice require two additional days of trials to perform as well as the control mice in locating all platforms. The WRAM results indicate that ZC3H14 is required in adult mice for proper cognitive function, particularly spatio-temporal working memory, which is consistent

with the cognitive deficits seen in patients [247] and the behavioral defects observed in the *dNab2* mutant flies [277].

2.2.5 *Zc3h14*$^{\Delta ex13/\Delta ex13}$ mice have normal visual function and exhibit normal motor function and coordination

The WRAM test requires vision to locate environmental cues and motor coordination to swim efficiently. To rule out possible confounding variables that could lead to impaired performance of *Zc3h14*$^{\Delta ex13/\Delta ex13}$ mice in the WRAM test, we conducted several tests to examine visual function (Supplementary Material, Fig. S3 A-C), and motor function and coordination (Supplementary Material, Fig. S3 D-G). These tests were performed on independent cohorts of mice so they would not confound results of the WRAM. *Zc3h14*$^{\Delta ex13/\Delta ex13}$ mice performed at least as well as the *Zc3h14*$^{+/+}$ mice on the visual and motor coordination assays. We measured visual acuity and contrast sensitivity by using an optokinetic test apparatus (depicted in Supplementary Material, Fig. S3A) for rodents, which elicits a head- and body-turning response to a rotating visual field [308]. *Zc3h14*$^{\Delta ex13/\Delta ex13}$ mice showed no obvious deficit in their visual acuity represented by their ability to distinguish similar spatial frequencies of black and white gratings when compared to control mice (Supplementary Material, Fig. S3B). Furthermore, *Zc3h14*$^{\Delta ex13/\Delta ex13}$ mice showed no evidence of impaired contrast sensitivity, as measured by their ability to distinguish between gradients of dark- and light-gray gratings (Supplementary Material, Fig. S3C), when compared to *Zc3h14*$^{+/+}$ mice.

Next, we challenged mice using two assays to assess general motor function and coordination. *Zc3h14*$^{\Delta ex13/\Delta ex13}$ mice did not show a statistically significant difference in their ability to grip a wire mesh while up-side down (depicted in Supplementary Material, Fig. S3D)

when compared to *Zc3h14*$^{+/+}$ mice (Supplementary Material, Fig. S3E). Additionally, when challenged on a rotarod apparatus (depicted in Supplementary Material, Fig. S3F), *Zc3h14*$^{\Delta ex13/\Delta ex13}$ mice performed at least as well as the *Zc3h14*$^{+/+}$ mice (Supplementary Material, Fig. S3G). These data together indicate that, along with vision, general motor function, sensorimotor coordination, and motor learning are intact in *Zc3h14*$^{\Delta ex13/\Delta ex13}$ mice, and thus would not contribute to differences in performance in the WRAM. Furthermore, consistent with normal baseline behavior, *Zc3h14*$^{+/+}$ and *Zc3h14*$^{\Delta ex13/\Delta ex13}$ mice were comparable in assays to assess exploratory behavior (novel cage), fear conditioning, and anxiety (light/dark box) (Supplementary Material, Table S1). Together, these results indicate that the working memory deficit detected in the *Zc3h14*$^{\Delta ex13/\Delta ex13}$ mice is not likely to be confounded by these variables.

2.2.6 Zc3h14 is required for proper poly(A) tail length control

Our previous work demonstrates that one evolutionarily conserved molecular function of ZC3H14 is to restrict poly(A) tail length of bulk RNAs [247, 251, 263, 264]. However, no studies have been previously performed to assess the molecular function of vertebrate ZC3H14 *in vivo*. To assess the functional consequence of loss of ZC3H14, we compared poly(A) tail length of bulk RNA isolated from several different tissues of *Zc3h14*$^{+/+}$ and *Zc3h14*$^{\Delta ex13/\Delta ex13}$ mice (Fig. 5). We examined RNA isolated from two different brain regions, cortex and hippocampus, as well as liver. *ZC3H14* is highly expressed in all these tissues [249]. Poly(A) tail length of bulk RNA isolated from these tissues was assessed as described in Materials and Methods using an acrylamide gel to resolve end-labeled poly(A) tracts. A typical gel is shown in Figure 5A and results depicted as scans of the lanes in each gel are shown in Figure 5B. The *Zc3h14*$^{\Delta ex13/\Delta ex13}$ mice show an increase in bulk poly(A) tail length compared to *Zc3h14*$^{+/+}$ mice

in all tissues examined but the effect is very modest in the cortex and liver. The increase in bulk poly(A) tail length is far more striking in the samples isolated from the hippocampus. This result provides molecular and *in vivo* evidence that ZC3H14 plays a role in poly(A) tail length control in a region of the mouse brain that is important for learning and memory.

2.2.7 Increased expression of synaptic proteins in *Zc3h14*$^{\Delta ex13/\Delta ex13}$ mice

Patients with loss of function alleles of *ZC3H14* have intellectual disability [247] and our mice show some changes in the lateral ventricle of the brain and poly(A) tail length control in the hippocampus. To begin to explore mechanisms that could underlie these functional changes, we performed a quantitative proteomic analysis to compare the hippocampal proteomes of *Zc3h14*$^{+/+}$ and *Zc3h14*$^{\Delta ex13/\Delta ex13}$ mice (n = 4 each group). We focused on hippocampi for this analysis as this is the tissue that shows the most profound change in bulk poly(A) tail length. Following tissue homogenization and trypsin digestion, peptides from each sample were analyzed by LC-MS/MS on an Orbitrap Fusion mass spectrometer. Relative protein abundance was determined by peptide ion-intensity measurements across LC-MS runs using the label-free quantification (LFQ) algorithm in the MaxQuant computational platform [309]. In total, 56,423 peptides mapping to 4,450 protein groups were identified in *Zc3h14*$^{+/+}$ and *Zc3h14*$^{\Delta ex13/\Delta ex13}$ mouse hippocampi. The stochastic nature of LC-MS/MS based peptide sequencing required us to limit the number of missing protein measurements to no more than two per condition, resulting in the final quantification of 4,161 protein groups (henceforth referred to as proteins) mapping to 4,052 unique gene symbols (Table S2).

Figure 6A shows a volcano plot where each protein that has any change in steady state expression level between *Zc3h14*$^{+/+}$ and *Zc3h14*$^{\Delta ex13/\Delta ex13}$ hippocampi is represented by a colored

dot. In total 113 (62 increased, 51 decreased) proteins with at least a ±1.25 fold change (i.e., $|\log_2(Zc3h14^{+/+}/Zc3h14^{\Delta ex13/\Delta ex13})| \geq 0.32$) and a p value < 0.05 are highlighted as green (decreased) or red (increased) dots. Proteins that did not meet these criteria (shown as blue dots) fall within the shaded nonsignificant boundaries of the plot and were omitted from further analysis. The identities of the 10 most decreased and 10 most increased proteins are listed, and their corresponding positions are labeled (with Roman or Arabic numerals, respectively) on the plot. Note that the top protein with decreased expression is ZC3H14, which further validates the absence of the ZC3H14 protein from *Zc3h14*$^{\Delta ex13/\Delta ex13}$ mice and highlights the reliability of our proteomics approach. We further analyzed the proteins which met our significance criteria by creating a heatmap with hierarchical clustering of both samples and proteins (Supplemental Data, Fig S4). This analysis shows that the *Zc3h14*$^{+/+}$ and *Zc3h14*$^{\Delta ex13/\Delta ex13}$ samples segregate based on proteins levels, thus confirming by an independent method the distinctive proteomic profiles.

To analyze enrichment of proteins that participate in the same cellular components, biological processes, or molecular functions, we performed a GO (gene ontology) analysis of the decreased (50 proteins when ZC3H14 is omitted from the list) and increased (62 proteins) sets of only those proteins significantly changed in *Zc3h14*$^{\Delta ex13/\Delta ex13}$ mice compared to *Zc3h14*$^{+/+}$mice. The criteria used to cluster proteins into a GO term were Z-score ≥ 1.96, p value < 0.05, and ≥ 3 gene symbols per GO term. As shown in Fig. 6B, only two GO terms were identified using the decreased protein set (n = 50), as most of these proteins do not cluster into GO terms. These GO terms are nuclear-specific and suggest these pathways are most affected in the nucleus at the protein level as a result of loss of ZC3H14. The small number of proteins that do cluster into common GO terms are depicted in Fig. 6C. Thus, the majority of proteins with decreased expression do not cluster into common pathways recognized by GO terms.

We then analyzed the set of increased proteins (n = 62) for GO enrichment. In striking contrast to the decreased protein set, many of the increased proteins cluster into several biologically meaningful GO terms. In fact, this result holds true even after more stringent inclusion criteria (Z-score ≥ 2.58, p value < 0.01, and ≥ 5 gene symbols per GO term) than that used for analyzing the decreased gene set (Fig. 6D) are applied. Many of the GO terms, such as "synapse," "signal transduction," and "behavior," have neuronal or brain-specific functions. For example, the top GO term categorized under cellular component is "synapse" (large green asterisk in Fig. 6E), which contains the following genes that increase in expression in *Zc3h14*$^{\Delta ex13/\Delta ex13}$ hippocampus when compared to *Zc3h14*$^{+/+}$ hippocampus: Atp1a2, CaMK2α, Nrgn, Psd3, Slc1a2, Slc1a3, Sparcl1, Sv2a (small green asterisks). Furthermore, the majority of the top 10 increased proteins cluster into the GO terms "signal transduction" and/or "membrane." In contrast, none of the top 10 decreased proteins cluster into common GO terms. This global GO term analysis of the increased protein set suggests that mutation of *Zc3h14* causes increased steady state levels of proteins in cellular components or processes important for brain function such as the synapse and signal transduction.

To validate the proteomic results, we selected several candidate proteins that showed a statistically significant change in the mass spectrometry data and compared expression in hippocampal lysates prepared from *Zc3h14*$^{\Delta ex13/\Delta ex13}$ mice to hippocampal lysates prepared from *Zc3h14*$^{+/+}$ mice (Fig. 7). We validated the decrease in the level of the ZC3H14 protein and also examined two proteins that were increase in *Zc3h14*$^{\Delta ex13/\Delta ex13}$ mice compared to *Zc3h14*$^{+/+}$ mice, Calcium/Calmodulin Dependent Protein Kinase II Alpha (CaMK2α/CaMKIIα) and WW domain-containing oxidoreductase (Wwox). The CaMK2α protein plays a key role in signaling within the hippocampus including a role in learning and memory [310]. While most extensively

characterized as a tumor suppressor, the Wwox protein has been implicated in neural development and in the pathogenesis of Alzheimer's disease [311]. As a control, we also examined the expression of the Synaptic Vesicle Glycoprotein 2c (SV2c), which showed no statistically significant difference between the mice. Results of a representative immunoblot are shown in Figure 7A. We quantitated the results of the immunoblotting using hippocampal lysates prepared from three *Zc3h14*$^{+/+}$ or *Zc3h14*$^{\Delta ex13/\Delta ex13}$ mice (Figure 7B). As predicted by the proteomic analysis, both Wwox and CaMK2α increase in *Zc3h14*$^{\Delta ex13/\Delta ex13}$ mice compared to *Zc3h14*$^{+/+}$ with no change in Sv2a.

To provide an initial test of whether proteins that show altered expression in *Zc3h14*$^{\Delta ex13/\Delta ex13}$ mice compared to *Zc3h14*$^{+/+}$ mice could be directly regulated by ZC3H14, we performed an RNA immunoprecipitation experiment (Fig. 7C). For this experiment, we immunoprecipitated endogenous ZC3H14 from mouse hippocampi and used qRT-PCR to detect bound transcripts. We focused on the *CaMK2a* transcript for these initial experiments both because it is an important regulator of neuronal activity [310] and our studies in *Drosophila* reveal that fly ZC3H14/dNab2 can regulate the expression of a CaMK2α translational reporter and bind to the *CaMK2a* transcript in a comparable RNA immunoprecipitation assay [312]. As shown in Figure 7C, the *CaMK2a* transcript is highly enriched (>15-fold) when ZC3H14 is immunoprecipitated from *Zc3h14*$^{+/+}$ hippocampus as compared to *Zc3h14*$^{\Delta ex13/\Delta ex13}$ hippocampus, which lacks ZC3H14. A previously validated target of ZC3H14 in cultured cells, *Atp5g1* [313], is also enriched in the ZC3H14 immunoprecipitation while the *Zc3h14* transcript is not. These results suggest that ZC3H14 could modulate the steady-state levels of hippocampal proteins through directly binding and regulating the corresponding transcripts.

2.3 Discussion

We have generated a *Zc3h14*$^{\Delta ex13/\Delta ex13}$ mouse to study the function of the evolutionarily conserved, ubiquitously expressed polyadenosine RNA-binding protein, ZC3H14. The mutation eliminates exon 13, the first common exon of all four isoforms of ZC3H14, which encodes the start of the critical zinc finger RNA-binding domain essential for the function of the *S. cerevisiae* orthologue of ZC3H14, Nab2 [253]. We have performed an initial characterization of the homozygous *Zc3h14*$^{\Delta ex13/\Delta ex13}$ mice, which revealed that they show an increase in the size of the lateral brain ventricles with no gross change in hippocampal morphology, and modest deficits in some behavioral paradigms including the WRAM. Interestingly, bulk RNA isolated from hippocampi of *Zc3h14*$^{\Delta ex13/\Delta ex13}$ mice has extended poly(A) tails, and parallel quantitative proteomic analysis comparing the hippocampi of *Zc3h14*$^{\Delta ex13/\Delta ex13}$ mice to *Zc3h14*$^{+/+}$ mice revealed an increase in the steady-state level of proteins important for synaptic plasticity and function including CaMK2α. Taken together, this work provides a model in which to study the function of ZC3H14 in the mammalian brain.

ZC3H14 orthologues in *S. cerevisiae* [251] and *Drosophila* [247] are essential for viability. However, patients who lack expression of ZC3H14 isoforms (isoforms 1-3), which most closely resemble the evolutionarily conserved gene product shared by the yeast and flies [288], are alive [247]. Furthermore, these patients suffer from nonsyndromic intellectual disability showing that, despite ubiquitous expression of ZC3H14 isoforms 1-3, functional consequences of loss of these protein isoforms is limited to the brain [249]. Unlike the patients, which retain at least one ZC3H14 isoform, the mice were engineered to remove an exon common to all splice variants and thus eliminate all protein isoforms. Although no full length ZC3H14 protein is present in these mice, we detect a very small amount of a truncated protein (Fig. 1D

and S1). These results suggest that ZC3H14 is not essential for viability with the caveat that the small amount of ZC3H14 that lacks the C-terminal RNA binding domain could confer some as yet undetermined function. The *Zc3h14*$^{\Delta ex13/\Delta ex13}$ mice are fertile and appear to show normal growth as evidenced by analysis of overall body weight as well as brain and hippocampal weights. We did detect a decrease in litter size at weaning, which could reveal developmental consequences of loss of ZC3H14 or altered maternal care. Adult *Zc3h14*$^{\Delta ex13/\Delta ex13}$ mice exhibited normal visual acuity and contrast sensitivity as well as general motor function and coordination. Taken together, these results suggest that ZC3H14 function is not critical for viability in mammals.

Two tissues that are highly dependent on spatial and temporal control of gene expression are the brain [284, 314, 315] and the testes [316, 317]. Consequently, changes in testis size are commonly associated with disorders of intellectual disability [318-322]. A striking phenotype we observe in the *Zc3h14*$^{\Delta ex13/\Delta ex13}$ mice is the decreased size of the testes, which suggests a requirement for ZC3H14 in proper testes development or maintenance. In fact, the testes have high expression of all ZC3H14 isoforms including the testes-enriched isoform d [249]. The testes themselves are rich in RNA-binding proteins [316, 317], many of which are expressed as testes-specific isoforms [323, 324]. Furthermore, spermatogenesis is highly dependent on post-transcriptional processing [325]. Additional studies are necessary to understand the requirement for ZC3H14 in the testes and the role ZC3H14, in particular the mammalian-specific isoform 4, plays in the testes.

Previous studies of the *Drosophila* orthologue of ZC3H14, dNab2, identified a requirement for dNab2 in supporting normal brain function and structure [277]. In *dNab2* mutant flies, the lobes of the mushroom bodies, neuropil which are essential for learning in flies [278],

are malformed and show crossing-over defects of axons across the midline [277]. Interestingly, such defects have also been reported in the fragile X syndrome fly model [326]. Our analysis of the brain morphology of *Zc3h14*$^{\Delta ex13/\Delta ex13}$ mice thus far reveals an increase in the size of the lateral ventricles with no gross change in the hippocampus. Enlargement of lateral ventricles in mouse models has been observed in a variety of brain disorders with cognitive impairment, including fragile X syndrome [327], down syndrome [328], and the autism spectrum disorder, Smith-Lemli-Opitz syndrome [329]. Furthermore, enlargement of lateral ventricles is a hallmark of developmental disability [330] and age-related cognitive decline [331, 332] in humans. Many potential mechanisms could underlie the increase in the size of the lateral ventricles observed in *Zc3h14*$^{\Delta ex13/\Delta ex13}$ mice including cerebrospinal fluid (CSF) overproduction, decreased resorption, or obstruction of outflow [328]. Alternatively, enlarged ventricles could arise from degeneration, impaired proliferation, or delayed maturation of ependymal cells that line the ventricles [328]. More detailed analyses will be required to define the nature of this defect in mice lacking ZC3H14.

With respect to the key function of ZC3H14, previous studies established that ZC3H14 and its orthologues play an evolutionarily conserved role in regulating poly(A) tail length of RNAs in budding yeast [263], *Drosophila* [247], and a murine neuroblastoma cell line [264]. Utilizing the *Zc3h14*$^{\Delta ex13/\Delta ex13}$ mice, we present the first functional characterization of the mammalian ZC3H14 protein *in vivo*. Our results reveal that ZC3H14 is required for proper control of poly(A) tail length in the hippocampus. Control of poly(A) tail length is crucial for proper post-transcriptional regulation [333], especially in neurons that require precise temporal and spatial control of gene expression [334] [41, 42, 335, 336]. An elongated poly(A) tail could increase the half-life [333] of specific target RNAs and/or increase translation through a

cytoplasmic polyadenylation element binding protein (CPEB)-dependent mechanism [269, 337]. Either mechanism could lead to an increase in the steady state level of the encoded protein. In fact, GO-term analysis of our mass spectrometry results revealed a unilateral increase in the expression of proteins (e.g. CaMK2α) important for processes such as signal transduction and synaptic function. Such changes could be mediated by direct binding of ZC3H14 to target transcripts as ZC3H14 enriches the *CaMK2a* transcript in RNA immunoprecipitation.

Results of the behavioral analyses reveal that the *Zc3h14*$^{\Delta ex13/\Delta ex13}$ mice apparently have intact spatio-temporal learning but a detectable deficit in working memory revealed in the WRAM. These data are remarkably consistent with studies in a *Drosophila* model, in which flies depleted of dNab2 specifically in neurons, show defects in short-term memory but preserved learning ability [277]. Working memory is closely related to attention [338], and measures of working memory capacity predict higher performance on executive function tasks [339]. Not only is working memory critical to brain development [340], but it is also a marker for age-related declines in cognitive function [341]. Taken together, it is possible that the human phenotype is, at least in part, recapitulated by the behavioral results in our rodent model.

This initial characterization of *Zc3h14*$^{\Delta ex13/\Delta ex13}$ mice reveal some parallel results to mice lacking the RNA binding protein Fmr1, which serve as a model of fragile X syndrome [342]. Studies in *Drosophila* support a close functional link as well as genetic interactions between *dNab2* and *dFmr1* [312]. Many years of analysis of the *Fmr1* knockout mice have identified changes at both the molecular and behavioral levels [342] some of which can be compared to this initial characterization of *Zc3h14*$^{\Delta ex13/\Delta ex13}$ mice. While *Fmr1* knockout mice have not been analyzed in the WRAM, some studies report deficits in either the Morris water maze or in maze learning while others found no difference [342]. Studies also revealed no statistically significant

difference in a novel object recognition paradigm for *Fmr1* knockout mice compared to control [342] as we report here for *Zc3h14*$^{\Delta ex13/\Delta ex13}$ mice. The extensive behavioral studies performed with *Fmr1* mice provide direction for future analyses of the mice lacking ZC3H14.

Another point of comparison for the *Zc3h14*$^{\Delta ex13/\Delta ex13}$ mice and the *Fmr1* knockout mice is proteomic changes that occur in the absence of these key regulatory RNA binding proteins. While an analysis of the hippocampal proteome directly comparable to the one reported here for *Zc3h14*$^{\Delta ex13/\Delta ex13}$ has not been carried out for *Fmr1* knockout mice, there are proteomic studies that analyzed primary cortical neurons [343] or synaptic membranes [344] [345]. The only study that employed samples derived from the hippocampus used iTRAQ analysis [344] and detected low fold changes with the largest difference 1.24-fold. That study identified 23 proteins that met the criteria set forth to define statistically significant changes. We detected all 23 of these proteins in our analysis of the *Zc3h14*$^{\Delta ex13/\Delta ex13}$ hippocampal proteome, and of these 23, we detected changes in 18 with the overlap primarily among proteins that show an increase in steady state levels in in the mutant compared to the wildtype control animals. Some of these changes did not meet our strict criteria for statistical significance so are not reported in the Supplemental Data. While the previous study detected an increase in CaMK2α levels in the *Fmr1* proteomic analysis, they were unable to validate a statistically significant change by immunoblotting. However, other studies have identified *CaMK2a* as an RNA regulated by FMRP/Fmr1 in multiple experimental systems [346] [312]. These results are consistent with our finding that CaMK2α protein levels increase in the hippocampus of *Zc3h14*$^{\Delta ex13/\Delta ex13}$ mice compared to control and that *CaMK2a* mRNA is enriched in an RNA immunoprecipitation of ZC3H14 from hippocampus. These results support the possibility that ZC3H14 could regulate some of the same target RNAs as FMRP that are critical for proper neuronal function.

In conclusion, we have generated a *Zc3h14*$^{\Delta ex13/\Delta ex13}$ mouse as a tool to study the role ZC3H14 plays in the mammalian brain. We establish here that ZC3H14 is required for proper brain function in mice and also demonstrate the ZC3H14 plays a conserved role in poly(A) tail length control within the hippocampus. Based on our proteomic analysis, we suggest a model where ZC3H14 regulates the expression of proteins critical for brain function. Utilizing this mouse model, future work will focus on characterizing specific target mRNAs, such as *CaMK2a*, which ZC3H14 could regulate to ensure proper brain function.

Figures:

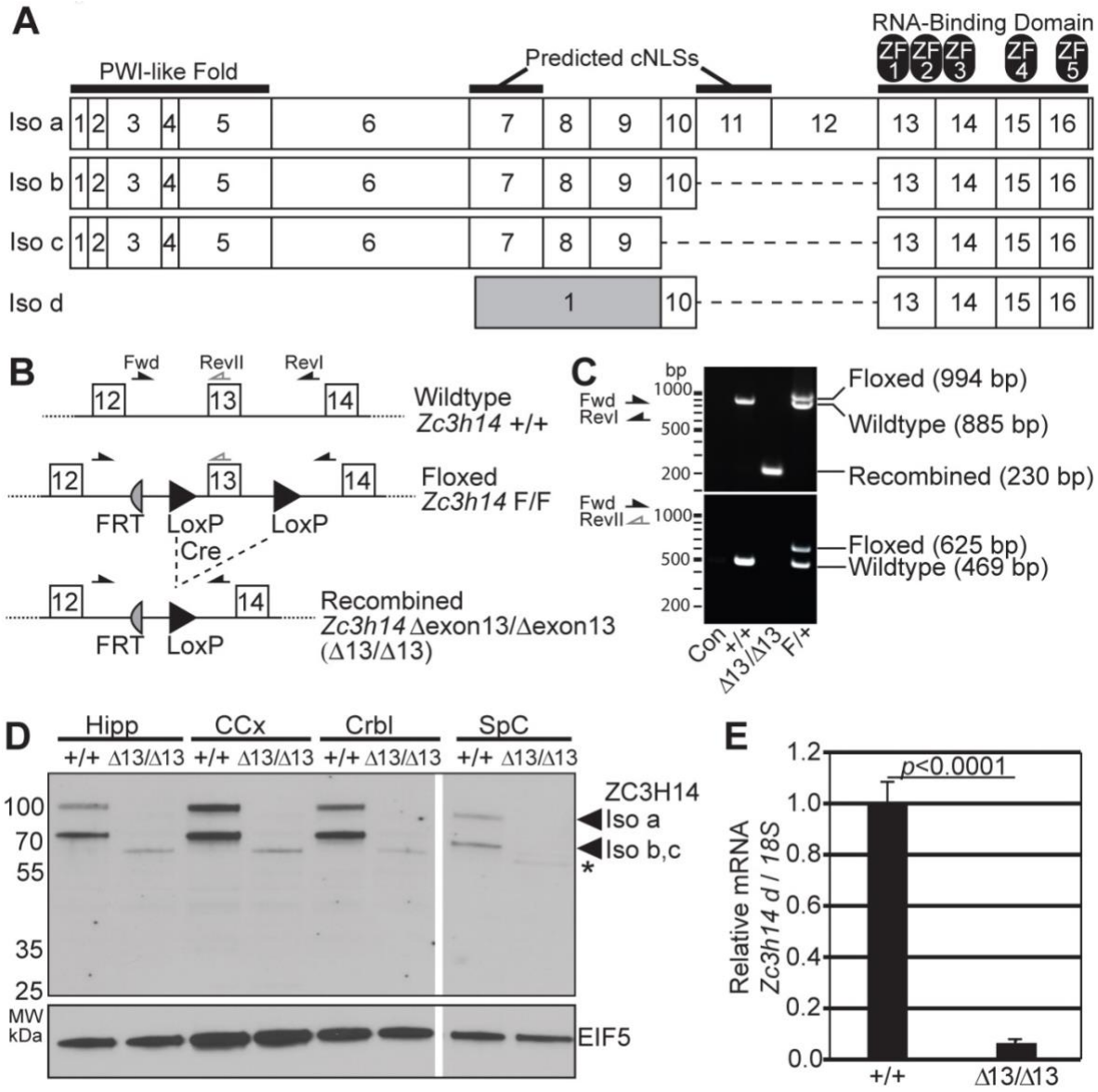

Figure 2-1: Generation of *Zc3h14*$^{\Delta ex13/\Delta ex13}$ mice. (A) Schematic of four protein isoforms of murine *Zc3h14* gene (Isoforms a-d). All isoforms generated contain the C-terminal RNA-binding domain, composed of five CCCH (Cys-Cys-Cys-His) zinc fingers (labelled as ZF1-5). Isoforms a-c contain the N-terminal PWI-like fold, important for poly(A) RNA export from nucleus in budding yeast [293] and predicted classical nuclear localization signal (NLS) motifs. Isoform d contains an alternative first exon (gray) that splices directly to exon 10 encoding a smaller

protein isoform. Note that exon 13 is the first common exon among all *Zc3h14* splice variants and encodes the beginning of the critical RNA-binding domain [248, 252]. (B) A map illustrating the location of the *loxP* and *FRT* sites adjacent to *Zc3h14* exon 13 in the floxed allele. The recombined allele illustrates the removal of *Zc3h14* exon 13 following Cre-mediated recombination. The position of the forward (Fwd) and reverse (RevI, RevII) primers used for genotyping are indicated. FRT, Flippase Recognition Target; +, control allele; F, floxed allele; Δex13, recombined allele lacking exon 13. (C) Genotyping of the *Zc3h14* allele by PCR using primers illustrated in (B). Representative agarose gels are shown for PCR (*top gel*) using the primers flanking *Zc3h14* exon 13, including *LoxP* sites (Fwd and RevI, black arrows), or (*bottom gel*) using the Fwd primer and reverse primer located in exon 13 (RevII, grey reverse arrow). Results are shown for no genomic DNA control (Con); a +/+ control mouse; a Δex13/Δex13 (Δ/Δ) homozygous recombined mouse; and a heterozygously floxed/+ (F/+) mouse. The size of the products generated is indicated to the right, and markers in bp are shown on the left. (D) ZC3H14 protein was analyzed in tissue samples collected from $Zc3h14^{+/+}$ or $Zc3h14^{\Delta ex13/\Delta ex13}$ mouse hippocampus (Hipp), cerebral cortex (CCx), cerebellum (Crbl), and spinal cord (SpC). The top panel shows an immunoblot for ZC3H14 using an N-terminal antibody that recognizes the PWI-like fold [249]. The band corresponding to isoform a is located at ~100 kDa; and the shorter isoforms, b and c, are detected as a single band at ~70 kDa. The bottom panel shows an immunoblot for EIF5, eukaryotic Initiation Factor 5, as a loading control [347]. (*) denotes a truncated N-terminal fragment of ZC3H14 (see Supplementary Material, Fig. S1). (E) Quantitative PCR analysis of *Zc3h14* splice variant d (which lacks the PWI-like Fold recognized by the antibody), normalized to 18S rRNA as an internal control, isolated from $Zc3h14^{+/+}$ or $Zc3h14^{\Delta ex13/\Delta ex13}$ mouse brain. Error bars indicate SEM. $P < 0.0001$.

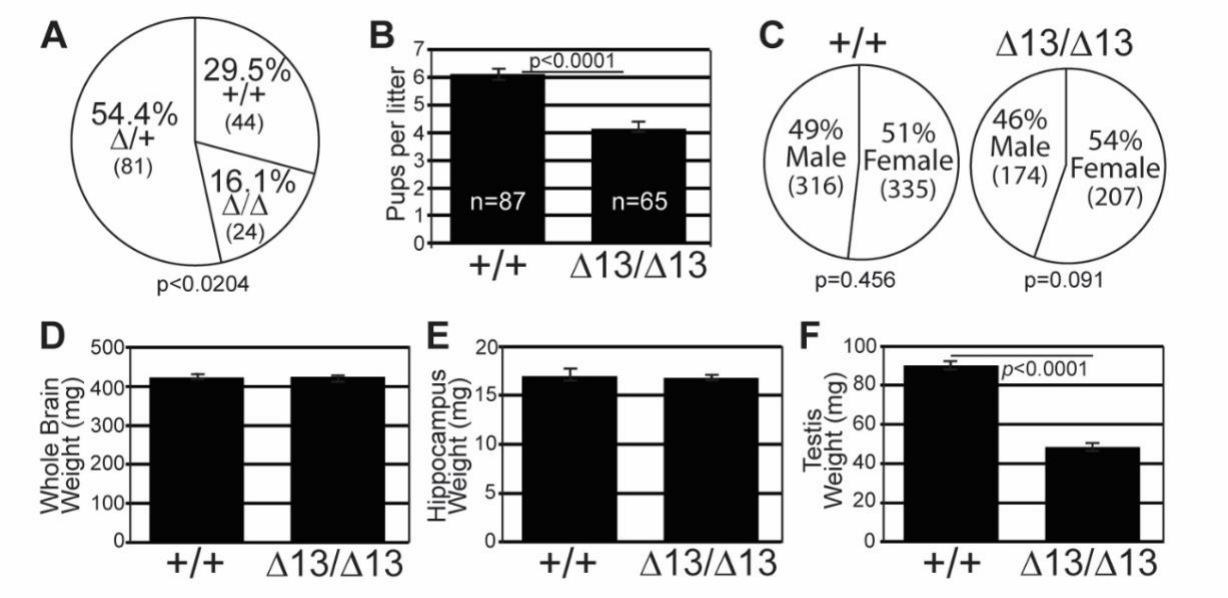

Figure 2-2: *Zc3h14*$^{\Delta ex13/\Delta ex13}$ mice are viable. (A) *Zc3h14* genotype percentages produced by heterozygous *Zc3h14*$^{\Delta/+}$ breeding pairs. The total numbers of mice obtained for each genotype are indicated in parentheses. *P*=0.0.0204. (B) The average number of pups per litter generated from *Zc3h14*$^{+/+}$ pairings or *Zc3h14*$^{\Delta ex13/\Delta ex13}$ parings are indicated in the bar graph. *P*<0.0001. (C) The percent of males and females of *Zc3h14*$^{+/+}$ and *Zc3h14*$^{\Delta ex13/\Delta ex13}$ mice born from *Zc3h14*$^{+/+}$ pairings or *Zc3h14*$^{\Delta ex13/\Delta ex13}$ parings is presented by genotype. Means of (D) whole brain weight and (E) hippocampus weight for *Zc3h14*$^{+/+}$ and *Zc3h14*$^{\Delta ex13/\Delta ex13}$ adult male mice. *Zc3h14*$^{+/+}$, n=3; *Zc3h14*$^{\Delta ex13/\Delta ex13}$, n=3. (F) Testis weight (mg) comparison between *Zc3h14*$^{+/+}$ and *Zc3h14*$^{\Delta ex13/\Delta ex13}$ adult mice. *P*<0.0001. *Zc3h14*$^{+/+}$, n=9; *Zc3h14*$^{\Delta ex13/\Delta ex13}$, n=9. Error bars indicate SEM for (B), (D), (E), (F).

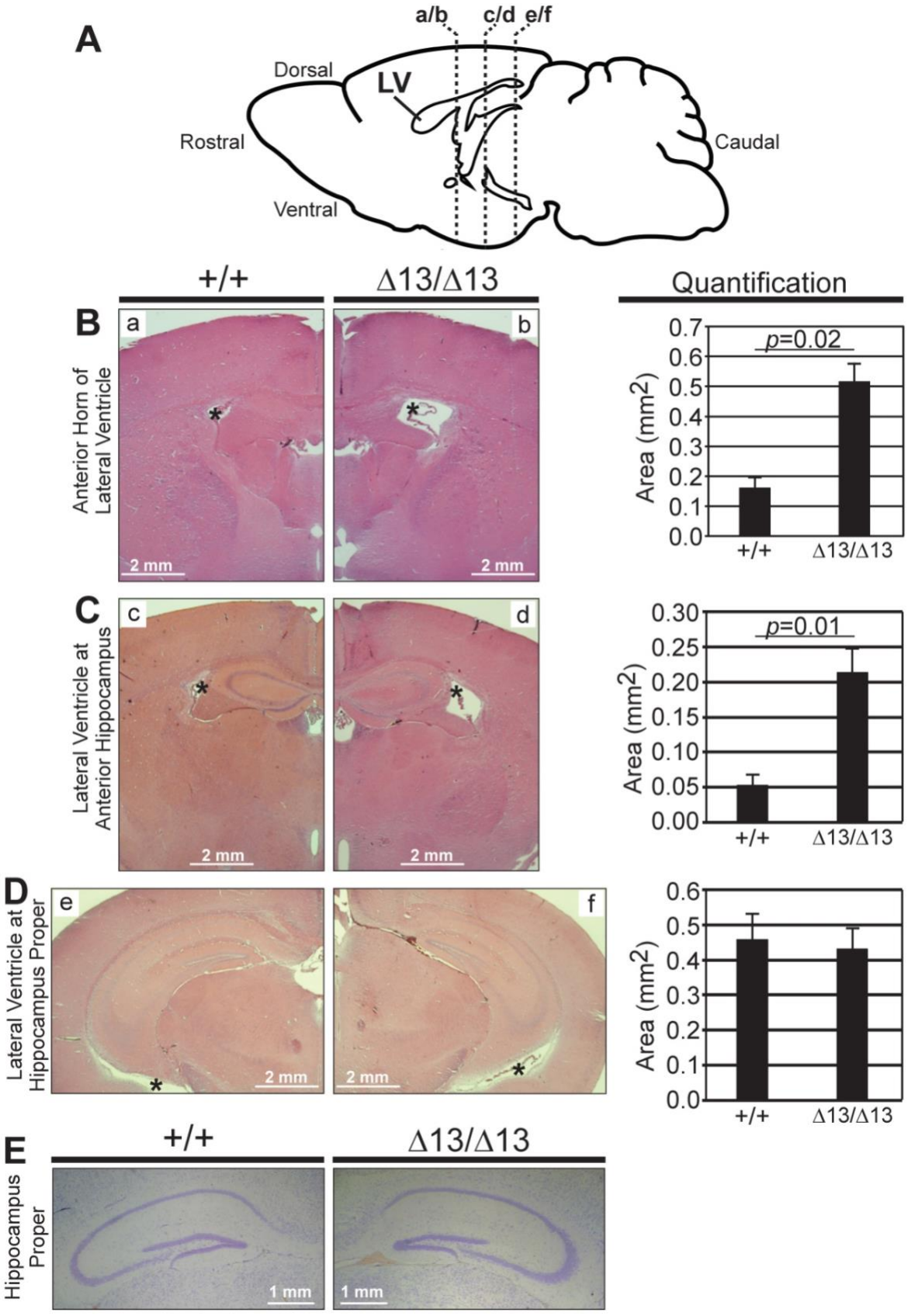
A
a/b
c/d
e/f
Dorsal
LV
Rostral
Caudal
Ventral
+/+
Δ13/Δ13
Quantification
B
a
b
Anterior Horn of Lateral Ventricle
2 mm
Area (mm2)
p=0.02
0.7
0.6
0.5
0.4
0.3
0.2
0.1
0.0
+/+
Δ13/Δ13
C
c
d
Lateral Ventricle at Anterior Hippocampus
p=0.01
0.30
0.25
0.20
0.15
0.10
0.05
0.00
D
e
f
Lateral Ventricle at Hippocampus Proper
0.6
E
Hippocampus Proper
1 mm

Figure 2-3: Analysis of brain and hippocampal morphology in *Zc3h14*$^{\Delta ex13/\Delta ex13}$ mice. (A) Diagram of lateral view of mouse brain and location of coronal sections shown in the following histological images. LV, lateral ventricle. Representative H&E stains of lateral ventricles of *Zc3h14*$^{+/+}$ (+/+) and *Zc3h14*$^{\Delta ex13/\Delta ex13}$ (Δex13/Δex13) adult mice at the following level of slices: (B) anterior horns of ventricles (***a***/***b*** in diagram), (C) anterior hippocampus (***c***/***d*** in diagram), and (D) hippocampus proper (***e***/***f*** in diagram). Magnification x2. Scale bars, 1 mm. *, lateral ventricle. H, hippocampus. Shown to the right are the corresponding quantifications of the area (mm^2) of the lateral ventricles at the indicated levels for *Zc3h14*$^{+/+}$ and *Zc3h14*$^{\Delta ex13/\Delta ex13}$mice. Error bars indicate SEM. For quantification of anterior horns of lateral ventricles; *Zc3h14*$^{+/+}$, n=3; *Zc3h14*$^{\Delta ex13/\Delta ex13}$, n=5. For quantification of lateral ventricles at anterior hippocampus; *Zc3h14*$^{+/+}$, n=3; *Zc3h14*$^{\Delta ex13/\Delta ex13}$, n=3. For quantification of lateral ventricles at hippocampus proper; *Zc3h14*$^{+/+}$, n=6; *Zc3h14*$^{\Delta ex13/\Delta ex13}$, n=6. (E) Comparable brain sections from *Zc3h14*$^{+/+}$ (+/+) and *Zc3h14*$^{\Delta ex13/\Delta ex13}$ (Δex13/Δex13) adult mice were stained with cresyl violet. Scale bars equal 100 µM.

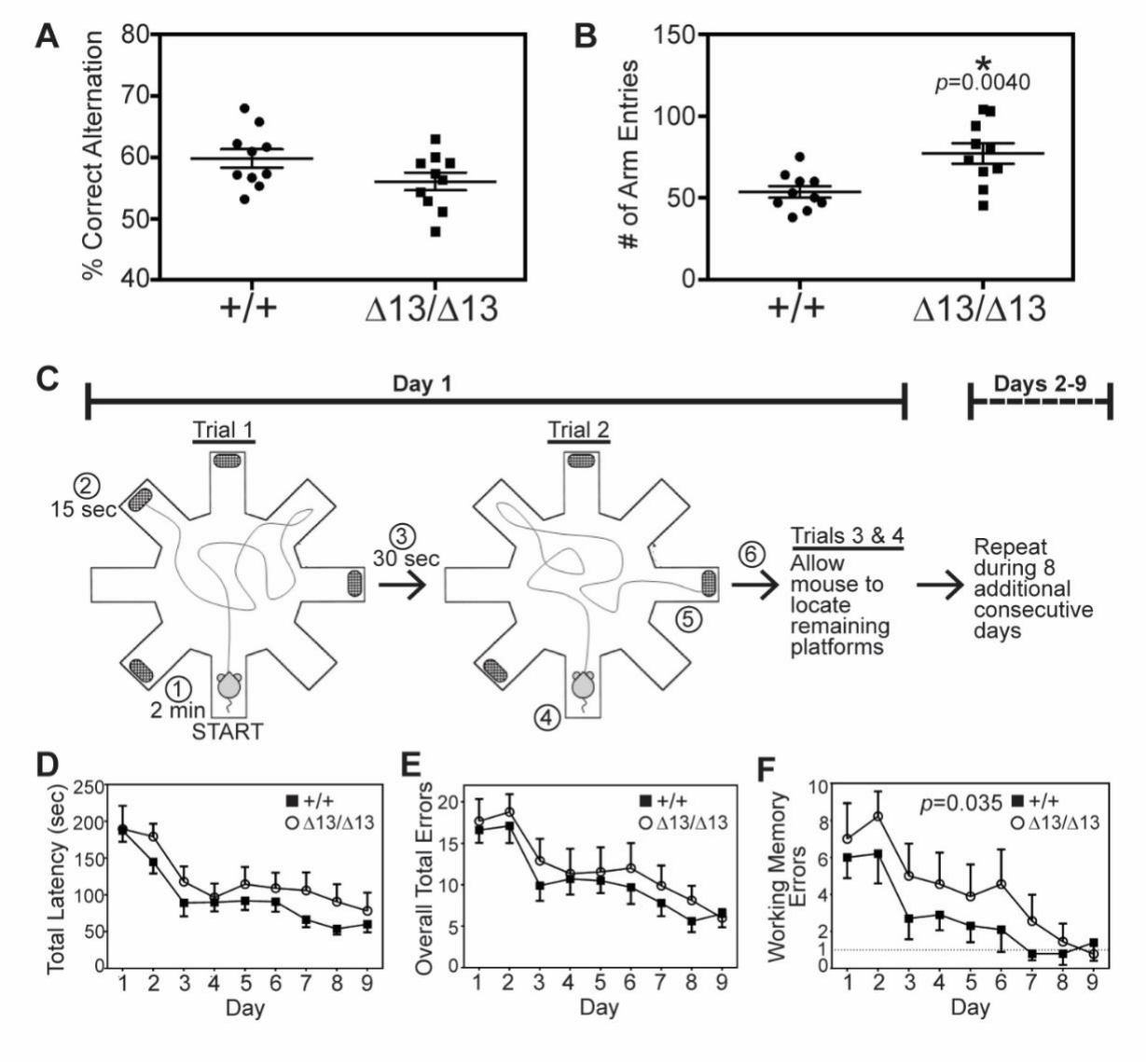

Figure 2-4: Analysis of *Zc3h14*$^{\Delta ex13/\Delta ex13}$ mice in behavioral paradigms. Mice were first tested in a Y-maze paradigm to analyze (A) %Correct Alternation between arms and (B) number of Arm Entries. We compared *Zc3h14*$^{+/+}$ (+/+) and *Zc3h14*$^{\Delta ex13/\Delta ex13}$ (Δex13/Δex13) adult mice in 20 independent trials as described in Materials and Methods. (A) There was no statistically significant difference detected in the %Correct Alternation between arms of the maze. (B) There was a statistically significant increase (p=0.004) in the number of arm entries (~40% increase) for *Zc3h14*$^{\Delta ex13/\Delta ex13}$ (Δex13/Δex13) compared to *Zc3h14*$^{+/+}$ (+/+). (C) Schematic of the WRAM

apparatus and 9-day testing procedure [306]. Mice are given two minutes to locate a hidden platform positioned at the far ends of four of eight arms. If a mouse is unable to locate a platform within two minutes of beginning the trial, it is gently guided to the nearest platform. Upon successful escape from water onto platform, mice are rewarded with 15 sec of rest on platform, followed by 30 sec of rest in a heated, dry cage. At the start of trial 2, the previously located platform is taken away and mice proceed to find one of the remaining hidden platforms. This process is repeated until all platforms are found, one in each trial. These four trials are repeated daily for a total of 9 consecutive days. Circled numbers indicate sequence of events in trials. The experiment compares *Zc3h14*$^{+/+}$ (+/+, closed squares) to *Zc3h14*$^{\Delta ex13/\Delta ex13}$ (Δ/Δ, open circles) mice. (D) Total latency is the average time (seconds) required per subject to complete all four trials for a specified day of testing. Comparing by test day, $p<0.0001$; comparing by genotype, $p=0.11$, indicating no difference. (E) Overall total errors is the average number of errors made per subject for all four trials for a specified day. Comparing by test day, $p<0.0001$; comparing by genotype, $p=0.20$, indicating no difference. (F) The average number of working memory errors, represented by reentry into any maze arm during a given trial, per subject for a specified day, is shown. Dashed line at 1 working memory error represents sufficient performance on WRAM. Comparing by test day, $p<0.0001$; comparing by genotype, $p=0.035$, revealing a statistically significant difference. Open circles indicate *Zc3h14*$^{\Delta/\Delta}$. Closed squares indicate *Zc3h14*$^{+/+}$. Behavioral tests were performed on independent cohorts of 3-4 month old mice. All tested mice were male. *Zc3h14*$^{+/+}$, n=10; *Zc3h14*$^{\Delta ex13/\Delta ex13}$, n=9. Error bars indicate SEM for (B), (C), (D).

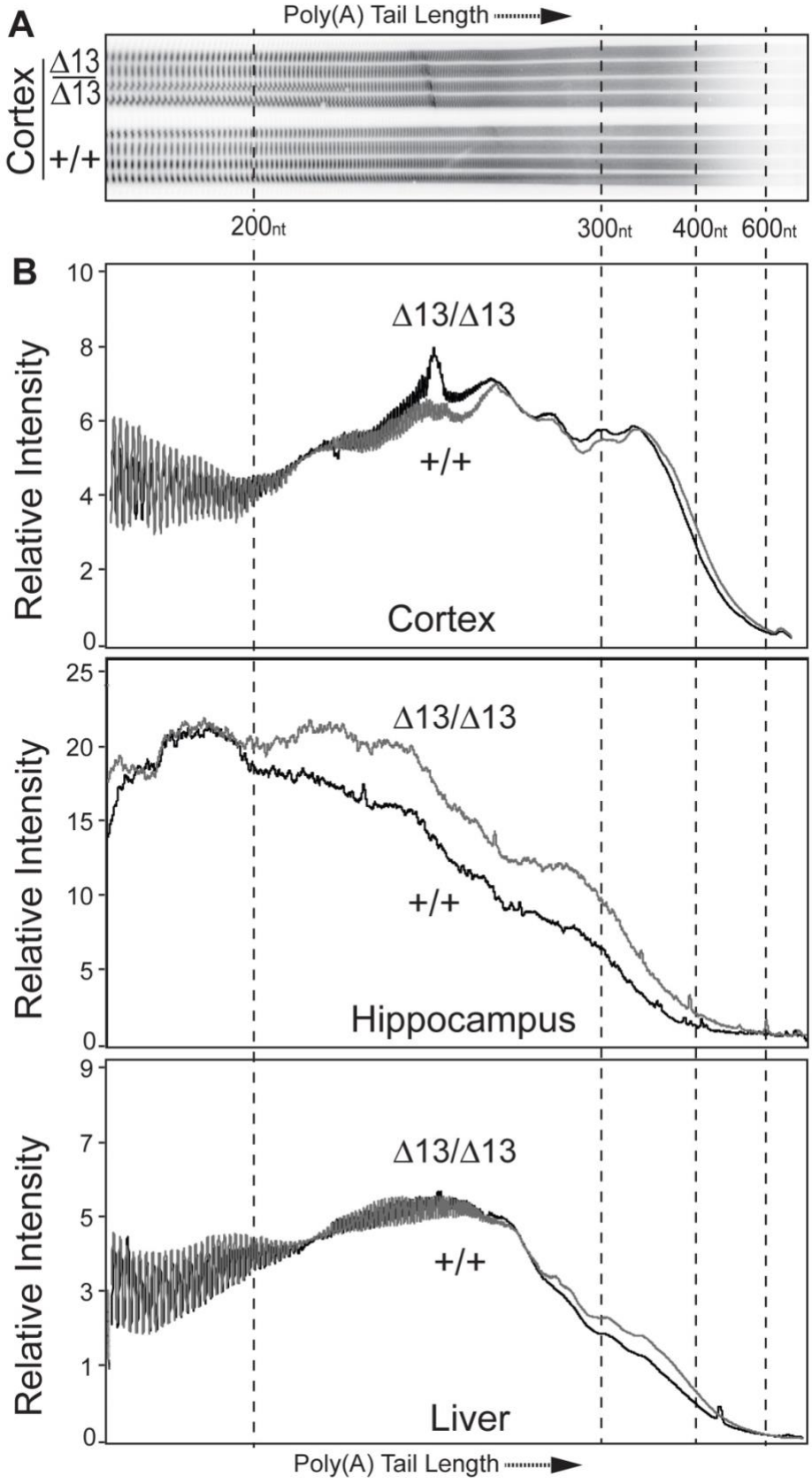
A
Poly(A) Tail Length
Cortex
Δ13/Δ13
+/+
200nt
300nt
400nt
600nt
B
Relative Intensity
Δ13/Δ13
+/+
Cortex
Hippocampus
Liver
Poly(A) Tail Length

Figure 2-5: ZC3H14 is required for proper poly(A) tail length control in mice. Bulk poly(A) tail length was analyzed from brain (cortex and hippocampus) and liver tissue. (A) A representative gel of the resolved bulk poly(A) sample isolated from cortex is shown for *Zc3h14*$^{\Delta ex13/\Delta ex13}$ (Δex13/Δex13) and *Zc3h14*$^{+/+}$ (+/+) hippocampal samples isolated from three independent mice. Approximate positions of nucleotide size markers (nt) are indicated. (B-D) To provide a quantitative measure of poly(A) tail length across samples, the Relative Intensity of the signal is plotted along the length of the poly(A) tail as determined by the size markers. The positions of the scan corresponding to 200, 300, 400, and 600 nucleotides (nt) are indicated. Results are presented for (B) Cortex, (C) Hippocampus and (D) Liver.

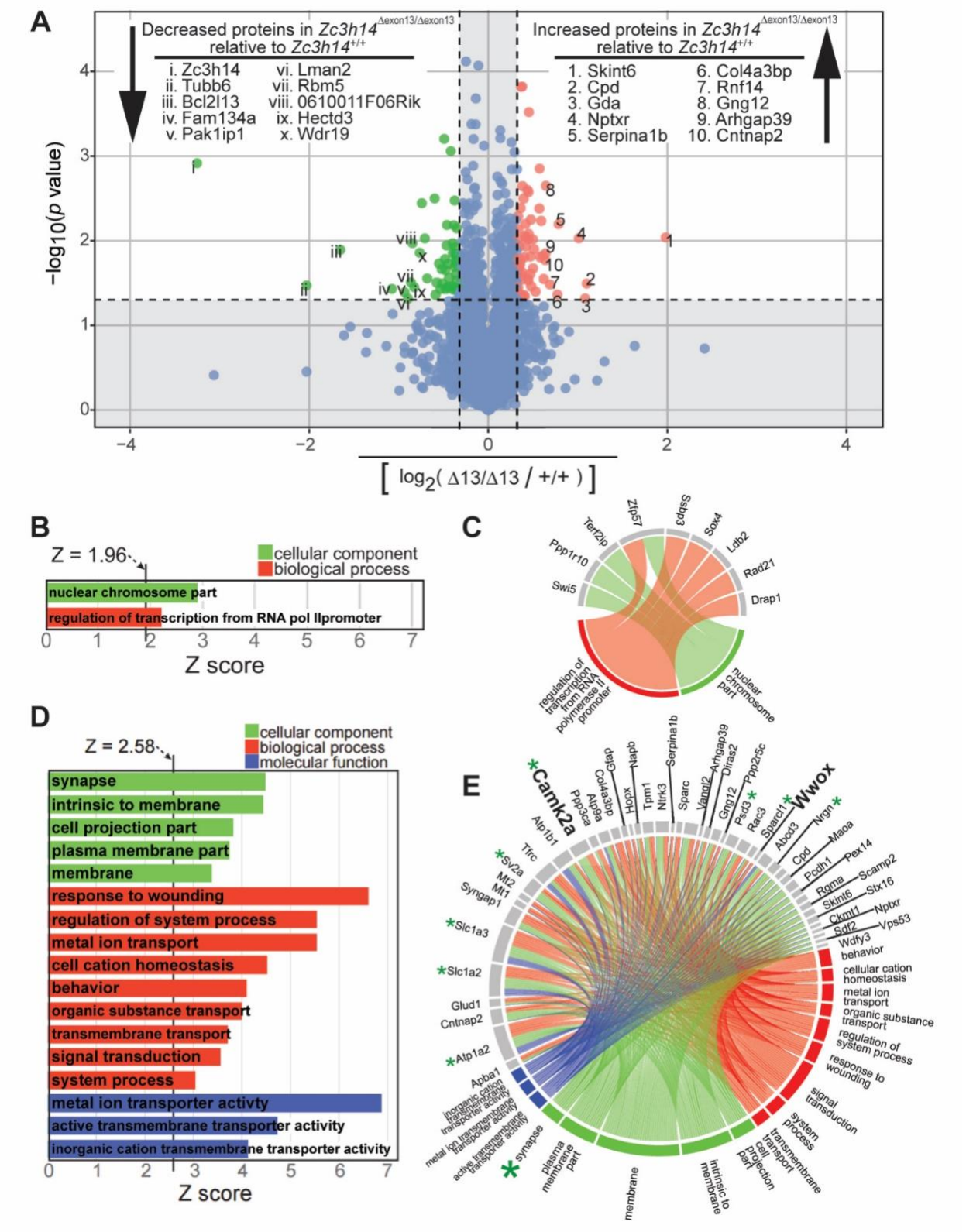
A
Decreased proteins in Zc3h14 Δexon13/Δexon13 relative to Zc3h14 +/+
i. Zc3h14
ii. Tubb6
iii. Bcl2l13
iv. Fam134a
v. Pak1ip1
vi. Lman2
vii. Rbm5
viii. 0610011F06Rik
ix. Hectd3
x. Wdr19
Increased proteins in Zc3h14 Δexon13/Δexon13 relative to Zc3h14 +/+
1. Skint6
2. Cpd
3. Gda
4. Nptxr
5. Serpina1b
6. Col4a3bp
7. Rnf14
8. Gng12
9. Arhgap39
10. Cntnap2
−log10(p value)
[log2(Δ13/Δ13 / +/+)]
B
Z = 1.96
cellular component
biological process
nuclear chromosome part
regulation of transcription from RNA pol IIpromoter
Z score
C
Zfp57
Ssbp3
Sox4
Ldb2
Rad21
Drap1
Ppp1r10
Terf2ip
Swi5
regulation of transcription from RNA polymerase II promoter
nuclear chromosome part
D
Z = 2.58
cellular component
biological process
molecular function
synapse
intrinsic to membrane
cell projection part
plasma membrane part
membrane
response to wounding
regulation of system process
metal ion transport
cell cation homeostasis
behavior
organic substance transport
transmembrane transport
signal transduction
system process
metal ion transporter activty
active transmembrane transporter activity
inorganic cation transmembrane transporter activity
Z score
E
Camk2a
Wwox
Atp1b1
Tfrc
Sv2a
Mt2
Mt1
Syngap1
Slc1a3
Slc1a2
Glud1
Cntnap2
Atp1a2
Apba1
synapse
plasma membrane part
membrane
intrinsic to membrane
cell projection part
transmembrane transport
system process
signal transduction
response to wounding
regulation of system process
organic substance transport
metal ion transport
cellular cation homeostasis
behavior
Wdfy3
Sdf2
Ckmt1
Skint6
Rgma
Pcdh1
Cpd
Abcd3
Sparcl1
Rac3
Psd3
Gng12
Vangl2
Dtnas2
Arhgap39
Ppp2r5c
Nptxr
Vps53
Stx16
Scamp2
Pex14
Maoa
Nrgn
Gtad
Col4a3bp
Atp6a
Ppp3ca
Hopx
Napb
Tpm1
Ntrk3
Sparc
Serpina1b

Figure 2-6: Proteomic analysis of *Zc3h14*$^{+/+}$ versus *Zc3h14*$^{\Delta ex13/\Delta ex13}$ hippocampi. (A) Volcano plot of all proteins with changed expression levels between *Zc3h14*$^{+/+}$ and *Zc3h14*$^{\Delta ex13/\Delta ex13}$ hippocampi, represented as colored dots. Statistically significantly changed proteins are highlighted as green dots and red dots. Among these, 51 proteins (including ZC3H14) have decreased expression (green dots) in *Zc3h14*$^{\Delta ex13/\Delta ex13}$ hippocampi when compared to *Zc3h14*$^{+/+}$ hippocampi, and 63 proteins have increased expression (red dots). Inclusion criteria for statistically significance are 1.25 fold change and $p < 0.05$. The top 10 hits for decreased and increased proteins are listed, along with their relative positions (Roman or Arabic numerals, respectively) on the volcano plot. The remaining proteins that did not meet statistical significance are represented as teal dots and fall within the shaded region of the plot, the boundaries of which are set by the aforementioned inclusion criteria. (B) For the decreased gene set, the two GO terms along with their Z-scores are listed. Inclusion criteria for this analysis are Z-score ≥ 1.96, *p* value < 0.05, and ≥ 3 genes per GO term. (C) The nine decreased genes that cluster and their corresponding GO terms are shown by a connecting line. (D) For the increased gene set, the list of GO terms along with their Z-scores are listed. Inclusion criteria for this analysis are Z-score ≥ 2.58, *p* value < 0.01, and ≥ 5 genes per GO term. (E) The increased genes that cluster into the listed GO terms in (D) are depicted. The corresponding GO terms are shown by a connecting line. For example, the large green asterisk indicates a GO term (synapse) and small green asterisks indicates the genes (Atp1a2, CaMK2α, Nrgn, Psd3, Slc1a2, Slc1a3, Sparcl1, Sv2a) that cluster to the GO term, also shown by connecting lines.

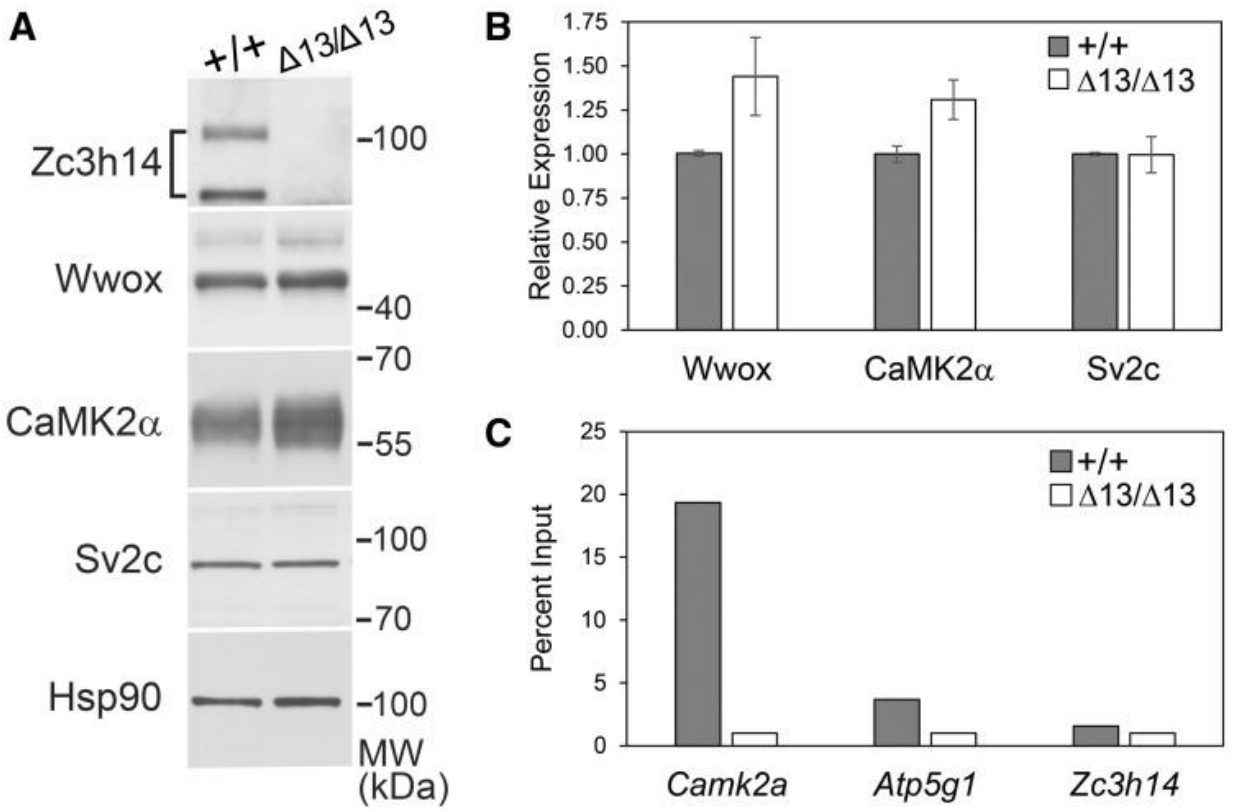

Figure 2-7: Validation of proteomic changes in *Zc3h14*$^{+/+}$ compared to *Zc3h14*$^{\Delta ex13/\Delta ex13}$ hippocampi. Total lysate was prepared from hippocampi of three *Zc3h14*$^{+/+}$ and three *Zc3h14*$^{\Delta ex13/\Delta ex13}$ hippocampi. Samples were probed with antibodies to ZC3H14, Wwox, Cank2a, and a control protein Hsp90. A representative immunobot is shown in (A) and the results from three independent samples are quantitated as a fold increase in (B). (C) To test whether ZC3H14 can bind to the *CaMK2a* transcript, we performed RNA immunoprecipitation from hippocampal lysates. Results are presented as fold enrichment compared to input for *CaMK2a*, a known target *Atp5g1*, and a control *Zc3h14*.

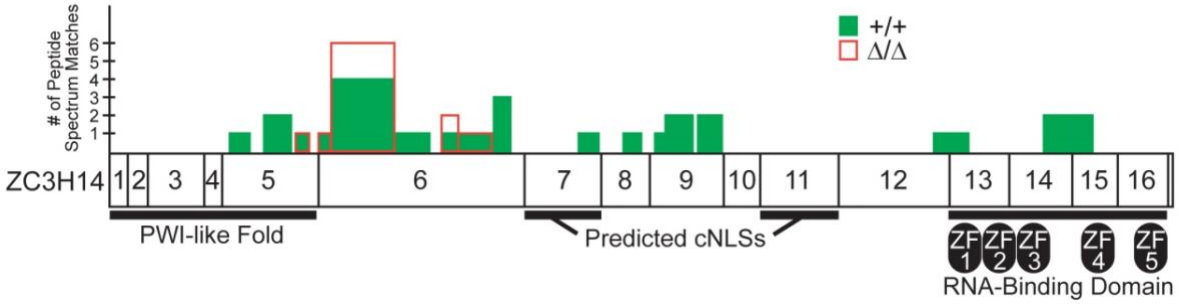

Figure 2-S1: Mass spectrometry analysis of *Zc3h14*$^{\Delta ex13/\Delta ex13}$ truncation products. A schematic of ZC3H14 with individual exons denoted is shown. The functional domains are indicated on the bottom of the schematic. The top shows peptide spectrum matches (PSM) for immunoprecipitation using an N-terminal ZC3H14 antibody of ZC3H14 isolated from *Zc3h14*$^{+/+}$ (green) or *Zc3h14*$^{\Delta ex13/\Delta ex13}$ (red) mouse whole brain lysate. The total number of identified PSMs for ZC3H14 is indicated. The location of the peptides identified is indicated by the position on the schematic. A scale bar to the left indicates the number of times fragment was identified. ZF, zinc finger.

A

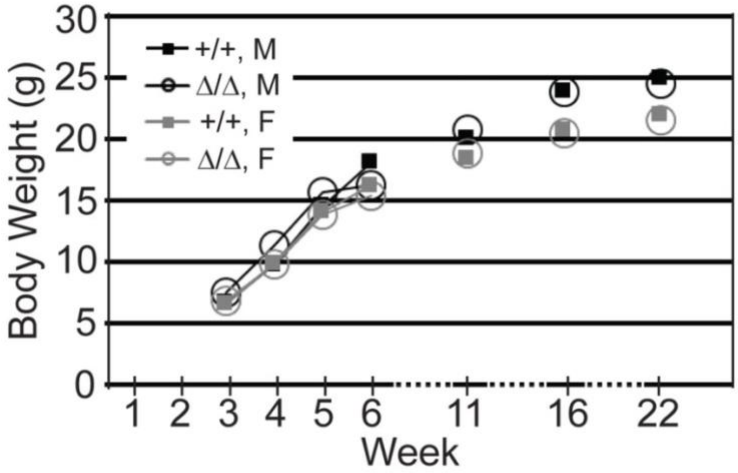

B

N values for Body Weight							
Week	3	4	5	6	11	16	22
Male +/+	7	7	8	5	7	8	6
Male Δ/Δ	3	9	8	4	5	10	6
Female +/+	6	6	8	7	6	9	5
Female Δ/Δ	4	13	9	7	8	13	9

C

SEM for Body Weight							
Week	3	4	5	6	11	16	22
Male +/+	0.46	0.96	0.93	0.32	1.07	0.40	0.60
Male Δ/Δ	1.63	0.94	0.81	1.23	1.66	0.91	1.84
Female +/+	0.33	0.43	0.33	0.32	0.44	0.44	0.73
Female Δ/Δ	0.98	0.63	0.65	0.61	0.73	0.49	0.56

D

P values for Body Weight							
Week	3	4	5	6	11	16	22
Male	0.49	0.26	0.41	0.16	0.87	0.97	0.82
Female	0.73	0.94	0.75	0.26	0.67	0.7	0.63

Figure 2-S2: Statistical values for body weight. (A) Mean weight (grams) of animals measured from juvenile to adult age is shown. M, male. F, female. For individual data points on mouse body weight reported, the following tables show (B) n values, (C) standard error of the means (SEMs), and (D) *p* values. +/+, wildtype. Δ/Δ, *Zc3h14*$^{\Delta ex13/\Delta ex13}$.

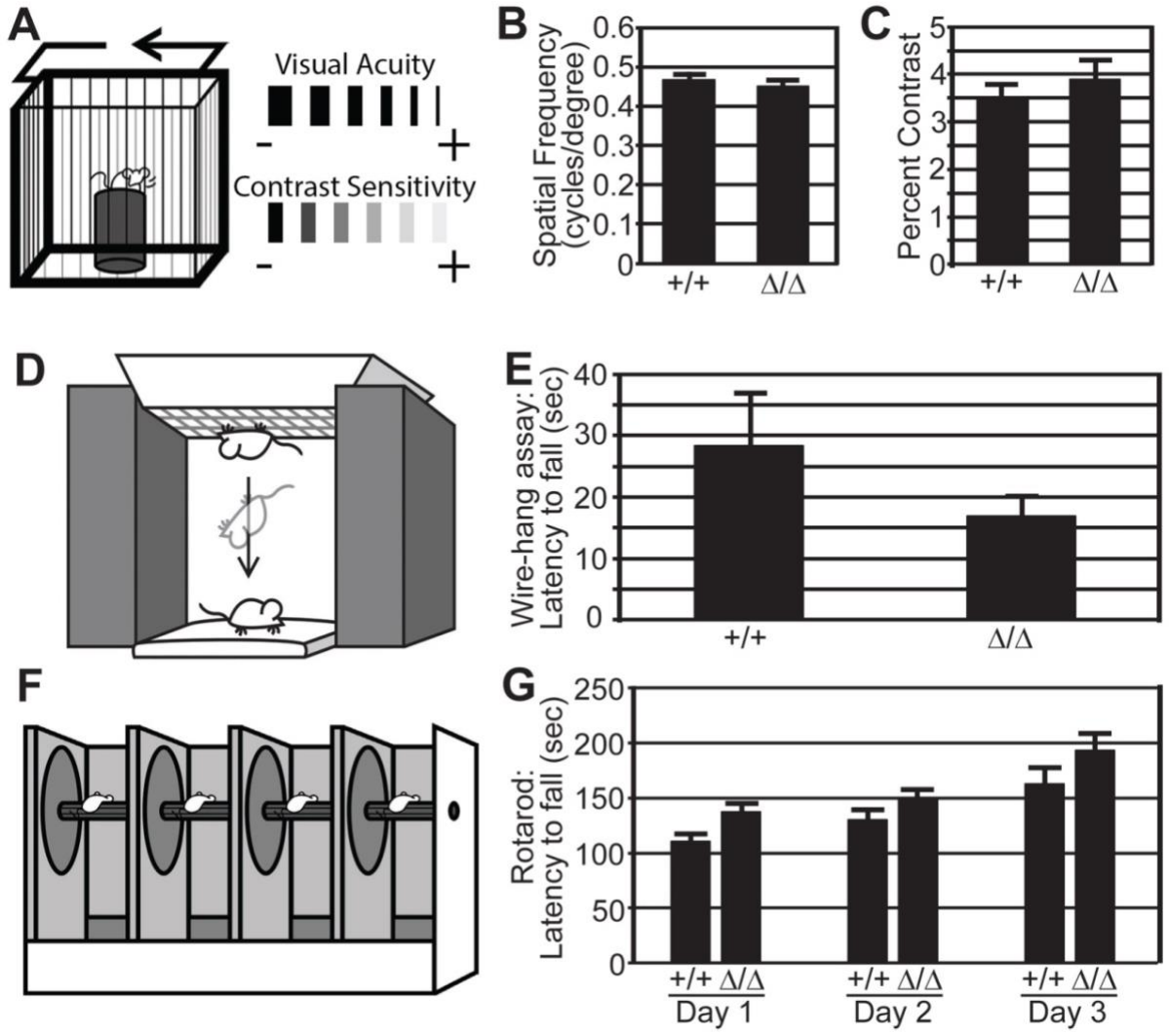

Figure 2-S3: Visual function and motor coordination assessments. To rule out possible visual or motor coordination deficits that could interfere with performance during water radial arm maze, we tested the visual and motor capabilities of the mice. When compared to controls (+/+), mutant (Δ/Δ, *Zc3h14*$^{\Delta ex13/\Delta ex13}$) mice performed at least as well on all visual and motor coordination assays. (A) Illustration of Optokinetic apparatus and visual cues. Visual acuity was measured by the ability of the mice to discern small spatial frequencies of white and black bars [348-350]. Contrast sensitivity was measured by the ability of the mice to discern alternating bars of similar shades of gray [348-350]. (B) Average of lowest spatial frequencies able to be

detected by mice by genotype is shown. (C) Average of lowest percent contrast able to be detected by mice by genotype is shown. For (B) and (C) *Zc3h14*$^{+/+}$, n=4; *Zc3h14*$^{\Delta ex13/\Delta ex13}$, n=4. (D) Illustration of wire-hang assay setup. (E) Latency to fall is the average time in seconds for mice, by genotype, to fall from a wire mesh when placed upside down against gravity. *Zc3h14*$^{+/+}$, n=9; *Zc3h14*$^{\Delta ex13/\Delta ex13}$, n=14. Comparing by genotype, p=0.1828. (F) Illustration of rotarod apparatus, which measures the ability of mice to balance on a rotating rod, tested across three days. (G) Latency to fall is the average time for mice to fall from the rotating rod, grouped by genotype. *Zc3h14*$^{+/+}$, n=9; *Zc3h14*$^{\Delta ex13/\Delta ex13}$, n=10. Differences between *Zc3h14*$^{+/+}$ and *Zc3h14*$^{\Delta ex13/\Delta ex13}$ on a given test day were not statistically significant after applying the Bonferroni correction for repeated measures. Error bars indicate SEM for all panels in figure.

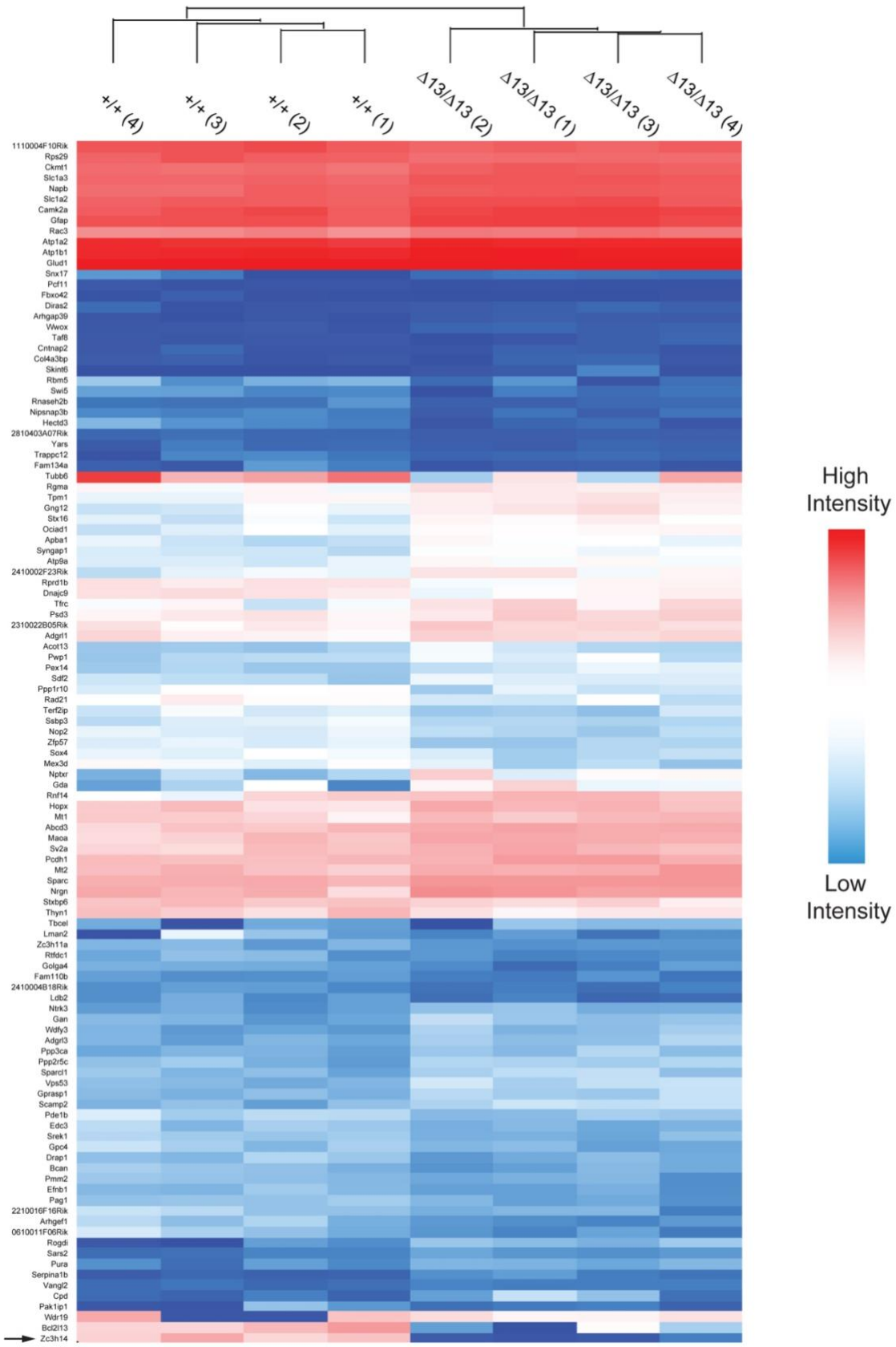
+/+ (4)
+/+ (3)
+/+ (2)
+/+ (1)
Δ13/Δ13 (2)
Δ13/Δ13 (1)
Δ13/Δ13 (3)
Δ13/Δ13 (4)
1110004F10Rik
Rps29
Ckmt1
Slc1a3
Napb
Slc1a2
Camk2a
Gfap
Rac3
Atp1a2
Atp1b1
Glud1
Snx17
Pcf11
Fbxo42
Diras2
Arhgap39
Wwox
Taf8
Cntnap2
Col4a3bp
Skint6
Rbm5
Swi5
Rnaseh2b
Nipsnap3b
Hectd3
2810403A07Rik
Yars
Trappc12
Fam134a
Tubb6
Rgma
Tpm1
Gng12
Stx16
Ociad1
Apba1
Syngap1
Atp9a
2410002F23Rik
Rprd1b
Dnajc9
Tfrc
Psd3
2310022B05Rik
Adgrl1
Acot13
Pwp1
Pex14
Sdf2
Ppp1r10
Rad21
Terf2ip
Sbbp3
Nop2
Zfp57
Sox4
Mex3d
Nptxr
Gda
Rnf14
Hopx
Mt1
Abcd3
Maoa
Sv2a
Pcdh1
Mt2
Sparc
Nrgn
Stxbp6
Thyn1
Tbcel
Lman2
Zc3h11a
Rtfdc1
Golga4
Fam110b
2410004B18Rik
Ldb2
Ntrk3
Gan
Wdfy3
Adgrl3
Ppp3ca
Ppp2r5c
Sparcl1
Vps53
Gprasp1
Scamp2
Pde1b
Edc3
Srek1
Gpc4
Drap1
Bcan
Pmm2
Efnb1
Pag1
2210016F16Rik
Arhgef1
0610011F06Rik
Rogdi
Sars2
Pura
Serpina1b
Vangl2
Cpd
Pak1ip1
Wdr19
Bcl2l13
Zc3h14
High Intensity
Low Intensity

Figure 2-S4: Heatmap with hierarchical clustering of significantly different proteins. Proteins identified as significantly different between *Zc3h14*$^{+/+}$ and *Zc3h14*$^{\Delta ex13/\Delta ex13}$ are presented in a heatmap with hierarchical clustering. It should be noted that the clustering discriminates between *Zc3h14*$^{+/+}$ and *Zc3h14*$^{\Delta ex13/\Delta ex13}$. Blue represents low protein levels and red represents high proteins levels.

Test	Measurement	Genotype	Average	SEM	*P*
Open Field	Time in center (sec)	+/+	35.10	5.18	0.03
		Δ13/Δ13	77.00	17.54	
	Number of entries into the center	+/+	18.20	9.38	0.05
		Δ13/Δ13	27.70	12.37	
	Total distance traveled (cm)	+/+	36.60	2.67	0.62
		Δ13/Δ13	34.50	3.28	
	Average speed (cm/sec)	+/+	0.10	0.00	0.61
		Δ13/Δ13	0.10	0.01	
Novel Cage	Time spent rearing (sec)	+/+	133.00	14.05	0.38
		Δ13/Δ13	117.40	10.27	
	Time spent digging (sec)	+/+	44.50	10.96	0.45
		Δ13/Δ13	34.30	7.38	
	Time spent grooming (sec)	+/+	13.80	1.81	0.81
		Δ13/Δ13	13.00	2.48	
Light-Dark Box	Latency to first dark entry (sec)	+/+	15.70	4.28	0.56
		Δ13/Δ13	21.20	8.34	
	Number of transitions between light/dark	+/+	23.80	1.79	0.22
		Δ13/Δ13	26.80	1.63	
	Time in dark (sec)	+/+	393.60	19.63	0.86
		Δ13/Δ13	386.60	33.20	
	Time in light (sec)	+/+	206.30	19.62	0.86
		Δ13/Δ13	386.60	33.20	
Fear Conditioning	Percent Freezing (%)	+/+	67.76	67.76	0.32
		Δ13/Δ13	61.14	61.14	

Table 2-S1: General behavioral tests. Twelve male *Zc3h14*$^{+/+}$ (+/+) and twelve *Zc3h14*$^{\Delta ex13/\Delta ex13}$(Δ/Δ) mice were evaluated using several paradigms as described in Materials and Methods to assess general activity in open field, exploratory behavior in novel cage, and anxiety in light-dark box.

Chapter 3

The Polyadenosine RNA Binding Protein ZC3H14 is Required in Mice for Proper Dendritic Spine Density

This paper is available on *bioRxiv* (*bioRxiv* 2020.10.08.331827; doi: https://doi.org/10.1101/2020.10.08.331827):

Outside contributions:

Dr. Kenneth Myers executed and generated all the data in Figure 2, which includes primary hippocampal neuronal culture and dendritic arborization analysis. He also performed the primary hippocampal neuronal culture, *in vitro* transfection of hippocampal neurons, and immunofluorescence microscopy in Figures 3-6. I performed all other studies and analyzed all the data collected for all the Figures presented.

3.1 Introduction

Brain development requires the formation of complex neural circuits where individual neurons communicate with one another at sites of connections termed synapses [351, 352]. The majority of excitatory synapses are positioned at dendritic spines, small protrusions found on the dendritic branches of neurons [353, 354]. These spines function as discrete biochemical signaling centers and are one of the primary sites of information processing in the brain [355-357]. During development, spines are generally thought to transition from thin filopodia through a maturation process that involves interim spine types into mature mushroom-shaped spines [139]. These spines remain dynamic even in mature neurons to support synaptic plasticity [358]. The size of the spine head positively correlates with the number of glutamate receptors at the postsynaptic surface [160, 359, 360]. Thus, the morphology of dendritic spines is tightly linked to synaptic strength. Consequently, defects in dendrite spine morphology are associated with numerous neurological disorders, including fragile X syndrome, autism, and epilepsy [235, 361-363].

Because dendrites and axons extend far away from the neuronal cell body, tight regulation of gene expression is essential for normal neuronal development and synaptic plasticity. Once exported from the nucleus, mRNAs are transported to local sites for translation, allowing new proteins to be rapidly synthesized at or near individual synapses in response to stimuli such as synaptic activity [364, 365]. This translation in dendrites provides a mechanism for maintaining and modifying the local proteome that is more rapid and efficient than synthesizing proteins in the cell body and transporting them to a specific site [366]. Numerous studies have directly linked synaptic plasticity to local translation and have identified specific subsets of mRNAs that localize preferentially to dendrites and dendritic spines [102, 113, 367, 368]. A large number of RNA binding proteins mediate the many events that comprise post-transcriptional gene

regulation, including events that occur in the nucleus prior to export to the cytoplasm [369], such as splicing, editing, and polyadenylation and the cytoplasmic events that contribute to local translation [366]. Numerous studies have linked RNA binding proteins to synaptic plasticity, learning and memory, and neurological disease [19, 370-374].

Many of the RNA binding proteins linked to neurological disease play multiple roles in post-transcriptional regulation of gene expression [375]. ZC3H14 (Zinc Finger CCCH-Type Containing 14) is an evolutionarily conserved, ubiquitously expressed polyadenosine RNA-binding protein [249]. Mutations in the *ZC3H14* gene cause an autosomal-recessive, non-syndromic form of intellectual disability [247, 288, 376]. Studies examining the essential budding yeast orthologue, Nab2, have identified roles in regulating poly(A) tail length, RNA splicing, and mRNA decay [251, 253, 263, 290, 377]. The *Drosophila* orthologue of ZC3H14, Nab2, also plays a role in poly(A) tail length control [247, 264, 277]. Studies in mammalian cells show that regulation of poly(A) tail length is a conserved function of ZC3H14 [264]. Loss of Nab2 function in yeast or flies is lethal [247, 251] and mutant flies exhibit defects in locomotor behavior as well as abnormal brain morphology [247, 277]. Work exploiting the *Drosophila* system showed that Nab2 function is essential in neurons as phenotypes observed in flies lacking Nab2 can be rescued by neuronal-specific expression of Nab2 [247]. These studies provide insight into why mutations in the ubiquitously expressed *ZC3H14* gene cause neurological deficits.

Multiple isoforms of ZC3H14 are produced in mammals through alternative splicing (See Fig. 3C) [249]. All four ZC3H14 isoforms include the essential zinc finger RNA-binding domain [252]; however, isoforms 1-3 contain an N-terminal Proline-Tryptophan-Isoleucine (PWI)-like domain as well as a predicted nuclear localization signal, while isoform 4 contains an alternative

first exon. ZC3H14 isoforms 1-3 are ubiquitously expressed, whereas isoform 4 is expressed primarily in testis [249]. While ZC3H14 isoforms 1-3 are primarily localized to nuclear speckles [249, 276], analysis of cultured primary rat hippocampal neurons shows that ZC3H14 is found in both the nucleus and in neuronal processes [312]. Studies of cultured primary *Drosophila* neurons reveal that Nab2 is present within puncta in neurites, associated with both ribonucleoprotein complexes and polyribosomes [312]. In addition, cell fractionation assays from whole mouse brain reveal a cytoplasmic pool of ZC3H14, although the majority of the protein is found in the nucleus [378]. These observations regarding the localization of ZC3H14 are consistent with studies of the budding yeast Nab2 protein, which show that Nab2 is a shuttling RNA binding protein that can exit the nucleus in an poly(A) RNA-dependent manner [255]. This dynamic localization of Nab2/ZC3H14, means that ZC3H14 could regulate target RNAs in the nucleus and/or the cytoplasm.

To explore the function of ZC3H14 in mammals, a *Zc3h14* mutant mouse was generated [379]. This mouse model removes exon 13 of *Zc3h14*, which is the first common exon present in all *Zc3h14* splice variants. This exon encodes part of the essential zinc finger RNA binding domain and thus no functional ZC3H14 protein is produced in homozygous $Zc3h14^{\Delta ex13/\Delta ex13}$ mice [253, 379]. These studies revealed that the ZC3H14 protein is not essential in mice; however $Zc3h14^{\Delta ex13/\Delta ex13}$ mice show defects in working memory, further supporting a role for ZC3H14 in normal brain function [379]. Proteomic analysis comparing hippocampi from $Zc3h14^{\Delta ex13/\Delta ex13}$ mice to control $Zc3h14^{+/+}$ mice identified a number of proteomic changes that occur upon the loss of ZC3H14, including many changes in proteins with key synaptic functions. Mice lacking ZC3H14 show an increase in the steady-state levels of CaMKIIα, a protein kinase that plays a key role in learning and memory [379-383]. Furthermore, the ZC3H14 protein binds

to *CaMKIIα* mRNA [379]. Complementary work in *Drosophila* shows that Nab2 associates with *CaMKII* mRNA and represses a *CaMKII* translational reporter [312]. Taken together, these studies suggest a role for ZC3H14 in regulating expression of CaMKII. As CaMKIIα plays key roles in regulating dendritic spine morphology [384], these results suggest that the loss of ZC3H14 could alter dendritic spine development; however, whether ZC3H14 is required for proper dendritic spine density or morphology has not yet been examined.

In this study, we analyze the *Zc3h14*$^{\Delta ex13/\Delta ex13}$ mouse model and find that loss of ZC3H14 decreases dendritic spine density both *in situ* and *in vitro*. This decrease in spine density corresponds to a reduction in the number of mushroom-shaped spines. Conversely, overexpression of ZC3H14 increases the density of spines, in a ZC3H14 isoform-specific manner. Finally, ZC3H14 is present in synaptosomes and the loss of ZC3H14 leads to an increase in the steady-state level of CaMKIIα in synaptosomes. Together, our results demonstrate that ZC3H14 is required for proper dendritic spine density and suggest a role for ZC3H14 in regulating dendritic spine morphogenesis.

3.2 Results

3.2.1 Spine density in the dentate gyrus is decreased in adult mice upon loss of ZC3H14

To assess whether the loss of ZC3H14 alters dendritic spine density, we performed Golgi staining [385, 386] on *Zc3h14*$^{+/+}$ (+/+) and *Zc3h14*$^{\Delta ex13/\Delta ex13}$ (Δ*13*/Δ*13*) whole male mouse brains at postnatal day 7 (P7) and 5 months (Fig. 1). Samples were prepared as described in Materials and Methods and dentate gyrus granule neurons were imaged by brightfield microscopy (Fig. 1A). We did not observe any obvious qualitative difference in dendritic spine density comparing granule cells from *Zc3h14*$^{+/+}$ and *Zc3h14*$^{\Delta ex13/\Delta ex13}$ mice at P7. Quantification

of dendritic spine density (Fig. 1B) reveals no statistically significant difference in spine density upon the loss of ZC3H14 as assessed at this time point (p>0.05; +/+ n=43 neurons, 6 mice; Δ*13*/Δ*13* n=35 neurons, 5 mice). However, dentate gyrus granule cells at 5 months (Fig. 1C) show reduced spine density in *Zc3h14*$^{\Delta ex13/\Delta ex13}$ mice as compared to *Zc3h14*$^{+/+}$ mice. Indeed, quantification of the samples from 5 months (Fig. 1D) confirms that spine density is significantly decreased in *Zc3h14*$^{\Delta ex13/\Delta ex13}$ mice at 5 months (p<.0005; +/+ n=33 neurons, 3 mice; Δ*13*/Δ*13* n=33 neurons, 3 mice). Together, these data demonstrate that loss of ZC3H14 in mice results in reduced dendritic spine density in the dentate gyrus at 5 months, with no statistically significant difference detected in this brain region at P7.

3.2.2 Loss of ZC3H14 does not alter dendritic arbor development in cultured primary hippocampal neurons

We previously showed that ZC3H14 is found in neurites of cultured neurons [312]. To determine whether ZC3H14 is required for normal dendritic development, we cultured primary hippocampal neurons from *Zc3h14*$^{+/+}$ (+/+) and *Zc3h14*$^{\Delta ex13/\Delta ex13}$ (Δ*13*/Δ*13*) E17.5 mouse brains as described in Materials and Methods. Neurons were transfected with GFP, to visualize neuronal morphology, and then fixed at DIV12. We did not detect any qualitative differences between the dendritic arbors of *Zc3h14*$^{+/+}$ and *Zc3h14*$^{\Delta ex13/\Delta ex13}$ hippocampal neurons (Fig. 2A). To analyze the morphology of these cultured neurons (+/+ n=54 neurons, Δ*13*/Δ*13* n=54 neurons), we measured both the total dendritic length (Fig. 2B) and the number of dendritic tips (Fig. 2C). To assess dendritic arbor complexity, we performed Sholl analysis [387], which counts the number of dendritic branches crossing concentric circles at regular radial distances away from the soma (+/+ n=51 neurons, Δ*13*/Δ*13* n=51 neurons) (Fig. 2D). In all these analyses,

no statistically significant differences were identified between *Zc3h14*$^{+/+}$ and *Zc3h14*$^{\Delta ex13/\Delta ex13}$ neurons (p>0.05), suggesting that ZC3H14 is not required for proper dendritic arbor development *in vitro*.

3.2.3 Loss of ZC3H14 causes a decrease in dendritic spine density in cultured primary hippocampal neurons

As *Zc3h14*$^{\Delta ex13/\Delta ex13}$ neurons show reduced spine density in brain tissue compared to control *Zc3h14*$^{+/+}$ neurons (Fig. 1B,D), we employed an *in vitro* culture system to further analyze dendritic spine density and morphology. DIV11 primary hippocampal neurons were co-transfected with GFP and mRuby-tagged Lifeact (Lifeact-mRuby), a small actin-binding peptide that labels dendritic spines [388], to visualize dendritic spines. Neurons were then fixed and imaged at DIV19. We first compared neurons from control *Zc3h14*$^{+/+}$ mice to neurons from *Zc3h14*$^{\Delta ex13/\Delta ex13}$ mice (Fig. 3A). Semi-automated quantification reveals a statistically significant decrease (p<0.03) in dendritic spine density in neurons lacking ZC3H14 (Fig. 3B).

To confirm that the decrease in spine density observed in neurons cultured from *Zc3h14*$^{\Delta ex13/\Delta ex13}$ mice results from the loss of ZC3H14 specifically, we performed a rescue experiment. Exogenous ZC3H14 was co-transfected into DIV11 hippocampal neurons along with Lifeact-mRuby, and cells were then fixed and imaged at DIV19. For this experiment, we included two different isoforms of ZC3H14 (Fig. 3A,C) generated by alternative splicing [249]. Both ZC3H14 Isoform 1 (Iso 1) and Isoform 3 (Iso 3) include the functionally important domains of ZC3H14, namely the zinc finger RNA binding domain [252, 389] and the N-terminal PWI-like domain [389, 390], as well as a predicted nuclear localization signal (Fig. 3C). These ZC3H14 isoforms are primarily localized to the nucleus but can be detected in the cytoplasm of

neurons [263, 276, 312, 378]. As shown in Figure 3A (Δ*13/*Δ*13* +Iso1 *and* Δ*13/*Δ*13* +Iso3), exogenous expression of either ZC3H14 Iso1 or ZC3H14 Iso3 appears to rescue dendritic spine density, which is confirmed through a semi-automated quantitative analysis of dendritic spine density [Δ*13/*Δ*13* (+Iso1) $p<0.01$; Δ*13/*Δ*13* (+Iso3) $p<0.02$] (Fig. 3B). These data indicate that the loss of ZC3H14 reduces dendritic spine density in mature primary hippocampal neurons *in vitro*.

The morphology of dendritic spines is heterogeneous, often representing differences in their stability and function [353, 391]. To determine if the loss of ZC3H14 affects spine morphology in DIV19 hippocampal neurons, we classified each spine as "Stubby", "Thin", or "Mushroom" [144, 392-394] according to both length and the head width to neck width ratio (Fig. 4A). For this analysis, 3D reconstructions of dendritic branches were generated, and individual spines from control $Zc3h14^{+/+}$ (+/+), $Zc3h14^{\Delta ex13/\Delta ex13}$ (Δ*13/*Δ*13*), $Zc3h14^{\Delta ex13/\Delta ex13}$ + ZC3H14 Isoform 1 (Δ*13/*Δ*13 (+Iso1)*) and $Zc3h14^{\Delta ex13/\Delta ex13}$ + ZC3H14 Isoform 3 (Δ*13/*Δ*13 (+Iso3)*) neurons were classified as stubby- (purple), thin- (light blue), or mushroom- (dark red) type (Fig. 4B). Semi-automated quantitation revealed no statistically significant changes in the density of either stubby- or thin-type spines for any of the samples examined (Fig. 4C). In contrast, we detected a statistically significant decrease in the density of mushroom-type spines present in Δ*13/*Δ*13* neurons as compared to control +/+ neurons ($p=0.0002$; +/+ n=18 neurons, Δ*13/*Δ*13* n=18 neurons). This decrease in mushroom-type spines is rescued by exogenous expression of either ZC3H14 Isoform 1 [compare Δ*13/*Δ*13 (+Iso1)* neurons to Δ*13/*Δ*13* neurons ($p<0.0001$; Δ*13/*Δ*13 (+Iso1)* n=23 neurons)] or ZC3H14 Isoform 3 [compare Δ*13/*Δ*13 (+Iso3)* neurons to Δ*13/*Δ*13* neurons ($p<0.002$; Δ*13/*Δ*13 (+Iso3)* n=19 neurons)]. Taken together, these

results demonstrate that loss of ZC3H14 leads to an overall decrease in the number of mushroom-shaped spines in cultured hippocampal neurons at DIV19.

3.2.4 Overexpression of ZC3H14 increases dendritic spine density, specifically by increasing the number of thin spines

Loss of ZC3H14 causes a decrease in dendritic spine density (Fig. 3,4). To further test a role for ZC3H14 in modulating dendritic spine morphology, we examined whether an increase in the level of ZC3H14 impacts dendritic spine density. For this analysis, primary hippocampal neurons from control *Zc3h14*$^{+/+}$ mice were co-transfected at DIV11 with Lifeact-mRuby and GFP (+/+), GFP-ZC3H14-Isoform1 (+/+ *(+Iso1)*), or GFP-ZC3H14-Isofom3 *(+/+ (+Iso3)*), and then fixed and imaged at DIV19 (Fig. 5A). Semi-automated quantification of spine density shows a statistically significant increase in spine density in +/+ *(+Iso1)* neurons as compared to control +/+ [(p<0.0005; +/+ n=21 neurons, +/+ *(+Iso1)* n=14 neurons)], but no significant difference in spine density in +/+ *(+Iso3)* neurons as compared to control +/+ [(p>0.05; +/+ *(+Iso3)* n=19 neurons)] (Fig. 5B). This analysis reveals that overexpression of ZC3H14 Isoform 1, but not ZC3H14 isoform 3, causes a statistically significant increase in dendritic spine density *in vitro*.

To assess whether overexpression of ZC3H14 alters the density of specific dendritic spine subtypes, individual spines were 3D reconstructed to measure their morphology and classify each spine as stubby- (purple), thin- (light blue), or mushroom-type (dark red). Representative reconstructions for +/+, +/+ *(+Iso1)*, and +/+ *(+Iso3)* DIV19 primary hippocampal neurons are shown in Figure 6A. Semi-automated analysis revealed a significant increase in thin-type spines in neurons overexpressing ZC3H14 Isoform 1 [(compare +/+ and

+/+ (+Iso1) neurons (p<0.0001)] with no statistically significant differences in stubby- or mushroom-type (Fig 6B).There were no significant changes in any of the dendritic spine classifications in neurons overexpressing ZC3H14 Isoform 3 compared to +/+. The increase specifically in thin-type spines, with no difference in stubby- or mushroom-type spines, in *+/+ (+Iso1)* DIV19 hippocampal neurons is consistent with a model where levels of ZC3H14 must be tightly regulated to ensure proper dendritic spine morphology.

3.2.5 ZC3H14 is present in synaptosomes and loss of ZC3H14 results in increased steady state levels of CaMKIIα in synaptosomes

Previous work has demonstrated that there is a pool of ZC3H14 present in the cytoplasm of neurons [312, 378]. To determine whether ZC3H14 is present in synaptosomes, which contain postsynaptic dendritic spines and presynaptic terminals [395], fractionation was performed as illustrated in Figure 7A. We isolated three fractions from postnatal day 0 (P0) whole brains: the homogenate (Hom), cytosol (Cyt), and synaptosomes (Syn). Synaptophysin, a protein localized specifically to synaptic vesicle membranes [396], is enriched in the synaptosome (Syn) fraction from this preparation (Fig. 7B), providing evidence for successful enrichment of synaptosomal proteins. Immunoblotting performed on Hom, Cyt, and Syn fractions collected from *Zc3h14*$^{+/+}$ (+/+) and *Zc3h14*$^{\Delta ex13/\Delta ex13}$ (Δ*13*/Δ*13*) P0 whole brains show that ZC3H14 is detected in all three fractions, including synaptosomes (Fig. 7C). As a control, no full length ZC3H14 protein is detected in the samples from the Δ*13*/Δ*13* brains. This demonstrates that ZC3H14 is present in synaptosomes.

As previous studies have implicated ZC3H14 in regulating the expression of CaMKII [312, 379], immunoblotting was performed to assess levels of CaMKII and PSD-95, a protein critical

for maintaining the post synaptic density in dendritic spines [397], specifically in synaptosomes (Fig. 7D). Results of this analysis show an increase in the level of CaMKIIα detected in the Δ*13/*Δ*13* synaptosomes compared to control, which is statistically significant ($p<0.04$; +/+ n=3, Δ*13/*Δ*13* n=3) (Fig. 7E). In contrast, no statistically significant difference ($p>0.05$) was detected in the level of PSD-95 present in these synaptosomal fractions (Fig. 7D,E). Taken together, these data support a model where ZC3H14 is required for proper steady-state levels of CaMKIIα protein in synaptosomes.

3.3 Discussion

This study employs a previously generated mouse model, *Zc3h14*$^{\Delta ex13/\Delta ex13}$ [379], to explore the requirement for ZC3H14 in dendritic spine density and morphology. Results of this analysis demonstrate that ZC3H14 is essential for proper dendritic spine density based on both *in situ* analysis of mouse brain and studies of cultured primary hippocampal neurons. In both cases, loss of ZC3H14 causes a decrease in overall dendritic spine density. Studies in the cultured primary hippocampal neurons reveal that this decrease in spine density is primarily due to loss of mushroom-type spines. Overexpression of ZC3H14 in cultured hippocampal neurons increases overall dendritic spine density, primarily driven by an increase in the number of thin-type spines. As ZC3H14 is present in synaptosomes, these changes in dendritic spine morphology could result from altered local translation. Finally, loss of ZC3H14 causes an increase in levels of CaMKIIα in synaptosomes, which could be linked to changes in dendritic spine morphology.

Either loss of ZC3H14 or an increase in levels achieved through transfection of cultured primary hippocampal neurons alters overall dendritic spine density. While the loss of ZC3H14 causes a decrease in dendritic spine density, overexpression of ZC3H14, causes an increase. The

subtypes of dendritic spines affected in these two cases are distinct from one another. Loss of ZC3H14 affects mushroom-type spines, while overexpression of ZC3H14 increases the number of thin-type spines. The decrease in mushroom-type spines observed in neurons cultured from *Zc3h14*$^{\Delta ex13/\Delta ex13}$ mouse hippocampi compared to control (Fig. 4) is rescued by restoring levels of ZC3H14 via transfection, providing evidence that the changes are due to loss of ZC3H14. The overexpression studies are more challenging to interpret because levels of overexpression of ZC3H14 likely vary among the neurons transfected. The neuronal cultures were co-stained to detect ZC3H14, but endogenous ZC3H14 is already abundant in nuclear speckles [249, 276], making identification of neurons with overexpression of ZC3H14 difficult to identify. However, transfection of ZC3H14 into +/+ neurons did cause a statistically significant increase specifically in thin-type spines, providing some evidence that ZC3H14 can regulate different types of spines. Future studies could employ variants of ZC3H14 with decreased RNA binding, which would first need to be generated and characterized, to assess whether this function is required both for the rescue and the effects observed upon overexpression of ZC3H14.

Dendritic spines are highly heterogeneous in both function and morphology [398]. Here, we detected different effects with regard to stubby, thin, and mushroom-type spines in response to loss or gain of ZC3H14. Stubby spines are characterized by their lack of a definable head or neck, as well as their short squat appearance. While they contain large excitatory synapses, stubby spines are considered to be immature, and hence are not found as readily in adult brains [399]. Thin spines are fairly dynamic with long thin necks and small bulbous heads, which contain small excitatory synapses. Mushroom spines are more static with thin necks and broad heads that contain the largest excitatory synapses. Previous studies have linked spine head volume with the size of the postsynaptic density (PSD), a dense and dynamic meshwork of

proteins that mediate postsynaptic signaling [393, 399]. Moreover, spine head volume correlates with AMPA receptor density and NMDA receptor-dependent calcium signaling, thus connecting spine morphology with synaptic strength [132, 359, 400]. Loss of ZC3H14 leads to a reduction in dendritic spine density, both i*n situ* and *in vitro*. This reduction *in vitro* is the result of a decrease specifically in the number of mushroom-shaped spines. Importantly, we were able to rescue both the overall and mushroom-specific reductions in spine density, by exogenously expressing ZC3H14 in individual hippocampal neurons from *Zc3h14*$^{\Delta ex13/\Delta ex13}$ mice. Together, this suggests that ZC3H14 could be required for the development of mature mushroom-shaped spines. Alternatively or in addition, ZC3H14 could play a role in the maintenance or stability of mushroom spines. Future experiments capable of monitoring spine dynamics would be required to distinguish between these possible roles for ZC3H14 in modulating mushroom-type spines.

Our *in situ* studies examined the dentate gyrus. The dentate gyrus is a region of the hippocampus highly associated with learning and memory, particularly spatially-based tasks [401-403]. Likely due to the tight level of control required at excitatory synapses for proper neuronal function, a number of neurological disorders show alterations in spine density in various regions of the brain, including the dentate gyrus [235, 242, 404, 405]. Of particular note, altered spine density in the dentate gyrus has been observed in a knockout mouse model of Fragile X Syndrome [242] , the most common form of inherited intellectual disability [406]. The Fragile X Mental Retardation (FMRP) RNA binding protein, which is lost in Fragile X Syndrome, is implicated in proper regulation of local translation in neurons [407, 408], providing an example of a ubiquitously expressed RNA-binding proteins required to regulate dendritic spine properties [409]. Our studies show a significant decrease in spine density in the dentate granule neurons of adult *Zc3h14*$^{\Delta ex13/\Delta ex13}$ mice *in situ*, which is consistent with prior studies of

these mice where a defect in working memory was detected in adult *Zc3h14*$^{\Delta ex13/\Delta ex13}$ mice in a spatially-based learning/memory behavioral assay [379]. These results suggest that the ZC3H14 RNA binding protein could play a similar role to FMRP in regulating transcripts critical for proper dendritic spine function. Consistent with this idea, studies in *Drosophila* identified functional and physical interactions between fly FMRP and the ZC3H14 orthologue Nab2 [312].

Interestingly, altered spine density of dentate granule neurons in *Zc3h14*$^{\Delta ex13/\Delta ex13}$ mice was detected at five months, but not at postnatal day 7 (P7). Regulation of dendritic spines in the brain is a highly spatiotemporally dynamic process and is dependent on both the stage of brain development and the brain region [148, 410]. This age-specific phenotype could suggest a role for ZC3H14 in dendritic spine maintenance, which is an age-dependent stage of neuronal development that initiates in mice during early adulthood. By contrast, mice at P7 are in the spinogenesis phase of neuronal development. Often neurological disorders show altered dendritic spine density at specific stages of neuronal development rather than as a constant phenotype across developmental stages [235, 363]. Performing Golgi staining of *Zc3h14*$^{\Delta ex13/\Delta ex13}$ mouse brain tissue during the spine pruning stage of neuronal development, which occurs between the spinogenesis and spine maintenance phases, could help to more precisely define the role of ZC3H14. These investigations could be important to understand how loss of ZC3H14 in humans leads to intellectual disability.

The finding that loss of ZC3H14 leads to a reduction in mushroom-shaped spines raises the question of what consequences this change could have for neuronal function in *Zc3h14*$^{\Delta ex13/\Delta ex13}$ mice. First, it is important to note that individual spines undergo changes in shape during development and in response to stimuli [139, 411]. The turnover of dendritic spines, as well as changes in their growth and retraction, is tied to alterations in brain circuitry that underlie

learning and memory [351, 363]. For example, early longitudinal studies of the mouse barrel cortex demonstrated how spine and synapse formation/stabilization, as well as destabilization, occur in response to novel sensory experiences [412, 413]. Similarly, the size of individual spines and synapses from cultured neurons *in vitro*, can be increased or decreased in response to specific patterns of activity [391, 414]. For this reason, thin spines, which are more dynamic and structurally flexible, are thought to represent "learning spines" [144]. Conversely, stable mature mushroom-shaped spines likely represent "memory spines" [144, 160]. Thus, our data showing that *Zc3h14*$^{\Delta ex13/\Delta ex13}$ mice have a reduction in mushroom-shaped spines are consistent with earlier findings that *Zc3h14*$^{\Delta ex13/\Delta ex13}$ mice exhibit defects in working memory, but display intact learning [312]. These findings are also remarkably consistent with results from *Drosophila* where pan-neuronal depletion of the fly ZC3H14 orthologue, Nab2, caused short-term memory defects while learning remained intact [277]. Thus, changes in the dendritic spine morphology upon loss of ZC3H14 are consistent with behavioral consequences that have been documented in multiple model organisms lacking ZC3H14.

Zc3h14$^{\Delta ex13/\Delta ex13}$ mice display an approximately 140% increase in CaMKIIα levels in synaptosomes as compared to control *Zc3h14*$^{+/+}$ mice. CaMKIIα is a well-known regulator of synaptic plasticity and dendritic spine morphology [380-383]. Thus, regulation of CaMKIIα levels could provide a possible mechanism by which the loss of ZC3H14 induces changes in spine density and morphology. Interestingly, we also identified ZC3H14 itself as a component of synaptosomes. This raises the intriguing possibility that ZC3H14 could regulate the local translation of target transcripts, including the *CaMKIIα* RNA. In a previous study characterizing the *Zc3h14*$^{\Delta ex13/\Delta ex13}$ mice, we provided evidence that ZC3H14 may regulate CaMKIIα expression [379]. Specifically, ZC3H14 binds to the *CaMKIIα* transcript and loss of ZC3H14

increases steady state levels of CaMKIIα in the brain [379]. These findings are bolstered by a study in *Drosophila* in which Nab2 not only interacts with the *CaMKII* transcript but also represses a CaMKII translational reporter in neurons [312]. Previous studies have shown that *CaMKIIα* mRNA is localized to dendrites, and that CaMKIIα expression in dendrites is dynamically regulated by local translation [80, 415-417]. Consequently, inhibiting CaMKIIα synthesis specifically in dendrites, but not in the soma, negatively affects synaptic plasticity and long-term memory but not learning [110, 418-420]. Our current results providing evidence that ZC3H14 is present in synaptosomes raises the possibility that ZC3H14 directly regulates the levels of CaMKIIα, potentially via modulating local translation. Further studies will be required to test this model.

Taken together, the results presented here provide the first evidence that ZC3H14 is important for proper dendritic spine density and specifically for dendrites to maintain normal numbers of mushroom-type spines. These findings are consistent with behavioral results showing that mice lacking ZC3H14 show defects in spatially-based memory tasks [379]. Growing evidence places the RNA binding protein ZC3H14 in a group with other RNA binding proteins such as FMRP and others that are implicated in regulating local translation at the synapse [375]. While further work is required to define the molecular mechanism by which ZC3H14 contributes to proper dendritic spine morphology, this work adds to our understanding of how loss of ZC3H14 could contribute to neuronal dysfunction.

Figures:

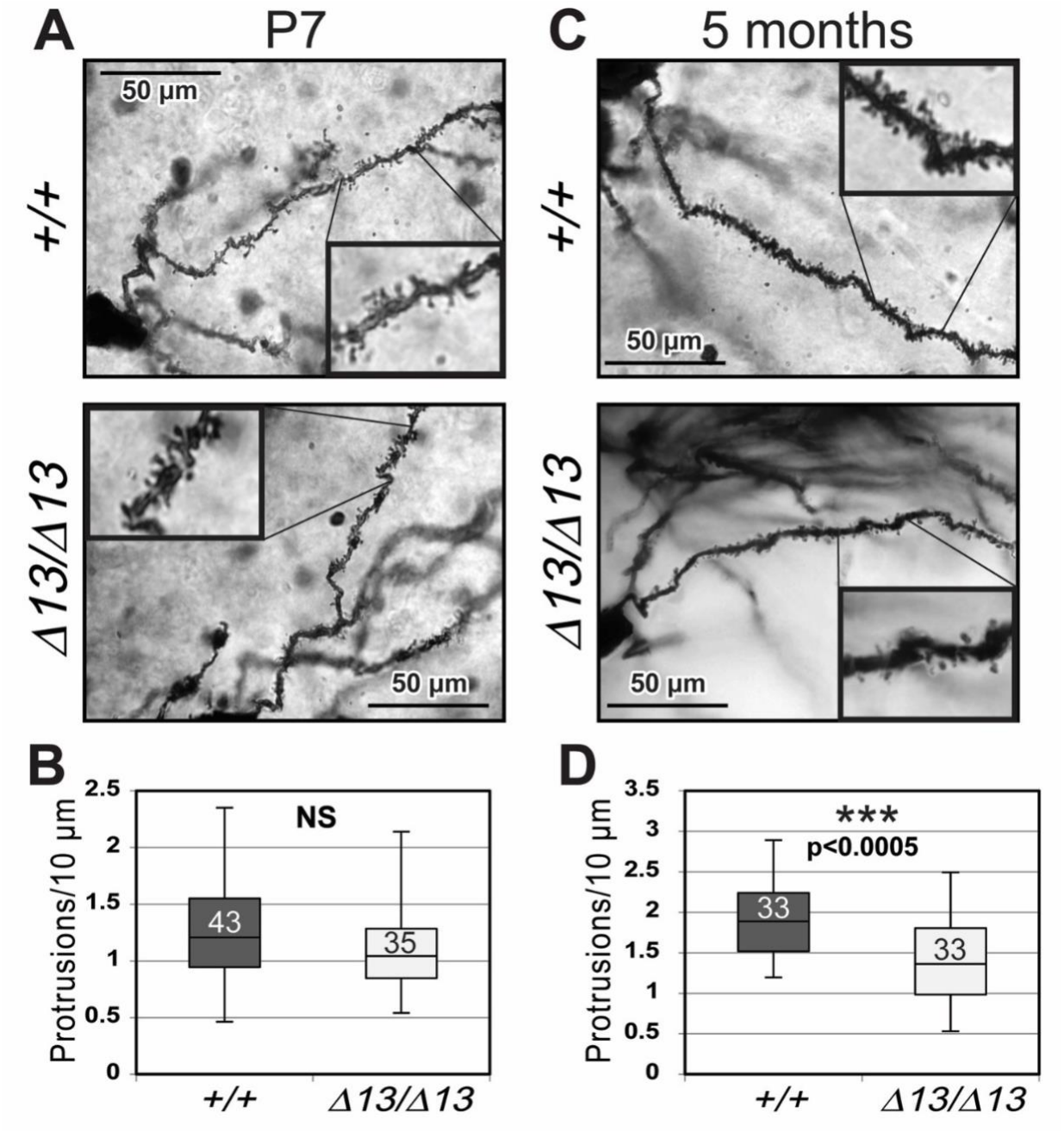

Figure 3.1: *Zc3h14*$^{\Delta ex13/\Delta ex13}$ mice show decreased neuronal dendritic spines compared to control. A) Representative dentate gyrus granule neurons from postnatal day 7 (P7) *Zc3h14*$^{+/+}$ (+/+) and *Zc3h14*$^{\Delta ex13/\Delta ex13}$ (Δ*13*/Δ*13*) mice visualized as Golgi-stained brain tissue are shown. B) Quantification of the number of dendritic spines per 10 µm, comparing +/+ and Δ*13*/Δ*13*

mice at P7 from (A). The total number of dendrites sampled is shown in the boxplots, with significance calculated by an unpaired *t* test (NS: $p>0.05$). C) Representative dentate gyrus granule neuron of 5 month +/+ and Δ*13*/Δ*13* Golgi-stained brain tissue are shown. D) Quantification of the number of protrusions per 10 μm, comparing +/+ and Δ*13*/Δ*13* mice at 5 months from (C). The number of dendrites sampled is shown in the boxplots, with statistical significance calculated by an unpaired *t* test (***$p<0.005$).

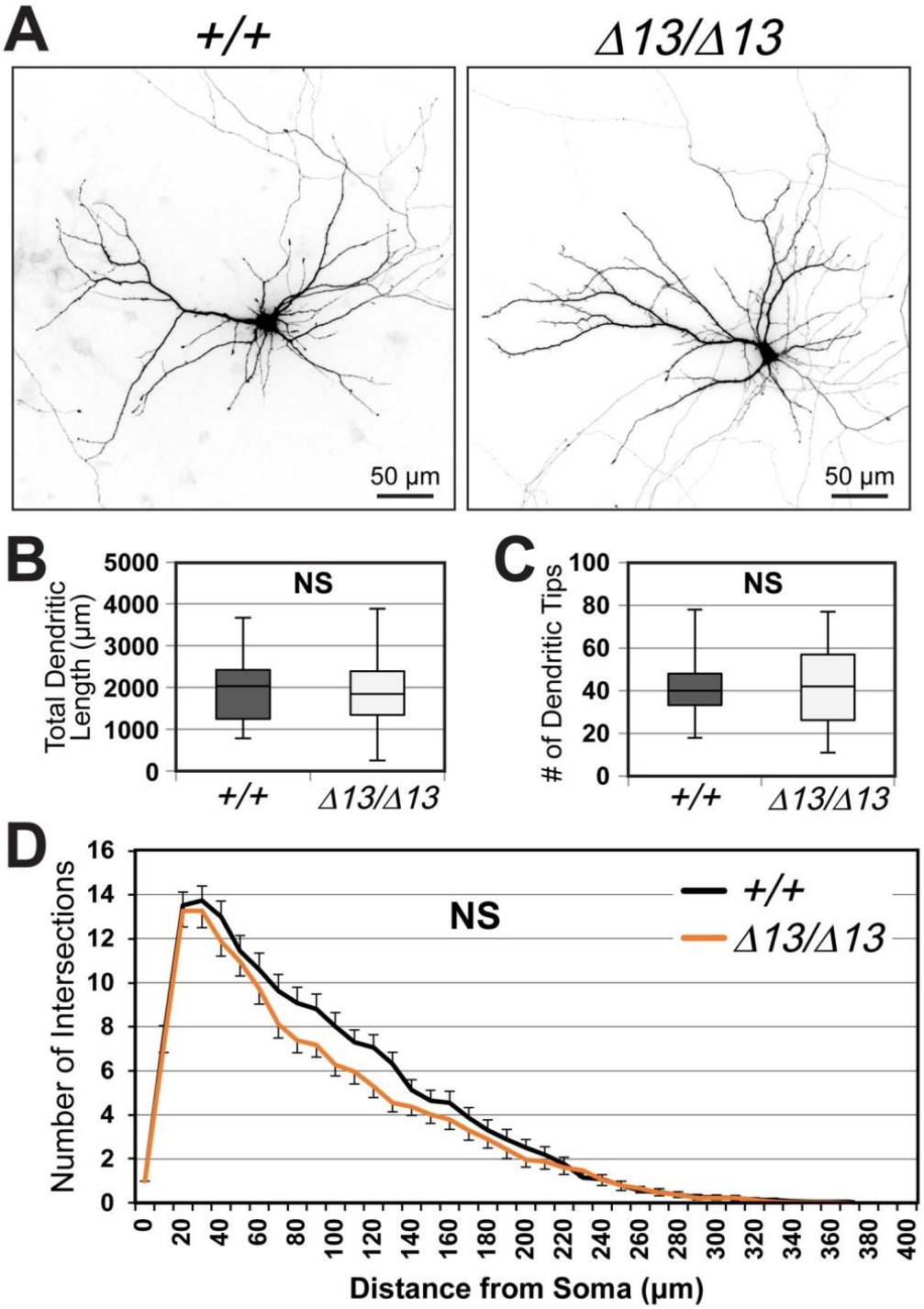

Figure 3-2: Primary hippocampal neurons from *Zc3h14*$^{\Delta ex13/\Delta ex13}$ mice exhibit no significant difference in dendritic arborization at DIV12. A) Representative inverted immunofluorescence images of *Zc3h14*$^{+/+}$ (+/+) and *Zc3h14*$^{\Delta ex13/\Delta ex13}$ (Δ*13*/Δ*13*) primary

hippocampal cells grown 12 days *in vitro* (DIV12). B-C) Quantification of total dendritic length and number of dendritic tips, respectively, comparing +/+ (n=54) and Δ*13*/Δ*13* (n=54). Statistical significance was calculated by an unpaired *t* test (NS: $p>0.05$). D) Sholl analysis quantification between +/+ (n=51) and Δ*13*/Δ*13* (n=51) DIV12 primary hippocampal neurons, by number of dendritic intersections made with concentric sholl rings in 10 μm increments, starting from the soma. Statistical significance was calculated by two-way ANOVA (NS: $p>0.05$).

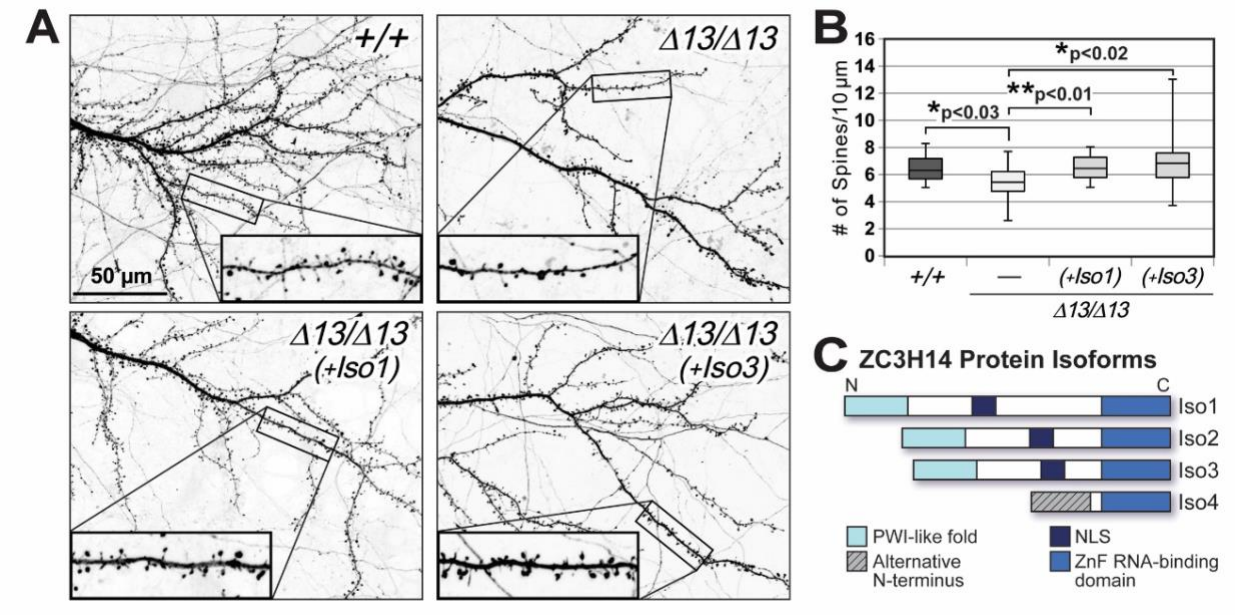

Figure 3-3: Primary hippocampal neurons from *Zc3h14*$^{\Delta ex13/\Delta ex13}$ mice cultured *in vitro* (DIV19) shows a statistically significant decrease in total dendritic spine density. A) Representative inverted fluorescence images of *Zc3h14*$^{+/+}$ (+/+), *Zc3h14*$^{\Delta ex13/\Delta ex13}$ (Δ*13*/Δ*13*), *Zc3h14*$^{\Delta ex13/\Delta ex13}$ transfected with ZC3H14 isoform 1 (Δ*13*/Δ*13 (+Iso1)*), and *Zc3h14*$^{\Delta ex13/\Delta ex13}$ transfected with ZC3H14 isoform 3 (Δ*13*/Δ*13 (+Iso3)*) primary hippocampal neurons cultured for 19 days *in vitro* (DIV19). Cultured neurons were fluorescently labeled by LifeAct-mRuby transfection. *Insets*, 2.6X magnification. B) Quantification of the number of dendritic spines per 10 μm, comparing +/+ (n=18 neurons), Δ*13*/Δ*13* (n=18 neurons), Δ*13*/Δ*13 (+Iso1)* (n=23 neurons); and Δ*13*/Δ*13 (+Iso3)* (n=19 neurons) at DIV19. Statistical significance was calculated by an unpaired *t* test (**p*<0.05). C) A schematic of ZC3H14 protein isoforms 1-4 (Iso1-4) with labeled domains [249] is shown: Proline-Tryptophan-Isoleucine (PWI)-like fold domain, Alternative N-terminus, predicted Nuclear Localization Sequence (NLS), and CysCysCysHis (CCCH) zinc finger (ZnF) RNA-binding domain.

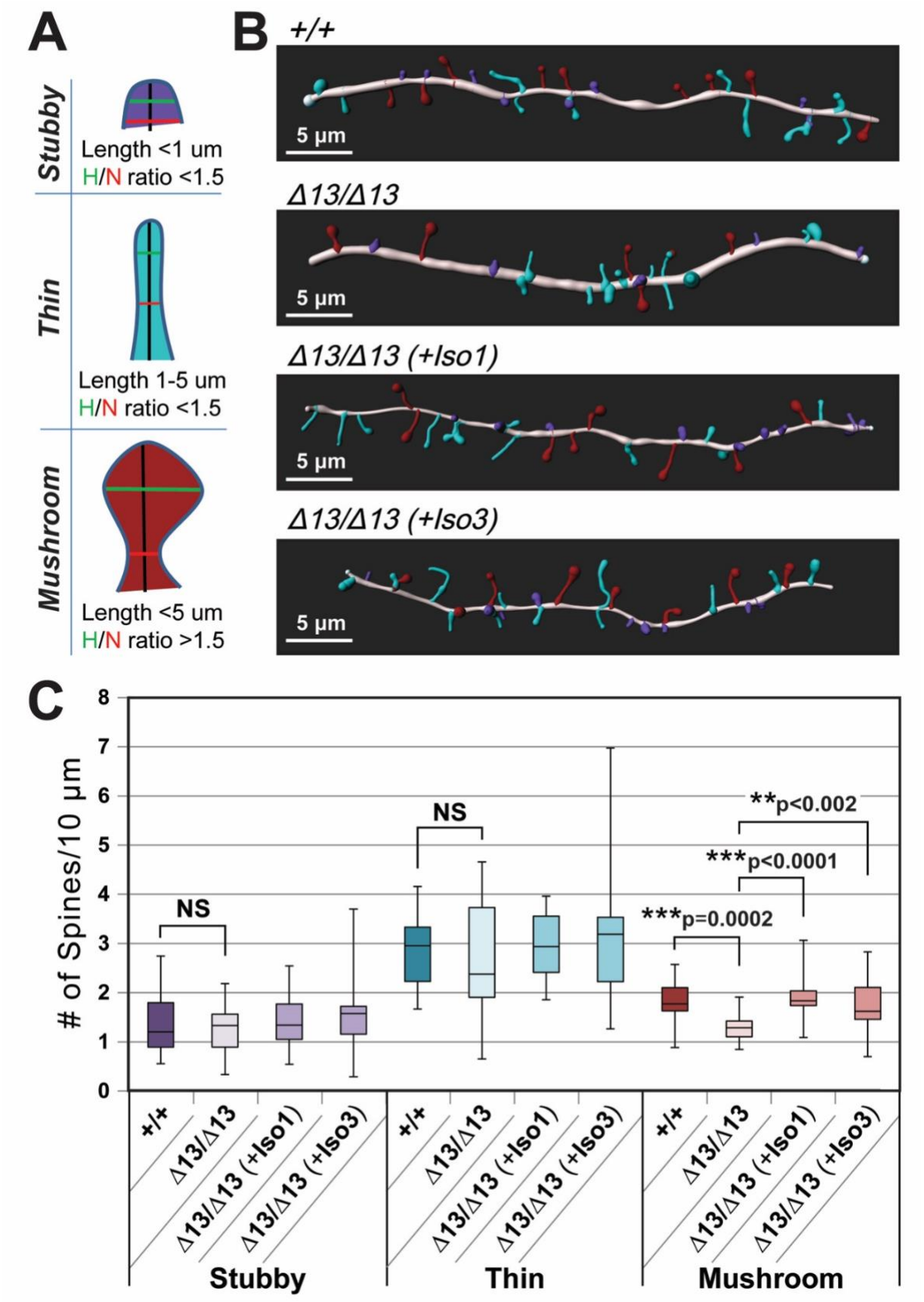
A
Stubby
Length <1 um
H/N ratio <1.5
Thin
Length 1-5 um
H/N ratio <1.5
Mushroom
Length <5 um
H/N ratio >1.5
B
+/+
5 µm
Δ13/Δ13
5 µm
Δ13/Δ13 (+Iso1)
5 µm
Δ13/Δ13 (+Iso3)
5 µm
C
# of Spines/10 µm
0
1
2
3
4
5
6
7
8
NS
NS
**p<0.002
***p<0.0001
***p=0.0002
+/+
Δ13/Δ13
Δ13/Δ13 (+Iso1)
Δ13/Δ13 (+Iso3)
Stubby
Thin
Mushroom

Figure 3-4: Primary hippocampal neurons from *Zc3h14*$^{\Delta ex13/\Delta ex13}$ mice cultured *in vitro* (DIV19) show a statistically significant decrease in mushroom-shaped dendritic spines that can be rescued by expressing ZC3H14 Isoform 1 or 3. A) A schematic illustrating the measurements used to classify "Stubby" (purple), "Thin" (light blue), and "Mushroom" (dark red) type dendritic spines, in terms of spine length, head width (H, green), and neck width (N, red). B) Representative Imaris software reconstructions of dendritic spines from *Zc3h14*$^{+/+}$ (+/+), *Zc3h14*$^{\Delta ex13/\Delta ex13}$ (Δ*13*/Δ*13*), *Zc3h14*$^{\Delta ex13/\Delta ex13}$ transfected with ZC3H14 isoform 1 (Δ*13*/Δ*13 (+Iso1)*), and *Zc3h14*$^{\Delta ex13/\Delta ex13}$ transfected with ZC3H14 isoform 3 (Δ*13*/Δ*13 (+Iso3)*), were constructed from fluorescent images of 19 days *in vitro* (DIV19) cultured primary hippocampal neurons. C) Quantification of the number of each spine type per 10 μm, comparing +/+ (n=18 neurons), Δ*13*/Δ*13* (n=18 neurons), Δ*13*/Δ*13 + (+Iso1)* (n=23 neurons); and Δ*13*/Δ*13 (+Iso3)* (n=19 neurons). The color intensity for each box plot is used as a general comparative indicator for the level of functional ZC3H14 protein present. Statistical significance was calculated by an unpaired *t* test (NS: $p>0.05$; **$p<0.01$; ***$p<0.001$).

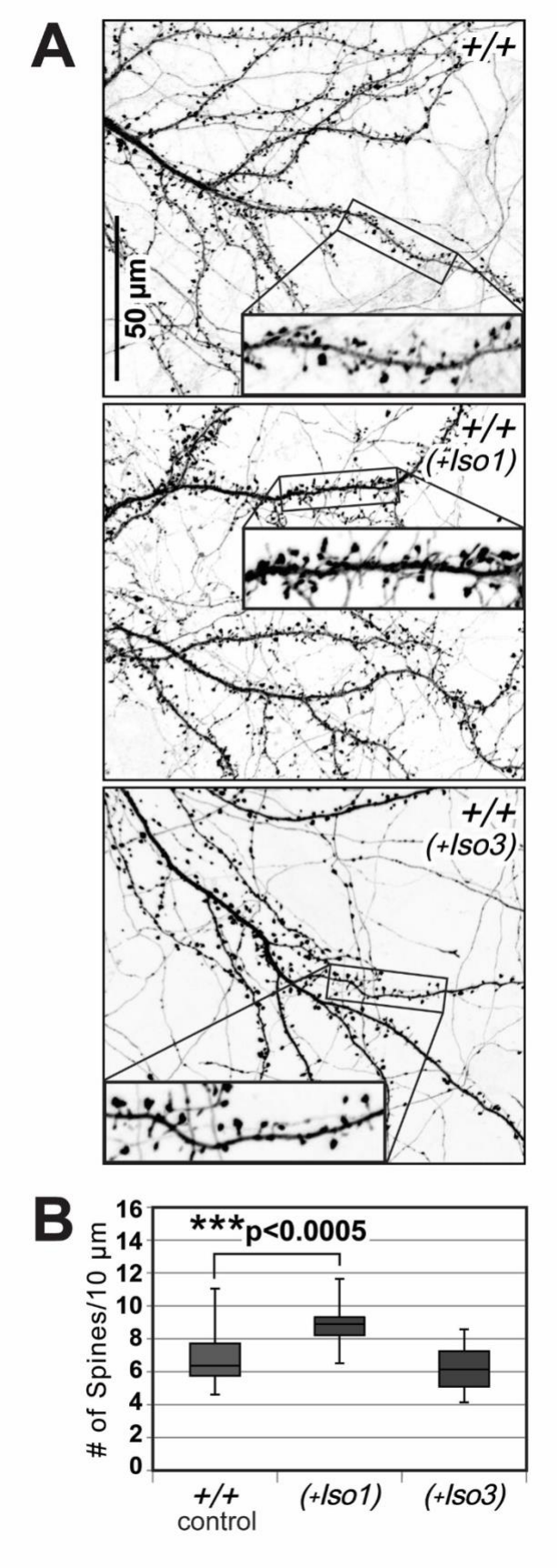
A
+/+
50 µm
+/+
(+Iso1)
+/+
(+Iso3)
B
***p<0.0005
# of Spines/10 µm
16
14
12
10
8
6
4
2
0
+/+
control
(+Iso1)
(+Iso3)

Figure 3-5: Overexpression of ZC3H14 Isoform 1 in cultured primary hippocampal neurons (DIV19) increases dendritic spine density. A) Representative inverted fluorescence images of control primary *Zc3h14*$^{+/+}$ (+/+) hippocampal neurons are shown together with *Zc3h14*$^{+/+}$ primary hippocampal neurons transfected with ZC3H14 Isoform 1 (+/+ *(+Iso1)*) or ZC3H14 Isoform 3 (+/+ *(+Iso3)*). The primary hippocampal neurons were cultured for 19 days *in vitro* (DIV19). Cultured neurons were fluorescently labeled by LifeAct-mRuby transfection. *Insets*, 2.4X magnification. B) Quantification of the number of dendritic spines per 10 μm, comparing +/+ (n=21 neurons), +/+ *(+Iso1)* (n=14 neurons), and +/+ *(+Iso3)* (n=19 neurons) at DIV19 is shown. Statistical significance was calculated by an unpaired *t* test (NS>0.05; ***p<0.0005).

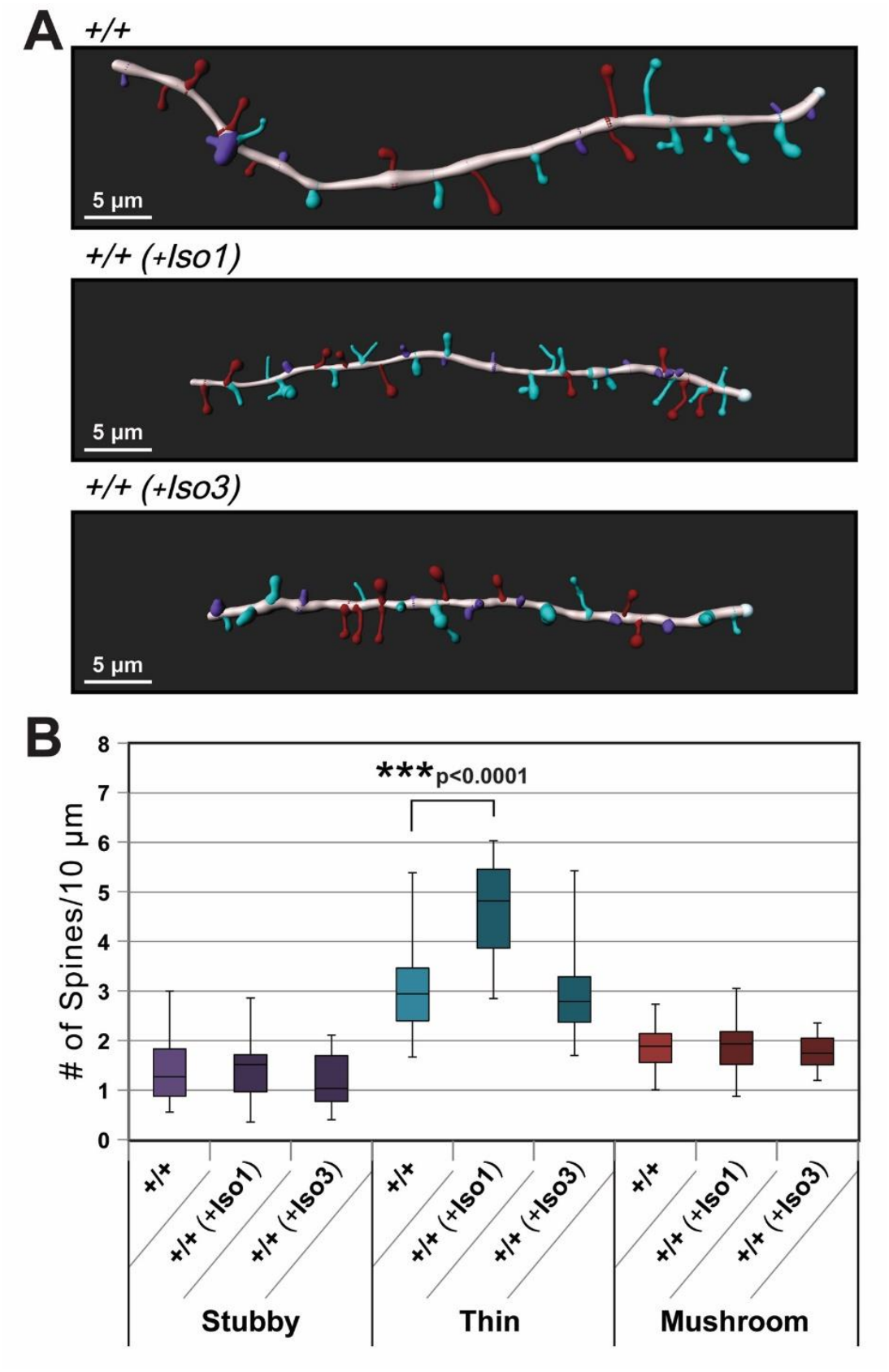
A
+/+
5 µm
+/+ (+Iso1)
5 µm
+/+ (+Iso3)
5 µm
B
***p<0.0001
# of Spines/10 µm
0
1
2
3
4
5
6
7
8
+/+
+/+ (+Iso1)
+/+ (+Iso3)
+/+
+/+ (+Iso1)
+/+ (+Iso3)
+/+
+/+ (+Iso1)
+/+ (+Iso3)
Stubby
Thin
Mushroom

Figure 3-6: The increase in spine density detected in DIV19 primary hippocampal neurons that overexpress ZC3H14 Isoform 1 is due to an increase in the number of thin-type dendritic spines. A) Representative Imaris software reconstructions of dendritic spines from *Zc3h14*$^{+/+}$ (+/+) primary hippocampal neurons (control), *Zc3h14*$^{+/+}$ neurons transfected with ZC3H14 Isoform 1 (+/+ *(+Iso1)*), and *Zc3h14*$^{+/+}$ neurons transfected with ZC3H14 Isoform 3 (+/+ *(+Iso3)*), were constructed from fluorescent images of 19 days *in vitro* (DIV19) cultured primary hippocampal neurons. B) Quantification of the number of each spine type per 10 μm, comparing +/+ (n=21 neurons), +/+ *(+Iso1)* (n=14 neurons), and +/+ *(+Iso3)* (n=19 neurons) samples. Statistical significance was calculated by an unpaired *t* test (NS>0.05; ***p<0.001).

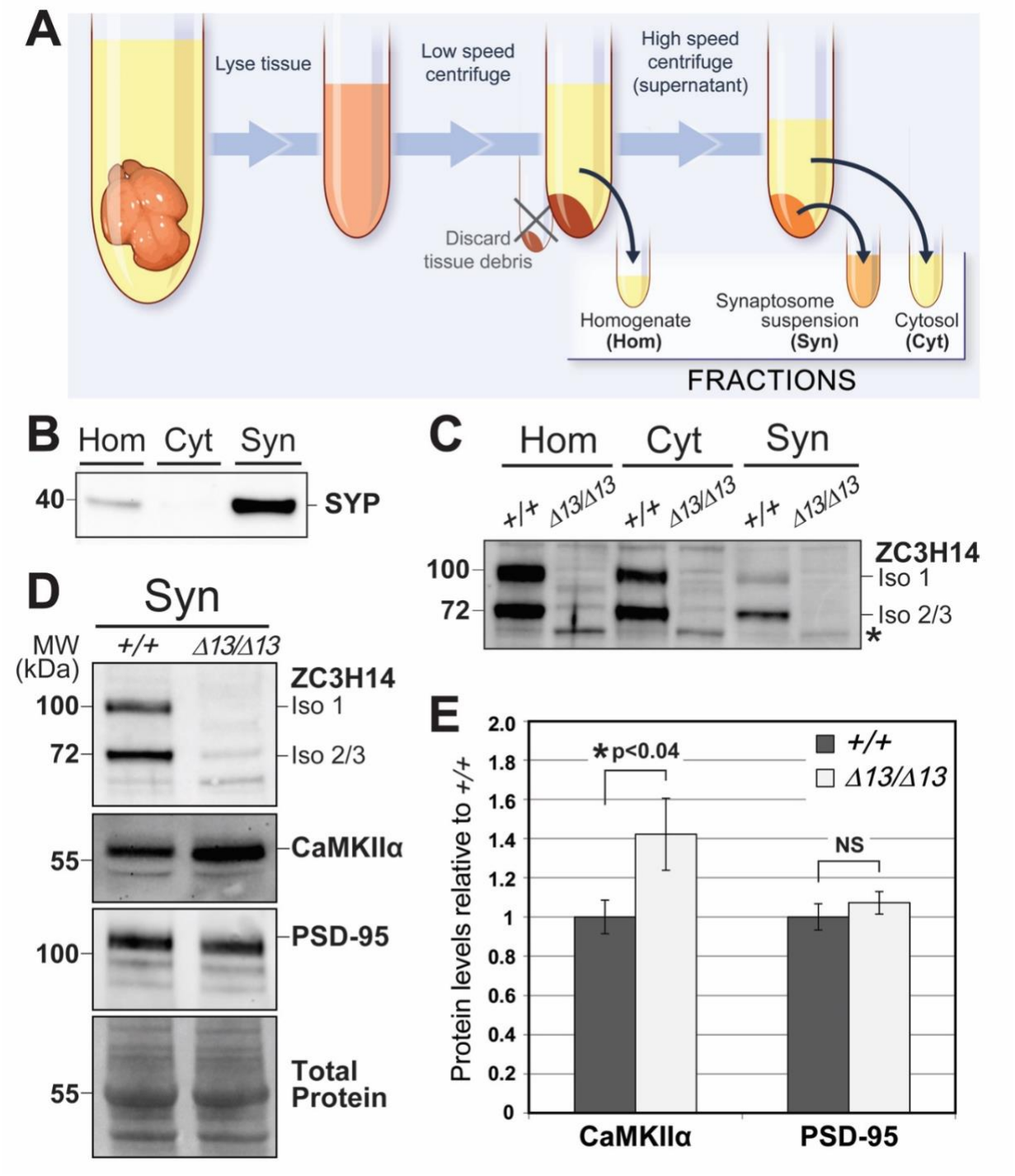

Figure 3-7: ZC3H14 is present in synaptosomes and CaMKIIα levels are increased in synaptosomal fractions from *Zc3h14*$^{\Delta ex13/\Delta ex13}$ mice compared to control. A) A schematic illustrates the synaptosomal fractionation procedure, which produces fractions corresponding to total homogenate (Hom), cytosol (Cyt) and synaptosome (Syn) derived from a single postnatal

day 0 (P0) whole mouse brain. B) Immunoblotting for synaptophysin (SYP, ~38 kDa), in the Hom, Cyt, and Syn fractions from a *Zc3h14*$^{+/+}$ (+/+) male whole mouse brain demonstrates the enrichment for this synaptic protein in the Syn fraction. C) An immunoblot analysis of Hom, Cyt, and Syn fractions comparing +/+ and *Zc3h14*$^{\Delta ex13/\Delta ex13}$ (Δ*13*/Δ*13*) P0 whole mouse brain samples is shown. The top panel shows an immunoblot to detect ZC3H14, using an N-terminal antibody that detects Zc3H14 Isoforms 1 (~100 kDa) and 2/3 (~70 kDa) [249]. The position of a truncated, nonfunctional ZC3H14 protein that is detected in the *Zc3h14*$^{\Delta ex13/\Delta ex13}$ mouse [379] is indicated by the *. D) Immunoblots shown compare the Syn fractions from +/+ and Δ*13*/Δ*13* P0 whole mouse brain samples. Panels show immunoblots for ZC3H14, CaMKIIα (~50kDa), and postsynaptic density protein 95 (PSD-95, ~95 kDa). The bottom panel shows total protein detected by Ponceau, which serves as a loading control. E) Quantification of CaMKIIα and PSD-95 levels in the Syn fraction comparing +/+ (n=3) and Δ*13*/Δ*13* (n=3) where n=independent male mice. For each protein, the level of protein detected was set to 1.0 for the +/+ control and results are plotted as Relative to this control sample. Statistical significance was calculated by an unpaired *t* test (NS>0.05; *p=0.04).

Chapter 4

Discussion:

Conclusions, implications and future directions

4.1 Introduction

A large number of RNA binding proteins are linked to tissue-specific disorders despite ubiquitous expression. ZC3H14 is a ubiquitous polyadenosine RNA binding protein that is lost in an autosomal recessive form of nonsyndromic intellectual disability. While the cellular and functional roles of ZC3H14 orthologues have been characterized in model systems such as *S. cerevisiae*, *D. melanogaster*, and *C. elegans*, far less research had been performed in a mammalian context where the process of RNA regulation is more complex and the effects on higher order brain function could be analyzed. This dissertation covers the generation and subsequent characterization of the first ZC3H14 ubiquitous loss of function mouse model (*Zc3h14*$^{\Delta ex13/\Delta ex13}$). Our findings show that, similar to humans, ZC3H14 is not essential in mice. Upon generation of this ZC3H14 mutant mouse strain, early experimentation was performed to determine whether *Zc3h14*$^{\Delta ex13/\Delta ex13}$ mice could serve as an appropriate model to assess the role of ZC3H14 in brain function. Behavioral analysis revealed loss of ZC3H14 specifically impairs working memory, providing evidence that *Zc3h14*$^{\Delta ex13/\Delta ex13}$ mice show a phenotype linked to higher order brain dysfunction. Results from *Drosophila* defined a key role for Nab2/ZC3H14 in neurons [264], and neuronal enrichment of ZC3H14 in mouse hippocampus [247]. Using the novel *Zc3h14*$^{\Delta ex13/\Delta ex13}$ mouse model, the primary hypothesis tested was that ZC3H14 is necessary for higher order brain function by regulating critical RNA targets that maintain proper neuronal function. This hypothesis was tested in this thesis by the generation and characterization of the first *Zc3h14* mouse model as well as a more in depth analysis of dendritic spine morphology in hippocampal neurons from these mice. The following chapter will discuss several overarching questions related to this main hypothesis, which have been raised and

addressed over the course of this thesis, as separate sections. Each section will also address unanswered questions, as well as open areas of study and potential future directions.

4.2 Discussion of Questions and Answers to the Main Thesis Hypothesis

4.2.1 Which step(s) in RNA regulation is ZC3H14 involved in in mice?

RNA binding proteins play numerous roles in regulating gene expression. Like other RNA binding proteins, ZC3H14/Nab2 has been implicated in several key regulatory steps. ZC3H14 plays an evolutionarily conserved role in regulating poly(A) tail length [247, 263, 264], which we also observed in mouse hippocampus [379]. Loss of ZC3H14 leads to increased bulk poly(A) tail length in various mouse tissues, but it is surprising that there is a very noticeable difference in the magnitude of the change observed between tissues [379] given that restriction of poly(A) tail length is considered a key ZC3H14 molecular function [247, 263]. The hippocampus exhibits the clearest increase in bulk poly(A) tail length as compared to cerebral cortex or liver [379], even though the levels of ZC3H14 protein are similar between these tissues (as presented by the Human Protein Atlas). This potentially indicates a differential requirement of poly(A) tail length regulation by ZC3H14 depending on tissue type, or even different regions of the same tissue. Whether ZC3H14 modulates poly(A) tail length through limiting polyadenylation, or promoting trimming of extended poly(A) tails to a shorter length is not yet known [265]. Regardless, altered poly(A) tail length can affect various steps of RNA processing/regulation, including translation, nuclear export, and RNA stability [266-271]. For example, elongated poly(A) tails are associated with promoting translation [267-269], due to the increased polysome formation and translation initiation via poly(A) tail-bound PABP recruiting the 40S ribosomal subunit to the 5’ mRNA end [364]. Therefore, loss of ZC3H14 may produce a

more robust change in RNA regulation within the hippocampus than other brain regions, not only in altering poly(A) tail length but in subsequent downstream steps of RNA regulation such as translation.

Currently, there are multiple pieces of evidence that implicate ZC3H14 in regulating translation. ZC3H14 associates with polysomes in mouse brain tissue [312] and loss of Nab2 in flies leads to increased expression of a CaMKII translational reporter [312]. Furthermore, Nab2 genetically and physically interact in neurites with FMRP [312], an RNA-binding protein that mediates translational repression [36, 37]. Together, these data suggest a role of ZC3H14 as a negative regulator of translation. This becomes especially relevant in evaluating tissue-specific roles of ZC3H14, in which impaired regulation of local translation may provide rationale for neuron-specific dysfunction. Loss of ZC3H14 in mice results in altered steady-state protein levels as determined through mass spectrometry analysis of P0 whole mouse brain tissue [379]. While there are a comparable number of significantly increased and decreased proteins identified, there is a distinct trend in increased steady-state targets grouping into GO terms relevant to neuronal function, particularly relating to synapses and cellular membrane. In comparison, the GO terms for those proteins that show a decrease in steady-state levels appear largely unrelated with regard to cellular function. Consistent with a potential role for ZC3H14 in regulating translation, ZC3H14 is present in synaptosomes [421], which are a major compartment for local translation. However, while these findings are consistent with a role in local translation, further studies are required to define the mechanism by which ZC3H14 could regulate translation. One possible model is that the poly(A) binding protein ZC3H14 blocks interaction of mRNA with PABP which is known to stimulate translation [262, 422]. Future experiments that could further address the role of ZC3H14 in translation and even local

translation may include real-time tracking of mRNAs/nascent protein translation comparing *Zc3h14*$^{+/+}$ and *Zc3h14*$^{\Delta ex13/\Delta ex13}$ neurons [423-425].

In addition to a suggested role in regulating translation, ZC3H14 is also implicated in other nuclear RNA processing steps, such as splicing and quality control of RNA export from the nucleus. ZC3H14 interacts with numerous components of the spliceosome [290]. In both budding yeast [290]and flies (unpublished) loss of Nab2 increases levels of unspliced intron-containing pre-mRNAs. In cultured cells, ZC3H14 is required to prevent nuclear export of intron-containing *ATP5G1* pre-mRNA [313]. This suggests an evolutionarily conserved role for ZC3H14 in processes that ensure proper pre-mRNA splicing, maturation, and quality control of mRNA export. Nab2 also physically interacts with the nuclear pore complex [256] and the THO mRNA processing complex in mouse brain [378]. The THO complex is an evolutionarily conserved complex with suggested roles in transcription elongation, mRNA splicing, and nuclear mRNA export [426-429]. ZC3H14 associate with components of the THO complex in an RNA-independent manner (unpublished) to regulate shared RNA targets *Atp5g1* and *Psd95* in N2a cells [378]. However, there is also evidence that these partners do not regulate the exact same set of mRNAs. For example, depletion of ZC3H14 but not THO complex components significantly reduces steady-state levels of *Mapt* mRNA [378]. This implies additional independent ZC3H14 function beyond association with the THO complex. Neurons depend on numerous tightly regulated alternative splicing events [84, 85], which can make the brain susceptible to deleterious consequences from impaired splicing, including such neurological diseases as spinal muscular dystrophy (SMA), amyotrophic lateral sclerosis (ALS), and autism spectrum disorder (ASD) [430]. To further investigate the role of ZC3H14 in neuronal RNA splicing, it would be of interest to perform fractionation on mouse brains and either perform RNA-seq to identify all

transcripts with splicing errors present in cytoplasm, or analyze specific transcripts of interest for splicing errors, such as *CaMKIIα.* Continuing to characterize the role of ZC3H14 in regulating splicing and export may create a more comprehensive view of how loss of ZC3H14 results in higher order brain dysfunction.

In summary, ZC3H14 is required to restrict poly(A) tail length, especially in the hippocampus, but the precise mechanism for how this regulation is achieved is still not known. This function is evolutionarily conserved [247, 263, 264, 379], but ZC3H14-mediated poly(A) tail restriction may be differentially required depending on tissue type. The function of ZC3H14 in restricting poly(A) tail length may have consequences for downstream steps in gene expression. Multiple lines of evidence support the idea that ZC3H14 could function as a translational repressor. A role in regulating translation, particularly local translation, may help to explain why loss of ZC3H14 causes detectable defects only in higher order brain function in humans. ZC3H14 is also implicated in additional steps of RNA regulation, including a conserved role in quality control of splicing and nuclear RNA export, which may be mediated through interactions with the spliceosome and THO complex, so these additional roles could also contribute to brain dysfunction. Indeed, like *ZC3H14*, genes encoding components of the THO complex are linked to neurological disorders[431-434], so these additional roles could also contribute to brain dysfunction.

4.2.2 Does ZC3H14 regulate all polyadenylated RNA?

ZC3H14/Nab2 binds with high affinity to polyadenosine RNA [248, 252]. This RNA binding profile means that ZC3H14/Nab2 could bind to and regulate every polyadenylated RNA. Multiple pieces of evidence suggest ZC3H14 demonstrates RNA target specificity. Although

ZC3H14 could bind and regulate all poly(A) RNAs, multiple experiments show that loss of ZC3H14/Nab2 alters only a subset of steady-state transcripts [313] and proteins [379]. For instance, ATP synthase F_0 subunit C is a protein required for the majority of ATP production in eukaryotic cells [435]. Identical mature proteins are produced from multiple independent genes, *ATP5G1*, *ATP5G2*, and *ATP5G3*, although each gene encodes a unique mature mRNA transcript. Remarkably, RNA-IP of ZC3H14 in MCF-7 cells shows differential ZC3H14 enrichment between these three transcripts, with highly significant enrichment specifically for *ATP5G1* and *ATP5G3* despite all three transcripts encoding the same mature protein [313]. This result strongly implies ZC3H14 can preferentially bind to specific RNA targets. The finding that ZC3H14 can bind to and potentially regulate specific RNA transcripts rather than the entire polyadenylated RNA pool may provide additional insight as to why ubiquitous loss of ZC3H14 in humans results in a brain tissue-specific disorder, especially if some ZC3H14-specific RNA targets are expressed specifically in neurons. Consistent with this hypothesis, both ZC3H14 and Nab2 associate with *CaMKIIα* mRNA in mice [379] and flies [312], but not with several other abundant polyadenylated mRNA transcripts such as *rp49* [312]. This enriched association specifically with *CaMKIIα* mRNA in conjunction with increased steady-state levels of CaMKIIα protein in mouse hippocampus and the requirement of Nab2 to specifically repress a *CaMKII-3'UTR* translational reporter (but not a *SV40-3'UTR* translational reporter) in flies [312] strongly suggests *CaMKIIα* mRNA is an evolutionarily conserved functional target of ZC3H14.

The mechanism that confers specificity of ZC3H14 for a subset of poly(A) RNAs is not known. While ZC3H14 binds with high affinity to polyadenosine RNA [248, 252], specificity may be conferred through binding A-rich sites outside of the poly(A) tail, as Nab2 binding can be observed throughout the body of mRNAs [275]. In support of this model, RNAs associated

with Nab2 have a consensus $A_{11}G$ sequence [274], and Nab2 binds to $A_{11}G$ RNA with higher affinity than A_{12} RNA [436]. The crystal structure of Nab2 ZnF5-7 associated with a polyadenosine RNA tract shows specific adenine binding only in select regions of the binding motif (XXXAAAXXXAAX) [436]. This potential sequence flexibility may underlie the capacity for ZC3H14 to target specific transcripts through binding A-rich RNA sequences beyond a simple tract of As such as that found in the poly(A) tail. Recent Nab2 structural data may provide critical additional insight into how Nab2 could exhibit specificity. Binding of A-rich RNA by Nab2 induces Nab2 dimerization, consisting of two RNAs and two Nab2 proteins [436]. Each RNA is bound to ZnF 5/7 by one Nab2 protein and the ZnF 6 of the other Nab2 [436]. This may provide additional parameters to convey transcript specificity of Nab2/ZC3H14 binding; not only through the requirement for two independent A-rich sites, but also the unexplored possibility of requiring specific spatial configurations between these binding regions that would optimize ZC3H14 binding. The possibility for additional ZC3H14 protein-protein interactions may also contribute to defining transcript binding specificity.

To address a model where ZC3H14 demonstrates transcript specificity, cross-linking immunoprecipitation sequencing (CLIP-seq) of the mouse brain could in theory identify: 1) the potential range of flexibility in ZC3H14-bound RNA target sites and 2) specific transcripts bound by ZC3H14 as each bound RNA read is typically ~35-50nt [437]. However, such an experiment could be complicated by a predicted enrichment for A-rich sequences by an overwhelming volume of A-only sequences due to poly(A) tail binding. Still, results of such an approach could address a fundamental question about ZC3H14 and help define how loss of a ubiquitous poly(A) RNA binding protein results in tissue-specific disease.

In summary, although ZC3H14 has the capacity to bind to all polyadenylated RNA, evidence suggests that ZC3H14 functions in a transcript-specific manner, with *CaMKIIα* mRNA as a noteworthy example. Transcript specificity could result from sequence specificity and/or interaction with partner proteins that confer specificity.

4.2.3 What functional impact does loss of ZC3H14 have on higher order brain function?

The hallmark phenotype identified in individuals with loss of ZC3H14 is nonsyndromic intellectual disability. This is consistent even with a newly identified individual with a novel homozygous *ZC3H14* mutation (N309fs) [438]. However, while this cognitive diagnosis is relatively consistent, some degree of phenotypic variability may be linked to the differing natures of the specific inherited mutation, possibly in relation to intellectual disability severity. Additional characterization of the N309fs individual also shows a potential link with global developmental delay, as demonstrated through delayed ability to walk, grasp, and talk. Among the small number of individuals identified with homozygous loss of function *ZC3H14* mutations, this is the first individual that was identified as a young child. This supports the link between ZC3H14 and intellectual disability as opposed to adult-onset, and subsequently may imply a requirement for ZC3H14 during early brain development. However, no additional functional or behavioral studies have been performed with ZC3H14 homozygous recessive individuals since the initial IQ test administered in 2011 [250]. Interestingly, all seven identified individuals thus far are male. However, this observation could very likely just be coincidence, as there is no evidence of significant sex skewing in the *Zc3h14*$^{\Delta ex13/\Delta ex13}$ mice [379] and there are only two females out of the 13 siblings within the three affected families. The small number of individuals with *ZC3H14* mutations that have been identified thus far poses a major limiting factor in

understanding ZC3H14 function in the human brain, and will require the identification and characterization of additional patients to better understand the potential cellular, developmental, and functional consequences of ZC3H14 loss in humans.

In place of investigating loss of ZC3H14 in the human brain, behavioral assays were performed with the *Zc3h14*$^{\Delta ex13/\Delta ex13}$ mice. This approach served to identify and characterize whether loss of ZC3H14 in mice would cause higher order brain dysfunction to model the human disease. The visuospatially-based water radial arm maze (WRAM) paradigm allows for analysis of specific subtypes of memory deficits defined by the type of navigational errors made as the mice explore the WRAM. *Zc3h14*$^{\Delta ex13/\Delta ex13}$ mice exhibited memory impairment and made significantly more errors in entering the same arm more than once during the same trial, specifically indicating a working memory deficit [379]. However, while working memory is impaired, learning remains intact, as *Zc3h14*$^{\Delta ex13/\Delta ex13}$ mice committed fewer errors each day over the course of nine days [379]. This is strikingly consistent with independent findings from Nab2-mutant flies which exhibit impairment in short term memory but retain learning capacity [277]. This was determined using a courtship conditioning assay, a non-spatial behavioral task that tracks attempted fly courtship behavior. This correlation between mice and flies strongly suggests a conserved functional role for ZC3H14 in memory.

Working memory refers to “the ability to hold information in mind while manipulating and integrating information to perform some cognitive goal” [439]. In the human brain, learning and memory are largely attributed to the medial temporal lobe, including the hippocampus, as the center for learning and memory. In addition, while elongation of bulk poly(A) tails upon loss of ZC3H14 is present in different tissues, this phenotype is far more robust in the hippocampus than in the cerebral cortex [379], indicating the hippocampus may be more sensitive to loss of

ZC3H14 than other brain regions. Therefore, most of our brain region-specific investigations of *Zc3h14*$^{\Delta ex13/\Delta ex13}$ mice have focused on the hippocampus. However, while the hippocampus is a highly interconnected structure, general associations have been made between hippocampal subregions (DG, CA1, and CA3) and varying roles in learning and memory [440]. Working memory is associated with each of these subregions, but each contributes to different facets of working memory [441-444]. Therefore, if the deficit in *Zc3h14*$^{\Delta ex13/\Delta ex13}$ working memory is attributed to loss of ZC3H14 within the hippocampus, it is possible that working memory impairment could occur in either a pan-hippocampal or sub-hippocampal manner. To address this, one interesting option for future experimentation would be to cross the *Zc3h14*$^{F/F}$ mice with different Cre recombinase drivers to selectively remove ZC3H14 protein from specific regions of the hippocampus [445-447].

While the hippocampus plays a foundational role in learning and memory, other brain regions such as the amygdala [448, 449], striatum [450, 451], medial prefrontal cortex (mPFC) [452, 453], and cerebellum [454, 455] support different types of memory and learning. In fact, growing evidence has led to the idea that working memory is produced from synchronous activity between the hippocampus and mPFC [453, 456, 457]. ZC3H14 could play critical roles in multiple brain regions rather than just a single region, and the combined impairment may trigger the working memory deficit. Therefore future functional, morphological, and molecular experimentation should consider investigating additional brain regions beyond the hippocampus, especially the mPFC.

In summary, loss of ZC3H14 in mice results in working memory impairment with intact learning, which is remarkably consistent with loss of Nab2 in flies [277]. Impairment of a specific type of memory may imply loss of ZC3H14 differentially affects certain brain regions.

While the focus of investigation has been based on whole hippocampus, disruption of working memory in *Zc3h14*$^{\Delta ex13/\Delta ex13}$ mice may be due in part to differentially affected subregions within the hippocampus. Furthermore, brain regions besides the hippocampus may contribute to the working memory deficit, with the mPFC as a prime candidate given the implication for synchronous signaling with the hippocampus to elicit working memory.

4.2.4 Is loss of ZC3H14 accompanied by structural changes in the brain?

No data has yet been collected regarding potential structural/morphological changes in the brains of humans lacking ZC3H14. Structural changes in the brain are not an uncommon phenotype in patients with neurological disorders, so *Zc3h14*$^{\Delta ex13/\Delta ex13}$ mouse brains were analyzed at six months old to identify any noticeable gross morphological defects. Whole brain and hippocampal weight are unchanged; the only large-scale morphological change noted in *Zc3h14*$^{\Delta ex13/\Delta ex13}$ mice is an increase in anterior lateral ventricle size [379]. Enlarged lateral ventricles are associated with various abnormalities, such as developmental defects, weakening or increased degeneration of surrounding tissue, increased cerebrospinal fluid (CSF) volume, altered circulation/obstructed interventricular connections, and/or decreased resorption [458-461]. Interestingly, increased lateral ventricle size is a phenotype shared in ASD [462], schizophrenia [463], bipolar disorder [464], and of particular interest, Alzheimer's disease (AD) [465]. This commonality with AD is a particularly noteworthy parallel as analysis of post-mortem tissue from Alzheimer's disease cases show reduced expression of ZC3H14 (MSUT2) in brain regions affected by tau pathology, including the temporal lobe, and little change in regions lacking tau pathology [276]. One hypothesis is that loss of ZC3H14 leads to increased neurodegeneration around the lateral ventricles through regulation of RNAs involved in

suppression of tau pathology. While possible, the lack of obvious structural changes detected in additional regions of the *Zc3h14*$^{\Delta ex13/\Delta ex13}$ brain is generally inconsistent with a role for loss of ZC3H14 causing a neurodegenerative disorder such as Alzheimer's disease. In addition, studies in *C. elegans* identified the worm ZC3H14 orthologue SUT-2 to suppress tauopathy phenotypes [254, 276], suggesting loss of SUT-2 may protect from tauopathy-related neurodegeneration. Furthermore, while ZC3H14 binds and regulates *Mapt* mRNA, depletion of ZC3H14 results in significantly reduced steady-state levels of *Mapt* [378], which seems counterintuitive when compared to tauopathy models [466]. To further investigate this possibility, *Zc3h14*$^{\Delta ex13/\Delta ex13}$ brain sections could be histologically stained with antibodies directed against tau and/or neurodegenerative markers to determine whether there is an increase in neurodegeneration and/or insoluble tau present in the brain upon loss of ZC3H14. *Zc3h14*$^{\Delta ex13/\Delta ex13}$ lateral ventricle size has also only been quantified at one time point (six months), so there is no insight yet as to when enlargement of lateral ventricles emerges and whether or not this phenotype is progressive in *Zc3h14*$^{\Delta ex13/\Delta ex13}$ mice. It would be straightforward to quantify *Zc3h14*$^{\Delta ex13/\Delta ex13}$ lateral ventricle size at additional time points, and these results could provide crucial insight as to whether enlarged lateral ventricles represent a stable or progressive phenotype upon loss of ZC3H14.

Another hypothesis for the presence of enlarged lateral ventricles in *Zc3h14*$^{\Delta ex13/\Delta ex13}$ mice is related to a potential role of ZC3H14 in regulating planar cell polarity (PCP). PCP is "the polarization of a field of cells within the plane of a cell sheet" [467]. PCP plays a central role in various cellular functions, including ciliogenesis and cilia-mediated fluid flow [468]. Within the brain, cilia are present only in two specific cell types, both of which are involved in ventricular function: choroid plexus cells which protrude into the ventricles and produce CSF [469], and

ependymal cells which line the ventricle walls and control ventricular CSF flow through coordinated ciliary beating [470, 471]. Disruption of cilia and associated PCP regulators can result in abnormal CSF accumulation and hydrocephalus, potentially leading to enlarged ventricular space [469, 472-475]. One such core PCP regulator, Van Gogh-like 2 (Vangl2), is required for ependymal cilia orientation [476] and contributes to both single-cell polarity as well as polarity across the ependymal [473]. Interestingly, Vangl2 protein is significantly increased (1.31-fold) in *Zc3h14*$^{\Delta ex13/\Delta ex13}$ mice at P0 [379]. While overexpression of Vangl2 has not been directly investigated in ventricular cells, Vangl2 overexpression yields asymmetric basal body positioning in zebrafish embryos [477], which may affect cilia-mediated fluid flow [478]. In summary, loss of ZC3H14 in *Zc3h14*$^{\Delta ex13/\Delta ex13}$ mice may dysregulate PCP components, especially Vangl2, in ependymal and/or choroid plexus cells, thereby potentially impairing CSF volume and/or flow and result in enlarged lateral ventricles. Consistent with a role in regulating PCP, *Zc3h14*$^{\Delta ex13/\Delta ex13}$ mice also exhibit disorganization of sensory hair cells in the organ of Corti (unpublished data), which is an auditory sensory organ classically used to study PCP defects [467, 479]. Additionally, multiple pieces of evidence in flies associate Nab2 with PCP regulation [480], strongly suggesting an evolutionarily conserved role for ZC3H14 in PCP.

With this degree of evidence suggesting a role for ZC3H14 involvement in PCP, it would be extremely relevant to examine whether the enlarged lateral ventricle phenotype in *Zc3h14*$^{\Delta ex13/\Delta ex13}$ mice is linked to PCP impairment. One interesting experiment would be to dissect, fix, and stain the lateral ventricle walls of *Zc3h14*$^{\Delta ex13/\Delta ex13}$ mice to analyze the epithelial cells for such PCP defects as altered cilia organization or orientation [473]. Analysis of fluid flow would also help address whether enlarged lateral ventricles in *Zc3h14*$^{\Delta ex13/\Delta ex13}$ mice may be associated with impaired CSF flow [473]. Beyond solely the presence of enlarged lateral

ventricles, linking this structural phenotype to PCP impairment upon loss of ZC3H14 would raise the question of whether additional PCP component-associated aberrations in the brain of these mice could be present. Of particular interest, dysregulation of Vangl2 is associated with impairment of various neuronal processes, including neuronal migration [481, 482], axon guidance and outgrowth [483-485], neuronal maturation [486, 487], and synapse formation [488-490]. Overall, this may open a completely new area of future study in understanding the molecular and functional consequences of ZC3H14 loss, as well as exploring Vangl2 as a potential ZC3H14 target.

Finally, given the obvious and highly penetrant morphological differences observed in the mushroom bodies in Nab2-null flies [277], it is fairly surprising that we did not detect any gross morphological differences in the *Zc3h14*$^{\Delta ex13/\Delta ex13}$ hippocampus [379]. However, this may be at least partially due to the increased regulatory complexity of the mouse brain in which some functions of ZC3H14 in the hippocampus may be redundantly covered by other proteins. This suggestion is consistent with the fact that Nab2 is essential in flies while ZC3H14 is not essential in mammals, despite Nab2 and ZC3H14 sharing sufficient functional overlap for viability of Nab2-null flies [264]. While gross differences in hippocampal morphology are not evident in the *Zc3h14*$^{\Delta ex13/\Delta ex13}$ mice, more subtle morphological changes may exist, which would require more detailed analysis. For example, morphological defects in Nab2-null fly mushroom bodies could result from either defects in axon projection, or altered trimming [277]. Given that ZC3H14 is detected in axonal projections [312], loss of ZC3H14 may affect axon projection, which could be assessed within the hippocampus through calbindin immunohistochemistry to visualize altered projection length of infrapyramidal mossy fibers from the DG to the CA3 region [491]. Such studies would help to more clearly define the role of ZC3H14 in the brain.

In summary, further analysis of mechanisms that cause enlarged lateral ventricles in *Zc3h14*$^{\Delta ex13/\Delta ex13}$ mice will be critical to define the pathway(s) affected, such as tauopathy or PCP dysfunction. Disorganization of sensory hair cells and increased steady-state levels of Vangl2 protein further suggest dysregulation of PCP upon loss of ZC3H14. Further investigation of the regions of the brain to detect any subtle morphological differences, especially in the hippocampus would also be important. These studies could contribute to further defining what neuronal pathways are affected by loss of ZC3H14 and how these defects relate to functional consequences for higher order brain function.

4.2.5 Is ZC3H14 required for proper neuronal morphology?

While the vast majority of ZC3H14 is localized in the nucleus, a fraction can be detected in the cytoplasm, particularly in neurons or brain tissue [249]. ZC3H14 can be detected in neurites of cultured neurons [312], suggesting ZC3H14 may play a specific role within neurites. One possibility is loss of ZC3H14 may affect neurite morphology, such as dendritic length or arborization, as these phenotypes are not uncommon in neurological disorders [492]. Proper dendrite morphology is critical for neuronal function, as this enables neurons to receive and integrate input from other cells [493]. DIV12 primary hippocampal neurons cultured from *Zc3h14*$^{\Delta ex13/\Delta ex13}$ mice did not show a difference in dendritic length or arborization [421] compared to control mice, suggesting ZC3H14 is not required for dendrite development *in vitro*. However, whether ZC3H14 could be important for proper dendrite morphology *in vivo* needs to be addressed in the future. Regardless, while dendrite development may not be affected by loss of ZC3H14, other structures such as dendritic spines were affected *in vitro* and thus may also show defects *in vivo*.

The increase observed in steady-state levels of several synaptic proteins in the hippocampus of *Zc3h14*$^{\Delta ex13/\Delta ex13}$ mice [379] prompted us to analyze the effect of ZC3H14 loss on hippocampal synapses. One common parameter assayed in neuronal disorders is dendritic spine density, where an increase or decrease in density is often associated with neurological impairment [235-237, 240, 405]. Furthermore, neurological disorders often exhibit distinct spatiotemporal dendritic spine landscape, in which spine density may be altered or unchanged with respect to brain region and age [235, 240, 405]. Due to this potential for spatiotemporal hit-or-miss detection of altered spine density in *Zc3h14*$^{\Delta ex13/\Delta ex13}$ mice, we first investigated spine density in a single hippocampal subregion at two different time points: during early brain development at postnatal day 7 (P7), and in mature adult brain at 5 months. Spatially, while there is potential for any hippocampal subregion to exhibit dendritic spine changes upon loss of ZC3H14, the DG was examined due to its association with spatial navigation [494-496] and the suggested role of the DG to act as the predominant point of entry for synaptic input to the rest of the hippocampus [224]. Temporally, changes in the relative rates between dendritic spine formation/elimination forms three distinct stages over the course of life: spinogenesis (early life), spine pruning (adolescence), and spine maintenance (adult) [148].

In situ, *Zc3h14*$^{\Delta ex13/\Delta ex13}$ mice show no dendritic spine density difference in the DG at P7, but decreased spine density is detected at 5 months [421]. Unaltered spine density during spinogenesis suggests loss of ZC3H14 generally does not affect spine formation, but the decrease in density during spine maintenance suggests loss of ZC3H14 could contribute to spine elimination during the spine pruning and/or spine maintenance phase. However, ZC3H14 may in fact also modulate spine formation, as altered spine density during spinogenesis may occur in brain regions other than the DG. A major gap in this set of experiments is the lack of

Zc3h14$^{\Delta ex13/\Delta ex13}$ spine density measurements during spine pruning. Spine pruning is characterized by the widespread removal of preexisting spines formed during spinogenesis. Incorporating the analysis of spine density during the pruning stage would help to further understand how loss of ZC3H14 generally affects spine formation and/or elimination, as well as potentially reveal ZC3H14 involvement in pathways required for specific spine regulation phases [497-499].

Unlike the DG, CA1 spine density is unchanged at 5 months in *Zc3h14*$^{\Delta ex13/\Delta ex13}$ mice (unpublished). This finding could indicate a spatially-based model for differential spine density impairment upon loss of ZC3H14, where spine density is specifically reduced in the DG but not CA1 region. Such region-specific differences have been documented for a number of neurological disorders. For example, Fragile X syndrome demonstrates heterogeneous dendritic spine phenotypes dependent on brain region, including between hippocampal subregions [240, 244]. If decreased adult spine density is unique to the DG in the *Zc3h14*$^{\Delta ex13/\Delta ex13}$ brain, one major characteristic that distinguishes the DG from the rest of the hippocampus, as well as most of the rest of the brain [500], is the presence of adult neurogenesis. Adult hippocampal neurogenesis is proposed to be important in learning and memory [501-503], which could include working memory [504-506]. Impaired adult neurogenesis in the DG may also influence spine dynamics and density [447, 507]. One follow up approach to determine whether reduced DG spine density in adult *Zc3h14*$^{\Delta ex13/\Delta ex13}$ mice is associated with altered neurogenesis would be to compare *Zc3h14*$^{+/+}$ and *Zc3h14*$^{\Delta ex13/\Delta ex13}$ DG for the presence of neurogenesis-indicative molecular biomarkers, such as PCNA, PH3, NeuroD,Pax6, and/or DCX [508]. These experiments would begin to refine the requirement for ZC3H14 in distinct brain regions and development stages.

With respect to CA1, making decisive conclusions about whether spine density is altered or not is complex. Detecting differences in CA1 spine density upon loss of ZC3H14 may depend upon analyzing apical versus basal dendrites [509-511], distance from the soma [511], or dorsal/ventral positioning along the hippocampus [512]. Even if after accounting for these variables, if CA1 adult spine density is unchanged, CA1 dendritic spines could still be affected by loss of ZC3H14. Other characteristics such as spine morphology can be impacted without affecting overall spine density [513]. Defining the complete spectrum of changes to spine density and/or morphology as well as any accompanying spatiotemporal parameters will help further contextualize neuronal ZC3H14 function. Overall, further analysis in brain regions (both within and outside the hippocampus) and developmental time points will need to be performed to comprehensively define the effect loss of ZC3H14 has on these essential and neuron-specific postsynaptic dendritic spines, as well as neuronal function and higher order brain function.

Beyond these *in situ* data, we also performed an analysis in cultured primary hippocampal neurons. This analysis revealed a significant decrease in spine density in *Zc3h14*$^{\Delta ex13/\Delta ex13}$ primary hippocampal neurons grown for 19 days *in vitro* (DIV19). Importantly, this decrease in spine density was rescued upon expression of ZC3H14 isoform 1 or 3 [421]. This consistent phenotype even outside the context of developmentally distinct brain regions strengthens a model where ZC3H14 is required to maintain proper dendritic spine density in hippocampal neurons. In contrast, i*n vivo* brain development may set spatiotemporal parameters that help determine the presence or absence of spine density alterations upon loss of ZC3H14. This *in vitro* decrease in spine density occurs specifically in mushroom “memory” spines, while the density of thin and stubby spines is unchanged [421]. This specific loss of mushroom spines is remarkably consistent with our WRAM behavioral data demonstrating impairment specifically

in working memory [379]. The reason why loss of ZC3H14 results specifically in reduced mushroom spines is not yet clear, but could be related to different dendritic spine properties such as spine maturation [514-516], stability [517-519], or degree of synaptic input [131].

In tandem with the rescue of dendritic spine density and mushroom spines by expression of ZC3H14 isoforms 1 or 3 in *Zc3h14*$^{\Delta ex13/\Delta ex13}$ neurons, overexpression of isoform 1 in *Zc3h14*$^{+/+}$ neurons results in an opposite trend in dendritic spine density, causing an increase in spine density [421]. Interestingly, this specifically increases thin "learning" spines as opposed to modulating mushroom spines [421]. This result is the first experimental indication of isoform-specific ZC3H14 function, as overexpression of ZC3H14 isoform 3 did not recapitulate the increased thin spine density phenotype [421]. Of the three nuclear ZC3H14 isoforms (1, 2, and 3), isoform 1 includes all exons while alternative splicing to generate isoform 3 excludes exons 10-12 [249]. The ZC3H14 isoform 1 protein possesses a unique phosphorylation site present in exon 12 (unpublished). This phosphorylation site introduces the possibility of isoform-specific regulation of ZC3H14 as well as phosphorylation-dependent regulation of ZC3H14. These data together provide evidence that ZC3H14 is required to regulate both dendritic spine density and morphology, which may be at least partially dependent upon isoform-specific functions of ZC3H14.

Dendritic spines are categorized as stubby, thin, and mushroom spines on the basis of measurements of the spine length and ratio between head and neck width, thereby generating a range of values that constitute each spine category. Interestingly, analyzing the average morphology within each spine type revealed mushroom spines in DIV19 *Zc3h14*$^{\Delta ex13/\Delta ex13}$ neurons have on average significantly larger head volume than those from control neurons (unpublished). This implies that while there are reduced mushroom spines in *Zc3h14*$^{\Delta ex13/\Delta ex13}$

neurons, the existing mushroom spines are larger on average than those in *Zc3h14*$^{+/+}$ neurons *in vitro*. This finding suggests two possible models for the effect of loss of ZC3H14 on mushroom spines: 1) loss of ZC3H14 promotes enlargement of all existing mushroom spine heads, or 2) loss of ZC3H14 promotes specific loss of mushroom spines with smaller heads. The first model would possibly indicate ZC3H14 normally acts to inhibit the size and/or stability of mushroom spines, while the latter might indicate ZC3H14 normally inhibits mushroom spine turnover. The first model is consistent with increased steady-state levels of CaMKIIα protein upon loss of ZC3H14, which is associated with dendritic spine enlargement [193, 195, 196]. The second model is consistent with small-headed mushroom spines being more susceptible to turnover than large-headed mushroom spines due to the inherent difference in maturity/stability [148, 154]. Regardless, either model cannot be directly addressed with single snapshots of dendritic spines. Defining what mechanism(s) drive specific reduction of mushroom spines upon loss of ZC3H14 may be accomplished through live-cell imaging of spine dynamics comparing *Zc3h14*$^{+/+}$ and *Zc3h14*$^{\Delta ex13/\Delta ex13}$ hippocampal neurons [141, 520-522]. This would ideally be tested with additional ZC3H14 conditions, including rescue and overexpression of ZC3H14 isoforms in *Zc3h14*$^{\Delta ex13/\Delta ex13}$ and *Zc3h14*$^{+/+}$neurons, respectively. This approach would help to test for a direct role of ZC3H14 in regulating dendritic spines *in vivo* and further assess isoform-specific functionality. Of particular interest would be to perform this analysis after mice undergo a learning/memory task, to evaluate potential impairment in learning/memory-induced dendritic spine dynamics [140, 143, 523-525]. Ultimately, analyzing dynamic processes such as rates of dendritic spine formation and turnover, maturity, and stability will provide crucial insight as to how ZC3H14 regulation impacts dendritic spine density and morphology, as well as narrow the range of potential pathways and targets for require ZC3H14-mediated regulation.

In summary, *in situ* analyses of *Zc3h14*$^{\Delta ex13/\Delta ex13}$ DG reveal spine density at P7 is unchanged, but spine density at 5 months is significantly reduced, indicating ZC3H14 may normally inhibit dendritic spine elimination. Spine density was unaltered in the *Zc3h14*$^{\Delta ex13/\Delta ex13}$ CA1 region at 5 months, potentially indicating a spatial distinction in the presence or absence of spine density changes within the hippocampus. DIV19 *Zc3h14*$^{\Delta ex13/\Delta ex13}$ primary hippocampal neurons also exhibit reduced spine density, specifically with fewer mushroom spines but larger mushroom spine heads. Transgenic expression of ZC3H14 isoform 1 or 3 is sufficient to rescue mushroom spine density in *Zc3h14*$^{\Delta ex13/\Delta ex13}$neurons. However, overexpression only of isoform 1in *Zc3h14*$^{+/+}$ neurons caused increased spine density, specifically an increase in thin spines, indicating isoform-specific ZC3H14 function. Overall, these results suggest ZC3H14 regulates both dendritic spine density and morphology, but any spatiotemporal parameters will need to be further defined to characterize the requirement for ZC3H14 specifically in neurons.

4.2.6 Does ZC3H14 affect the proteomic composition of dendritic spines?

A subset of hippocampal proteins show significant altered steady-state levels upon loss of ZC3H14, including many with functions related to the synapse [379]. Of particular interest, total CaMKIIα protein is significantly increased [379], which is consistent with significantly increased CaMKIIα detected in synaptosomes prepared from *Zc3h14*$^{\Delta ex13/\Delta ex13}$ mice [421]. CaMKIIα, which is one of the most highly enriched proteins in dendritic spines, plays a central role in synaptic plasticity, which underlies memory formation [526]. Numerous CaMKII mutant models exhibit impaired LTP and/or learning and memory [174-178], and dysregulated CaMKII is associated with a wide range of neurological disorders [179-184, 527]. Interestingly, ZC3H14 shows enriched association for *CaMKIIα* mRNA in the hippocampus [379] and ZC3H14 is

present in synaptosomes [421]. Together with the evidence that CaMKIIα is increased in hippocampal synaptosomes upon loss of ZC3H14 [421] and Nab2 is required in flies to repress a CaMKII translational reporter [312], suggest *CaMKIIα* as an RNA target of ZC3H14. Additional data implicating ZC3H14 as a negative regulator of translation [312, 379] suggests a model where ZC3H14 negatively represses local CaMKIIα translation. This may be mediated through ZC3H14 limiting poly(A) tail length [379], as altered poly(A) tail length is associated with translational defects [267-269]. Consistent with this model, induced extension of *CaMKIIα* poly(A) tail length following visual experience in rats is accompanied by an increase in CaMKIIα protein in synaptosomes [272]. One future approach that may address whether loss of ZC3H14 affects local translation of CaMKIIα would be to test polysomal association of *CaMKIIα* mRNA between *Zc3h14*$^{+/+}$ and *Zc3h14*$^{\Delta ex13/\Delta ex13}$ synaptosomes [528], both in a stimulated and unstimulated context.

Dysregulated CaMKIIα is associated with learning/memory impairment [174-178], including working memory [194], as well as altered dendritic spine density [529, 530]. In addition, CaMKIIα is implicated in modulating dendritic spine volume, where loss of CaMKIIα activity is associated with impaired dendritic spine enlargement [193] and accumulation of postsynaptic CaMKIIα is associated with increased spine volume [195, 196]. This indicates CaMKIIα may be required in regulating both dendritic spine density and morphology. Loss of ZC3H14 results in decreased dendritic spine density *in situ* and *in vitro* [421] and altered dendritic spine morphology (unpublished). Therefore, CaMKIIα as a functional target of ZC3H14 serves as a particularly attractive molecular link between loss of ZC3H14, dysregulated dendritic spine density and morphology, and memory deficits.

Given the requirement for CaMKIIα to stabilize developed spines [531], it is interesting to consider how increased CaMKIIα upon loss of ZC3H14 might cause a reduction in mushroom spines rather than an increase, especially considering the remaining mushroom spines exhibit larger spine heads, which is a phenotype typically associated with increased synaptic strength/stability [159]. Increased CaMKIIα in *Zc3h14*$^{\Delta ex13/\Delta ex13}$ neurons may impair maturation of thin spines into mushroom spines, but this seems improbable as this would likely be accompanied by an increase in thin spines upon loss of ZC3H14. Another model is that increased CaMKIIα may in fact inhibit mushroom spine stability in *Zc3h14*$^{\Delta ex13/\Delta ex13}$ neurons and therefore increase spine turnover. Spine stability is established through the joint activity of CaMKIIα and CaMKIIβ, with CaMKIIβ facilitating high binding affinity to F-actin [157, 199, 200]. Therefore, spine stability may be inhibited due to a reduction in the ratio of CaMKIIβ:CaMKIIα contained in heteromeric CaMKII holoenzymes, meaning each holoenzyme could have reduced F-actin binding [532]. However, reduced F-actin binding seems to be an inconsistent mechanism when accounting for the larger spine head phenotype exhibited by the remaining mushroom spines. One future experiment that could address this model would be to compare the ratio of insoluble to soluble CaMKIIα in *Zc3h14*$^{+/+}$ and *Zc3h14*$^{\Delta ex13/\Delta ex13}$ synaptosomes, to gauge whether amount of F-actin-bound CaMKIIα is dependent on the presence of ZC3H14. A third and rather intriguing model is that while increased CaMKIIα results in larger mushroom spine heads, additional CaMKIIα activity may be impaired or dysregulated in *Zc3h14*$^{\Delta ex13/\Delta ex13}$ mice and in fact promote spine turnover. Spine size is a general indicator of synaptic strength, but cannot be considered completely equivalent parameters. Correlation between spine size and synaptic strength depends heavily on multiple CaMKII phosphorylation sites, in which certain configurations can increase dendritic spine size while decreasing in synaptic strength [533]. For

example, autonomous CaMKII (T286) increases spine size regardless of synaptic strength, but an increase or decrease in synaptic strength is determined by the phosphorylation state of a separate site (T305/T306) [533]. Synaptic strength is tied to spine stability, so a decrease in synaptic strength may promote spine turnover and potentially result in decreased spine density. This mechanism may explain how an increase in CaMKIIα can result in both decreased dendritic spine density and increased mushroom head volume in *Zc3h14*$^{\Delta ex13/\Delta ex13}$ neurons. Therefore, it would be extremely informative to compare the activation status of different CaMKIIα phosphorylation sites between the *Zc3h14*$^{+/+}$ and *Zc3h14*$^{\Delta ex13/\Delta ex13}$ synaptosomes, to investigate whether the CaMKIIα phosphorylation profile changes upon loss of ZC3H14. Overall, while CaMKIIα is increased in *Zc3h14*$^{\Delta ex13/\Delta ex13}$ synaptosomes, there are still many open questions regarding how this may lead to altered dendritic spine characteristics such as decreased spine density or morphological changes upon loss of ZC3H14.

In addition to accounting for the effects that increased CaMKIIα has on individual dendritic spines, increased CaMKIIα may also differentially affect certain brain regions. While CaMKIIα is abundantly detected throughout the brain, the highest levels are detected in the hippocampus [189]. CaMKIIα distribution in a transgenic CaMKIIα-GFP mouse line yields similar results, with strongest CaMKIIα-GFP expression occurring in the hippocampus, specifically the DG [534]. This may imply that while CaMKIIα is expressed throughout the brain [189, 535], the DG may be of particular interest to examine upon CaMKIIα dysregulation. Interestingly, CaMKIIα deficiency impairs neuronal development in the DG, causing DG immaturity [194]. Immature DG is shared in patients/mouse models of neurological disorders such as schizophrenia, epilepsy, and major depressive disorder [536-539], in which CaMKIIα can be dysregulated [182, 540-542]. In addition, immature DG is associated with behavioral

abnormalities such as working memory deficit and hyperlocomotor activity [194, 543, 544], which is strikingly similar to defects observed in the *Zc3h14*$^{\Delta ex13/\Delta ex13}$ mice [379]. Finally, a link has recently been found between disrupted Vangl2, a core PCP component which is increased in *Zc3h14*$^{\Delta ex13/\Delta ex13}$ hippocampi [379], impaired CaMKIIα phosphorylation, impaired DG granule cell maturation, and defects in pattern completion behavior [486]. This provides a very interesting potential link between increased CaMKIIα and Vangl2 upon loss of ZC3H14 and altered dendritic spine density and/or morphology in *Zc3h14*$^{\Delta ex13/\Delta ex13}$ neurons. In addition, the potential link between dysregulated CaMKIIα and DG-specific impairment may further suggest the existence of differential brain region dysfunction upon loss of ZC3H14. Overall, increased synaptosomal CaMKIIα in *Zc3h14*$^{\Delta ex13/\Delta ex13}$ mice has the potential to dysregulate neuronal function in the dendritic spines, but the mechanism by which this may be accomplished is a subject of intense future investigation, as the roles of CaMKIIα are multifaceted and subject to a high degree of regulation. However, the potential for *CaMKIIα* as a specific mRNA target of ZC3H14 regulation could be fundamental in understanding how loss of ZC3H14 results in neuronal dysfunction, as well as why loss of ZC3H14 as a ubiquitous RNA binding protein results in a tissue-specific disorder.

In summary, CaMKIIα is increased in *Zc3h14*$^{\Delta ex13/\Delta ex13}$ synaptosomes [421]. The presence of ZC3H14 in synaptosomes along with enriched association with *CaMKIIα* mRNA [421] suggests *CaMKIIα* as an RNA target of ZC3H14. Association of ZC3H14 with polysomes and the requirement of Nab2 in flies to repress a CaMKII translational reporter [312] further suggest ZC3H14 may act to repress CaMKIIα local translation in neurites. Increased synaptosomal CaMKIIα may be responsible for the decreased mushroom spine density and/or increased mushroom head volume phenotypes observed in *Zc3h14*$^{\Delta ex13/\Delta ex13}$ hippocampal neurons

[421], but the method in which this may occur through CaMKIIα is unknown, and may rely on such factors as CaMKIIα phosphorylation or altered binding to F-actin. In addition, a potential link between dysregulated CaMKIIα and DG impairment may provide additional context as to how loss of ZC3H14 results specifically in higher order brain dysfunction, but further characterization of both the brain and CaMKIIα in *Zc3h14*$^{\Delta ex13/\Delta ex13}$ mice is necessary.

4.3 Concluding remarks

ZC3H14 is a ubiquitously expressed polyadenosine RNA binding protein that is associated with autosomal recessive nonsyndromic intellectual disability. Prior to this thesis, no studies had been performed to characterize the role of ZC3H14 in vertebrates, let alone in the mammalian brain, which depends on a complex regulatory system of RNA processing. We created a novel *Zc3h14*$^{\Delta ex13/\Delta ex13}$ mutant mouse model to characterize the role of ZC3H14 in the mammalian brain and gain insight as to how ZC3H14 contributes to maintaining higher order brain function. This was investigated across multiple levels of function, including changes in behavior, brain structure, neuron morphology, proteomic composition, and altered RNA regulation, upon loss of ZC3H14.

We hypothesized that ZC3H14 is necessary for higher order brain function by regulating critical RNA targets that maintain proper neuronal function. Critically, we identified loss of ZC3H14 results in working memory defects and altered steady-state levels of a subset of proteins in the hippocampus, including a number of proteins with roles related to the synaptic function. Among these, CaMKIIα is significantly increased in *Zc3h14*$^{\Delta ex13/\Delta ex13}$ hippocampi, including in synaptosomes. This provides a critical link between ZC3H14 regulation of RNAs and higher order brain function, as CaMKIIα is a known modulator of synaptic plasticity and

learning/memory, and ZC3H14 shows enriched association for *CaMKIIα* mRNA, suggesting *CaMKIIα* as an RNA target of ZC3H14. Analyzing dendritic spines, where CaMKIIα is enriched, *Zc3h14*$^{\Delta ex13/\Delta ex13}$ hippocampal neurons show altered dendritic spine density, which is rescued upon exogenous ZC3H14 expression. This finding provides a model by which dysregulated CaMKIIα upon loss of ZC3H14 may alter the dendritic spine landscape in *Zc3h14*$^{\Delta ex13/\Delta ex13}$ mice and ultimately impair processes critical for higher order brain function, such as working memory.

Together, these findings support a model, illustrated in **Figure 4-1**, where ZC3H14 plays a critical role in higher order brain function by regulating specific RNAs, such as *CaMKIIα.* Loss of ZC3H14 results in increased CaMKIIα in synaptosomes and impaired neuronal function, including altered dendritic spine density. More investigation will be required to understand precisely how ZC3H14 regulates specific RNA targets in the brain to produce these specific morphological and functional impairments in neurons. A puzzling question remains as to why an RNA binding protein with high affinity for polyadenosine RNAs does not regulate a larger set of RNAs. However, this thesis provides the first characterization of ZC3H14 function in the mammalian brain and provides some initial insight as to how loss of a ubiquitous RNA binding protein could result in a disorder that manifests primarily as a defect in higher order brain function.

Figures

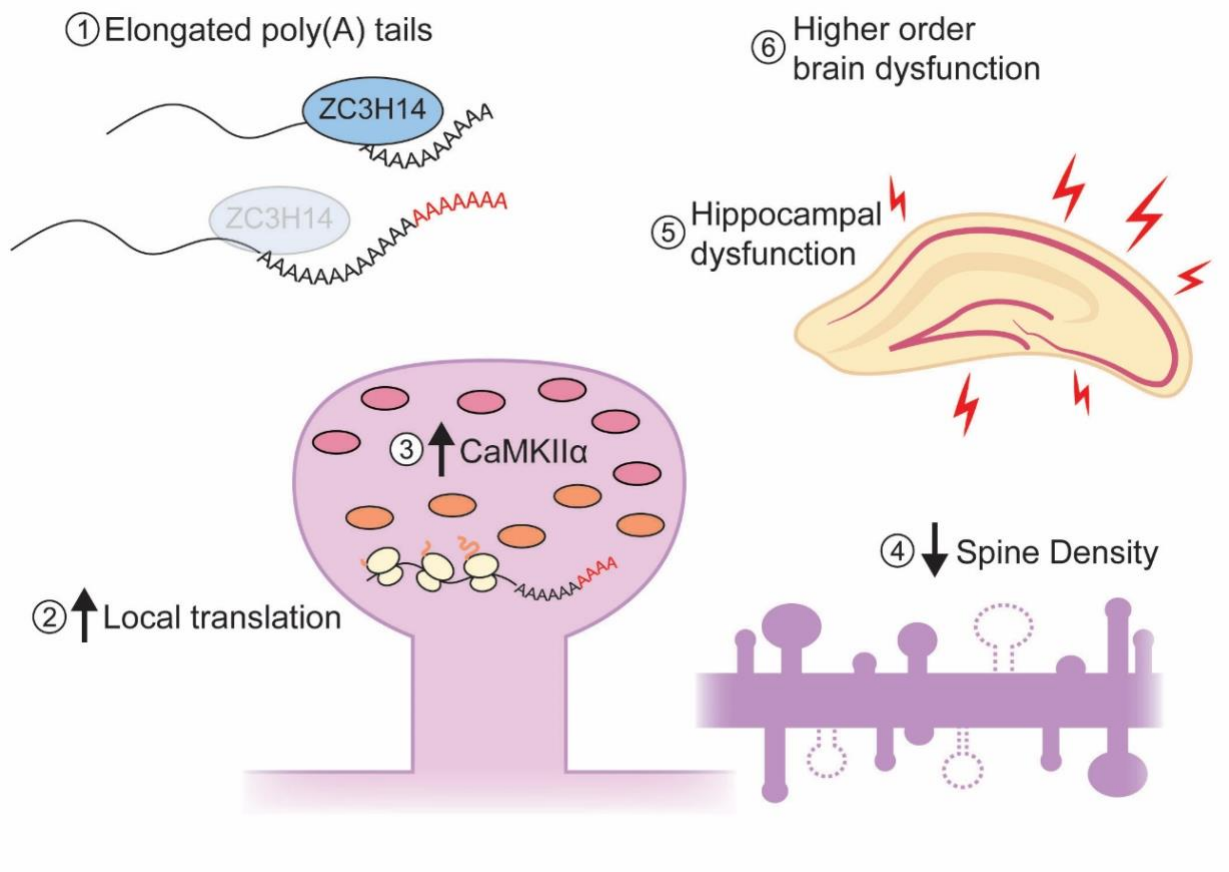

Figure 4-1: Model of RNA Regulation by ZC3H14 in Neurons. This speculative model presents a way in which loss of ZC3H14 (blue) results in impaired higher order brain function in *Zc3h14*$^{\Delta ex13/\Delta ex13}$ mice, based on evidence gathered over the course of this thesis. 1) Bulk RNA poly(A) tails are elongated upon loss of ZC3H14. It is predicted that ZC3H14 preferentially binds to specific RNAs, including *CaMKIIα*, and may thus elongate *CaMKIIα* poly(A) tail length as well. 2) Elongated poly(A) tail length can result in various downstream regulatory effects, including increased translation. This is predicted to occur for *CaMKIIα* mRNA, which is subject to local translation in neurons. 3) ZC3H14 is suggested to act as a negative regulator of translation, thereby increasing CaMKIIα levels (pink and orange), which is detected in synaptosomes and is known to be enriched in dendritic spines. 4) Loss of ZC3H14 decreases

hippocampal dendritic spine density both *in situ* and *in vitro*, with morphological analyses *in vitro* indicating specific reduction in mushroom spines and enlarged mushroom spine heads. CaMKIIα is critical in synaptic plasticity and has been implicated to regulate both dendritic spine density and morphology, therefore increased CaMKIIα.may result in these altered dendritic spine characteristics. 5) Alterations in dendritic spines may contribute to impairment of brain regions, including the hippocampus, which serves as a major center for learning/memory. 6) Loss of ZC3H14 in the hippocampus may impair higher order brain function, including a deficit in working memory in *Zc3h14*$^{\Delta ex13/\Delta ex13}$ mice.

Chapter 5

Materials and Methods

5.1 Materials and Methods: Chapter 2

Generation of *Zc3h14*$^{\Delta ex13/\Delta ex13}$ mouse Mouse embryonic stem cells (clone EPD0366_5_F01, ES cell strain C57BL/6N, Parental Cell Line JM8A3.N1) were obtained from Knockout Mouse Project Repository (UC Davis, Davis, CA). This clone flanks with *loxP* sites exon 13, the first common exon among all four *Zc3h14* isoforms (a, b, c, d) (see Fig. 1 A and B). *In vitro* Flp-*FRT* recombination to eliminate the *LacZ*/*neomycin* cassette and subsequent blastocyst injections were performed by the Emory Mouse Transgenic and Gene Targeting Core. We generated heterozygously floxed *Zc3h14* exon 13 mice (*Zc3h14*$^{F/+}$) by mating adult male chimeras to C57BL/6N wildtype female mice (The Jackson Laboratory). Offspring generated from this mating were then mated to generate homozygously floxed mutant mice (*Zc3h14*$^{F/F}$). *EIIa-Cre* mice (purchased from The Jackson Laboratory, Stock #003724, mixed C57BL/6J and C57BL/6N genetic background) which express Cre-recombinase active at the zygotic stage [294], were mated to homozygously floxed *Zc3h14* exon 13 (*Zc3h14*$^{F/F}$) mice for 3-4 generations to generate a germline-transmissible *Zc3h14* allele lacking exon 13 (*Zc3h14*$^{\Delta ex13/\Delta ex13}$). These mice with confirmed proper recombination were mated to wildtype C57BL/6 mice (purchased from The Jackson Laboratory) to breed out the *EIIa-Cre* allele. *EIIa-Cre*-negative, *Zc3h14*$^{\Delta ex13/+}$ were mated to generate *Zc3h14*$^{\Delta ex13/\Delta ex13}$ mutant homozygous mice for at least four generations.

Control *Zc3h14*$^{+/+}$ were maintained in the colony as control counterparts from the heterozygous *Zc3h14*$^{\Delta ex13/+}$ breeders. Generations F4-F8 of *Zc3h14*$^{+/+}$ (and *Zc3h14*$^{\Delta ex13/\Delta ex13}$) homozygous pairings were used for experiments, and homozygous off-spring were routinely cross-bred to minimize genetic drift between *Zc3h14*$^{+/+}$ and *Zc3h14*$^{\Delta ex13/\Delta ex13}$ mice.

All procedures involving mice were done in accordance with the NIH guidelines for use and care of live animals and were approved by the Emory University Institutional Animal Care and Use Committee.

Genotyping Mice were screened for the conditional floxed allele, Cre-mediated recombination, and the Cre-recombinase gene by PCR of genomic DNA isolated from toe clippings using a standard DNA isolation protocol [545]. Tissue from toe clippings was lysed in 50 µl of standard lysis buffer supplemented with Proteinase K overnight at 55°C. Samples were centrifuged for 5 min at full speed to sediment cellular debris. Genomic DNA was precipitated using ice-cold 100% ethanol, washed two times in 75% ethanol, and allowed to air dry before being resuspended in 30 µl of water. Template DNA was amplified by standard PCR per the Qiagen *Taq DNA Polymerase* PCR kit manufacturing protocol (Qiagen 201205). The following primers were used to genotype mice at the *Zc3h14* locus (as illustrated in Fig. 1 B and C): Fwd (5'-GTTGGCTCATCTTCTGTAAAGC-3') and RevI (5'-GGTAAGGAAAACTAATCCACATCTAG-3') for the conditional floxed allele (generating a product of either 885 bp for control, 994 bp for floxed, or 230 bp for recombined alleles) or RevII (5'-GCCACACTCAGGTCAGTCATCTCG-3') for the direct detection of exon 13 (generating a product of either 469 bp for control or 625 bp for floxed, or no product for the recombined allele which excises exon 13). For detection of the Cre-recombinase gene, generic Cre-recombinase primers were used: Fwd-Cre (5'-GCGGTCTGGCAGTAAAAACTATC-3') and Rev-Cre (5'-GTGAAACAGCATTGCTGTCACTT-3').

Immunoblotting Mouse brain tissue samples were lysed in RIPA-2 buffer (50 mM Tris–HCl, pH 8.0, 150 mM NaCl, 1% IGEPAL or NP-40, 0.5% deoxycholic acid, 0.1% SDS) containing protease inhibitors (Complete Mini; Roche) and centrifuged at 9,200 x g for 10 min at 4°C. The pellet was discarded, and the supernatant was subjected to SDS-PAGE and immunoblotting. An equal amount of protein from each sample was loaded onto 10% SDS-polyacrylamide gels and transferred to a 0.2 μm nitrocellulose membrane (Bio-Rad Laboratories) [546]. After blocking non-specific binding, the membranes were incubated with the primary antibodies. Primary antibodies used were as follows: anti-ZC3H14 (rabbit polyclonal antibody generated against the N-terminal PWI-like domain) [249], EIF5 (Santa Cruz sc-282), α-Tubulin (Sigma T9026), Histone H3 (Abcam ab1791), THOC1 (kind gift from Dr. Robin Reed, Harvard University, Boston, MA), S6 Ribosomal Protein (5G10) (Cell Signaling 2217), followed by incubation with the appropriate horseradish peroxidase (HRP)-conjugated secondary IgG antibody (Jackson ImmunoResearch).

Real-time PCR analysis of *Zc3h14* splice variant d mRNA To obtain RNA from mouse tissue, brain was lysed using QIAzol, according to the guidelines of the manufacturer (Qiagen). cDNA was synthesized from RNA isolated from mouse whole brain using M-MLV Reverse Transcriptase kit (Invitrogen 28025), GoTaq DNA Polymerase (Promega M3001), and Recombinant RNasin Ribonuclease Inhibitor (Promega N2511). Briefly, 5 ng of cDNA was subjected to PCR amplification using SYBR Green PCR Master Mix (Applied Biosystems) and *Zc3h14* splice variant d-specific primers: Fwd (5’GGTTGAGAAAGGAACTCAACAGAGGC-3’) (junction of alternative exon 1 and exon 10) and Rev (5’-TCATCTCGGCTTGACTCATCTCCA-3’) (junction of exons 10 and 13). PCR amplification

was performed with an Applied Biosystems, StepOnePlus Real-Time PCR System. The 18S rRNA was used to normalize mRNA. Relative quantitation of mRNA expression level was determined using the relative standard curve method as previously described [547] and according to the instructions of the manufacturer (Applied Biosystems).

ZC3H14 immunoprecipitation for mass spectrometry analysis Brain tissue was homogenized in IP buffer (50 mM Tris-HCl, pH 7.4, 100 mM NaCl, 32 mM NaF, 0.5% NP-40 in DEPC-treated water) containing protease inhibitors (Complete Mini; Roche; 1 tablet/10 mL of IP buffer). Cells were sonicated on ice 5 times at 0.5% output for 10 sec, passed through a 27-gauge syringe 5 times, and placed back on ice for 20 minutes with occasional vortexing. Lysates were spun at 15,600 x g for 10 minutes at 4°C and protein concentrations were determined with a standard BCA assay. Protein G magnetic beads (DYNA beads, Invitrogen) were rinsed and resuspended in IP buffer and incubated with pre-immune rabbit serum or an equal volume of N-terminal ZC3H14 antibody for 1 hour at room temperature. Bead/antibody and bead/pre-immune samples were rinsed in IP buffer and added to clarified cell lysates. Ten percent of the sample was then removed and reserved for input analysis, and the remainder of the sample was incubated overnight at 4°C while tumbling end over end. Beads were then magnetized to collect bound and unbound species separately. The beads were washed 5 times with ice-cold IP buffer. ZC3H14 protein complexes were eluted with reducing sample buffer (RSB): 250 mM Tris HCL, 500 mM DTT, 10% SDS, 0.5% bromophenol blue, 50% glycerol. Upon submission to the Emory Proteomics Core for mass spectrometry analysis, the samples were further reduced with DTT and alkylated with Iodoacetamide (IAA), and then subjected to sequential in-solution digestion with LysC (1:100 enzyme-to-protein ratio) for 4 hrs and with trypsin (1:100 enzyme-to-protein ratio)

overnight. After desalting and sample cleanup with Water's Sep-Pak, the samples were submitted for analysis on the Orbitrap Fusion Mass Spectrometer (Thermo Scientific).

Determination of bulk poly(A) tail length Bulk poly(A) tails were analyzed using a standard poly(A) tail length assay [548] as described previously [549]. Total RNA was isolated from hippocampi of P0 *Zc3h14*$^{+/+}$ and *Zc3h14*$^{\Delta ex13/\Delta ex13}$ mice using a RNeasy mini kit (Qiagen 74104). Total RNA was 3'end labeled with [^{32}P]pCp using T4 RNA ligase and digested with a cocktail of RNAse A/T1. The resulting tracts of poly(A) RNA were resolved by gel electrophoresis and imaged by film or PhosphorImager. Three biological replicates were performed for each mouse genotype analyzed. Using ImageJ software, densitometry analysis of each experiment was performed in order to obtain profile curves for each sample that was analyzed, as described previously [264]. Profiles of the relative signal intensity at a given location on the gel were plotted in Microsoft Excel and a moving average (period = 25) calculated.

Immunohistochemical analysis of brain morphology Whole brains were fixed overnight in 4% PFA, processed for routine embedding in paraffin, and cut 9 μm in thickness onto glass slides. Slides were dewaxed in xylene and rehydrated through graded ethanol washes. Haematoxylin and eosin staining was performed using standard procedures. Alternatively, slices were stained with cresyl violet to assess hippocampal morphology.

Images were visualized on an Olympus BX51 microscope using a 2X magnification objective and captured using DP Controller (Olympus) software. Genotype of all brain images was blinded for the analyses, and the quantification of ventricular area was performed using ImageJ.

Y maze The Y-maze is made of three centrally-joined arms (8 in-tall x 15.5 in-long x 4 in-wide) made of opaque Plexiglas with an arm angle of 120°. Using 10 homozygous wildtype and 10 homozygous mutant male mice, mice were individually placed in the central intersection and allowed to explore the maze for 8 minutes. Arm entries were automatically recorded using TopScan software by CleverSys. The mouse's midpoint needed to be inside the arm to count as an entry. Correct alternation is defined as entry into an arm different from the last two arm entries (e.g. ABC, CAB, BCA, CBA, BAC, or ACB, but not ABA, CAC, etc.). The maze was cleaned with Virkon between each test to remove olfactory cues. % correct alternation was calculated as: % Correct Alternation= [(Number of Correct Alternations)/(Total arm entries)] x 100. The Y-maze assay was performed by Jason Schroeder with the Emory University Rodent Behavioral Core.

Fear Conditioning Fear conditioning was performed using an established Coulbourn system (7 x 7 x 12 in), utilizing a metal shock grid floor. On the training day, mice were allowed to acclimate to the chamber for three minutes followed by three trials of tone (85 dB)-shock (mA?) pairings. Each tone-shock session lasted 20 s, with the shock occurring within the last 0.5 s of the tone. Each trial was separated by one minute. To assay contextual freezing, mice were returned to the same chamber the following day for eight minutes with no tone or shocks administered and measured for percent freezing. To assay cued fear, mice were placed in a new chamber the next day for three minutes, followed by the 85 dB tone for six minutes and measured for percent freezing. Percent freezing (defined as a lack of any movement/total time x 100) was measured

each day in one minute intervals (FreezeFrame software; Actimetrics). The Fear Conditioning assay was performed by Jason Schroeder with the Emory University Rodent Behavioral Core.

Water radial arm maze (WRAM) The WRAM apparatus was used as previously described [306]. A radial maze, 2 m in diameter with 8 arms of equal width and length (10 cm wide and 60 cm long) at 45-degree angles surrounding an open center section, was filled with water at approximately 21ºC (see Fig. 5A). The water was made opaque by mixing in water-soluble, non-toxic paint of the same color (black) as the maze and the platforms. The water was filled to a level 0.5-1.0 cm above the top of all four total submerged platforms, placed one each at the far end of half of the arms. A specific orientation of platforms, constant for each mouse throughout the testing period, was placed in the arena with the following criteria: the “start” arm always contained no platform and no more than 2 adjacent arms contained platforms.

Ten *Zc3h14*$^{+/+}$ and nine *Zc3h14*$^{\Delta ex13/\Delta ex13}$ male adult (5 month old) mice were tested. At the start of each trial, a mouse was placed inside a clean, dry, empty cage heated with a lamp to approximately 40ºC. Once the platforms were placed in the correct orientation, the mouse was gently placed in the water at the far end of the "start" arm, and the timer was started. A blinded researcher monitored the progress of the mouse by recording both the sequence of arms the mouse entered and the time in seconds the mouse took to locate a platform, with a maximum trial length of 120 seconds before the trial was aborted and the mouse was gently guided to the nearest platform. When a mouse reached a platform, it was allowed to remain there for 15 seconds, allowing time for it to identify any visual cues placed on the walls to aid in spatial memory. The mouse was then returned to the heated and dry cage for a period of 30 seconds as a reward for successfully completing the trial. The platform on which the mouse was seated was

removed, and the next trial commenced in the same manner. Four trials were performed per mouse, per day, until each mouse had located all 4 platforms. Testing was conducted for 9 consecutive days.

We used the following criteria to analyze WRAM data. To plot *total latency*, time required to reach the platforms were recorded for each mouse and summed across the four trials per day. After groups were unblinded, these latencies were calculated across the 9-day testing period. To plot *overall total errors*, each entry into an arm that did not result in locating a platform was summed across the four trials for each mouse per day. These errors were then sorted into 3 types: I) errors in which the first time on a given trial a mouse enters any arm that contained a platform on a previous trial on the same day (shows good working and spatial memory but poor procedural memory); II) errors in which the first time on a given trial a mouse enters any arm that never contained a platform or else enters an arm with a platform but does not successfully locate the platform (shows poor spatial memory); III) errors in which a mouse makes a repeated entry into any arm for which it has previously registered a type I or type II error on the same trial (shows poor working memory). To plot *working memory errors*, groups were then unblinded, and type III errors were summed for the four trials per day across the 9-day testing period, at which point a steady-state minimum was achieved, indicating sufficient performance. Sufficient performance on the WRAM requires that a group make an average of no more than approximately 1.0 type III error per subject per day by the conclusion of testing in order to demonstrate learning.

Open field Open field was performed as previously described [550]. Briefly, the mice were acclimated to the testing room for two hours prior to initiating the task. Twelve *Zc3h14*$^{+/+}$ and

twelve *Zc3h14*$^{\Delta ex13/\Delta ex13}$ male adult mice (3-4 months) were examined. Each mouse was placed into the center of an opaque Plexiglas box (60 x 60 x 60 cm) and given 10 minutes to explore the apparatus. The center zone was defined as the region 15 cm from each side of the box. The time spent in the center, number of entries into the center, total distance traveled, and average speed were recorded and scored with AnyMaze video tracking software (Stoelting Co. IL) by a user blinded to genotype.

Novel cage Twelve *Zc3h14*$^{+/+}$ and twelve *Zc3h14*$^{\Delta ex13/\Delta ex13}$ male adult mice (3-4 months) were examined. Each mouse was placed into an uncovered cage with corncob bedding for 10 minutes. General mobility and exploratory actions such as rearing, digging, and grooming were scored.

Light-dark box Twelve *Zc3h14*$^{+/+}$ and twelve *Zc3h14*$^{\Delta ex13/\Delta ex13}$ male adult mice (3-4 months) were examined. The apparatus comprised a Plexiglas box (30 x 14 x 14.5 cm) was divided into a light (20 x 14 x 14.5 cm) and dark side (10 x 14 x 14.5 cm). The walls of the dark side were blackened to reduce external illumination. A hole in the divider between the two sides enabled movement of the mouse between the two sections. Each mouse was placed into the light side and given 10 minutes to explore freely. Latencies to first enter the dark side, the number of transitions between each side, and total time spent in each side was recorded for each mouse.

Optokinetic tracking (OKT) To assess visual function, we measured visual acuity and contrast sensitivity using optokinetic tracking behavior (OptoMotry, Cerebral Mechanics, Inc., Lethbridge, Alberta, Canada) [348-350]. Both mice employed for the WRAM analyses and independent cohorts were assessed in these assays. Four *Zc3h14*$^{+/+}$ and four *Zc3h14*$^{\Delta ex13/\Delta ex13}$

mice were placed on a platform in the center of a virtual optomotor drum consisting of four computer monitors. Spatial frequency thresholds were determined by varying the spatial frequency at 100% contrast. Contrast sensitivity thresholds were determined by varying contrast at peak contrast sensitivity (0.064 cycles/degree). Positive responses were noted as reflexive head-tracking in the direction of the moving gratings. Both eyes were tested by using clockwise and counter-clockwise rotations [308]. The values from the left and right eyes were averaged for analysis of differences between groups at 6 weeks of age using a two-way repeated ANOVA with Holm-Sidak post-hoc.

Wire-hang assay Testing was performed with 1- x 1-cm mesh hardware fixed to a 19- x 19-cm frame. Nine *Zc3h14*$^{+/+}$ and 14 *Zc3h14*$^{\Delta ex13/\Delta ex13}$ male adult mice were placed on the wire mesh, which was slowly inverted 27.5 cm over a soft, thick heating pad (unheated), lined with paper towels. Latency to fall was recorded in seconds as previously described [551]. The test was performed three trials a day for three days for each mouse. The maximum latency to fall for each day was averaged together for the three days for each mouse.

Rotarod A four-lane motorized rotarod (Rotamex-5 Controller, Columbus Instruments, Columbus, OH) was used according to manufacturer's instructions and as previously described [551]. Each rod was 3.0 cm in diameter and 9.5 cm long. The fall height from rod center was 44.5 cm to the base. Scanning infrared beam sensors monitored animals' absence from rod to detect time to fall. The acceleration interval (1.0 sec), acceleration step (0.1 RPM), and maximum speed (50.0 RPM) was the same for each mouse and for all testing days. Prior to

testing, mice were trained on a rotarod (AccuRotor Rota Rod RR4/M, AccuScan Instruments, Columbus, OH) that had a constant speed of 4.2 RPM.

Nine *Zc3h14*$^{+/+}$ and 10 *Zc3h14*$^{\Delta ex13/\Delta ex13}$ male adult mice were allowed to acclimate to the room for 15 min. All mice were oriented on the rod to walk forward to maintain balance. To avoid falling, mice were required to move forward in a coordinated manner. Training occurred over 3 days. Four mice at a time were trained for 10 min on the rotarod at constant speed, replacing mice back on the rod when subjects had fallen from the rotarod. After training on the third day, the mice started the 3-day testing phase. Each day of testing consisted of 3 trials, with at least 15 min of rest in between trials, for a total of 9 trials. Latency to fall was averaged for the three trials within a particular day and analyzed using the two-tailed Student's *t*-test with the Bonferroni correction for repeated measures. *P* values of 0.05 or less were taken as statistically significant. The genotype of the mice were blinded until all latency times were recorded.

Mass spectrometry analysis of *Zc3h14*$^{+/+}$ and *Zc3h14*$^{\Delta ex13/\Delta ex13}$ hippocampi Samples submitted for mass spectrometry analysis consisted of eight hippocampi from four *Zc3h14*$^{+/+}$ and eight hippocampi from four *Zc3h14*$^{\Delta ex13/\Delta ex13}$ mice at P0. Each tissue piece was uniformly homogenized in 300 µL of urea lysis buffer (8 M urea, 100 mM $NaHPO_4$, pH 8.5), including 3 µL (100x stock) HALT protease and phosphatase inhibitor cocktail (Pierce). All homogenization was performed using a Bullet Blender (Next Advance) according to manufacturer protocols. Briefly, each tissue piece was added to Urea lysis buffer in a 1.5 mL Rino tube (Next Advance) harboring 750 mg stainless steel beads (0.9-2 mm in diameter) and blended twice for 5 minute intervals in the cold room (4°C). Protein supernatants were transferred to 1.5 mL Eppendorf tubes and sonicated (Sonic Dismembrator, Fisher Scientific) 3 times for 5 s with 15 s intervals of

rest at 30% amplitude to disrupt nucleic acids and subsequently vortexed. Protein concentration was determined by the bicinchoninic acid (BCA) method, and samples were frozen in aliquots at −80°C. Protein homogenates (100 µg) were diluted with 50 mM NH_4HCO_3 to a final concentration of less than 2 M urea and then treated with 1 mM dithiothreitol (DTT) at 25°C for 30 minutes, followed by 5 mM iodoacetimide (IAA) at 25°C for 30 minutes in the dark. Protein was digested with 1:100 (w/w) lysyl endopeptidase (Wako) at 25°C for 2 hours and further digested overnight with 1:50 (w/w) trypsin (Promega) at 25°C. Resulting peptides were desalted with a Sep-Pak C18 column (Waters) and dried under vacuum.

For LC-MS/MS analysis, hippocampal derived peptides were resuspended in peptide 100 µL of loading buffer (0.1% formic acid, 0.03% trifluoroacetic acid, 1% acetonitrile). Peptide mixtures (2 µL) were separated on a self-packed C18 (1.9 µm Dr. Maisch, Germany) fused silica column (25 cm x 75 µM internal diameter (ID); New Objective, Woburn, MA) by a Dionex Ultimate 3000 RSLCNano and monitored on a Fusion mass spectrometer (ThermoFisher Scientific , San Jose, CA). Elution was performed over a 120 minute gradient at a rate of 400 nL/min with buffer B ranging from 3% to 80% (buffer A: 0.1% formic acid in water, buffer B: 0.1 % formic in acetonitrile). The mass spectrometer cycle was programmed to collect at the top speed for 3 second cycles. The MS scans (400-1600 m/z range, 200,000 AGC, 50 ms maximum ion time) were collected at a resolution of 120,000 at m/z 200 in profile mode and the HCD MS/MS spectra (0.7 m/z isolation width, 30% collision energy, 10,000 AGC target, 35 ms maximum ion time) were detected in the ion trap. Dynamic exclusion was set to exclude previous sequenced precursor ions for 20 seconds within a 10 ppm window. Precursor ions with +1, and +8 or higher charge states were excluded from sequencing.

MaxQuant for label-free quantification Raw data files were analyzed using MaxQuant v1.5.2.8 with Thermo Foundation 2.0 for RAW file reading capability. The search engine Andromeda was used to build and search a concatenated target-decoy IPI/Uniprot mouse reference (downloaded at Aug 14, 2015) supplement with eGFP protein sequence. Protein Methionine oxidation (+15.9949 Da) and protein N-terminal acetylation (+42.0106 Da) were variable modifications (up to 5 allowed per peptide); cysteine was assigned a fixed carbamidomethyl modification (+57.0215 Da). Only fully tryptic peptides were considered with up to 2 miscleavages in the database search. A precursor mass tolerance of ±10 ppm was applied prior to mass accuracy calibration and ±4.5 ppm after internal MaxQuant calibration. Other search settings included a maximum peptide mass of 6,000 Da, a minimum peptide length of 6 residues, 0.6 Da Tolerance for iron trap HCD MS/MS scans. The false discovery rate (FDR) for peptide spectral matches, proteins, and site decoy fraction were all set to 1%. The label free quantitation (LFQ) algorithm in MaxQuant [309, 552] was used for protein quantitation. LFQ intensity of each protein for each mouse was averaged from two hippocampi (left and right). No more than two missing values were considered per group ($Zc3h14^{\Delta ex13/\Delta ex13}$ or $Zc3h14^{+/+}$). Differentially expressed proteins were found by calculating Student's t-test p values and fold difference $|\log2(Zc3h14^{\Delta ex13/\Delta ex13}/Zc3h14^{+/+})| \geq 0.32$ ($\geq \pm 1.25$ fold change). Volcano plots were plotted with ggplot2 packages in R.

GO enrichment, network, and heatmap Functional enrichment of the modules was determined using the GO-Elite (v1.2.5) package [553]. The set of total proteins identified and quantified (n = 4,161) was used as the background. Input lists included proteins either significantly decreased (n = 50) or increased (n = 63) in $Zc3h14^{\Delta ex13/\Delta ex13}$ mice. Z-score determines overrepresentation of

ontologies in a module and permutation P-value was used to assess the significance of the Z-score. For these down regulated proteins in *Zc3h14*$^{\Delta ex13/\Delta ex13}$ mice, Z-score cut off of 1.96, *p* value cut off of 0.05 with a minimum of 3 proteins per category were used as filters in pruning the ontologies. For these up regulated proteins in *Zc3h14*$^{\Delta ex13/\Delta ex13}$ mice, Z-score cut off of 2.58, P value cut off of 0.01 with a minimum of 5 proteins per category were used as filters in pruning the ontologies. Horizontal bar graph was plotted in R. The networks were constructed using the igraph package in R [554]. The heatmap and hierarchical clustering were generated using the default parameters in Perseus [555].

Statistical analysis Data were analyzed using R, GraphPad Prism 6.0, or Microsoft Excel. R, Prism, or Microsoft Excel was also used to generate graphs, column and row means and standard error of the means (SEMs), and statistical analyses (two-way ANOVA, *t*-tests, and post-hoc analysis) to compare between genotypes. *P* values are > 0.05, unless otherwise noted. *P* values < 0.05 were considered statistically significant. Error bars indicate SEM unless otherwise noted.

5.2 Materials and Methods: Chapter 3

Mice Mouse lines *Zc3h14*$^{+/+}$ and *Zc3h14*$^{\Delta ex13/\Delta ex13}$ were bred and maintained as previously described [379].We previously generated heterozygously floxed *Zc3h14* exon 13 mice (*Zc3h14*$^{F/+}$) by mating adult male chimeras to C57BL/6N wild-type female mice (The Jackson Laboratory). Offspring generated from this mating were then mated to generate homozygously floxed mutant mice (*Zc3h14*$^{F/F}$). *EIIa-Cre* mice (purchased from The Jackson Laboratory, Stock #003724, mixed C57BL/6J and C57BL/6N genetic background) which express Cre-recombinase active at the zygotic stage [294], were mated to homozygously floxed *Zc3h14* exon 13

(*Zc3h14*$^{F/F}$) mice for 3-4 generations to generate a germline-transmissible *Zc3h14* allele lacking exon 13 (*Zc3h14*$^{\Delta ex13/\Delta ex13}$). These mice with confirmed proper recombination were mated to wild-type C57BL/6 mice (purchased from The Jackson Laboratory) to breed out the *EIIa-Cre* allele. *EIIa-Cre*-negative, *Zc3h14*$^{\Delta ex13/+}$ were mated to generate *Zc3h14*$^{\Delta ex13/\Delta ex13}$ mutant homozygous mice for at least four generations.

Control *Zc3h14*$^{+/+}$ were maintained in the colony as control counterparts from the heterozygous *Zc3h14*$^{\Delta ex13/+}$ breeders. *Zc3h14*$^{+/+}$ (and *Zc3h14*$^{\Delta ex13/\Delta ex13}$) homozygous pairings were used for experiments, and homozygous off-spring were routinely cross-bred to minimize genetic drift between *Zc3h14*$^{+/+}$ and *Zc3h14*$^{\Delta ex13/\Delta ex13}$ mice.

All procedures involving mice were performed in accordance with the NIH guidelines for use and care of live animals and were approved by the Emory University Institutional Animal Care and Use Committee.

Golgi Staining Male mice were sacrificed and whole brains isolated at either postnatal day 7 (P7) (six (6) *Zc3h14*$^{+/+}$, five (5) *Zc3h14*$^{\Delta ex13/\Delta ex13}$) or 5 months old (three (3) *Zc3h14*$^{+/+}$, three (3) *Zc3h14*$^{\Delta ex13/\Delta ex13}$). Whole brains were subsequently processed using the FD Rapid GolgiStain® Kit protocol [385, 386, 556]. After complete penetration of the Golgi stain solutions, brains were dip frozen in a block of optimal cutting temperature (OCT) compound and sliced coronally on a Leica CM1850 cryostat at a slice thickness of 240 μm onto gelatin-coated slides. Slides were stained and counterstained with cresyl violet, cleared, and mounted with Permount as according to the FD Rapid Golgi stain Kit protocol.

Images of dendrites from dentate gyrus granule cells were captured using an Olympus BX51 brightfield microscope at 100x. Cells were required to have at least one unbroken dendrite at least 75 μm long and originating from the soma to be considered for imaging. The fine focus was manually adjusted every ~0.5 μm to capture the whole image area, with stacking and compositing performed in Adobe Photoshop CS5. Dendritic spines were manually called and counted. Experimenters were blinded to genotype while both imaging and counting. Significance was calculated using an unpaired *t* test.

Primary hippocampal neuronal culture Dissociated hippocampal neurons were cultured from embryonic day 17.5 (E17.5) mouse embryos of both sexes from a single litter. Briefly, brains were removed from embryos, and then hippocampi were dissected in ice cold Hank's Balanced Salt Solution (HBSS). Hippocampi were pooled together and dissociated using trypsin for 12 minutes, then triturated and plated on 25 mm coverslips coated overnight with 100 μg/ml poly-L-lysine (Sigma). Neurons were plated at a density of approximately 350,000 cells per 35 mm dish. Cells were maintained in Neurobasal medium (ThermoFisher) supplemented with B-27 (ThermoFisher), penicillin/streptomycin, and GlutaMax (Invitrogen). Cells were fed once a week by replacing half of the medium with fresh growth medium.

Transfection of hippocampal neurons Hippocampal neurons were transfected at 11 days in vitro (DIV 11) using Calphos calcium phosphate transfection reagent (Takara) according to manufacturer's protocol. The following DNA plasmids were used: GFP-ZC3H14-Isoform 1 and GFP-ZC3H14-Isoform 3 [249] , LifeAct-mRuby [388] (provided by Dr. Gary Bassell, Emory

University), and eGFP-N1 (GFP). All DNA constructs were prepared using Endotoxin-free Maxi Prep kits (Qiagen).

Immunofluorescence microscopy Hippocampal neurons were fixed at either DIV 12 or DIV 19 using freshly prepared 4% paraformaldehyde (PFA) and 4% sucrose in phosphate-buffered saline (PBS) for 15 minutes at room temperature. Neurons were washed in PBS, then blocked and permeabilized in PBS supplemented with 5% normal goat serum, and 0.2% Triton X-100 for 1 hour at room temperature. Cells were incubated with primary antibodies (rabbit anti-RFP (600-401-279; Rockland; 1:1000) and mouse anti-GFP (A-11120; Invitrogen; 1;2000) for 1 hour, then with Alexa Fluor (Alexa-488 or Alexa-546; 1:750; ThermoFisher Scientific) secondary antibodies for 1 hour, and finally mounted with Fluoromount-G (Southern Biotech). All samples were blinded prior to image acquisition and their identities revealed after image analysis was completed. Dendritic arbors were imaged using an epifluorescent Nikon Eclipse Ti inverted microscope with a 20x objective (Plan Fluor, 0.5 NA). Analysis, including tracing and Sholl analysis, was carried out using the ImageJ Simple Neurite Tracer plugin [557]. Dendritic spines were imaged as Z-stacks comprised of 21 optical sections (0.2 µm step-size) using a Nikon C2 laser-scanning confocal system with an inverted Nikon Ti2 microscope (60x Plan Apo objective, 1.4 NA). For display purposes, 2D images were generated from maximum intensity projections of Z-stacks. For image analysis, dendrite and spine volumes were reconstructed from Z-stacks using the Filament Tracer module in Imaris (Bitplane). Spine heads were manually seeded prior to spine volume reconstruction. Density and classification of dendritic spines were determined using automated measurements produced from the Filament Tracer module. For each neuron imaged, spines were analyzed from four separate secondary or tertiary dendritic branches (a

minimum of 25 μm long) at least 50 μm away from the soma. Spines were classified as either stubby, mushroom, or thin, following parameters previously described [392]. Briefly, stubby spines are defined as having a length <1 μm and a head/neck width ratio <1.5; thin spines are defined as having a length 1-5 μm and a head/neck width ratio <1.5; mushroom spines are defined as having a length <5 μm and a head/neck width ratio >1.5.

Synaptosomal Fractionation Mice were sacrificed and whole brains isolated at postnatal day 0 (P0). Brains were immediately frozen on dry ice, and stored at -80°C. We employed validated PCR primers to confirm the genotype of these P0 brains [379]. These whole brains were homogenized in Thermo Scientific Syn-PER Synaptic Protein Extraction Reagent with EDTA-free protease inhibitor, using a Dounce tissue grinder [three (3) *Zc3h14*$^{+/+}$, three (3) *Zc3h14*$^{\Delta ex13/\Delta ex13}$]. Fractionation to obtain the homogenate (Hom), cytosol (Cyt), and synaptosome (Syn) fractions was performed as described in the Thermo Scientific Syn-PER Synaptic Protein Extraction Reagent protocol.

Immunoblotting Samples from the synaptosomal fractionation were resolved by SDS-PAGE and transferred to a 0.2 μm nitrocellulose membrane (Bio-Rad Laboratories). After blocking non-specific binding with 5% nonfat milk in 1X TBST (Tris-Buffered Saline, 0.1% Tween 20) solution, the membranes were incubated with primary antibody [anti-ZC3H14 [249], CaMKIIα (Thermo Fisher 13-7300), PSD-95 (Sigma-Aldrich MAB1598), Synaptophysin (Sigma-Aldrich MAB5258)], followed by incubation with the appropriate horseradish peroxidase (HRP)-conjugated secondary IgG antibody (Jackson ImmunoResearch). Total protein was visualized by

Ponceau staining. Quantification of chemiluminescence and Ponceau staining was carried out in ImageJ, with significance calculated with an unpaired *t* test.

Chapter 6

References

1. Kun, A., et al., *The dynamics of the RNA world: insights and challenges.* Ann N Y Acad Sci, 2015. **1341**: p. 75-95.
2. Kruger, K., et al., *Self-splicing RNA: autoexcision and autocyclization of the ribosomal RNA intervening sequence of Tetrahymena.* Cell, 1982. **31**(1): p. 147-57.
3. Guerrier-Takada, C., et al., *The RNA moiety of ribonuclease P is the catalytic subunit of the enzyme.* Cell, 1983. **35**(3 Pt 2): p. 849-57.
4. Sprengel, G.F., H., *Evidence for the reductive pathway of deoxyribonucleotide synthesis in an archaebacterium.* FEBS Lett, 1981. **132**: p. 207-209.
5. Chen, X., N. Li, and A.D. Ellington, *Ribozyme catalysis of metabolism in the RNA world.* Chem Biodivers, 2007. **4**(4): p. 633-55.
6. Martin, L.L., P.J. Unrau, and U.F. Muller, *RNA synthesis by in vitro selected ribozymes for recreating an RNA world.* Life (Basel), 2015. **5**(1): p. 247-68.
7. Pereira, I.T., et al., *Cardiomyogenic differentiation is fine-tuned by differential mRNA association with polysomes.* BMC Genomics, 2019. **20**(1): p. 219.
8. Liu, H., et al., *Alternative splicing analysis in human monocytes and macrophages reveals MBNL1 as major regulator.* Nucleic Acids Res, 2018. **46**(12): p. 6069-6086.
9. Kretz, M., et al., *Control of somatic tissue differentiation by the long non-coding RNA TINCR.* Nature, 2013. **493**(7431): p. 231-5.
10. Warren, L. and C. Lin, *mRNA-Based Genetic Reprogramming.* Mol Ther, 2019. **27**(4): p. 729-734.
11. Lianoglou, S., et al., *Ubiquitously transcribed genes use alternative polyadenylation to achieve tissue-specific expression.* Genes Dev, 2013. **27**(21): p. 2380-96.
12. Gerstberger, S., M. Hafner, and T. Tuschl, *A census of human RNA-binding proteins.* Nat Rev Genet, 2014. **15**(12): p. 829-45.
13. Ramanathan, A., G.B. Robb, and S.H. Chan, *mRNA capping: biological functions and applications.* Nucleic Acids Res, 2016. **44**(16): p. 7511-26.
14. Fu, X.D. and M. Ares, Jr., *Context-dependent control of alternative splicing by RNA-binding proteins.* Nat Rev Genet, 2014. **15**(10): p. 689-701.
15. Tian, B. and J.L. Manley, *Alternative polyadenylation of mRNA precursors.* Nat Rev Mol Cell Biol, 2017. **18**(1): p. 18-30.
16. Xie, Y. and Y. Ren, *Mechanisms of nuclear mRNA export: A structural perspective.* Traffic, 2019. **20**(11): p. 829-840.
17. Geuens, T., D. Bouhy, and V. Timmerman, *The hnRNP family: insights into their role in health and disease.* Hum Genet, 2016. **135**(8): p. 851-67.
18. Buxbaum, A.R., G. Haimovich, and R.H. Singer, *In the right place at the right time: visualizing and understanding mRNA localization.* Nat Rev Mol Cell Biol, 2015. **16**(2): p. 95-109.
19. Wang, E.T., et al., *Dysregulation of mRNA Localization and Translation in Genetic Disease.* J Neurosci, 2016. **36**(45): p. 11418-11426.
20. Kim, Y.K. and L.E. Maquat, *UPFront and center in RNA decay: UPF1 in nonsense-mediated mRNA decay and beyond.* RNA, 2019. **25**(4): p. 407-422.
21. Castello, A., et al., *RNA-binding proteins in Mendelian disease.* Trends Genet, 2013. **29**(5): p. 318-27.
22. Gerstberger, S., et al., *Evolutionary conservation and expression of human RNA-binding proteins and their role in human genetic disease.* Adv Exp Med Biol, 2014. **825**: p. 1-55.

23. Ng, C.K., et al., *Loss of the scavenger mRNA decapping enzyme DCPS causes syndromic intellectual disability with neuromuscular defects.* Hum Mol Genet, 2015. **24**(11): p. 3163-71.
24. Papaemmanuil, E., et al., *Somatic SF3B1 mutation in myelodysplasia with ring sideroblasts.* N Engl J Med, 2011. **365**(15): p. 1384-95.
25. Wheeler, T.M., et al., *Correction of ClC-1 splicing eliminates chloride channelopathy and myotonia in mouse models of myotonic dystrophy.* J Clin Invest, 2007. **117**(12): p. 3952-7.
26. Brais, B., et al., *Short GCG expansions in the PABP2 gene cause oculopharyngeal muscular dystrophy.* Nat Genet, 1998. **18**(2): p. 164-7.
27. Nousiainen, H.O., et al., *Mutations in mRNA export mediator GLE1 result in a fetal motoneuron disease.* Nat Genet, 2008. **40**(2): p. 155-7.
28. Lefebvre, S., et al., *Identification and characterization of a spinal muscular atrophy-determining gene.* Cell, 1995. **80**(1): p. 155-65.
29. Santoro, M.R., S.M. Bray, and S.T. Warren, *Molecular mechanisms of fragile X syndrome: a twenty-year perspective.* Annu Rev Pathol, 2012. **7**: p. 219-45.
30. Morton, D.J., et al., *The RNA exosome and RNA exosome-linked disease.* RNA, 2018. **24**(2): p. 127-142.
31. Balcerak, A., et al., *RNA-protein interactions: disorder, moonlighting and junk contribute to eukaryotic complexity.* Open Biol, 2019. **9**(6): p. 190096.
32. Rousseau, F., et al., *Prevalence of carriers of premutation-size alleles of the FMRI gene--and implications for the population genetics of the fragile X syndrome.* Am J Hum Genet, 1995. **57**(5): p. 1006-18.
33. Tassone, F., et al., *FMR1 CGG allele size and prevalence ascertained through newborn screening in the United States.* Genome Med, 2012. **4**(12): p. 100.
34. Sutcliffe, J.S., et al., *DNA methylation represses FMR-1 transcription in fragile X syndrome.* Hum Mol Genet, 1992. **1**(6): p. 397-400.
35. Pieretti, M., et al., *Absence of expression of the FMR-1 gene in fragile X syndrome.* Cell, 1991. **66**(4): p. 817-22.
36. Khandjian, E.W., et al., *The fragile X mental retardation protein is associated with ribosomes.* Nat Genet, 1996. **12**(1): p. 91-3.
37. Li, Z., et al., *The fragile X mental retardation protein inhibits translation via interacting with mRNA.* Nucleic Acids Res, 2001. **29**(11): p. 2276-83.
38. Ronesi, J.A., et al., *Disrupted Homer scaffolds mediate abnormal mGluR5 function in a mouse model of fragile X syndrome.* Nat Neurosci, 2012. **15**(3): p. 431-40, S1.
39. Napoli, I., et al., *The fragile X syndrome protein represses activity-dependent translation through CYFIP1, a new 4E-BP.* Cell, 2008. **134**(6): p. 1042-54.
40. Stefani, G., et al., *Fragile X mental retardation protein is associated with translating polyribosomes in neuronal cells.* J Neurosci, 2004. **24**(33): p. 7272-6.
41. Udagawa, T., et al., *Genetic and acute CPEB1 depletion ameliorate fragile X pathophysiology.* Nat Med, 2013. **19**(11): p. 1473-7.
42. Richter, J.D., G.J. Bassell, and E. Klann, *Dysregulation and restoration of translational homeostasis in fragile X syndrome.* Nat Rev Neurosci, 2015. **16**(10): p. 595-605.
43. Muddashetty, R.S., et al., *Dysregulated metabotropic glutamate receptor-dependent translation of AMPA receptor and postsynaptic density-95 mRNAs at synapses in a mouse model of fragile X syndrome.* J Neurosci, 2007. **27**(20): p. 5338-48.

44. Lu, R., et al., *The fragile X protein controls microtubule-associated protein 1B translation and microtubule stability in brain neuron development.* Proc Natl Acad Sci U S A, 2004. **101**(42): p. 15201-6.
45. Bagni, C. and R.S. Zukin, *A Synaptic Perspective of Fragile X Syndrome and Autism Spectrum Disorders.* Neuron, 2019. **101**(6): p. 1070-1088.
46. Banerjee, A., et al., *Aberrant RNA translation in fragile X syndrome: From FMRP mechanisms to emerging therapeutic strategies.* Brain Res, 2018. **1693**(Pt A): p. 24-36.
47. Ramirez-Cheyne, J.A., et al., *Fragile X syndrome and connective tissue dysregulation.* Clin Genet, 2019. **95**(2): p. 262-267.
48. Moore, B.C., et al., *Fragile X-linked mental retardation of macro-orchidism.* West J Med, 1982. **137**(4): p. 278-81.
49. Trollet, C., et al., *Oculopharyngeal Muscular Dystrophy*, in *GeneReviews((R))*, M.P. Adam, et al., Editors. 1993: Seattle (WA).
50. Raz, Y. and V. Raz, *Oculopharyngeal muscular dystrophy as a paradigm for muscle aging.* Front Aging Neurosci, 2014. **6**: p. 317.
51. Banerjee, A., et al., *PABPN1: molecular function and muscle disease.* FEBS J, 2013. **280**(17): p. 4230-50.
52. Richard, P., et al., *Correlation between PABPN1 genotype and disease severity in oculopharyngeal muscular dystrophy.* Neurology, 2017. **88**(4): p. 359-365.
53. Kerwitz, Y., et al., *Stimulation of poly(A) polymerase through a direct interaction with the nuclear poly(A) binding protein allosterically regulated by RNA.* EMBO J, 2003. **22**(14): p. 3705-14.
54. Wahle, E., *A novel poly(A)-binding protein acts as a specificity factor in the second phase of messenger RNA polyadenylation.* Cell, 1991. **66**(4): p. 759-68.
55. Kuhn, U., et al., *Poly(A) tail length is controlled by the nuclear poly(A)-binding protein regulating the interaction between poly(A) polymerase and the cleavage and polyadenylation specificity factor.* J Biol Chem, 2009. **284**(34): p. 22803-14.
56. Muniz, L., L. Davidson, and S. West, *Poly(A) Polymerase and the Nuclear Poly(A) Binding Protein, PABPN1, Coordinate the Splicing and Degradation of a Subset of Human Pre-mRNAs.* Mol Cell Biol, 2015. **35**(13): p. 2218-30.
57. Bresson, S.M. and N.K. Conrad, *The human nuclear poly(a)-binding protein promotes RNA hyperadenylation and decay.* PLoS Genet, 2013. **9**(10): p. e1003893.
58. Ogino, S., R.B. Wilson, and B. Gold, *New insights on the evolution of the SMN1 and SMN2 region: simulation and meta-analysis for allele and haplotype frequency calculations.* Eur J Hum Genet, 2004. **12**(12): p. 1015-23.
59. Rochette, C.F., N. Gilbert, and L.R. Simard, *SMN gene duplication and the emergence of the SMN2 gene occurred in distinct hominids: SMN2 is unique to Homo sapiens.* Hum Genet, 2001. **108**(3): p. 255-66.
60. Lefebvre, S., et al., *Correlation between severity and SMN protein level in spinal muscular atrophy.* Nat Genet, 1997. **16**(3): p. 265-9.
61. Ottesen, E.W., et al., *High-affinity RNA targets of the Survival Motor Neuron protein reveal diverse preferences for sequence and structural motifs.* Nucleic Acids Res, 2018. **46**(20): p. 10983-11001.
62. Fischer, U., Q. Liu, and G. Dreyfuss, *The SMN-SIP1 complex has an essential role in spliceosomal snRNP biogenesis.* Cell, 1997. **90**(6): p. 1023-9.

63. Pellizzoni, L., J. Yong, and G. Dreyfuss, *Essential role for the SMN complex in the specificity of snRNP assembly.* Science, 2002. **298**(5599): p. 1775-9.
64. Wahl, M.C., C.L. Will, and R. Luhrmann, *The spliceosome: design principles of a dynamic RNP machine.* Cell, 2009. **136**(4): p. 701-18.
65. Wan, L., et al., *The survival of motor neurons protein determines the capacity for snRNP assembly: biochemical deficiency in spinal muscular atrophy.* Mol Cell Biol, 2005. **25**(13): p. 5543-51.
66. Gabanella, F., et al., *Ribonucleoprotein assembly defects correlate with spinal muscular atrophy severity and preferentially affect a subset of spliceosomal snRNPs.* PLoS One, 2007. **2**(9): p. e921.
67. Jangi, M., et al., *SMN deficiency in severe models of spinal muscular atrophy causes widespread intron retention and DNA damage.* Proc Natl Acad Sci U S A, 2017. **114**(12): p. E2347-E2356.
68. See, K., et al., *SMN deficiency alters Nrxn2 expression and splicing in zebrafish and mouse models of spinal muscular atrophy.* Hum Mol Genet, 2014. **23**(7): p. 1754-70.
69. Custer, S.K., et al., *Altered mRNA Splicing in SMN-Depleted Motor Neuron-Like Cells.* PLoS One, 2016. **11**(10): p. e0163954.
70. Baumer, D., et al., *Alternative splicing events are a late feature of pathology in a mouse model of spinal muscular atrophy.* PLoS Genet, 2009. **5**(12): p. e1000773.
71. Fallini, C., et al., *Deficiency of the Survival of Motor Neuron Protein Impairs mRNA Localization and Local Translation in the Growth Cone of Motor Neurons.* J Neurosci, 2016. **36**(13): p. 3811-20.
72. Akten, B., et al., *Interaction of survival of motor neuron (SMN) and HuD proteins with mRNA cpg15 rescues motor neuron axonal deficits.* Proc Natl Acad Sci U S A, 2011. **108**(25): p. 10337-42.
73. Khalil, B., et al., *mRNP assembly, axonal transport, and local translation in neurodegenerative diseases.* Brain Res, 2018. **1693**(Pt A): p. 75-91.
74. Kapitein, L.C. and C.C. Hoogenraad, *Building the Neuronal Microtubule Cytoskeleton.* Neuron, 2015. **87**(3): p. 492-506.
75. Konietzny, A., J. Bar, and M. Mikhaylova, *Dendritic Actin Cytoskeleton: Structure, Functions, and Regulations.* Front Cell Neurosci, 2017. **11**: p. 147.
76. Fiala, J.C.H., K.M., ed. *Dendrite Structure*. Dendrites, ed. G.S. Stuart, N.; Hausser, M. 1999, Oxford University Press.
77. Gao, Y., et al., *Multiplexed dendritic targeting of alpha calcium calmodulin-dependent protein kinase II, neurogranin, and activity-regulated cytoskeleton-associated protein RNAs by the A2 pathway.* Mol Biol Cell, 2008. **19**(5): p. 2311-27.
78. Mikl, M., G. Vendra, and M.A. Kiebler, *Independent localization of MAP2, CaMKIIalpha and beta-actin RNAs in low copy numbers.* EMBO Rep, 2011. **12**(10): p. 1077-84.
79. Batish, M., et al., *Neuronal mRNAs travel singly into dendrites.* Proc Natl Acad Sci U S A, 2012. **109**(12): p. 4645-50.
80. Mayford, M., et al., *The 3'-untranslated region of CaMKII alpha is a cis-acting signal for the localization and translation of mRNA in dendrites.* Proc Natl Acad Sci U S A, 1996. **93**(23): p. 13250-5.
81. Blichenberg, A., et al., *Identification of a cis-acting dendritic targeting element in MAP2 mRNAs.* J Neurosci, 1999. **19**(20): p. 8818-29.

82. Kobayashi, H., et al., *Identification of a cis-acting element required for dendritic targeting of activity-regulated cytoskeleton-associated protein mRNA.* Eur J Neurosci, 2005. **22**(12): p. 2977-84.
83. An, J.J., et al., *Distinct role of long 3' UTR BDNF mRNA in spine morphology and synaptic plasticity in hippocampal neurons.* Cell, 2008. **134**(1): p. 175-87.
84. Xu, Q., B. Modrek, and C. Lee, *Genome-wide detection of tissue-specific alternative splicing in the human transcriptome.* Nucleic Acids Res, 2002. **30**(17): p. 3754-66.
85. Yeo, G., et al., *Variation in alternative splicing across human tissues.* Genome Biol, 2004. **5**(10): p. R74.
86. Yan, Q., et al., *Systematic discovery of regulated and conserved alternative exons in the mammalian brain reveals NMD modulating chromatin regulators.* Proc Natl Acad Sci U S A, 2015. **112**(11): p. 3445-50.
87. Ciolli Mattioli, C., et al., *Alternative 3' UTRs direct localization of functionally diverse protein isoforms in neuronal compartments.* Nucleic Acids Res, 2019. **47**(5): p. 2560-2573.
88. Tushev, G., et al., *Alternative 3' UTRs Modify the Localization, Regulatory Potential, Stability, and Plasticity of mRNAs in Neuronal Compartments.* Neuron, 2018. **98**(3): p. 495-511 e6.
89. Das, S., R.H. Singer, and Y.J. Yoon, *The travels of mRNAs in neurons: do they know where they are going?* Curr Opin Neurobiol, 2019. **57**: p. 110-116.
90. Harvey, R.F., et al., *Trans-acting translational regulatory RNA binding proteins.* Wiley Interdiscip Rev RNA, 2018. **9**(3): p. e1465.
91. Hirokawa, N., S. Niwa, and Y. Tanaka, *Molecular motors in neurons: transport mechanisms and roles in brain function, development, and disease.* Neuron, 2010. **68**(4): p. 610-38.
92. Ravanidis, S., F.G. Kattan, and E. Doxakis, *Unraveling the Pathways to Neuronal Homeostasis and Disease: Mechanistic Insights into the Role of RNA-Binding Proteins and Associated Factors.* Int J Mol Sci, 2018. **19**(8).
93. Sephton, C.F. and G. Yu, *The function of RNA-binding proteins at the synapse: implications for neurodegeneration.* Cell Mol Life Sci, 2015. **72**(19): p. 3621-35.
94. Miyashiro, K.Y., et al., *RNA cargoes associating with FMRP reveal deficits in cellular functioning in Fmr1 null mice.* Neuron, 2003. **37**(3): p. 417-31.
95. Fallini, C., et al., *The survival of motor neuron (SMN) protein interacts with the mRNA-binding protein HuD and regulates localization of poly(A) mRNA in primary motor neuron axons.* J Neurosci, 2011. **31**(10): p. 3914-25.
96. Follwaczny, P., et al., *Pumilio2-deficient mice show a predisposition for epilepsy.* Dis Model Mech, 2017. **10**(11): p. 1333-1342.
97. Vessey, J.P., et al., *Dendritic localization of the translational repressor Pumilio 2 and its contribution to dendritic stress granules.* J Neurosci, 2006. **26**(24): p. 6496-508.
98. Huang, Y.S., et al., *Facilitation of dendritic mRNA transport by CPEB.* Genes Dev, 2003. **17**(5): p. 638-53.
99. Fujii, R. and T. Takumi, *TLS facilitates transport of mRNA encoding an actin-stabilizing protein to dendritic spines.* J Cell Sci, 2005. **118**(Pt 24): p. 5755-65.
100. Klein, M.E., et al., *RNA-binding protein Sam68 controls synapse number and local beta-actin mRNA metabolism in dendrites.* Proc Natl Acad Sci U S A, 2013. **110**(8): p. 3125-30.

101. Nakayama, K., et al., *RNG105/caprin1, an RNA granule protein for dendritic mRNA localization, is essential for long-term memory formation.* Elife, 2017. **6**.
102. Cajigas, I.J., et al., *The local transcriptome in the synaptic neuropil revealed by deep sequencing and high-resolution imaging.* Neuron, 2012. **74**(3): p. 453-66.
103. Chicurel, M.E., D.M. Terrian, and H. Potter, *mRNA at the synapse: analysis of a synaptosomal preparation enriched in hippocampal dendritic spines.* J Neurosci, 1993. **13**(9): p. 4054-63.
104. Donato, A., et al., *Neuronal sub-compartmentalization: a strategy to optimize neuronal function.* Biol Rev Camb Philos Soc, 2019. **94**(3): p. 1023-1037.
105. Duchaine, T.F., et al., *Staufen2 isoforms localize to the somatodendritic domain of neurons and interact with different organelles.* J Cell Sci, 2002. **115**(Pt 16): p. 3285-95.
106. Mitsumori, K., Y. Takei, and N. Hirokawa, *Components of RNA granules affect their localization and dynamics in neuronal dendrites.* Mol Biol Cell, 2017. **28**(11): p. 1412-1417.
107. Yoon, Y.J., et al., *Glutamate-induced RNA localization and translation in neurons.* Proc Natl Acad Sci U S A, 2016. **113**(44): p. E6877-E6886.
108. Rangaraju, V., S. Tom Dieck, and E.M. Schuman, *Local translation in neuronal compartments: how local is local?* EMBO Rep, 2017. **18**(5): p. 693-711.
109. Torre, E.R. and O. Steward, *Demonstration of local protein synthesis within dendrites using a new cell culture system that permits the isolation of living axons and dendrites from their cell bodies.* J Neurosci, 1992. **12**(3): p. 762-72.
110. Miller, S., et al., *Disruption of dendritic translation of CaMKIIalpha impairs stabilization of synaptic plasticity and memory consolidation.* Neuron, 2002. **36**(3): p. 507-19.
111. Mathur, C., et al., *Demonstration of ion channel synthesis by isolated squid giant axon provides functional evidence for localized axonal membrane protein translation.* Sci Rep, 2018. **8**(1): p. 2207.
112. Leung, K.M., et al., *Asymmetrical beta-actin mRNA translation in growth cones mediates attractive turning to netrin-1.* Nat Neurosci, 2006. **9**(10): p. 1247-56.
113. Kang, H. and E.M. Schuman, *A requirement for local protein synthesis in neurotrophin-induced hippocampal synaptic plasticity.* Science, 1996. **273**(5280): p. 1402-6.
114. Costa-Mattioli, M., et al., *Translational control of long-lasting synaptic plasticity and memory.* Neuron, 2009. **61**(1): p. 10-26.
115. Buffington, S.A., W. Huang, and M. Costa-Mattioli, *Translational control in synaptic plasticity and cognitive dysfunction.* Annu Rev Neurosci, 2014. **37**: p. 17-38.
116. Pernice, H.F., et al., *mTOR and MAPK: from localized translation control to epilepsy.* BMC Neurosci, 2016. **17**(1): p. 73.
117. Jackson, R.J., C.U. Hellen, and T.V. Pestova, *The mechanism of eukaryotic translation initiation and principles of its regulation.* Nat Rev Mol Cell Biol, 2010. **11**(2): p. 113-27.
118. Fukao, A., et al., *The ELAV protein HuD stimulates cap-dependent translation in a Poly(A)- and eIF4A-dependent manner.* Mol Cell, 2009. **36**(6): p. 1007-17.
119. Kahvejian, A., et al., *Mammalian poly(A)-binding protein is a eukaryotic translation initiation factor, which acts via multiple mechanisms.* Genes Dev, 2005. **19**(1): p. 104-13.
120. Craig, A.W., et al., *Interaction of polyadenylate-binding protein with the eIF4G homologue PAIP enhances translation.* Nature, 1998. **392**(6675): p. 520-3.

121. Pineiro, D., et al., *Gemin5: A Multitasking RNA-Binding Protein Involved in Translation Control.* Biomolecules, 2015. **5**(2): p. 528-44.
122. Kawahara, H., et al., *Neural RNA-binding protein Musashi1 inhibits translation initiation by competing with eIF4G for PABP.* J Cell Biol, 2008. **181**(4): p. 639-53.
123. Kraushar, M.L., et al., *Temporally defined neocortical translation and polysome assembly are determined by the RNA-binding protein Hu antigen R.* Proc Natl Acad Sci U S A, 2014. **111**(36): p. E3815-24.
124. Darnell, J.C., et al., *FMRP stalls ribosomal translocation on mRNAs linked to synaptic function and autism.* Cell, 2011. **146**(2): p. 247-61.
125. Graber, T.E., et al., *UPF1 Governs Synaptic Plasticity through Association with a STAU2 RNA Granule.* J Neurosci, 2017. **37**(38): p. 9116-9131.
126. Graber, T.E., et al., *Reactivation of stalled polyribosomes in synaptic plasticity.* Proc Natl Acad Sci U S A, 2013. **110**(40): p. 16205-10.
127. Ivanov, A., et al., *PABP enhances release factor recruitment and stop codon recognition during translation termination.* Nucleic Acids Res, 2016. **44**(16): p. 7766-76.
128. Ivanov, A., et al., *Polyadenylate-binding protein-interacting proteins PAIP1 and PAIP2 affect translation termination.* J Biol Chem, 2019. **294**(21): p. 8630-8639.
129. Ivanov, P.V., et al., *Interactions between UPF1, eRFs, PABP and the exon junction complex suggest an integrated model for mammalian NMD pathways.* EMBO J, 2008. **27**(5): p. 736-47.
130. Petzoldt, A.G. and S.J. Sigrist, *Synaptogenesis.* Curr Biol, 2014. **24**(22): p. R1076-80.
131. Matsuzaki, M., et al., *Structural basis of long-term potentiation in single dendritic spines.* Nature, 2004. **429**(6993): p. 761-6.
132. Matsuzaki, M., et al., *Dendritic spine geometry is critical for AMPA receptor expression in hippocampal CA1 pyramidal neurons.* Nat Neurosci, 2001. **4**(11): p. 1086-92.
133. Hasegawa, S., et al., *Dendritic spine dynamics leading to spine elimination after repeated inductions of LTD.* Sci Rep, 2015. **5**: p. 7707.
134. Tonnesen, J., et al., *Spine neck plasticity regulates compartmentalization of synapses.* Nat Neurosci, 2014. **17**(5): p. 678-85.
135. Risher, W.C., et al., *Rapid Golgi analysis method for efficient and unbiased classification of dendritic spines.* PLoS One, 2014. **9**(9): p. e107591.
136. Urban, P., et al., *Dendritic Spines Taxonomy: The Functional and Structural Classification * Time-Dependent Probabilistic Model of Neuronal Activation.* J Comput Biol, 2019. **26**(4): p. 322-335.
137. Su, R., et al., *A novel method for dendritic spines detection based on directional morphological filter and shortest path.* Comput Med Imaging Graph, 2014. **38**(8): p. 793-802.
138. Swanger, S.A., et al., *Automated 4D analysis of dendritic spine morphology: applications to stimulus-induced spine remodeling and pharmacological rescue in a disease model.* Mol Brain, 2011. **4**: p. 38.
139. Berry, K.P. and E. Nedivi, *Spine Dynamics: Are They All the Same?* Neuron, 2017. **96**(1): p. 43-55.
140. Xu, T., et al., *Rapid formation and selective stabilization of synapses for enduring motor memories.* Nature, 2009. **462**(7275): p. 915-9.
141. Attardo, A., J.E. Fitzgerald, and M.J. Schnitzer, *Impermanence of dendritic spines in live adult CA1 hippocampus.* Nature, 2015. **523**(7562): p. 592-6.

142. Yang, G., et al., *Sleep promotes branch-specific formation of dendritic spines after learning.* Science, 2014. **344**(6188): p. 1173-8.
143. Yang, G., F. Pan, and W.B. Gan, *Stably maintained dendritic spines are associated with lifelong memories.* Nature, 2009. **462**(7275): p. 920-4.
144. Bourne, J. and K.M. Harris, *Do thin spines learn to be mushroom spines that remember?* Curr Opin Neurobiol, 2007. **17**(3): p. 381-6.
145. Nishiyama, J., *Plasticity of dendritic spines: Molecular function and dysfunction in neurodevelopmental disorders.* Psychiatry Clin Neurosci, 2019. **73**(9): p. 541-550.
146. Yasuda, R., *Biophysics of Biochemical Signaling in Dendritic Spines: Implications in Synaptic Plasticity.* Biophys J, 2017. **113**(10): p. 2152-2159.
147. Borovac, J., M. Bosch, and K. Okamoto, *Regulation of actin dynamics during structural plasticity of dendritic spines: Signaling messengers and actin-binding proteins.* Mol Cell Neurosci, 2018. **91**: p. 122-130.
148. Chen, C.C., J. Lu, and Y. Zuo, *Spatiotemporal dynamics of dendritic spines in the living brain.* Front Neuroanat, 2014. **8**: p. 28.
149. Cruz-Martin, A., M. Crespo, and C. Portera-Cailliau, *Delayed stabilization of dendritic spines in fragile X mice.* J Neurosci, 2010. **30**(23): p. 7793-803.
150. Rakic, P., et al., *Concurrent overproduction of synapses in diverse regions of the primate cerebral cortex.* Science, 1986. **232**(4747): p. 232-5.
151. Markus, E.J. and T.L. Petit, *Neocortical synaptogenesis, aging, and behavior: lifespan development in the motor-sensory system of the rat.* Exp Neurol, 1987. **96**(2): p. 262-78.
152. Zuo, Y., et al., *Development of long-term dendritic spine stability in diverse regions of cerebral cortex.* Neuron, 2005. **46**(2): p. 181-9.
153. Dickstein, D.L., et al., *Dendritic spine changes associated with normal aging.* Neuroscience, 2013. **251**: p. 21-32.
154. Holtmaat, A.J., et al., *Transient and persistent dendritic spines in the neocortex in vivo.* Neuron, 2005. **45**(2): p. 279-91.
155. Honkura, N., et al., *The subspine organization of actin fibers regulates the structure and plasticity of dendritic spines.* Neuron, 2008. **57**(5): p. 719-29.
156. Dosemeci, A., et al., *Composition of the synaptic PSD-95 complex.* Mol Cell Proteomics, 2007. **6**(10): p. 1749-60.
157. Okamoto, K., M. Bosch, and Y. Hayashi, *The roles of CaMKII and F-actin in the structural plasticity of dendritic spines: a potential molecular identity of a synaptic tag?* Physiology (Bethesda), 2009. **24**: p. 357-66.
158. Koganezawa, N., et al., *The role of drebrin in dendritic spines.* Mol Cell Neurosci, 2017. **84**: p. 85-92.
159. El-Husseini, A.E., et al., *PSD-95 involvement in maturation of excitatory synapses.* Science, 2000. **290**(5495): p. 1364-8.
160. Borczyk, M., et al., *Neuronal plasticity affects correlation between the size of dendritic spine and its postsynaptic density.* Sci Rep, 2019. **9**(1): p. 1693.
161. Mori, Y., et al., *Two cis-acting elements in the 3' untranslated region of alpha-CaMKII regulate its dendritic targeting.* Nat Neurosci, 2000. **3**(11): p. 1079-84.
162. Lisman, J., R. Yasuda, and S. Raghavachari, *Mechanisms of CaMKII action in long-term potentiation.* Nat Rev Neurosci, 2012. **13**(3): p. 169-82.
163. Hudmon, A. and H. Schulman, *Structure-function of the multifunctional Ca2+/calmodulin-dependent protein kinase II.* Biochem J, 2002. **364**(Pt 3): p. 593-611.

164. Rosenberg, O.S., et al., *Structure of the autoinhibited kinase domain of CaMKII and SAXS analysis of the holoenzyme.* Cell, 2005. **123**(5): p. 849-60.
165. Meyer, T., et al., *Calmodulin trapping by calcium-calmodulin-dependent protein kinase.* Science, 1992. **256**(5060): p. 1199-202.
166. De Koninck, P. and H. Schulman, *Sensitivity of CaM kinase II to the frequency of Ca2+ oscillations.* Science, 1998. **279**(5348): p. 227-30.
167. Strack, S., et al., *Differential inactivation of postsynaptic density-associated and soluble Ca2+/calmodulin-dependent protein kinase II by protein phosphatases 1 and 2A.* J Neurochem, 1997. **68**(5): p. 2119-28.
168. Rellos, P., et al., *Structure of the CaMKIIdelta/calmodulin complex reveals the molecular mechanism of CaMKII kinase activation.* PLoS Biol, 2010. **8**(7): p. e1000426.
169. Abraham, W.C., *How long will long-term potentiation last?* Philos Trans R Soc Lond B Biol Sci, 2003. **358**(1432): p. 735-44.
170. Lee, S.J., et al., *Activation of CaMKII in single dendritic spines during long-term potentiation.* Nature, 2009. **458**(7236): p. 299-304.
171. Sanhueza, M. and J. Lisman, *The CaMKII/NMDAR complex as a molecular memory.* Mol Brain, 2013. **6**: p. 10.
172. Jourdain, P., K. Fukunaga, and D. Muller, *Calcium/calmodulin-dependent protein kinase II contributes to activity-dependent filopodia growth and spine formation.* J Neurosci, 2003. **23**(33): p. 10645-9.
173. Lucchesi, W., K. Mizuno, and K.P. Giese, *Novel insights into CaMKII function and regulation during memory formation.* Brain Res Bull, 2011. **85**(1-2): p. 2-8.
174. Yasuda, M. and M.R. Mayford, *CaMKII activation in the entorhinal cortex disrupts previously encoded spatial memory.* Neuron, 2006. **50**(2): p. 309-18.
175. Silva, A.J., et al., *Deficient hippocampal long-term potentiation in alpha-calcium-calmodulin kinase II mutant mice.* Science, 1992. **257**(5067): p. 201-6.
176. Giese, K.P., et al., *Autophosphorylation at Thr286 of the alpha calcium-calmodulin kinase II in LTP and learning.* Science, 1998. **279**(5352): p. 870-3.
177. Achterberg, K.G., et al., *Temporal and region-specific requirements of alphaCaMKII in spatial and contextual learning.* J Neurosci, 2014. **34**(34): p. 11180-7.
178. Wang, H., et al., *Inducible protein knockout reveals temporal requirement of CaMKII reactivation for memory consolidation in the brain.* Proc Natl Acad Sci U S A, 2003. **100**(7): p. 4287-92.
179. Guo, W., et al., *Elevated CaMKIIalpha and Hyperphosphorylation of Homer Mediate Circuit Dysfunction in a Fragile X Syndrome Mouse Model.* Cell Rep, 2015. **13**(10): p. 2297-311.
180. Weeber, E.J., et al., *Derangements of hippocampal calcium/calmodulin-dependent protein kinase II in a mouse model for Angelman mental retardation syndrome.* J Neurosci, 2003. **23**(7): p. 2634-44.
181. Ghosh, A. and K.P. Giese, *Calcium/calmodulin-dependent kinase II and Alzheimer's disease.* Mol Brain, 2015. **8**(1): p. 78.
182. Ogundele, O.M. and C.C. Lee, *CaMKIIalpha expression in a mouse model of NMDAR hypofunction schizophrenia: Putative roles for IGF-1R and TLR4.* Brain Res Bull, 2018. **137**: p. 53-70.
183. Thompson, C.H., et al., *CaMKII modulates sodium current in neurons from epileptic Scn2a mutant mice.* Proc Natl Acad Sci U S A, 2017. **114**(7): p. 1696-1701.

184. Siarey, R.J., et al., *Altered signaling pathways underlying abnormal hippocampal synaptic plasticity in the Ts65Dn mouse model of Down syndrome.* J Neurochem, 2006. **98**(4): p. 1266-77.
185. Tombes, R.M., M.O. Faison, and J.M. Turbeville, *Organization and evolution of multifunctional Ca(2+)/CaM-dependent protein kinase genes.* Gene, 2003. **322**: p. 17-31.
186. Gaertner, T.R., et al., *Comparative analyses of the three-dimensional structures and enzymatic properties of alpha, beta, gamma and delta isoforms of Ca2+-calmodulin-dependent protein kinase II.* J Biol Chem, 2004. **279**(13): p. 12484-94.
187. Zalcman, G., N. Federman, and A. Romano, *CaMKII Isoforms in Learning and Memory: Localization and Function.* Front Mol Neurosci, 2018. **11**: p. 445.
188. Vallano, M.L., *Separation of isozymic forms of type II calcium/calmodulin-dependent protein kinase using cation-exchange chromatography.* J Neurosci Methods, 1989. **30**(1): p. 1-9.
189. Erondu, N.E. and M.B. Kennedy, *Regional distribution of type II Ca2+/calmodulin-dependent protein kinase in rat brain.* J Neurosci, 1985. **5**(12): p. 3270-7.
190. Tobimatsu, T. and H. Fujisawa, *Tissue-specific expression of four types of rat calmodulin-dependent protein kinase II mRNAs.* J Biol Chem, 1989. **264**(30): p. 17907-12.
191. Kool, M.J., et al., *CAMK2-Dependent Signaling in Neurons Is Essential for Survival.* J Neurosci, 2019. **39**(28): p. 5424-5439.
192. Elgersma, Y., et al., *Inhibitory autophosphorylation of CaMKII controls PSD association, plasticity, and learning.* Neuron, 2002. **36**(3): p. 493-505.
193. Yamagata, Y., et al., *Kinase-dead knock-in mouse reveals an essential role of kinase activity of Ca2+/calmodulin-dependent protein kinase IIalpha in dendritic spine enlargement, long-term potentiation, and learning.* J Neurosci, 2009. **29**(23): p. 7607-18.
194. Yamasaki, N., et al., *Alpha-CaMKII deficiency causes immature dentate gyrus, a novel candidate endophenotype of psychiatric disorders.* Mol Brain, 2008. **1**: p. 6.
195. Otmakhov, N., et al., *Persistent accumulation of calcium/calmodulin-dependent protein kinase II in dendritic spines after induction of NMDA receptor-dependent chemical long-term potentiation.* J Neurosci, 2004. **24**(42): p. 9324-31.
196. Zhang, Y.P., N. Holbro, and T.G. Oertner, *Optical induction of plasticity at single synapses reveals input-specific accumulation of alphaCaMKII.* Proc Natl Acad Sci U S A, 2008. **105**(33): p. 12039-44.
197. Cho, M.H., et al., *Dentate gyrus-specific manipulation of beta-Ca2+/calmodulin-dependent kinase II disrupts memory consolidation.* Proc Natl Acad Sci U S A, 2007. **104**(41): p. 16317-22.
198. Borgesius, N.Z., et al., *betaCaMKII plays a nonenzymatic role in hippocampal synaptic plasticity and learning by targeting alphaCaMKII to synapses.* J Neurosci, 2011. **31**(28): p. 10141-8.
199. Lin, Y.C. and L. Redmond, *CaMKIIbeta binding to stable F-actin in vivo regulates F-actin filament stability.* Proc Natl Acad Sci U S A, 2008. **105**(41): p. 15791-6.
200. Shen, K., et al., *CaMKIIbeta functions as an F-actin targeting module that localizes CaMKIIalpha/beta heterooligomers to dendritic spines.* Neuron, 1998. **21**(3): p. 593-606.
201. Backus, A.R., et al., *Mnemonic convergence in the human hippocampus.* Nat Commun, 2016. **7**: p. 11991.

202. Eichenbaum, H., *A cortical-hippocampal system for declarative memory.* Nat Rev Neurosci, 2000. **1**(1): p. 41-50.
203. Squire, L.R., et al., *Memory consolidation.* Cold Spring Harb Perspect Biol, 2015. **7**(8): p. a021766.
204. Yonelinas, A.P., *The hippocampus supports high-resolution binding in the service of perception, working memory and long-term memory.* Behav Brain Res, 2013. **254**: p. 34-44.
205. Olson, I.R., et al., *Working memory for conjunctions relies on the medial temporal lobe.* J Neurosci, 2006. **26**(17): p. 4596-601.
206. Hartley, T., et al., *The hippocampus is required for short-term topographical memory in humans.* Hippocampus, 2007. **17**(1): p. 34-48.
207. Jeneson, A. and L.R. Squire, *Working memory, long-term memory, and medial temporal lobe function.* Learn Mem, 2012. **19**(1): p. 15-25.
208. Dede, A.J., et al., *Learning and remembering real-world events after medial temporal lobe damage.* Proc Natl Acad Sci U S A, 2016. **113**(47): p. 13480-13485.
209. Covington, N.V., S. Brown-Schmidt, and M.C. Duff, *The Necessity of the Hippocampus for Statistical Learning.* J Cogn Neurosci, 2018. **30**(5): p. 680-697.
210. Palombo, D.J., et al., *Hippocampal contributions to value-based learning: Converging evidence from fMRI and amnesia.* Cogn Affect Behav Neurosci, 2019. **19**(3): p. 523-536.
211. Kates, W.R., et al., *Reliability and validity of MRI measurement of the amygdala and hippocampus in children with fragile X syndrome.* Psychiatry Res, 1997. **75**(1): p. 31-48.
212. Grossman, A.W., et al., *Hippocampal pyramidal cells in adult Fmr1 knockout mice exhibit an immature-appearing profile of dendritic spines.* Brain Res, 2006. **1084**(1): p. 158-64.
213. Braak, H., E. Braak, and J. Bohl, *Staging of Alzheimer-related cortical destruction.* Eur Neurol, 1993. **33**(6): p. 403-8.
214. Belfiore, R., et al., *Temporal and regional progression of Alzheimer's disease-like pathology in 3xTg-AD mice.* Aging Cell, 2019. **18**(1): p. e12873.
215. Sussman, D., et al., *The autism puzzle: Diffuse but not pervasive neuroanatomical abnormalities in children with ASD.* Neuroimage Clin, 2015. **8**: p. 170-9.
216. Zamarbide, M., et al., *Male-Specific cAMP Signaling in the Hippocampus Controls Spatial Memory Deficits in a Mouse Model of Autism and Intellectual Disability.* Biol Psychiatry, 2019. **85**(9): p. 760-768.
217. Huberfeld, G., T. Blauwblomme, and R. Miles, *Hippocampus and epilepsy: Findings from human tissues.* Rev Neurol (Paris), 2015. **171**(3): p. 236-51.
218. Zeidler, Z., et al., *Targeting the Mouse Ventral Hippocampus in the Intrahippocampal Kainic Acid Model of Temporal Lobe Epilepsy.* eNeuro, 2018. **5**(4).
219. Heckers, S. and C. Konradi, *GABAergic mechanisms of hippocampal hyperactivity in schizophrenia.* Schizophr Res, 2015. **167**(1-3): p. 4-11.
220. Marissal, T., et al., *Restoring wild-type-like CA1 network dynamics and behavior during adulthood in a mouse model of schizophrenia.* Nat Neurosci, 2018. **21**(10): p. 1412-1420.
221. Aylward, E.H., et al., *MRI volumes of the hippocampus and amygdala in adults with Down's syndrome with and without dementia.* Am J Psychiatry, 1999. **156**(4): p. 564-8.
222. Gotti, S., E. Caricati, and G. Panzica, *Alterations of brain circuits in Down syndrome murine models.* J Chem Neuroanat, 2011. **42**(4): p. 317-26.

223. Cheng, S., *The CRISP theory of hippocampal function in episodic memory.* Front Neural Circuits, 2013. **7**: p. 88.
224. Treves, A., et al., *What is the mammalian dentate gyrus good for?* Neuroscience, 2008. **154**(4): p. 1155-72.
225. Nakazawa, K., et al., *Hippocampal CA3 NMDA receptors are crucial for memory acquisition of one-time experience.* Neuron, 2003. **38**(2): p. 305-15.
226. Stepan, J., J. Dine, and M. Eder, *Functional optical probing of the hippocampal trisynaptic circuit in vitro: network dynamics, filter properties, and polysynaptic induction of CA1 LTP.* Front Neurosci, 2015. **9**: p. 160.
227. Vinogradova, O.S., *Hippocampus as comparator: role of the two input and two output systems of the hippocampus in selection and registration of information.* Hippocampus, 2001. **11**(5): p. 578-98.
228. Bui, A.D., et al., *Dentate gyrus mossy cells control spontaneous convulsive seizures and spatial memory.* Science, 2018. **359**(6377): p. 787-790.
229. Tunc-Ozcan, E., et al., *Activating newborn neurons suppresses depression and anxiety-like behaviors.* Nat Commun, 2019. **10**(1): p. 3768.
230. Hagihara, H., et al., *Immature dentate gyrus: an endophenotype of neuropsychiatric disorders.* Neural Plast, 2013. **2013**: p. 318596.
231. Padurariu, M., et al., *Hippocampal neuronal loss in the CA1 and CA3 areas of Alzheimer's disease patients.* Psychiatr Danub, 2012. **24**(2): p. 152-8.
232. Lopez-Santiago, L.F., et al., *Neuronal hyperexcitability in a mouse model of SCN8A epileptic encephalopathy.* Proc Natl Acad Sci U S A, 2017. **114**(9): p. 2383-2388.
233. Varghese, M., et al., *Autism spectrum disorder: neuropathology and animal models.* Acta Neuropathol, 2017. **134**(4): p. 537-566.
234. Bartsch, T., et al., *Selective neuronal vulnerability of human hippocampal CA1 neurons: lesion evolution, temporal course, and pattern of hippocampal damage in diffusion-weighted MR imaging.* J Cereb Blood Flow Metab, 2015. **35**(11): p. 1836-45.
235. Phillips, M. and L. Pozzo-Miller, *Dendritic spine dysgenesis in autism related disorders.* Neurosci Lett, 2015. **601**: p. 30-40.
236. Kim, H., et al., *Maternal Loss of Ube3a Impairs Experience-Driven Dendritic Spine Maintenance in the Developing Visual Cortex.* J Neurosci, 2016. **36**(17): p. 4888-94.
237. Ferrer, I. and F. Gullotta, *Down's syndrome and Alzheimer's disease: dendritic spine counts in the hippocampus.* Acta Neuropathol, 1990. **79**(6): p. 680-5.
238. Belichenko, P.V., et al., *Synaptic structural abnormalities in the Ts65Dn mouse model of Down Syndrome.* J Comp Neurol, 2004. **480**(3): p. 281-98.
239. Dindot, S.V., et al., *The Angelman syndrome ubiquitin ligase localizes to the synapse and nucleus, and maternal deficiency results in abnormal dendritic spine morphology.* Hum Mol Genet, 2008. **17**(1): p. 111-8.
240. He, C.X. and C. Portera-Cailliau, *The trouble with spines in fragile X syndrome: density, maturity and plasticity.* Neuroscience, 2013. **251**: p. 120-8.
241. Irwin, S.A., R. Galvez, and W.T. Greenough, *Dendritic spine structural anomalies in fragile-X mental retardation syndrome.* Cereb Cortex, 2000. **10**(10): p. 1038-44.
242. Grossman, A.W., et al., *Developmental characteristics of dendritic spines in the dentate gyrus of Fmr1 knockout mice.* Brain Res, 2010. **1355**: p. 221-7.
243. Bhattacharya, A., et al., *Genetic removal of p70 S6 kinase 1 corrects molecular, synaptic, and behavioral phenotypes in fragile X syndrome mice.* Neuron, 2012. **76**(2): p. 325-37.

244. Levenga, J., et al., *Subregion-specific dendritic spine abnormalities in the hippocampus of Fmr1 KO mice.* Neurobiol Learn Mem, 2011. **95**(4): p. 467-72.
245. Nimchinsky, E.A., A.M. Oberlander, and K. Svoboda, *Abnormal development of dendritic spines in FMR1 knock-out mice.* J Neurosci, 2001. **21**(14): p. 5139-46.
246. Su, T., et al., *Early continuous inhibition of group 1 mGlu signaling partially rescues dendritic spine abnormalities in the Fmr1 knockout mouse model for fragile X syndrome.* Psychopharmacology (Berl), 2011. **215**(2): p. 291-300.
247. Pak, C., et al., *Mutation of the conserved polyadenosine RNA binding protein, ZC3H14/dNab2, impairs neural function in Drosophila and humans.* Proc Natl Acad Sci U S A, 2011. **108**(30): p. 12390-5.
248. Kelly, S.M., et al., *Recognition of polyadenosine RNA by zinc finger proteins.* Proc Natl Acad Sci U S A, 2007. **104**(30): p. 12306-11.
249. Leung, S.W., et al., *Splice variants of the human ZC3H14 gene generate multiple isoforms of a zinc finger polyadenosine RNA binding protein.* Gene, 2009. **439**(1-2): p. 71-8.
250. Kuss, A.W., et al., *Autosomal recessive mental retardation: homozygosity mapping identifies 27 single linkage intervals, at least 14 novel loci and several mutation hotspots.* Hum Genet, 2011. **129**(2): p. 141-8.
251. Anderson, J.T., et al., *NAB2: a yeast nuclear polyadenylated RNA-binding protein essential for cell viability.* Mol Cell Biol, 1993. **13**(5): p. 2730-41.
252. Kelly, S.M., et al., *Recognition of polyadenosine RNA by the zinc finger domain of nuclear poly(A) RNA-binding protein 2 (Nab2) is required for correct mRNA 3'-end formation.* J Biol Chem, 2010. **285**(34): p. 26022-32.
253. Marfatia, K.A., et al., *Domain analysis of the Saccharomyces cerevisiae heterogeneous nuclear ribonucleoprotein, Nab2p. Dissecting the requirements for Nab2p-facilitated poly(A) RNA export.* J Biol Chem, 2003. **278**(9): p. 6731-40.
254. Guthrie, C.R., G.D. Schellenberg, and B.C. Kraemer, *SUT-2 potentiates tau-induced neurotoxicity in Caenorhabditis elegans.* Hum Mol Genet, 2009. **18**(10): p. 1825-38.
255. Green, D.M., et al., *Nab2p is required for poly(A) RNA export in Saccharomyces cerevisiae and is regulated by arginine methylation via Hmt1p.* J Biol Chem, 2002. **277**(10): p. 7752-60.
256. Fasken, M.B., M. Stewart, and A.H. Corbett, *Functional significance of the interaction between the mRNA-binding protein, Nab2, and the nuclear pore-associated protein, Mlp1, in mRNA export.* J Biol Chem, 2008. **283**(40): p. 27130-43.
257. Amrani, N., et al., *Yeast Pab1 interacts with Rna15 and participates in the control of the poly(A) tail length in vitro.* Mol Cell Biol, 1997. **17**(7): p. 3694-701.
258. Zhang, X., et al., *Translation repression via modulation of the cytoplasmic poly(A)-binding protein in the inflammatory response.* Elife, 2017. **6**.
259. Bernstein, P., S.W. Peltz, and J. Ross, *The poly(A)-poly(A)-binding protein complex is a major determinant of mRNA stability in vitro.* Mol Cell Biol, 1989. **9**(2): p. 659-70.
260. Caponigro, G. and R. Parker, *Mechanisms and control of mRNA turnover in Saccharomyces cerevisiae.* Microbiol Rev, 1996. **60**(1): p. 233-49.
261. Dunn, E.F., et al., *Yeast poly(A)-binding protein, Pab1, and PAN, a poly(A) nuclease complex recruited by Pab1, connect mRNA biogenesis to export.* Genes Dev, 2005. **19**(1): p. 90-103.

262. Chekanova, J.A. and D.A. Belostotsky, *Evidence that poly(A) binding protein has an evolutionarily conserved function in facilitating mRNA biogenesis and export.* RNA, 2003. **9**(12): p. 1476-90.
263. Hector, R.E., et al., *Dual requirement for yeast hnRNP Nab2p in mRNA poly(A) tail length control and nuclear export.* EMBO J, 2002. **21**(7): p. 1800-10.
264. Kelly, S.M., et al., *A conserved role for the zinc finger polyadenosine RNA binding protein, ZC3H14, in control of poly(A) tail length.* RNA, 2014. **20**(5): p. 681-8.
265. Soucek, S., A.H. Corbett, and M.B. Fasken, *The long and the short of it: the role of the zinc finger polyadenosine RNA binding protein, Nab2, in control of poly(A) tail length.* Biochim Biophys Acta, 2012. **1819**(6): p. 546-54.
266. Fuke, H. and M. Ohno, *Role of poly (A) tail as an identity element for mRNA nuclear export.* Nucleic Acids Res, 2008. **36**(3): p. 1037-49.
267. Chorghade, S., et al., *Poly(A) tail length regulates PABPC1 expression to tune translation in the heart.* Elife, 2017. **6**.
268. Peng, J., E.L. Murray, and D.R. Schoenberg, *In vivo and in vitro analysis of poly(A) length effects on mRNA translation.* Methods Mol Biol, 2008. **419**: p. 215-30.
269. Weill, L., et al., *Translational control by changes in poly(A) tail length: recycling mRNAs.* Nat Struct Mol Biol, 2012. **19**(6): p. 577-85.
270. Beckel-Mitchener, A.C., et al., *Poly(A) tail length-dependent stabilization of GAP-43 mRNA by the RNA-binding protein HuD.* J Biol Chem, 2002. **277**(31): p. 27996-8002.
271. Prieto, S., B.J. de la Cruz, and I.E. Scheffler, *Glucose-regulated turnover of mRNA and the influence of poly(A) tail length on half-life.* J Biol Chem, 2000. **275**(19): p. 14155-66.
272. Wu, L., et al., *CPEB-mediated cytoplasmic polyadenylation and the regulation of experience-dependent translation of alpha-CaMKII mRNA at synapses.* Neuron, 1998. **21**(5): p. 1129-39.
273. Kuhlmann, S.I., E. Valkov, and M. Stewart, *Structural basis for the molecular recognition of polyadenosine RNA by Nab2 Zn fingers.* Nucleic Acids Res, 2014. **42**(1): p. 672-80.
274. Kim Guisbert, K., et al., *Functional specificity of shuttling hnRNPs revealed by genome-wide analysis of their RNA binding profiles.* RNA, 2005. **11**(4): p. 383-93.
275. Tuck, A.C. and D. Tollervey, *A transcriptome-wide atlas of RNP composition reveals diverse classes of mRNAs and lncRNAs.* Cell, 2013. **154**(5): p. 996-1009.
276. Guthrie, C.R., et al., *MSUT2 is a determinant of susceptibility to tau neurotoxicity.* Hum Mol Genet, 2011. **20**(10): p. 1989-99.
277. Kelly, S.M., et al., *The Drosophila ortholog of the Zc3h14 RNA binding protein acts within neurons to pattern axon projection in the developing brain.* Dev Neurobiol, 2016. **76**(1): p. 93-106.
278. Heisenberg, M., *Mushroom body memoir: from maps to models.* Nat Rev Neurosci, 2003. **4**(4): p. 266-75.
279. Medioni, C., K. Mowry, and F. Besse, *Principles and roles of mRNA localization in animal development.* Development, 2012. **139**(18): p. 3263-76.
280. Moore, M.J., *From birth to death: the complex lives of eukaryotic mRNAs.* Science, 2005. **309**(5740): p. 1514-8.
281. Shyu, A.B., M.F. Wilkinson, and A. van Hoof, *Messenger RNA regulation: to translate or to degrade.* EMBO J, 2008. **27**(3): p. 471-81.

282. Neelamraju, Y., S. Hashemikhabir, and S.C. Janga, *The human RBPome: From genes and proteins to human disease.* J Proteomics, 2015. **127**(Pt A): p. 61-70.
283. Lukong, K.E., et al., *RNA-binding proteins in human genetic disease.* Trends Genet, 2008. **24**(8): p. 416-25.
284. Dredge, B.K., A.D. Polydorides, and R.B. Darnell, *The splice of life: alternative splicing and neurological disease.* Nat Rev Neurosci, 2001. **2**(1): p. 43-50.
285. Squire, L.R. and E.R. Kandel, *Memory: from mind to molecules*. Scientific American Library paperbacks. 2000, New York: Scientific American Library. xi, 235 p.
286. Lenzken, S.C., et al., *Neuronal RNA-binding proteins in health and disease.* Wiley Interdiscip Rev RNA, 2014. **5**(4): p. 565-76.
287. Xing, L. and G.J. Bassell, *mRNA localization: an orchestration of assembly, traffic and synthesis.* Traffic, 2013. **14**(1): p. 2-14.
288. Kelly, S., et al., *New kid on the ID block: neural functions of the Nab2/ZC3H14 class of Cys_3His tandem zinc-finger polyadenosine RNA binding proteins.* RNA Biol, 2012. **9**(5): p. 555-62.
289. Reuter, L.M., D.M. Meinel, and K. Sträßer, *The poly(A)-binding protein Nab2 functions in RNA polymerase III transcription.* Genes Dev, 2015. **29**(14): p. 1565-75.
290. Soucek, S., et al., *The Evolutionarily-conserved Polyadenosine RNA Binding Protein, Nab2, Cooperates with Splicing Machinery to Regulate the Fate of pre-mRNA.* Mol Cell Biol, 2016. **36**(21): p. 2697-2714.
291. Lee, D.C. and J.D. Aitchison, *Kap104p-mediated nuclear import. Nuclear localization signals in mRNA-binding proteins and the role of Ran and Rna.* J Biol Chem, 1999. **274**(41): p. 29031-7.
292. Duncan, K., J.G. Umen, and C. Guthrie, *A putative ubiquitin ligase required for efficient mRNA export differentially affects hnRNP transport.* Curr Biol, 2000. **10**(12): p. 687-96.
293. Brockmann, C., et al., *Structural basis for polyadenosine-RNA binding by Nab2 Zn fingers and its function in mRNA nuclear export.* Structure, 2012. **20**(6): p. 1007-18.
294. Lakso, M., et al., *Efficient in vivo manipulation of mouse genomic sequences at the zygote stage.* Proc Natl Acad Sci U S A, 1996. **93**(12): p. 5860-5.
295. Dooley, T.P., et al., *Transactivation of the adenovirus EIIa promoter in the absence of adenovirus E1A protein is restricted to mouse oocytes and preimplantation embryos.* Development, 1989. **107**(4): p. 945-56.
296. Abdeen, S.K., et al., *Conditional inactivation of the mouse Wwox tumor suppressor gene recapitulates the null phenotype.* J Cell Physiol, 2013. **228**(7): p. 1377-82.
297. Gerber, E.E., et al., *Integrin-modulating therapy prevents fibrosis and autoimmunity in mouse models of scleroderma.* Nature, 2013. **503**(7474): p. 126-30.
298. Wang, Y., et al., *Cosmc is an essential chaperone for correct protein O-glycosylation.* Proc Natl Acad Sci U S A, 2010. **107**(20): p. 9228-33.
299. Cao, Y., et al., *Regulators of G protein signaling RGS7 and RGS11 determine the onset of the light response in ON bipolar neurons.* Proc Natl Acad Sci U S A, 2012. **109**(20): p. 7905-10.
300. Chandra, D., et al., *GABAA receptor alpha 4 subunits mediate extrasynaptic inhibition in thalamus and dentate gyrus and the action of gaboxadol.* Proc Natl Acad Sci U S A, 2006. **103**(41): p. 15230-5.

301. Bergo, M.O., et al., *Zmpste24 deficiency in mice causes spontaneous bone fractures, muscle weakness, and a prelamin A processing defect.* Proc Natl Acad Sci U S A, 2002. **99**(20): p. 13049-54.
302. Higashi, Y., et al., *Generation of the floxed allele of the SIP1 (Smad-interacting protein 1) gene for Cre-mediated conditional knockout in the mouse.* Genesis, 2002. **32**(2): p. 82-4.
303. Deacon, R.M. and J.N. Rawlins, *T-maze alternation in the rodent.* Nat Protoc, 2006. **1**(1): p. 7-12.
304. Vorhees, C.V. and M.T. Williams, *Assessing spatial learning and memory in rodents.* ILAR J, 2014. **55**(2): p. 310-32.
305. Bunge, S.A., et al., *Prefrontal regions involved in keeping information in and out of mind.* Brain, 2001. **124**(Pt 10): p. 2074-86.
306. Penley, S.C., C.M. Gaudet, and S.W. Threlkeld, *Use of an eight-arm radial water maze to assess working and reference memory following neonatal brain injury.* J Vis Exp, 2013(82): p. 50940.
307. Morris, R.G., et al., *Place navigation impaired in rats with hippocampal lesions.* Nature, 1982. **297**(5868): p. 681-3.
308. Douglas, R.M., et al., *Independent visual threshold measurements in the two eyes of freely moving rats and mice using a virtual-reality optokinetic system.* Vis Neurosci, 2005. **22**(5): p. 677-84.
309. Cox, J., et al., *Accurate proteome-wide label-free quantification by delayed normalization and maximal peptide ratio extraction, termed MaxLFQ.* Mol Cell Proteomics, 2014. **13**(9): p. 2513-26.
310. Shonesy, B.C., et al., *CaMKII: a molecular substrate for synaptic plasticity and memory.* Prog Mol Biol Transl Sci, 2014. **122**: p. 61-87.
311. Chang, H.T., et al., *WW domain-containing oxidoreductase in neuronal injury and neurological diseases.* Oncotarget, 2014. **5**(23): p. 11792-9.
312. Bienkowski, R.S., et al., *The Conserved, Disease-Associated RNA Binding Protein dNab2 Interacts with the Fragile X Protein Ortholog in Drosophila Neurons.* Cell Rep, 2017. **20**(6): p. 1372-1384.
313. Wigington, C.P., et al., *The Polyadenosine RNA-binding Protein, Zinc Finger Cys3His Protein 14 (ZC3H14), Regulates the Pre-mRNA Processing of a Key ATP Synthase Subunit mRNA.* J Biol Chem, 2016. **291**(43): p. 22442-22459.
314. Zhou, H., et al., *RNA-binding proteins in neurological diseases.* Sci China Life Sci, 2014. **57**(4): p. 432-44.
315. Kapeli, K. and G.W. Yeo, *Genome-wide approaches to dissect the roles of RNA binding proteins in translational control: implications for neurological diseases.* Front Neurosci, 2012. **6**: p. 144.
316. Paronetto, M.P. and C. Sette, *Role of RNA-binding proteins in mammalian spermatogenesis.* Int J Androl, 2010. **33**(1): p. 2-12.
317. Venables, J.P. and I. Eperon, *The roles of RNA-binding proteins in spermatogenesis and male infertility.* Curr Opin Genet Dev, 1999. **9**(3): p. 346-54.
318. Cheng, C.Y., et al., *ENU mutagenesis identifies mice modeling Warburg Micro Syndrome with sensory axon degeneration caused by a deletion in Rab18.* Exp Neurol, 2015. **267**: p. 143-51.

319. Bakker, N.E., et al., *Testes in infants with Prader-Willi syndrome: human chorionic gonadotropin treatment, surgery and histology.* J Urol, 2015. **193**(1): p. 291-8.
320. Sammour, Z.M., et al., *Congenital genitourinary abnormalities in children with Williams-Beuren syndrome.* J Pediatr Urol, 2014. **10**(5): p. 804-9.
321. Yi, T., et al., *LGR4/GPR48 inactivation leads to aniridia-genitourinary anomalies-mental retardation syndrome defects.* J Biol Chem, 2014. **289**(13): p. 8767-80.
322. Cabezas, D.A., et al., *A new X linked mental retardation (XLMR) syndrome with short stature, small testes, muscle wasting, and tremor localises to Xq24-q25.* J Med Genet, 2000. **37**(9): p. 663-8.
323. Siffroi, J.P., et al., *Expression of the TAR RNA binding protein in human testis.* Mol Hum Reprod, 2001. **7**(3): p. 219-25.
324. Kimura, M., et al., *Characterization of two cytoplasmic poly(A)-binding proteins, PABPC1 and PABPC2, in mouse spermatogenic cells.* Biol Reprod, 2009. **80**(3): p. 545-54.
325. Sutherland, J.M., et al., *RNA binding proteins in spermatogenesis: an in depth focus on the Musashi family.* Asian J Androl, 2015. **17**(4): p. 529-36.
326. Michel, C.I., R. Kraft, and L.L. Restifo, *Defective neuronal development in the mushroom bodies of Drosophila fragile X mental retardation 1 mutants.* J Neurosci, 2004. **24**(25): p. 5798-809.
327. Reiss, A.L., et al., *Neurodevelopmental effects of the FMR-1 full mutation in humans.* Nat Med, 1995. **1**(2): p. 159-67.
328. Ishihara, K., et al., *Enlarged brain ventricles and impaired neurogenesis in the Ts1Cje and Ts2Cje mouse models of Down syndrome.* Cereb Cortex, 2010. **20**(5): p. 1131-43.
329. Correa-Cerro, L.S., et al., *Development and characterization of a hypomorphic Smith-Lemli-Opitz syndrome mouse model and efficacy of simvastatin therapy.* Hum Mol Genet, 2006. **15**(6): p. 839-51.
330. White, N.S., M.T. Alkire, and R.J. Haier, *A voxel-based morphometric study of nondemented adults with Down Syndrome.* Neuroimage, 2003. **20**(1): p. 393-403.
331. Pearlson, G.D., et al., *MRI brain changes in subjects with Down syndrome with and without dementia.* Dev Med Child Neurol, 1998. **40**(5): p. 326-34.
332. Driscoll, I., et al., *Longitudinal pattern of regional brain volume change differentiates normal aging from MCI.* Neurology, 2009. **72**(22): p. 1906-13.
333. Eckmann, C.R., C. Rammelt, and E. Wahle, *Control of poly(A) tail length.* Wiley Interdiscip Rev RNA, 2011. **2**(3): p. 348-61.
334. Curinha, A., et al., *Implications of polyadenylation in health and disease.* Nucleus, 2014. **5**(6): p. 508-19.
335. Darnell, J.C. and J.D. Richter, *Cytoplasmic RNA-binding proteins and the control of complex brain function.* Cold Spring Harb Perspect Biol, 2012. **4**(8): p. a012344.
336. Liu-Yesucevitz, L., et al., *Local RNA Translation at the Synapse and in Disease.* The Journal of Neuroscience, 2011. **31**(45): p. 16086-16093.
337. Richter, J.D., *CPEB: a life in translation.* Trends in Biochemical Sciences, 2007. **32**(6): p. 279-285.
338. Kreitz, C., et al., *Working-memory performance is related to spatial breadth of attention.* Psychol Res, 2015. **79**(6): p. 1034-41.

339. Rummel, J. and C.D. Boywitt, *Controlling the stream of thought: working memory capacity predicts adjustment of mind-wandering to situational demands.* Psychon Bull Rev, 2014. **21**(5): p. 1309-15.
340. Kail, R.V., A. Lervag, and C. Hulme, *Longitudinal evidence linking processing speed to the development of reasoning.* Dev Sci, 2015.
341. Nagel, I.E., et al., *Human aging magnifies genetic effects on executive functioning and working memory.* Front Hum Neurosci, 2008. **2**: p. 1.
342. Kazdoba, T.M., et al., *Modeling fragile X syndrome in the Fmr1 knockout mouse.* Intractable Rare Dis Res, 2014. **3**(4): p. 118-33.
343. Liao, L., et al., *Quantitative proteomic analysis of primary neurons reveals diverse changes in synaptic protein content in fmr1 knockout mice.* Proc Natl Acad Sci U S A, 2008. **105**(40): p. 15281-6.
344. Klemmer, P., et al., *Proteomics, ultrastructure, and physiology of hippocampal synapses in a fragile X syndrome mouse model reveal presynaptic phenotype.* J Biol Chem, 2011. **286**(29): p. 25495-504.
345. Tang, B., et al., *Fmr1 deficiency promotes age-dependent alterations in the cortical synaptic proteome.* Proc Natl Acad Sci U S A, 2015. **112**(34): p. E4697-706.
346. Sudhakaran, I.P., et al., *FMRP and Ataxin-2 function together in long-term olfactory habituation and neuronal translational control.* Proc Natl Acad Sci U S A, 2014. **111**(1): p. E99-E108.
347. Cheever, A., E. Blackwell, and S. Ceman, *Fragile X protein family member FXR1P is regulated by microRNAs.* RNA, 2010. **16**(8): p. 1530-9.
348. Prusky, G.T., et al., *Rapid quantification of adult and developing mouse spatial vision using a virtual optomotor system.* Invest Ophthalmol Vis Sci, 2004. **45**(12): p. 4611-6.
349. Aung, M.H., et al., *Early visual deficits in streptozotocin-induced diabetic long evans rats.* Invest Ophthalmol Vis Sci, 2013. **54**(2): p. 1370-7.
350. Aung, M.H., et al., *Dopamine deficiency contributes to early visual dysfunction in a rodent model of type 1 diabetes.* J Neurosci, 2014. **34**(3): p. 726-36.
351. Yuste, R., *Dendritic spines and distributed circuits.* Neuron, 2011. **71**(5): p. 772-81.
352. Sheng, M. and C.C. Hoogenraad, *The postsynaptic architecture of excitatory synapses: a more quantitative view.* Annu Rev Biochem, 2007. **76**: p. 823-47.
353. Bourne, J.N. and K.M. Harris, *Balancing structure and function at hippocampal dendritic spines.* Annu Rev Neurosci, 2008. **31**: p. 47-67.
354. Segal, M., *Dendritic spines and long-term plasticity.* Nat Rev Neurosci, 2005. **6**(4): p. 277-84.
355. Adrian, M., et al., *Barriers in the brain: resolving dendritic spine morphology and compartmentalization.* Front Neuroanat, 2014. **8**: p. 142.
356. Chen, Y. and B.L. Sabatini, *Signaling in dendritic spines and spine microdomains.* Curr Opin Neurobiol, 2012. **22**(3): p. 389-96.
357. Svoboda, K., D.W. Tank, and W. Denk, *Direct measurement of coupling between dendritic spines and shafts.* Science, 1996. **272**(5262): p. 716-9.
358. De Roo, M., et al., *Spine dynamics and synapse remodeling during LTP and memory processes.* Prog Brain Res, 2008. **169**: p. 199-207.
359. Noguchi, J., et al., *Spine-neck geometry determines NMDA receptor-dependent Ca2+ signaling in dendrites.* Neuron, 2005. **46**(4): p. 609-22.

360. Nusser, Z., et al., *Cell type and pathway dependence of synaptic AMPA receptor number and variability in the hippocampus.* Neuron, 1998. **21**(3): p. 545-59.
361. Fiala, J.C., J. Spacek, and K.M. Harris, *Dendritic spine pathology: cause or consequence of neurological disorders?* Brain Res Brain Res Rev, 2002. **39**(1): p. 29-54.
362. Newey, S.E., et al., *Rho GTPases, dendritic structure, and mental retardation.* J Neurobiol, 2005. **64**(1): p. 58-74.
363. Forrest, M.P., E. Parnell, and P. Penzes, *Dendritic structural plasticity and neuropsychiatric disease.* Nat Rev Neurosci, 2018. **19**(4): p. 215-234.
364. Besse, F. and A. Ephrussi, *Translational control of localized mRNAs: restricting protein synthesis in space and time.* Nat Rev Mol Cell Biol, 2008. **9**(12): p. 971-80.
365. Holt, C.E. and E.M. Schuman, *The central dogma decentralized: new perspectives on RNA function and local translation in neurons.* Neuron, 2013. **80**(3): p. 648-57.
366. Glock, C., M. Heumuller, and E.M. Schuman, *mRNA transport & local translation in neurons.* Curr Opin Neurobiol, 2017. **45**: p. 169-177.
367. Huber, K.M., M.S. Kayser, and M.F. Bear, *Role for rapid dendritic protein synthesis in hippocampal mGluR-dependent long-term depression.* Science, 2000. **288**(5469): p. 1254-7.
368. Poon, M.M., et al., *Identification of process-localized mRNAs from cultured rodent hippocampal neurons.* J Neurosci, 2006. **26**(51): p. 13390-9.
369. Scherrer, K., *Primary transcripts: From the discovery of RNA processing to current concepts of gene expression - Review.* Experimental Cell Research, 2018. **373**(1): p. 1-33.
370. Liu-Yesucevitz, L., et al., *Local RNA translation at the synapse and in disease.* J Neurosci, 2011. **31**(45): p. 16086-93.
371. Cooper, T.A., L. Wan, and G. Dreyfuss, *RNA and disease.* Cell, 2009. **136**(4): p. 777-93.
372. Kapur, M. and S.L. Ackerman, *mRNA Translation Gone Awry: Translation Fidelity and Neurological Disease.* Trends Genet, 2018. **34**(3): p. 218-231.
373. Scheper, G.C., M.S. van der Knaap, and C.G. Proud, *Translation matters: protein synthesis defects in inherited disease.* Nat Rev Genet, 2007. **8**(9): p. 711-23.
374. Thelen, M.P. and M.J. Kye, *The Role of RNA Binding Proteins for Local mRNA Translation: Implications in Neurological Disorders.* Front Mol Biosci, 2019. **6**: p. 161.
375. Thelen, M.P. and M.J. Kye, *The Role of RNA Binding Proteins for Local mRNA Translation: Implications in Neurological Disorders.* Frontiers in Molecular Biosciences, 2020. **6**(161).
376. Al-Nabhani, M., et al., *Reanalysis of exome sequencing data of intellectual disability samples: Yields and benefits.* Clinical Genetics, 2018. **94**(6): p. 495-501.
377. Schmid, M., et al., *The Nuclear PolyA-Binding Protein Nab2p Is Essential for mRNA Production.* Cell Rep, 2015. **12**(1): p. 128-139.
378. Morris, K.J. and A.H. Corbett, *The polyadenosine RNA-binding protein ZC3H14 interacts with the THO complex and coordinately regulates the processing of neuronal transcripts.* Nucleic Acids Res, 2018. **46**(13): p. 6561-6575.
379. Rha, J., et al., *The RNA-binding protein, ZC3H14, is required for proper poly(A) tail length control, expression of synaptic proteins, and brain function in mice.* Hum Mol Genet, 2017. **26**(19): p. 3663-3681.
380. Coultrap, S.J. and K.U. Bayer, *CaMKII regulation in information processing and storage.* Trends Neurosci, 2012. **35**(10): p. 607-18.

381. Herring, B.E. and R.A. Nicoll, *Long-Term Potentiation: From CaMKII to AMPA Receptor Trafficking.* Annu Rev Physiol, 2016. **78**: p. 351-65.
382. Kim, K. and Y. Hayashi, *CaMKII: the Swiss army knife of synaptic plasticity.* J Physiol, 2014. **592**(22): p. 4807-8.
383. Coultrap, S.J., et al., *Autonomous CaMKII mediates both LTP and LTD using a mechanism for differential substrate site selection.* Cell Rep, 2014. **6**(3): p. 431-7.
384. Fukunaga, K., N. Shioda, and E. Miyamoto, *The Function of CaM Kinase II in Synaptic Plasticity and Spine Formation*, in *Handbook of Neurochemistry and Molecular Neurobiology: Neural Signaling Mechanisms*, A. Lajtha and K. Mikoshiba, Editors. 2009, Springer US: Boston, MA. p. 163-183.
385. Ramón-Moliner, E., *The Golgi-Cox technique*, in *Contemporary Methods in Neuroanatomy*, W.J.H. Nauta and S.O.E. Ebbesson, Editors. 1970, Springer: New York. p. 32-55.
386. Du, F., *Golgi-Cox Staining of Neuronal Dendrites and Dendritic Spines With FD Rapid GolgiStain Kit.* Curr Protoc Neurosci, 2019. **88**(1): p. e69.
387. Sholl, D.A., *Dendritic organization in the neurons of the visual and motor cortices of the cat.* J Anat, 1953. **87**(4): p. 387-406.
388. Riedl, J., et al., *Lifeact: a versatile marker to visualize F-actin.* Nature Methods, 2008. **5**(7): p. 605-607.
389. Fasken, M.B., A.H. Corbett, and M. Stewart, *Structure-function relationships in the Nab2 polyadenosine-RNA binding Zn finger protein family.* Protein Sci, 2019. **28**(3): p. 513-523.
390. Grant, R.P., et al., *Structure of the N-terminal Mlp1-binding domain of the Saccharomyces cerevisiae mRNA-binding protein, Nab2.* J Mol Biol, 2008. **376**(4): p. 1048-59.
391. Bosch, M. and Y. Hayashi, *Structural plasticity of dendritic spines.* Curr Opin Neurobiol, 2012. **22**(3): p. 383-8.
392. Swanger, S.A., et al., *Automated 4D analysis of dendritic spine morphology: applications to stimulus-induced spine remodeling and pharmacological rescue in a disease model.* Molecular Brain, 2011. **4**(1): p. 38.
393. Arellano, J.I., et al., *Ultrastructure of dendritic spines: correlation between synaptic and spine morphologies.* Front Neurosci, 2007. **1**(1): p. 131-43.
394. Peters, A. and I.R. Kaiserman-Abramof, *The small pyramidal neuron of the rat cerebral cortex. The perikaryon, dendrites and spines.* Am J Anat, 1970. **127**(4): p. 321-55.
395. Chicurel, M.E., D.M. Terrian, and H. Potter, *mRNA at the synapse: analysis of a synaptosomal preparation enriched in hippocampal dendritic spines.* The Journal of neuroscience : the official journal of the Society for Neuroscience, 1993. **13**(9): p. 4054-4063.
396. Wiedenmann, B. and W.W. Franke, *Identification and localization of synaptophysin, an integral membrane glycoprotein of Mr 38,000 characteristic of presynaptic vesicles.* Cell, 1985. **41**(3): p. 1017-28.
397. Hunt, C.A., L.J. Schenker, and M.B. Kennedy, *PSD-95 is associated with the postsynaptic density and not with the presynaptic membrane at forebrain synapses.* The Journal of neuroscience : the official journal of the Society for Neuroscience, 1996. **16**(4): p. 1380-1388.

398. Alvarez, V.A. and B.L. Sabatini, *Anatomical and Physiological Plasticity of Dendritic Spines.* Annual Review of Neuroscience, 2007. **30**(1): p. 79-97.
399. Harris, K.M., F.E. Jensen, and B. Tsao, *Three-dimensional structure of dendritic spines and synapses in rat hippocampus (CA1) at postnatal day 15 and adult ages: implications for the maturation of synaptic physiology and long-term potentiation.* J Neurosci, 1992. **12**(7): p. 2685-705.
400. Majewska, A., A. Tashiro, and R. Yuste, *Regulation of spine calcium dynamics by rapid spine motility.* J Neurosci, 2000. **20**(22): p. 8262-8.
401. O'Malley, A., et al., *Transient spine density increases in the mid-molecular layer of hippocampal dentate gyrus accompany consolidation of a spatial learning task in the rodent.* Neuroscience, 2000. **99**(2): p. 229-32.
402. Xavier, G.F. and V.C. Costa, *Dentate gyrus and spatial behaviour.* Prog Neuropsychopharmacol Biol Psychiatry, 2009. **33**(5): p. 762-73.
403. Barak, B., et al., *Neuron-specific expression of tomosyn1 in the mouse hippocampal dentate gyrus impairs spatial learning and memory.* Neuromolecular Med, 2013. **15**(2): p. 351-63.
404. Scheff, S.W., D.L. Sparks, and D.A. Price, *Quantitative assessment of synaptic density in the outer molecular layer of the hippocampal dentate gyrus in Alzheimer's disease.* Dementia, 1996. **7**(4): p. 226-32.
405. Penzes, P., et al., *Dendritic spine pathology in neuropsychiatric disorders.* Nat Neurosci, 2011. **14**(3): p. 285-93.
406. Hagerman, R.J., et al., *Fragile X syndrome.* Nature Reviews Disease Primers, 2017. **3**(1): p. 17065.
407. Zalfa, F., T. Achsel, and C. Bagni, *mRNPs, polysomes or granules: FMRP in neuronal protein synthesis.* Curr Opin Neurobiol, 2006. **16**(3): p. 265-9.
408. Feng, Y., et al., *Fragile X mental retardation protein: nucleocytoplasmic shuttling and association with somatodendritic ribosomes.* J Neurosci, 1997. **17**(5): p. 1539-47.
409. Ifrim, M.F., K.R. Williams, and G.J. Bassell, *Single-Molecule Imaging of PSD-95 mRNA Translation in Dendrites and Its Dysregulation in a Mouse Model of Fragile X Syndrome.* J Neurosci, 2015. **35**(18): p. 7116-30.
410. Stein, I.S. and K. Zito, *Dendritic Spine Elimination: Molecular Mechanisms and Implications.* Neuroscientist, 2019. **25**(1): p. 27-47.
411. Hotulainen, P. and C.C. Hoogenraad, *Actin in dendritic spines: connecting dynamics to function.* J Cell Biol, 2010. **189**(4): p. 619-29.
412. Holtmaat, A., et al., *Experience-dependent and cell-type-specific spine growth in the neocortex.* Nature, 2006. **441**(7096): p. 979-83.
413. Zuo, Y., et al., *Long-term sensory deprivation prevents dendritic spine loss in primary somatosensory cortex.* Nature, 2005. **436**(7048): p. 261-5.
414. Ho, V.M., J.A. Lee, and K.C. Martin, *The cell biology of synaptic plasticity.* Science, 2011. **334**(6056): p. 623-8.
415. Burgin, K.E., et al., *In situ hybridization histochemistry of Ca2+/calmodulin-dependent protein kinase in developing rat brain.* J Neurosci, 1990. **10**(6): p. 1788-98.
416. Paradies, M.A. and O. Steward, *Multiple subcellular mRNA distribution patterns in neurons: a nonisotopic in situ hybridization analysis.* J Neurobiol, 1997. **33**(4): p. 473-93.

417. Scheetz, A.J., A.C. Nairn, and M. Constantine-Paton, *NMDA receptor-mediated control of protein synthesis at developing synapses.* Nat Neurosci, 2000. **3**(3): p. 211-6.
418. Aakalu, G., et al., *Dynamic visualization of local protein synthesis in hippocampal neurons.* Neuron, 2001. **30**(2): p. 489-502.
419. Ashraf, S.I., et al., *Synaptic protein synthesis associated with memory is regulated by the RISC pathway in Drosophila.* Cell, 2006. **124**(1): p. 191-205.
420. Neant-Fery, M., et al., *A role for dendritic translation of CaMKIIalpha mRNA in olfactory plasticity.* PLoS One, 2012. **7**(6): p. e40133.
421. Jones, S.K., et al., *The Polyadenosine RNA Binding Protein ZC3H14 is Required in Mice for Proper Dendritic Spine Density.* bioRxiv, 2020: p. 2020.10.08.331827.
422. Imataka, H., A. Gradi, and N. Sonenberg, *A newly identified N-terminal amino acid sequence of human eIF4G binds poly(A)-binding protein and functions in poly(A)-dependent translation.* EMBO J, 1998. **17**(24): p. 7480-9.
423. Wang, C., et al., *Real-Time Imaging of Translation on Single mRNA Transcripts in Live Cells.* Cell, 2016. **165**(4): p. 990-1001.
424. Wu, B., et al., *Translation dynamics of single mRNAs in live cells and neurons.* Science, 2016. **352**(6292): p. 1430-5.
425. Langille, J.J., K. Ginzberg, and W.S. Sossin, *Polysomes identified by live imaging of nascent peptides are stalled in hippocampal and cortical neurites.* Learn Mem, 2019. **26**(9): p. 351-362.
426. Masuda, S., et al., *Recruitment of the human TREX complex to mRNA during splicing.* Genes Dev, 2005. **19**(13): p. 1512-7.
427. Huertas, P., et al., *An hpr1 point mutation that impairs transcription and mRNP biogenesis without increasing recombination.* Mol Cell Biol, 2006. **26**(20): p. 7451-65.
428. Rougemaille, M., et al., *THO/Sub2p functions to coordinate 3'-end processing with gene-nuclear pore association.* Cell, 2008. **135**(2): p. 308-21.
429. Zenklusen, D., et al., *Stable mRNP formation and export require cotranscriptional recruitment of the mRNA export factors Yra1p and Sub2p by Hpr1p.* Mol Cell Biol, 2002. **22**(23): p. 8241-53.
430. Scotti, M.M. and M.S. Swanson, *RNA mis-splicing in disease.* Nat Rev Genet, 2016. **17**(1): p. 19-32.
431. Kumar, R., et al., *THOC2 Mutations Implicate mRNA-Export Pathway in X-Linked Intellectual Disability.* Am J Hum Genet, 2015. **97**(2): p. 302-10.
432. Di Gregorio, E., et al., *A de novo X;8 translocation creates a PTK2-THOC2 gene fusion with THOC2 expression knockdown in a patient with psychomotor retardation and congenital cerebellar hypoplasia.* J Med Genet, 2013. **50**(8): p. 543-51.
433. Beaulieu, C.L., et al., *Intellectual disability associated with a homozygous missense mutation in THOC6.* Orphanet J Rare Dis, 2013. **8**: p. 62.
434. Maeder, C.I., et al., *The THO Complex Coordinates Transcripts for Synapse Development and Dopamine Neuron Survival.* Cell, 2018. **174**(6): p. 1436-1449 e20.
435. Jonckheere, A.I., J.A. Smeitink, and R.J. Rodenburg, *Mitochondrial ATP synthase: architecture, function and pathology.* J Inherit Metab Dis, 2012. **35**(2): p. 211-25.
436. Aibara, S., et al., *Structural basis for the dimerization of Nab2 generated by RNA binding provides insight into its contribution to both poly(A) tail length determination and transcript compaction in Saccharomyces cerevisiae.* Nucleic Acids Res, 2017. **45**(3): p. 1529-1538.

437. Zhang, Z. and Y. Xing, *CLIP-seq analysis of multi-mapped reads discovers novel functional RNA regulatory sites in the human transcriptome.* Nucleic Acids Res, 2017. **45**(16): p. 9260-9271.
438. Al-Nabhani, M., et al., *Reanalysis of exome sequencing data of intellectual disability samples: Yields and benefits.* Clin Genet, 2018. **94**(6): p. 495-501.
439. Fernandez-Quezada, D., et al., *Male/female Differences in Radial Arm Water Maze Execution After Chronic Exposure to Noise.* Noise Health, 2019. **21**(98): p. 25-34.
440. Basu, J. and S.A. Siegelbaum, *The Corticohippocampal Circuit, Synaptic Plasticity, and Memory.* Cold Spring Harb Perspect Biol, 2015. **7**(11).
441. Niewoehner, B., et al., *Impaired spatial working memory but spared spatial reference memory following functional loss of NMDA receptors in the dentate gyrus.* Eur J Neurosci, 2007. **25**(3): p. 837-46.
442. Sasaki, T., et al., *Dentate network activity is necessary for spatial working memory by supporting CA3 sharp-wave ripple generation and prospective firing of CA3 neurons.* Nat Neurosci, 2018. **21**(2): p. 258-269.
443. Zhang, X.H., et al., *Delay-dependent impairment of spatial working memory with inhibition of NR2B-containing NMDA receptors in hippocampal CA1 region of rats.* Mol Brain, 2013. **6**: p. 13.
444. Song, D., et al., *The lateralization of left hippocampal CA3 during the retrieval of spatial working memory.* Nat Commun, 2020. **11**(1): p. 2901.
445. Tsien, J.Z., P.T. Huerta, and S. Tonegawa, *The essential role of hippocampal CA1 NMDA receptor-dependent synaptic plasticity in spatial memory.* Cell, 1996. **87**(7): p. 1327-38.
446. Nakazawa, K., et al., *Requirement for hippocampal CA3 NMDA receptors in associative memory recall.* Science, 2002. **297**(5579): p. 211-8.
447. Gao, X., G.M. Smith, and J. Chen, *Impaired dendritic development and synaptic formation of postnatal-born dentate gyrus granular neurons in the absence of brain-derived neurotrophic factor signaling.* Exp Neurol, 2009. **215**(1): p. 178-90.
448. Inman, C.S., et al., *Direct electrical stimulation of the amygdala enhances declarative memory in humans.* Proc Natl Acad Sci U S A, 2018. **115**(1): p. 98-103.
449. Schumann, D. and T. Sommer, *Dissociable contributions of the amygdala to the immediate and delayed effects of emotional arousal on memory.* Learn Mem, 2018. **25**(6): p. 283-293.
450. Knowlton, B.J., J.A. Mangels, and L.R. Squire, *A neostriatal habit learning system in humans.* Science, 1996. **273**(5280): p. 1399-402.
451. Yin, H.H., et al., *Dynamic reorganization of striatal circuits during the acquisition and consolidation of a skill.* Nat Neurosci, 2009. **12**(3): p. 333-41.
452. Horst, N.K. and M. Laubach, *Working with memory: evidence for a role for the medial prefrontal cortex in performance monitoring during spatial delayed alternation.* J Neurophysiol, 2012. **108**(12): p. 3276-88.
453. Wirt, R.A. and J.M. Hyman, *Integrating Spatial Working Memory and Remote Memory: Interactions between the Medial Prefrontal Cortex and Hippocampus.* Brain Sci, 2017. **7**(4).
454. Chang, D.I., et al., *Cerebellar Contribution to Context Processing in Extinction Learning and Recall.* Cerebellum, 2015. **14**(6): p. 670-6.
455. Marvel, C.L., O.P. Morgan, and S.I. Kronemer, *How the motor system integrates with working memory.* Neurosci Biobehav Rev, 2019. **102**: p. 184-194.

456. Hyman, J.M., et al., *Working Memory Performance Correlates with Prefrontal-Hippocampal Theta Interactions but not with Prefrontal Neuron Firing Rates.* Front Integr Neurosci, 2010. **4**: p. 2.
457. Benchenane, K., et al., *Coherent theta oscillations and reorganization of spike timing in the hippocampal- prefrontal network upon learning.* Neuron, 2010. **66**(6): p. 921-36.
458. Shen, M.D., *Cerebrospinal fluid and the early brain development of autism.* J Neurodev Disord, 2018. **10**(1): p. 39.
459. Gilmore, J.H., et al., *Prenatal mild ventriculomegaly predicts abnormal development of the neonatal brain.* Biol Psychiatry, 2008. **64**(12): p. 1069-76.
460. Feng, R., et al., *Forebrain degeneration and ventricle enlargement caused by double knockout of Alzheimer's presenilin-1 and presenilin-2.* Proc Natl Acad Sci U S A, 2004. **101**(21): p. 8162-7.
461. Ohtsuka, N., et al., *GABAergic neurons regulate lateral ventricular development via transcription factor Pax5.* Genesis, 2013. **51**(4): p. 234-45.
462. Turner, A.H., K.S. Greenspan, and T.G.M. van Erp, *Pallidum and lateral ventricle volume enlargement in autism spectrum disorder.* Psychiatry Res Neuroimaging, 2016. **252**: p. 40-45.
463. Del Re, E.C., et al., *Enlarged lateral ventricles inversely correlate with reduced corpus callosum central volume in first episode schizophrenia: association with functional measures.* Brain Imaging Behav, 2016. **10**(4): p. 1264-1273.
464. Hibar, D.P., et al., *Subcortical volumetric abnormalities in bipolar disorder.* Mol Psychiatry, 2016. **21**(12): p. 1710-1716.
465. Apostolova, L.G., et al., *Hippocampal atrophy and ventricular enlargement in normal aging, mild cognitive impairment (MCI), and Alzheimer Disease.* Alzheimer Dis Assoc Disord, 2012. **26**(1): p. 17-27.
466. Strang, K.H., T.E. Golde, and B.I. Giasson, *MAPT mutations, tauopathy, and mechanisms of neurodegeneration.* Lab Invest, 2019. **99**(7): p. 912-928.
467. Jones, C. and P. Chen, *Planar cell polarity signaling in vertebrates.* Bioessays, 2007. **29**(2): p. 120-32.
468. Wallingford, J.B. and B. Mitchell, *Strange as it may seem: the many links between Wnt signaling, planar cell polarity, and cilia.* Genes Dev, 2011. **25**(3): p. 201-13.
469. Narita, K. and S. Takeda, *Cilia in the choroid plexus: their roles in hydrocephalus and beyond.* Front Cell Neurosci, 2015. **9**: p. 39.
470. Del Bigio, M.R., *Ependymal cells: biology and pathology.* Acta Neuropathol, 2010. **119**(1): p. 55-73.
471. Lee, L., *Riding the wave of ependymal cilia: genetic susceptibility to hydrocephalus in primary ciliary dyskinesia.* J Neurosci Res, 2013. **91**(9): p. 1117-32.
472. Ohata, S., et al., *Loss of Dishevelleds disrupts planar polarity in ependymal motile cilia and results in hydrocephalus.* Neuron, 2014. **83**(3): p. 558-71.
473. Boutin, C., et al., *A dual role for planar cell polarity genes in ciliated cells.* Proc Natl Acad Sci U S A, 2014. **111**(30): p. E3129-38.
474. Ohata, S., et al., *Mechanosensory Genes Pkd1 and Pkd2 Contribute to the Planar Polarization of Brain Ventricular Epithelium.* J Neurosci, 2015. **35**(31): p. 11153-68.
475. Banizs, B., et al., *Dysfunctional cilia lead to altered ependyma and choroid plexus function, and result in the formation of hydrocephalus.* Development, 2005. **132**(23): p. 5329-39.

476. Guirao, B., et al., *Coupling between hydrodynamic forces and planar cell polarity orients mammalian motile cilia.* Nat Cell Biol, 2010. **12**(4): p. 341-50.
477. Borovina, A., et al., *Vangl2 directs the posterior tilting and asymmetric localization of motile primary cilia.* Nat Cell Biol, 2010. **12**(4): p. 407-12.
478. Wallingford, J.B., *Planar cell polarity signaling, cilia and polarized ciliary beating.* Curr Opin Cell Biol, 2010. **22**(5): p. 597-604.
479. May-Simera, H. and M.W. Kelley, *Planar cell polarity in the inner ear.* Curr Top Dev Biol, 2012. **101**: p. 111-40.
480. Lee, W.H., et al., *A Genetic Screen Links the Disease-Associated Nab2 RNA-Binding Protein to the Planar Cell Polarity Pathway in Drosophila melanogaster.* G3 (Bethesda), 2020.
481. Sawamoto, K., et al., *New neurons follow the flow of cerebrospinal fluid in the adult brain.* Science, 2006. **311**(5761): p. 629-32.
482. Glasco, D.M., et al., *The mouse Wnt/PCP protein Vangl2 is necessary for migration of facial branchiomotor neurons, and functions independently of Dishevelled.* Dev Biol, 2012. **369**(2): p. 211-22.
483. Ghimire, S.R., E.M. Ratzan, and M.R. Deans, *A non-autonomous function of the core PCP protein VANGL2 directs peripheral axon turning in the developing cochlea.* Development, 2018. **145**(12).
484. Shafer, B., et al., *Vangl2 promotes Wnt/planar cell polarity-like signaling by antagonizing Dvl1-mediated feedback inhibition in growth cone guidance.* Dev Cell, 2011. **20**(2): p. 177-91.
485. Dos-Santos Carvalho, S., et al., *Vangl2 acts at the interface between actin and N-cadherin to modulate mammalian neuronal outgrowth.* Elife, 2020. **9**.
486. Robert, B.J.A., et al., *Vangl2 in the Dentate Network Modulates Pattern Separation and Pattern Completion.* Cell Rep, 2020. **31**(10): p. 107743.
487. Hagiwara, A., et al., *The planar cell polarity protein Vangl2 bidirectionally regulates dendritic branching in cultured hippocampal neurons.* Mol Brain, 2014. **7**: p. 79.
488. Thakar, S., et al., *Evidence for opposing roles of Celsr3 and Vangl2 in glutamatergic synapse formation.* Proc Natl Acad Sci U S A, 2017. **114**(4): p. E610-E618.
489. Nagaoka, T., et al., *The Wnt/planar cell polarity pathway component Vangl2 induces synapse formation through direct control of N-cadherin.* Cell Rep, 2014. **6**(5): p. 916-27.
490. Okerlund, N.D., R.E. Stanley, and B.N. Cheyette, *The Planar Cell Polarity Transmembrane Protein Vangl2 Promotes Dendrite, Spine and Glutamatergic Synapse Formation in the Mammalian Forebrain.* Mol Neuropsychiatry, 2016. **2**(2): p. 107-14.
491. Bagri, A., et al., *Stereotyped pruning of long hippocampal axon branches triggered by retraction inducers of the semaphorin family.* Cell, 2003. **113**(3): p. 285-99.
492. Martinez-Cerdeno, V., *Dendrite and spine modifications in autism and related neurodevelopmental disorders in patients and animal models.* Dev Neurobiol, 2017. **77**(4): p. 393-404.
493. Prigge, C.L. and J.N. Kay, *Dendrite morphogenesis from birth to adulthood.* Curr Opin Neurobiol, 2018. **53**: p. 139-145.
494. Lee, J.W., et al., *Role of dentate gyrus in aligning internal spatial map to external landmark.* Learn Mem, 2009. **16**(9): p. 530-6.

495. Lee, I. and R.P. Kesner, *Encoding versus retrieval of spatial memory: double dissociation between the dentate gyrus and the perforant path inputs into CA3 in the dorsal hippocampus.* Hippocampus, 2004. **14**(1): p. 66-76.
496. Clelland, C.D., et al., *A functional role for adult hippocampal neurogenesis in spatial pattern separation.* Science, 2009. **325**(5937): p. 210-3.
497. Orefice, L.L., et al., *Control of spine maturation and pruning through proBDNF synthesized and released in dendrites.* Mol Cell Neurosci, 2016. **71**: p. 66-79.
498. Afroz, S., et al., *Synaptic pruning in the female hippocampus is triggered at puberty by extrasynaptic GABAA receptors on dendritic spines.* Elife, 2016. **5**.
499. Wang, M., et al., *Distinct Defects in Spine Formation or Pruning in Two Gene Duplication Mouse Models of Autism.* Neurosci Bull, 2017. **33**(2): p. 143-152.
500. Bergmann, O., K.L. Spalding, and J. Frisen, *Adult Neurogenesis in Humans.* Cold Spring Harb Perspect Biol, 2015. **7**(7): p. a018994.
501. Saxe, M.D., et al., *Ablation of hippocampal neurogenesis impairs contextual fear conditioning and synaptic plasticity in the dentate gyrus.* Proc Natl Acad Sci U S A, 2006. **103**(46): p. 17501-6.
502. Lazarov, O. and C. Hollands, *Hippocampal neurogenesis: Learning to remember.* Prog Neurobiol, 2016. **138-140**: p. 1-18.
503. Cameron, H.A. and L.R. Glover, *Adult neurogenesis: beyond learning and memory.* Annu Rev Psychol, 2015. **66**: p. 53-81.
504. Saxe, M.D., et al., *Paradoxical influence of hippocampal neurogenesis on working memory.* Proc Natl Acad Sci U S A, 2007. **104**(11): p. 4642-6.
505. Ouchi, Y., et al., *Reduced adult hippocampal neurogenesis and working memory deficits in the Dgcr8-deficient mouse model of 22q11.2 deletion-associated schizophrenia can be rescued by IGF2.* J Neurosci, 2013. **33**(22): p. 9408-19.
506. Pannangrong, W., et al., *Valproic acid withdrawal ameliorates impairments of hippocampal-spatial working memory and neurogenesis.* J Zhejiang Univ Sci B, 2019. **20**(3): p. 253-263.
507. Tensaouti, Y., et al., *ApoE Regulates the Development of Adult Newborn Hippocampal Neurons.* eNeuro, 2018. **5**(4).
508. Zhang, J. and J. Jiao, *Molecular Biomarkers for Embryonic and Adult Neural Stem Cell and Neurogenesis.* Biomed Res Int, 2015. **2015**: p. 727542.
509. Chakraborti, A., et al., *Cranial irradiation alters dendritic spine density and morphology in the hippocampus.* PLoS One, 2012. **7**(7): p. e40844.
510. Anton-Sanchez, L., et al., *Three-dimensional spatial modeling of spines along dendritic networks in human cortical pyramidal neurons.* PLoS One, 2017. **12**(6): p. e0180400.
511. Perez-Cruz, C., et al., *Reduced spine density in specific regions of CA1 pyramidal neurons in two transgenic mouse models of Alzheimer's disease.* J Neurosci, 2011. **31**(10): p. 3926-34.
512. McAvoy, K., et al., *Fluoxetine induces input-specific hippocampal dendritic spine remodeling along the septotemporal axis in adulthood and middle age.* Hippocampus, 2015. **25**(11): p. 1429-46.
513. Carrasco, P., et al., *Ceramide levels regulated by carnitine palmitoyltransferase 1C control dendritic spine maturation and cognition.* J Biol Chem, 2012. **287**(25): p. 21224-32.

514. Lin, L., et al., *Determination of dendritic spine morphology by the striatin scaffold protein STRN4 through interaction with the phosphatase PP2A.* J Biol Chem, 2017. **292**(23): p. 9451-9464.
515. Mucha, M., et al., *Lipocalin-2 controls neuronal excitability and anxiety by regulating dendritic spine formation and maturation.* Proc Natl Acad Sci U S A, 2011. **108**(45): p. 18436-41.
516. Magnowska, M., et al., *Transient ECM protease activity promotes synaptic plasticity.* Sci Rep, 2016. **6**: p. 27757.
517. Ryskamp, D., et al., *Pridopidine stabilizes mushroom spines in mouse models of Alzheimer's disease by acting on the sigma-1 receptor.* Neurobiol Dis, 2019. **124**: p. 489-504.
518. Zhang, L., Y. Huang, and B. Hu, *Olfactory experiences dynamically regulate plasticity of dendritic spines in granule cells of Xenopus tadpoles in vivo.* Sci Rep, 2016. **6**: p. 35009.
519. Pchitskaya, E., et al., *Stim2-Eb3 Association and Morphology of Dendritic Spines in Hippocampal Neurons.* Sci Rep, 2017. **7**(1): p. 17625.
520. Gu, L., et al., *Long-term in vivo imaging of dendritic spines in the hippocampus reveals structural plasticity.* J Neurosci, 2014. **34**(42): p. 13948-53.
521. Araki, Y., et al., *Rapid dispersion of SynGAP from synaptic spines triggers AMPA receptor insertion and spine enlargement during LTP.* Neuron, 2015. **85**(1): p. 173-189.
522. Chen, Y., et al., *Impairment of synaptic plasticity by the stress mediator CRH involves selective destruction of thin dendritic spines via RhoA signaling.* Mol Psychiatry, 2013. **18**(4): p. 485-96.
523. Moczulska, K.E., et al., *Dynamics of dendritic spines in the mouse auditory cortex during memory formation and memory recall.* Proc Natl Acad Sci U S A, 2013. **110**(45): p. 18315-20.
524. Lai, C.S., T.F. Franke, and W.B. Gan, *Opposite effects of fear conditioning and extinction on dendritic spine remodelling.* Nature, 2012. **483**(7387): p. 87-91.
525. Chu, C., et al., *The microbiota regulate neuronal function and fear extinction learning.* Nature, 2019. **574**(7779): p. 543-548.
526. Hell, J.W., *CaMKII: claiming center stage in postsynaptic function and organization.* Neuron, 2014. **81**(2): p. 249-65.
527. Chia, P.H., et al., *A homozygous loss-of-function CAMK2A mutation causes growth delay, frequent seizures and severe intellectual disability.* Elife, 2018. **7**.
528. Bagni, C., et al., *Chemical stimulation of synaptosomes modulates alpha - Ca2+/calmodulin-dependent protein kinase II mRNA association to polysomes.* J Neurosci, 2000. **20**(10): p. RC76.
529. Stephenson, J.R., et al., *A Novel Human CAMK2A Mutation Disrupts Dendritic Morphology and Synaptic Transmission, and Causes ASD-Related Behaviors.* J Neurosci, 2017. **37**(8): p. 2216-2233.
530. Cornelia Koeberle, S., et al., *Developmental stage-dependent regulation of spine formation by calcium-calmodulin-dependent protein kinase IIalpha and Rap1.* Sci Rep, 2017. **7**(1): p. 13409.
531. Jia, J.M., et al., *The schizophrenia susceptibility gene dysbindin regulates dendritic spine dynamics.* J Neurosci, 2014. **34**(41): p. 13725-36.

532. Thiagarajan, T.C., E.S. Piedras-Renteria, and R.W. Tsien, *alpha- and betaCaMKII. Inverse regulation by neuronal activity and opposing effects on synaptic strength.* Neuron, 2002. **36**(6): p. 1103-14.
533. Pi, H.J., et al., *CaMKII control of spine size and synaptic strength: role of phosphorylation states and nonenzymatic action.* Proc Natl Acad Sci U S A, 2010. **107**(32): p. 14437-42.
534. Wang, X., et al., *Distribution of CaMKIIalpha expression in the brain in vivo, studied by CaMKIIalpha-GFP mice.* Brain Res, 2013. **1518**: p. 9-25.
535. Cook, S.G., et al., *Analysis of the CaMKIIalpha and beta splice-variant distribution among brain regions reveals isoform-specific differences in holoenzyme formation.* Sci Rep, 2018. **8**(1): p. 5448.
536. Miyakawa, T., et al., *Conditional calcineurin knockout mice exhibit multiple abnormal behaviors related to schizophrenia.* Proc Natl Acad Sci U S A, 2003. **100**(15): p. 8987-92.
537. Walton, N.M., et al., *Detection of an immature dentate gyrus feature in human schizophrenia/bipolar patients.* Transl Psychiatry, 2012. **2**: p. e135.
538. Harrison, P.J., *The hippocampus in schizophrenia: a review of the neuropathological evidence and its pathophysiological implications.* Psychopharmacology (Berl), 2004. **174**(1): p. 151-62.
539. Shin, R., et al., *The immature dentate gyrus represents a shared phenotype of mouse models of epilepsy and psychiatric disease.* Bipolar Disord, 2013. **15**(4): p. 405-21.
540. Yabuki, Y., et al., *[Imaging monitoring method of CaMKII activity by immunohistochemical analysis in schizophrenic model rats].* Yakugaku Zasshi, 2013. **133**(5): p. 501-6.
541. Liu, X.B. and K.D. Murray, *Neuronal excitability and calcium/calmodulin-dependent protein kinase type II: location, location, location.* Epilepsia, 2012. **53 Suppl 1**: p. 45-52.
542. Yamagata, Y., K. Imoto, and K. Obata, *A mechanism for the inactivation of Ca2+/calmodulin-dependent protein kinase II during prolonged seizure activity and its consequence after the recovery from seizure activity in rats in vivo.* Neuroscience, 2006. **140**(3): p. 981-92.
543. Takao, K., et al., *Deficiency of schnurri-2, an MHC enhancer binding protein, induces mild chronic inflammation in the brain and confers molecular, neuronal, and behavioral phenotypes related to schizophrenia.* Neuropsychopharmacology, 2013. **38**(8): p. 1409-25.
544. Ohira, K., et al., *Synaptosomal-associated protein 25 mutation induces immaturity of the dentate granule cells of adult mice.* Mol Brain, 2013. **6**: p. 12.
545. Laird, P.W., et al., *Simplified mammalian DNA isolation procedure.* Nucleic Acids Res, 1991. **19**(15): p. 4293.
546. Simionescu-Bankston, A., et al., *The N-BAR domain protein, Bin3, regulates Rac1- and Cdc42-dependent processes in myogenesis.* Dev Biol, 2013. **382**(1): p. 160-71.
547. Rankin, E.B., et al., *Inactivation of the arylhydrocarbon receptor nuclear translocator (Arnt) suppresses von Hippel-Lindau disease-associated vascular tumors in mice.* Mol Cell Biol, 2005. **25**(8): p. 3163-72.
548. Chekanova, J.A., R.J. Shaw, and D.A. Belostotsky, *Analysis of an essential requirement for the poly(A) binding protein function using cross-species complementation.* Curr Biol, 2001. **11**(15): p. 1207-14.

549. Apponi, L.H., et al., *Loss of nuclear poly(A)-binding protein 1 causes defects in myogenesis and mRNA biogenesis.* Human Molecular Genetics, 2010. **19**(6): p. 1058-1065.
550. Makinson, C.D., et al., *An Scn1a epilepsy mutation in Scn8a alters seizure susceptibility and behavior.* Exp Neurol, 2016. **275 Pt 1**: p. 46-58.
551. Crawley, J.N., *What's Wrong With My Mouse: Behavioral Phenotyping of Transgenic and Knockout Mice*. 2000, New York: John Wiley & Sons, Inc. 52-55.
552. Luber, C.A., et al., *Quantitative proteomics reveals subset-specific viral recognition in dendritic cells.* Immunity, 2010. **32**(2): p. 279-89.
553. Zambon, A.C., et al., *GO-Elite: a flexible solution for pathway and ontology over-representation.* Bioinformatics, 2012. **28**(16): p. 2209-10.
554. Csardi G, N.T., *The igraph software package for complex network research.* InterJournal Complex Systems 2006. **1695**.
555. Tyanova, S., et al., *The Perseus computational platform for comprehensive analysis of (prote)omics data.* Nat Methods, 2016. **13**(9): p. 731-40.
556. Garcia-Lopez, P., V. Garcia-Marin, and M. Freire, *The discovery of dendritic spines by Cajal in 1888 and its relevance in the present neuroscience.* Prog Neurobiol, 2007. **83**(2): p. 110-30.
557. Longair, M.H., D.A. Baker, and J.D. Armstrong, *Simple Neurite Tracer: open source software for reconstruction, visualization and analysis of neuronal processes.* Bioinformatics, 2011. **27**(17): p. 2453-4.